University of Potsdam

Institute of Environmental Science and Geography

Understanding hydrological dynamics in the tropical Andes of Peru and Ecuador and their responses to climate change

Cumulative dissertation

for the degree of "doctor rerum naturalium" (Dr. rer. nat.)

in Hydrology

submitted to the
Faculty of Science
at the University of Potsdam, Germany

by
Carlos Antonio Fernandez Palomino

Date of disputation: 30 August 2024

Universität
Potsdam

Understanding hydrological dynamics in the tropical Andes of Peru and Ecuador and their responses to climate change

Dissertation submitted to the Faculty of Science at the University of Potsdam, Germany, for the degree of "doctor rerum naturalium" (Dr. rer. nat.) in Hydrology

Potsdam, March 2024

Author:
Carlos Antonio Fernandez Palomino

1st supervisor:
Prof. Dr. Axel Bronstert

2nd supervisor:
Prof. Dr. Eva Paton

Mentor:
Prof. Dr. Fred Hattermann

1st reviewer:
Prof. Dr. Axel Bronstert

2nd reviewer:
Prof. Dr. Fred Hattermann

3rd reviewer:
Prof. Dr. Wouter Buytaert

Examination committee members:
Prof. Dr. Andreas Guntner
Prof. Dr. Axel Bronstert
Prof. Dr. Fred Hattermann
Prof. Dr. Eva Paton
Prof. Dr. Wouter Buytaert
Prof. Dr. Wolfgang Schwanghardt
Prof. Dr. Jurgen Kropp

Author's declaration

I prepared this dissertation independently, without unauthorized assistance. All content is original, and proper references have been provided for any sources utilized. No portion of this dissertation has been submitted for evaluation towards any other degree. Furthermore, this dissertation has not been presented for examination at any other university, either in Germany or elsewhere.

Carlos Antonio Fernandez Palomino

Potsdam, March 2024

"Water is the driving force of all nature." — Leonardo da Vinci

"Climate change is the environmental challenge of this generation, and it is imperative that we act before it's too late." — John Delaney

Acknowledgements

Contents

Summary

Human-induced climate change is impacting the global water cycle by, e.g., causing changes in precipitation patterns, evapotranspiration dynamics, cryosphere shrinkage, and complex stream-flow trends. These changes, coupled with the increased frequency and severity of extreme hydrometeorological events like floods, droughts, and heatwaves, contribute to hydroclimatic disasters, posing significant implications for local and global infrastructure, human health, and overall productivity.

In the tropical Andes, climate change is evident through warming trends, glacier retreats, and shifts in precipitation patterns, leading to altered risks of floods and droughts, e.g., in the upper Amazon River basin. Projections for the region indicate rising temperatures, potential glacier disappearance or substantial shrinkage, and altered streamflow patterns, highlighting challenges in water availability due to these expected changes and growing human water demand. The evolving trends in hydroclimatic conditions in the tropical Andes present significant challenges to socioeconomic and environmental systems, emphasizing the need for a comprehensive understanding to guide effective adaptation policies and strategies in response to the impacts of climate change in the region.

The main objective of this thesis is to investigate current hydrological dynamics in the tropical Andes of Peru and Ecuador and their responses to climate change. Given the scarcity of hydrometeorological data in the region, this objective was accomplished through a comprehensive data preparation and analysis in combination with hydrological modeling using the Soil and Water Assessment Tool (SWAT) eco-hydrological model. In this context, the initial steps involved assessing, identifying, and/or generating more reliable climate input data to address data limitations.

The thesis introduces RAIN4PE, a high-resolution precipitation dataset for Peru and Ecuador, developed by merging satellite, reanalysis, and ground-based data with surface elevation through the random forest method. Further adjustments of precipitation estimates were made for catchments influenced by fog/cloud water input on the eastern side of the Andes using streamflow data and applying the method of reverse hydrology. RAIN4PE surpasses other global and local precipitation datasets, showcasing superior reliability and accuracy in representing precipitation patterns and simulating hydrological processes across the tropical Andes. This establishes it as the optimal precipitation product for hydrometeorological applications in the region.

Due to the significant biases and limitations of global climate models (GCMs) in representing key atmospheric variables over the tropical Andes, this study developed regionally adapted GCM simulations specifically tailored for Peru and Ecuador. These simulations are known as the BASD-CMIP6-PE dataset, and they were derived using reliable, high-resolution datasets like RAIN4PE as reference data. The BASD-CMIP6-PE dataset shows notable improvements over raw GCM simulations, reflecting enhanced representations of observed climate properties and accurate simulation of streamflow, including high and low flow indices. This renders it suitable for assessing regional climate change impacts on agriculture, water resources, and hydrological extremes.

In addition to generating more accurate climatic input data, a reliable hydrological model is essential for simulating watershed hydrological processes. To tackle this challenge, the thesis presents an innovative multiobjective calibration framework integrating remote sensing vegetation data, baseflow index, discharge goodness-of-fit metrics, and flow duration curve signatures. In contrast to traditional calibration strategies relying solely on discharge goodness-of-fit metrics, this approach enhances the simulation of vegetation, streamflow, and the partitioning of flow into surface runoff and baseflow in a typical Andean catchment. The refined hydrological model calibration strategy was applied to conduct reliable simulations and understand current and future hydrological trajectories in the tropical Andes.

By establishing a region-suitable and thoroughly tested hydrological model with high-resolution and reliable precipitation input data from RAIN4PE, this study provides new insights into the spatiotemporal distribution of water balance components in Peru and transboundary catchments. Key findings underscore the estimation of Peru's total renewable freshwater resource (total river runoff of 62,399 m^3/s), with the Peruvian Amazon basin contributing 97.7%. Within this basin, the Amazon-Andes transition region emerges as a pivotal hotspot for water yield (precipitation minus evapotranspiration), characterized by abundant rainfall and lower atmospheric water demand/evapotranspiration. This finding underlines its paramount role in influencing the hydrological variability of the entire Amazon basin.

Subsurface hydrological pathways, particularly baseflow from aquifers, strongly influence water yield in lowland and Andean catchments, sustaining streamflow, especially during the extended dry season. Water yield demonstrates an elevation- and latitude-dependent increase in the Pacific Basin (catchments draining into the Pacific Ocean), while it follows an unimodal curve in the Peruvian Amazon Basin, peaking in the Amazon-Andes transition region. This observation indicates an intricate relationship between water yield and elevation.

In Amazon lowlands rivers, particularly in the Ucayali River, floodplains play a significant role in shaping streamflow seasonality by attenuating and delaying peak flows for up to two months during periods of high discharge. This observation underscores the critical importance of incorporating floodplain dynamics into hydrological simulations and river management strategies for accurate modeling and effective water resource management.

Hydrological responses vary across different land use types in high Andean catchments. Pasture areas exhibit the highest water yield, while agricultural areas and mountain forests show lower yields, emphasizing the importance of puna (high-altitude) ecosystems, such as pastures, páramos, and bofedales, in regulating natural storage.

Projected future hydrological trajectories were analyzed by driving the hydrological model with regionalized GCM simulations provided by the BASD-CMIP6-PE dataset. The analysis considered sustainable (low warming, SSP1-2.6) and fossil fuel-based development (high-end warming, SSP5-8.5) scenarios for the mid (2035-2065) and end (2065-2095) of the century. The projected changes in water yield and streamflow across the tropical Andes exhibit distinct regional and seasonal variations, particularly amplified under a high-end warming scenario towards the end of the century. Projections suggest year-round increases in water yield and streamflow in the Andean regions and decreases in the Amazon lowlands, with exceptions such as the northern Amazon expecting increases during wet seasons. Despite these regional differences, the upper Amazon River's streamflow is projected to remain relatively stable throughout the 21st century. Additionally, projections anticipate a decrease in low flows in the Amazon lowlands and an increased risk of high flows (floods) in the Andean and northern Amazon catchments.

This thesis significantly contributes to enhancing climatic data generation, overcoming regional limitations that previously impeded hydrometeorological research, and creating new opportunities. It plays a crucial role in advancing hydrological model calibration, improving the representation of internal hydrological processes, and achieving accurate results for the right reasons. Novel insights into current hydrological dynamics in the tropical Andes are fundamental for improving water resource management. The anticipated intensified changes in water flows and hydrological extreme patterns under a high-end warming scenario highlight the urgency of implementing emissions mitigation and adaptation measures to address the heightened impacts on water resources.

In fact, the new datasets (RAIN4PE and BASD-CMIP6-PE) have already been utilized by researchers and experts in regional and local-scale projects and catchments in Peru and Ecuador. For instance, they have been applied in river catchments such as Mantaro, Piura, and San Pedro to analyze local historical and future developments in climate and water resources.

Zusammenfassung

Menschgemachter Klimawandel beeinflusst den globalen Wasserkreislauf durch Veränderungen in Niederschlagsmustern, Verdunstungsdynamiken, dem Rückgang der Gletscher und komplexen Trends in den Abflussraten in den Flüssen. Diese Veränderungen, gepaart mit der zunehmenden Häufigkeit und Schwere von extremen hydrometeorologischen Ereignissen wie Überschwemmungen, Dürren und Hitzewellen, tragen zu hydroklimatischen Katastrophen bei und haben erhebliche Auswirkungen auf lokale und globale Infrastruktur, die menschliche Gesundheit und die Gesamtproduktivität.

In den tropischen Anden zeigt sich der Klimawandel durch Erwärmungstrends, Gletscherschmelzen und Verschiebungen in den Niederschlagsmustern, was zu erhöhten Risiken von Überschwemmungen und Dürren führt, beispielsweise im oberen Amazonas-Einzugsgebiet. Projektionen für die Region deuten auf steigende Temperaturen, potenzielles Verschwinden oder erhebliche Schrumpfung von Gletschern und veränderte Abflussmuster hin, was die Herausforderungen bei der Wasserverfügbarkeit aufgrund dieser erwarteten Veränderungen und des wachsenden menschlichen Wasserbedarfs zeigt. Die Trends in den hydroklimatischen Bedingungen in den tropischen Anden stellen erhebliche Herausforderungen für sozioökonomische und Umweltsysteme dar und unterstreichen die Notwendigkeit eines umfassenden Verständnisses, um effektive Anpassungspolitiken und -strategien im Hinblick auf die Auswirkungen des Klimawandels in der Region zu steuern.

Das Hauptziel dieser Dissertation ist es, die aktuellen hydrologischen Dynamiken in den tropischen Anden von Peru und Ecuador und ihre Reaktionen auf den Klimawandel zu untersuchen. Aufgrund der Knappheit von hydrometeorologischen Daten in der Region wurde dieses Ziel durch eine umfassende Datenvorbereitung und -analyse in Kombination mit hydrologische Modellierung mithilfe des ökohydrologischen Modells Soil and Water Assessment Tool (SWAT) erreicht. Die ersten Schritte umfassten die Bewertung, Identifizierung und/oder Generierung zuverlässigerer Klimadaten, um Datenbeschränkungen zu bewältigen.

Die Arbeit beginnt mit der Vorstellung von RAIN4PE, einen hochauflösenden Niederschlagsdatensatz für Peru und Ecuador, der durch die Zusammenführung von Satelliten-, Reanalysen- und bodengestützten Daten mit der Geländeoberfläche durch die Methode des Random Forest entwickelt wurde. Weitere Anpassungen der Niederschlagsschätzungen erfolgen unter Verwendung von Abflussdaten für Einzugsgebiete, die durch den Einfluss von Nebel-/Wolkenwasser auf der östlichen Seite der Anden beeinflusst werden, und mit Hilfe der Methode der Reverse-Hydrologie. RAIN4PE übertrifft andere globale und lokale Niederschlagsdatensätze und zeigt

eine überlegene Zuverlässigkeit und Genauigkeit bei der Darstellung von Niederschlagsmustern und der Simulation hydrologischer Prozesse in den tropischen Anden. Dies etabliert ihn als das optimale Niederschlagsprodukt für hydrometeorologische Anwendungen in der Region.

Aufgrund der signifikanten Ungenauigkeiten und Beschränkungen globaler Klimamodelle (GCMs) bei der Darstellung wichtiger atmosphärischer Variablen über den tropischen Anden entwickelte diese Studie regional angepasste GCM-Simulationen, die speziell für Peru und Ecuador maßgeschneidert wurden. Diese Simulationen sind als der BASD-CMIP6-PE-Datensatz bekannt und wurden unter Verwendung zuverlässiger, hochauflösender Datensätze wie RAIN4PE als Referenzdaten abgeleitet. Der BASD-CMIP6-PE-Datensatz weist gegenüber rohen GCM-Ergebnissen bedeutende Verbesserungen auf, zeigt eine verbesserte Darstellung beobachteter Klimaeigenschaften und eine genaue Simulation des Wasserabflusses einschließlich seiner Hoch- und Niedrigflussindizes. Dies macht ihn geeignet, regionale Auswirkungen des Klimawandels auf Landwirtschaft, Wasserressourcen und hydrologische Extremereignisse zu bewerten.

Zusätzlich zur Generierung genauerer klimatischer Eingabedaten ist ein zuverlässiges hydrologisches Modell für die Simulation hydrologischer Dynamiken im Einzugsgebiet unerlässlich. Um diese Herausforderung zu bewältigen, stellt die Arbeit einen innovativen multiobjektiven Kalibrierungsrahmen vor, der fernerkundungsbasierte Vegetationsdaten, Basisabfluss-Index, Abflussgütemaße und Kennzeichen der Abflussdauerkurve integriert. Im Gegensatz zu traditionellen Kalibrierungsstrategien, die ausschließlich auf Abflussgütemaße beruhen, verbessert dieser Ansatz die Simulation von Vegetation, Wasserabfluss und Aufteilung des Abflusses in Oberflächen- und Basisabfluss in einem typischen Anden-Einzugsgebiet. Die verfeinerte Kalibrierungsstrategie des hydrologischen Modells wurde angewendet, um zuverlässigere Simulationen zu erzielen und aktuelle und zukünftige hydrologische Entwicklungen in den tropischen Anden zu verstehen.

Aufbauend auf einer der Region angepassten hydrologischen Modell mit hochauflösenden und zuverlässigen Niederschlagsdaten von RAIN4PE liefert diese Studie neue Einblicke in die räumlich-zeitliche Verteilung von Wasserbilanzkomponenten in Peru und grenzüberschreitenden Einzugsgebieten. Die wichtigsten Erkenntnisse betonen die Schätzung der Gesamtmenge an erneuerbarem Süßwasser in Peru (Gesamtwasserabfluss von 62.399 m^3/s), wobei das peruanische Amazonasbecken 97,7% dazu beiträgt. Innerhalb dieses Beckens wird die Übergangsregion Amazonas-Anden als zentraler Hotspot für Wasserertrag (Niederschlag minus Evapotranspiration) hervorgehoben, geprägt durch reichlichen Niederschlag und eine geringere atmosphärische Wassernachfrage/Evapotranspiration. Diese Erkenntnis unterstreicht ihre herausragende Rolle bei der Beeinflussung der hydrologischen Variabilität des gesamten Amazonasbeckens.

Unterirdische hydrologische Komponenten, insbesondere der Grundwasserabfluss, beeinflussen deutlich die Abflussbildung in Tiefland- und Anden-Einzugsgebieten und unterstützen den Abfluss in den Flüssen, insbesondere während der verlängerten Trockenzeit. Wasserertrag zeigt einen höhen- und breitengradabhängigen Anstieg im Pazifikbecken (Einzugsgebiete, die in den Pazifik münden), während er im peruanischen Amazonasbecken einer unimodalen Kurve folgt und im Übergangsgebiet Amazonas-Anden seinen Höhepunkt erreicht. Dieses Ergebnis verdeutlicht den Zusammenhang zwischen Abflussbildung und Geländehöhe.

In Flüssen der Tiefebenen des Amazonas, insbesondere im Ucayali-Fluss, spielen Überschwemmungsgebiete eine bedeutende Rolle bei der saisonalen Wasserflussdynamik, indem sie Spitzenflüsse für bis zu zwei Monate während Perioden hoher Abflüsse abschwächen und verzögern. Dieses Ergebnis unterstreicht die Wichtigkeit der Einbeziehung von Überschwemmungsdynamiken in hydrologische Simulationen und Flussmanagementstrategien für eine präzise Modellierung und effektive Wasserressourcenbewirtschaftung.

Hydrologische Reaktionen variieren je nach Landnutzungstypen in hohen Anden-Einzugsgebieten. Weideflächen zeigen den höchsten Wasserertrag, während landwirtschaftliche Flächen und Bergwälder geringere Wasserertrag aufweisen, was die Bedeutung von Puna (hochgelegenen) Ökosystemen wie Weiden, Páramos und Bofedales bei der Regulierung natürlicher Speicher betont.

Projektierte zukünftige hydrologische Entwicklungen wurden analysiert, indem das hydrologische Modell mit regionalisierten GCM-Simulationen des BASD-CMIP6-PE-Datensatzes

angetrieben wurde. Diese Analyse berücksichtigte nachhaltige (geringe Erwärmung, SSP1-2.6) und auf starker Nutzung fossiler Brennstoffe basierende (hochgradige Erwärmung, SSP5-8.5) Szenarien für die Mitte (2035-2065) und das Ende (2065-2095) des 21. Jahrhunderts. Die projektierten Veränderungen in Wasserertrag und Wasserabfluss in den tropischen Anden zeigen deutliche regionale und saisonale Variationen, insbesondere unter einem Szenario mit hoher Erwärmung gegen Ende des Jahrhunderts. Diese Projektionen deuten auf ganzjährige Zunahmen im Wasserertrag und Wasserabfluss in den Andenregionen und Rückgänge in den Tiefebenen des Amazonas hin, mit Ausnahmen wie im nördlichen Amazonasgebiet, wo Zunahmen während der Regenzeiten projektiert werden. Trotz dieser regionalen Unterschiede wird der jährliche Wasserabfluss des oberen Amazonas voraussichtlich im gesamten 21. Jahrhundert relativ stabil bleiben. Darüber hinaus deuten die Projektionen auf eine Abnahme der Niedrigabflüsse in den Tiefebenen des Amazonas und ein erhöhtes Risiko von Hochwasserabflüssen (Überschwemmungen) in den Anden- und nördlichen Amazonas-Einzugsgebieten hin.

Diese Arbeit trägt erheblich zur Verbesserung der Datenlage bzgl. des Klimas in dieser Region bei, überwindet regionale Datenbegrenzungen, die zuvor hydrometeorologische Forschung behinderten, und schafft neue Möglichkeiten. Sie trägt zur Fortentwicklung der Kalibrierung hydrologischer Modelle bei, der Verbesserung der Darstellung interner hydrologischer Prozesse und damit der Erzielung hydrologisch konsistenter Simulationsergebnisse. Diese neuen Erkenntnisse zu den hydrologischen Dynamiken in den tropischen Anden sind grundlegend für eine verbesserte Bewirtschaftung der regionalen Wasserressourcen. Die erwartete Intensivierung des regionalen Wasserkreislaufs unter einem Szenario mit hoher Erwärmung unterstreichen die Dringlichkeit der Umsetzung von Maßnahmen zur Emissionsminderung und Anpassung, um den verstärkten Auswirkungen auf Wasserressourcen zu begegnen.

Tatsächlich wurden die neuen Datensätze (RAIN4PE und BASD-CMIP6-PE) bereits von Forschern und Experten in regionalen und lokalen Projekten und Einzugsgebieten in Peru und Ecuador genutzt. Zum Beispiel wurden sie in Flusseinzugsgebieten wie Mantaro, Piura und San Pedro angewendet, um lokale historische und zukünftige Entwicklungen in Klima und Wasserressourcen zu analysieren.

1. Introduction

1.1 Motivation

1.1.1 Global climate change impacts

In its narrow sense, climate represents the long-term statistical portrayal of prevailing weather conditions, encompassing temperature and precipitation (IPCC, 2023a). In a broader context, climate extends to the overall state of the climate system, a result of intricate interactions among its components: the atmosphere, hydrosphere, cryosphere, lithosphere, and biosphere (IPCC, 2023a). These components continuously exchange elements such as heat, water, and gases, contributing to the complex dynamics of the climate system.

Over time, the climate system undergoes changes influenced by internal dynamics and external forcings, ranging from volcanic eruptions and solar variations to human-induced factors such as changes in land use and atmospheric composition (IPCC, 2023a). This interplay results in the current positive energy imbalance within the climate system, primarily attributed to escalating concentrations of greenhouse gases, particularly carbon dioxide and methane, which impedes the escape of infrared radiation, inducing warming across the atmosphere, land, cryosphere, and ocean (Hansen et al., 2011; Hansen et al., 2005; IPCC, 2023b; Trenberth and Cheng, 2022).

Human-induced climate change has altered the global water cycle, evident in warming, altered precipitation patterns and/or evapotranspiration dynamics, intensified rainfall, and a reduction in the global area of rainfall (Benestad et al., 2022; IPCC, 2023e). Rising temperatures have significantly impacted the global cryosphere, leading to the shrinkage of mountain glaciers, land and sea ice, and snow cover (IPCC, 2023d). Streamflow trends follow complex patterns (Gudmundsson et al., 2019), with certain regions experiencing drying trends (e.g., South Europe/Mediterranean, Southern Africa, and South Australia), while others exhibit wetting trends (e.g., Central North America, Southeastern South America, North Europe, and North Asia).

Concurrently, the frequency and severity of extreme hydrometeorological events, such as heatwaves, heavy precipitation, floods, and droughts, have increased globally, attributed to climate change (IPCC, 2023f; Vicente-Serrano et al., 2022; Zhang et al., 2022). The impact of increased floods is particularly evident in regions prone to rainstorm-induced and excessive soil moisture-induced floods, especially in tropical areas (Zhang et al., 2022). Regarding droughts, in some regions there is an increase in severity, particularly in agricultural and ecological
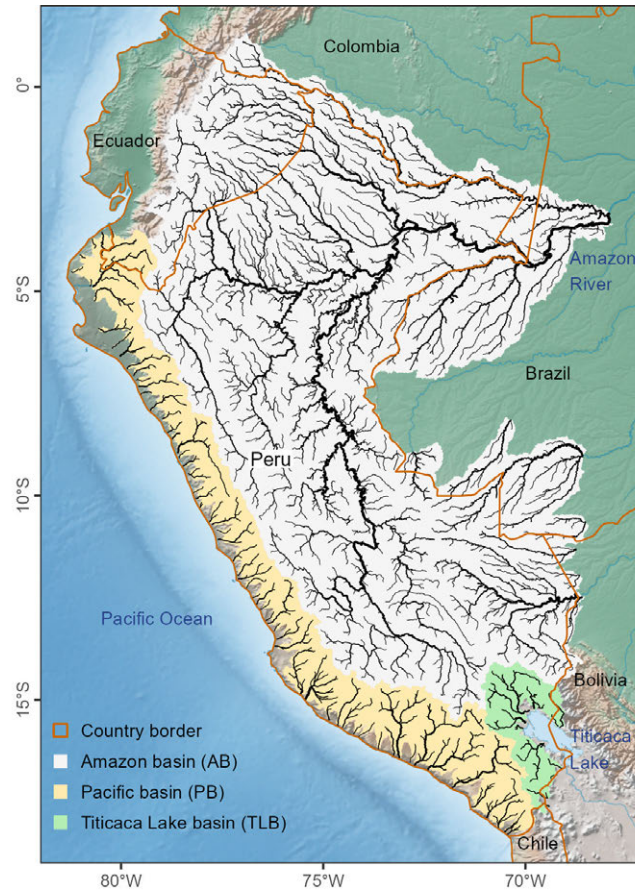
Figure 1.1: Study domain area in the Tropical Andes and simulated river catchments draining into the Amazon River (Amazon Basin), the Pacific Ocean (Pacific Basin), and Titicaca Lake (Titicaca Lake Basin).

droughts, influenced by the rise in atmospheric evaporative demand and/or reduced regional precipitation (Vicente-Serrano et al., 2022).

Consequently, these climate change effects can lead to hydroclimatic disasters, altering the distribution of water availability and damaging local and global infrastructure, human health, and total productivity (Abbass et al., 2022). In light of these global climate change effects, it becomes crucial to investigate the specific regional-scale impacts.

1.1.2 Climate change impact on the tropical Andes

The investigation conducted in the framework of this doctoral thesis addresses changes in the regional terrestrial water cycle in the tropical Andes region (19°S–2°N and 82°–67°W; see Fig. 1.1), covering Andean and Amazon lowland catchments. The primary focus is on changes in water budget components (precipitation, evapotranspiration, water yield (precipitation minus evapotranspiration), and streamflow) and hydrological extremes (low and high flows) across Peru and Ecuador, including transboundary catchments. The tropical Andes region is marked by complex, highly variable, and changing hydrological and climatic conditions, showcasing diverse ecosystems like deserts, punas, páramos, glaciers, mountain forests, tropical montane cloud forests, and rainforests (Espinoza et al., 2020; Pabón-Caicedo et al., 2020).

Peru includes three natural drainage basins (the Amazon basin, the Pacific basin, and the Titicaca Lake basin; Fig. 1.1) defined by the topography of the Andes mountain range. Despite being home to 66% of the population, the Pacific basin has natural access to only 2% of the country's total water resources (ANA, 2012; Bergmann et al., 2021); this highlights the uneven distribution of water across these basins. Climate change exacerbates this disparity.

Regionally, the impact of climate change includes warming along the tropical Andes, the retreat of the tropical Andean glaciers (loss of 42% of the total glacier area during the 1990-2020 period), alterations in summer precipitation and rainy season duration in the southern Peruvian Andes and southern Peruvian Amazon, and positive changes in precipitation and discharge over the west northern region of the Amazon (Cayo et al., 2022; Espinoza et al., 2019; Espinoza Villar et al., 2009a; Gloor et al., 2013; Imfeld et al., 2021; Lavado Casimiro et al., 2012; Marengo et al., 2018; da Motta Paca et al., 2020; Pabón-Caicedo et al., 2020; Segura et al., 2020; Torres-Batlló and Martí-Cardona, 2020). Additionally, floods and droughts have intensified in the Amazon River basin in recent decades, as documented by Marengo and Espinoza (2016).

Projections indicate an increased likelihood of more severe global and regional hydro-climatic conditions due to climate change. In the tropical Andes, temperatures are projected to rise throughout the 21st century, with expected changes in precipitation patterns—decreasing over the Amazon lowland and increasing over the Andes (Bradley et al., 2006; Pabón-Caicedo et al., 2020; Seiler et al., 2013; Vuille et al., 2018). Glaciers are projected to either disappear entirely or undergo substantial shrinkage by the end of the century (Masiokas et al., 2020). While hydrological projections are confined to specific Andean basins, the overall trend suggests a future increase in wet-season streamflow linked to climate change (Andres et al., 2014; Juen et al., 2007; Lavado Casimiro et al., 2011; Motschmann et al., 2022; Olsson et al., 2017; Zulkafli et al., 2016). Conversely, a reduction in dry-season flow is expected due to the retreat of glaciers and the rising demand for water resulting from anthropogenic activities (Goyburo et al., 2023; Motschmann et al., 2022). Additionally, there is an elevated risk of extreme hydrometeorological events, including heavy precipitation, floods, and droughts in the tropical Andes (Potter et al., 2023; Zubieta et al., 2021; Zulkafli et al., 2016).

Current and projected changes in hydroclimatic conditions pose significant challenges to regional socioeconomic and environmental systems, particularly fragile ecosystems. Hence, a comprehensive understanding of these trajectories is imperative to inform the development of adaptation policies and strategies addressing climate change impacts in this region.

1.1.3 Data limitation and uncertainty

Ground-based hydrometeorological observations, encompassing temperature, precipitation, and streamflow, are essential to meteorological, climatological, and hydrological studies. They support activities such as generating retrospective gridded products, conducting trend analyses, and driving and evaluating hydrological models. However, regions characterized by uneven and sparse observational gauges, such as the tropical Andes, pose challenges to these applications.

Researchers have explored alternative sources such as reanalysis data or satellite products in these regions. Nevertheless, uncertainties associated with estimating meteorological variables in these datasets, involving errors, biases, and underrepresenting annual cycles, underscore the indispensable role of ground-based data in mitigating such uncertainties (Condom et al., 2020).

Recent developments have generated global and regional products integrating satellite and/or reanalysis information with gauge-based data through merging procedures (e.g., Aybar et al., 2020; Beck et al., 2019b; Funk et al., 2015a). Despite these advancements, challenges persist, especially in data-sparse and complex terrain regions like the Andes-Amazon transition zone (Condom et al., 2020). In this zone, uncertainties in meteorological variables, particularly precipitation—a crucial water cycle component—result in poor hydrologic model performances and water budget imbalances (Aybar et al., 2020; Manz et al., 2016; Strauch et al., 2017; Zubieta et al., 2015, 2017; Zulkafli et al., 2014).

This imbalance can be attributed to the underestimation of precipitation due to the scarcity of meteorological gauges in these areas. Furthermore, this issue is aggravated by the fact that existing gauges do not account for cloud/fog water—a significant water source in tropical Andes ecosystems such as páramos and tropical montane cloud forests (Cárdenas et al., 2017; Clark et al., 2014; Gomez-Peralta et al., 2008). This source remains unquantified in existing precipitation datasets.

Hence, there is an urgent need for reliable and accurate meteorological datasets to enhance our understanding of hydrological processes in the tropical Andes and to facilitate the

regionalization of climate models for climate change impact assessments. In this context, a new precipitation dataset for Peru and Ecuador is developed, merging different precipitation sources and refining estimates using streamflow data through reverse hydrology.

The combined application of historical climate simulations and future climate projections from global climate models are crucial for evaluating the impact of climate change on the water sector. This assessment follows a standard modeling procedure (Krysanova et al., 2016), which includes bias adjustment and downscaling global climate model outputs to a regional scale. These outputs are then integrated into hydrological models for catchment-scale processes simulation. The results are subsequently utilized to assess impacts and guide decision-making for sustainable water resource management under diverse climate scenarios.

Regionalization can be achieved through either dynamical downscaling using regional climate models or statistical downscaling. Bias adjustment is necessary for global and regional climate model outputs, particularly in the tropical Andes, where high biases have been reported (Arias et al., 2021a; Firpo et al., 2022; Gutierrez et al., 2024; Monteverde et al., 2022). Consequently, bias adjustment and downscaling of raw global climate model outputs are imperative to produce reliable climate simulations and projections for finer-scale impact studies.

In alignment with this requirement, a high-resolution climate dataset containing historical climate simulations and future climate projections has been generated for Peru and Ecuador in this thesis. Generating reliable historical and projected meteorological data is crucial for comprehensive understanding of historical hydroclimatic conditions and developing future projections.

1.1.4 Hydrological modeling and calibration

Global and regional environmental changes, particularly in climate and land use, significantly impact hydrological processes and water resources. A comprehensive understanding of historical hydrological conditions and projections in the appropriate spatial scale (i.e. the hydrological meso-scale) is essential for informed water resources decision-making in the face of these changes.

In regions with limited data availability, such as the tropical Andes, hydrological models play a crucial role in simulating continuous time series of water balance components. These models, varying in complexity from lumped to distributed spatial representation of the basins, require calibration to identify parameters. This calibration becomes necessary due to limitations in measuring parameters of physical systems and data availability. Ensuring the accuracy of hydrological models through calibration and validation is crucial for improving their performance, increasing confidence in the projected impacts of climate change, and reducing uncertainty associated with hydrological model projections (Krysanova et al., 2018).

Calibration poses a significant challenge due to data input, model structure, and model parameter uncertainties. Interactions between parameters further intensify these challenges (Wang et al., 2020; Zhang et al., 2018b). Equifinality (Beven, 2006), where different model configurations and/or parameter values may yield equally acceptable performance, adds identifiability problems to the calibration process.

Addressing equifinality in calibration involves implementing strategies, such as incorporating additional target variables beyond streamflow data (Krysanova et al., 2018). This approach enhances the representation of specific hydrological cycle processes. Previous studies have employed multiobjective calibrations, including earth observations, in-situ measurements, and additional calibration metrics. These include evapotranspiration (Conradt et al., 2013; Rajib et al., 2018), vegetation data (Rane and Jayaraj, 2023), snow (Di Marco et al., 2021), soil moisture (Eini et al., 2023), and hydrological signatures based on the flow duration curve (Chilkoti et al., 2018; Shafii and Tolson, 2015).

Nonetheless, as argued by Shafii et al. (2017), these approaches do not always ensure accurate partitioning of flow among various pathways, which is critical when modeling hydrology-related processes such as solute transport, erosion, surface runoff, and baseflow contribution. To advance in addressing this issue, this thesis introduces a novel approach by integrating multiobjective calibration with vegetation data (e.g., leaf area index), flow duration curve signatures, and baseflow index. This innovative method aims to provide valuable insights into Andean catchment hydrological systems.

1.2 Objectives

As stated in the title, this thesis aims to enhance our understanding of the hydrological dynamics in the tropical Andes, with a specific focus on their responses to climate change. To achieve this, the following specific research questions are formulated:

1. How well do state-of-the-art regional and global precipitation datasets perform in the tropical Andes for hydrometeorological applications?
2. What is the performance of raw and regionally adapted global climate model simulations over the tropical Andes?
3. How does hydrological model calibration influence the model's reliability regarding vegetation, streamflow, and flow partitioning simulations?
4. How does the current spatiotemporal distribution of water balance components look like across Peru?
5. How do hydrological responses vary across areas with different land use types in the tropical Andes?
6. How do projected changes in water balance components vary spatially, along elevation, and over the seasons?
7. What is the potential impact of climate change on extreme hydrological conditions in the region?

Four studies outlined in the following section have been conducted to address these questions. Chapter 2 addresses Objective 1, Chapter 3 tackles Objective 2, Chapter 4 covers Objectives 3 and 5, and Objectives 4, 6, and 7 are explored in Chapter 5.

1.3 Thesis outline and author contribution

This cumulative thesis integrates three published articles and one manuscript under review by a scientific journal. These manuscripts were developed during my doctoral research at the University of Potsdam and the Potsdam Institute for Climate Impact Research and represent collaborative work involving various teams of authors. Below is an overview of the four papers, including a description of my contributions.

Chapter 2: "A novel high-resolution gridded precipitation dataset for Peruvian and Ecuadorian watersheds: development and hydrological evaluation"

This study introduces RAIN4PE (Rain for Peru and Ecuador), a new daily precipitation dataset tailored for the regions of Peru and Ecuador. The dataset is developed using a novel approach that employs a machine learning algorithm to merge various precipitation data sources (satellite, reanalysis, and ground-based measurements) with terrain elevation and the reverse hydrology technique to adjust the precipitation estimates over montane catchments based on streamflow data. Furthermore, this study presents a comprehensive evaluation of the accuracy and reliability of RAIN4PE by comparing it with other state-of-the-art local and global precipitation datasets, utilizing observed precipitation data and hydrological modeling. The study has been published as:

Fernandez-Palomino, C. A., Hattermann, F. F., Krysanova, V., Lobanova, A., Vega-Jácome, F., Lavado, W., Santini, W., Aybar, C., et al. (2022). "A Novel High-Resolution Gridded Precipitation Dataset for Peruvian and Ecuadorian Watersheds: Development and Hydrological Evaluation". In: *Journal of Hydrometeorology* 23.3, pp. 309–336. DOI: 10.1175/JHM-D-20-0285.1

Own contribution: study design, implementation, analysis, and manuscript writing with input from all co-authors.

Chapter 3: "High-resolution climate projection dataset based on CMIP6 for Peru and Ecuador: BASD-CMIP6-PE"

This study introduces BASD-CMIP6-PE, a high-resolution climate dataset for Peru and Ecuador based on the bias-adjusted and statistically downscaled CMIP6 climate projections of 10 global climate models (GCMs). Furthermore, this study presents a comprehensive evaluation of the reliability of both regionalized and raw CMIP6-GCM simulations in the historical period using observation-based data and hydrological modeling. The study has been published as:

Fernandez-Palomino, C. A., Hattermann, F. F., Krysanova, V., Vega-Jácome, F., Menz, C., Gleixner, S., and Bronstert, A. (2024). "High-resolution climate projection dataset based on CMIP6 for Peru and Ecuador: BASD-CMIP6-PE". in: *Scientific Data* 11.1, pp. 1–14. DOI: 10.1038/s41597-023-02863-z

Own contribution: I conceived the study and wrote the first version of the manuscript with inputs from all co-authors, and all authors contributed significantly to further revisions.

Chapter 4: "Towards a more consistent eco-hydrological modelling through multiobjective calibration: a case study in the Andean Vilcanota River basin, Peru"

This study presents a comprehensive multiobjective calibration framework for hydrological models using remote sensing vegetation data, discharge, and hydrological signatures to understand the hydrological responses of Andean catchments. The study has been published as:

Fernandez-Palomino, C. A., Hattermann, F. F., Krysanova, V., Vega-Jácome, F., and Bronstert, A. (2020). "Towards a more consistent eco-hydrological modelling through multi-objective calibration: a case study in the Andean Vilcanota River basin, Peru". In: *Hydrological Sciences Journal* 66.1, pp. 59–74. DOI: 10.1080/02626667.2020.1846740

Own contribution: study design, implementation, analysis, and manuscript writing with input from all co-authors.

Chapter 5: "Pan-Peruvian simulation of present and projected future hydrological conditions using novel data products and CMIP6 climate projections"

For the first time, this study provides insights into the spatiotemporal distribution of water balance components and hydrological extremes under both current and future climate scenarios across Peru. These insights are derived from state-of-the-art hydrological simulations conducted in Peruvian catchments, including transboundary river catchments, incorporating novel data products and CMIP6 climate projections. The study has been submitted to the Journal of Hydrology, and a preprint has been published as:

Fernandez-Palomino, C. A., Hattermann, F. F., Krysanova, V., Vega-Jácome, F., Lavado, W., Santini, W., Gutiérrez, R. R., and Bronstert, A. (2023a). "Pan-Peruvian Simulation of Present and Projected Future Hydrological Conditions Using Novel Data Products and CMIP6 Climate Projections". In: *SSRN*. DOI: 10.2139/SSRN.4602668

Own contribution: study design, implementation, analysis, and manuscript writing with input from all co-authors.

In addition to the manuscripts mentioned above, the author also participated in the following publications, which are not included in the thesis:

Aybar, C., Fernández, C., Huerta, A., Lavado, W., Vega, F., and Felipe-Obando, O. (2020). "Construction of a high-resolution gridded rainfall dataset for Peru from 1981 to the present day". In: *Hydrological Sciences Journal* 65.5, pp. 770–785. DOI: 10.1080/02626667.2019.1649411

Bergmann, J., Vinke, K., Fernandez Palomino, C., Gornott, C., Gleixner, S., Laudien, R., Lobanova, A., Ludescher, J., et al. (2021). *Assessing the Evidence: Climate Change and Migration in Peru*. Potsdam and Geneva: Potsdam Institute for Climate Impact Research (PIK) and International Organisation for Migration (IOM)

Harifidy, R. Z., Hiroshi, I., Kazuyoshi, S., Jun, M., Zy, R., Harivelo, M., and Fernández-Palomino, C. A. (2024). "Multi-gauge calibration comparison for simulating streamflow across the Major River Basins in Madagascar: SWAT + Toolbox, R-SWAT, and SWAT + Editor Hard calibration". In: *Hydrology Research*. DOI: 10.2166/NH.2024.188

2. A novel high-resolution gridded precipitation dataset for Peruvian and Ecuadorian watersheds – development and hydrological evaluation

Abstract

A novel approach for estimating precipitation patterns is developed here and applied to generate a new hydrologically corrected daily precipitation dataset, called RAIN4PE (Rain for Peru and Ecuador), at 0.1° spatial resolution for the period 1981–2015 covering Peru and Ecuador. It is based on the application of 1) the random forest method to merge multisource precipitation estimates (gauge, satellite, and reanalysis) with terrain elevation, and 2) observed and modeled streamflow data to first detect biases and second further adjust gridded precipitation by inversely applying the simulated results of the ecohydrological model SWAT (Soil and Water Assessment Tool). Hydrological results using RAIN4PE as input for the Peruvian and Ecuadorian catchments were compared against the ones when feeding other uncorrected (CHIRP and ERA5) and gauge-corrected (CHIRPS, MSWEP, and PISCO) precipitation datasets into the model. For that, SWAT was calibrated and validated at 72 river sections for each dataset using a range of performance metrics, including hydrograph goodness of fit and flow duration curve signatures. Results showed that gauge-corrected precipitation datasets outperformed uncorrected ones for streamflow simulation. However, CHIRPS, MSWEP, and PISCO showed limitations for streamflow simulation in several catchments draining into the Pacific Ocean and the Amazon River. RAIN4PE provided the best overall performance for streamflow simulation, including flow variability (low, high, and peak flows) and water budget closure. The overall good performance of RAIN4PE as input for hydrological modeling provides a valuable criterion of its applicability for robust countrywide hydrometeorological applications, including hydroclimatic extremes such as droughts and floods.

Significance statement

We developed a novel precipitation dataset RAIN4PE for Peru and Ecuador by merging multisource precipitation data (satellite, reanalysis, and ground-based precipitation) with terrain elevation using the random forest method. Furthermore, RAIN4PE was hydrologically corrected using streamflow data in watersheds with precipitation underestimation through reverse hydrology. The results of a comprehensive hydrological evaluation showed that RAIN4PE outperformed state-of-the-art precipitation datasets such as CHIRP, ERA5, CHIRPS, MSWEP, and PISCO in terms of daily and monthly streamflow simulations, including extremely low and high flows in almost all Peruvian and Ecuadorian catchments. This underlines the suitability of

RAIN4PE for hydrometeorological applications in this region. Furthermore, our approach for the generation of RAIN4PE can be used in other data-scarce regions.

2.1 Introduction

Precipitation is an essential component of the water cycle and reliable and accurate information about its spatiotemporal distribution is decisive for a multitude of scientific studies and operational applications. Rain gauge observations are the most used and—on a local scale—direct and accurate precipitation data sources. In addition, precipitation data can be derived from other sources such as rainfall radar stations, satellites, reanalysis products, or based on merging procedures (Sun et al., 2018). In many developing countries like Peru and Ecuador, rain gauges are unevenly and sparsely distributed (Aybar et al., 2020; Hunziker et al., 2017; Manz et al., 2016; Ochoa et al., 2014; Scheel et al., 2011). These features limit the precise estimation of spatial and temporal variability of precipitation using only gauge-based measurements in the tropical Andes.

Precipitation information derived from satellite data, e.g., CMORPH (Joyce et al., 2004), TMPA (Huffman et al., 2007), CHIRP (Funk et al., 2015b), and IMERG (Huffman et al., 2019), with a high spatiotemporal resolution, near-global coverage, and near-real-time availability have been produced in the last decades (see appendix 2.A.1 for abbreviations). These satellite-based precipitation products are promising alternative sources for regions with sparse observations. However, previous studies for the Andes domain (Baez-Villanueva et al., 2018; Chavez and Takahashi, 2017; Erazo et al., 2018; Kneis et al., 2014; Mantas et al., 2014; Manz et al., 2017; Ochoa et al., 2014; Satgé et al., 2016; Scheel et al., 2011; Zulkafli et al., 2014) have reported that precipitation estimates from satellites can be erroneous or biased, and that ground-based data are often needed to reduce their bias. Furthermore, the current short length of satellite records in this region constitutes an important restriction for the use of most of these products for long-term applications.

Reanalysis precipitation data, such as CFSR (Saha et al., 2010), JRA-55 (Kobayashi et al., 2015), and MERRA (Reichle et al., 2017), rely on uncertain parameterizations, and their spatial resolution is too coarse to represent orographic precipitation (Beck et al., 2020b). Recently, the state-of-the-art climate reanalysis ERA5 (Hersbach et al., 2020) was released, which has been shown to outperform previous reanalyses for precipitation estimation (Beck et al., 2019a; Fallah et al., 2020; Gleixner et al., 2020; Tall et al., 2019; Xu et al., 2019a), and has shown acceptable performance for hydrological modeling over North America (Tarek et al., 2020), the Amazon River basin (Towner et al., 2019), and at the global scale (Alfieri et al., 2020).

In recent years, global merged precipitation products that incorporate satellite and reanalysis information with gauge-based datasets such as CHIRPS (Funk et al., 2015a) and MSWEP (Beck et al., 2017, 2019b) have been published and are available. Many studies worldwide have shown that these products have higher accuracy than precipitation estimates based on one source only (e.g., either satellite- or reanalysis-based precipitation products) and have significant potential for hydrometeorological studies (Bai and Liu, 2018; Beck et al., 2019a; Wu et al., 2019; Xu et al., 2019b). CHIRPS has been used successfully to understand the precipitation variability over the Andes (Segura et al., 2019) and Amazonia (Espinoza et al., 2019; da Motta Paca et al., 2020; Paccini et al., 2018). In South America, the accuracy of merged precipitation products has been tested only in a few studies using ground-based precipitation (Baez-Villanueva et al., 2018; Satgé et al., 2019; Zambrano-Bigiarini et al., 2017) and hydrological modeling (Satgé et al., 2019; Wongchuig Correa et al., 2017). CHIRPS and MSWEP showed good performance for streamflow simulation in the Amazon River basin (Wongchuig Correa et al., 2017) and in catchments draining into Titicaca Lake (Satgé et al., 2020, 2019). To the best of our knowledge, there are no case studies in the literature on the hydrological evaluation of CHIRPS and MSWEP in Peruvian and Ecuadorian watersheds, which is addressed in this study.

At the regional scale, recently a high-resolution (0.1°) daily gridded precipitation dataset for Peru as part of PISCO datasets was developed (PISCO hereafter) (Aybar et al., 2020). PISCO is based on the merging of satellite estimates (CHIRP) and ground-based observations. It is used by SENAMHI for operational purposes in Peru for droughts and floods monitoring at the national scale, and was applied for hydrological modeling of the Andean Vilcanota River catchment (Fernandez-Palomino et al., 2020), catchments draining into the Pacific Ocean (Asurza-Véliz and Lavado-Casimiro, 2020), and Peruvian catchments (Llauca et al., 2021).

As the method used to generate PISCO mainly corrects the biases of CHIRP using in situ precipitation data, the higher accuracy of precipitation estimates is constrained to gauged regions such as the Pacific coast and the eastern and western slopes of the Andes of Peru (Aybar et al., 2020; Llauca et al., 2021). Hence, the application of PISCO for Peruvian Amazon and transboundary river catchments is limited. This motivated us to generate a new rainfall dataset for hydrometeorological applications at the national scale of Peru and Ecuador, exploiting the lessons learned from precipitation estimates derived not only from gauges and satellites but also from the state-of-the-art reanalysis ERA5. Indeed, ERA5 and CHIRP, which has long-term daily precipitation data available (1981–present) and hence appropriate for long-term hydrological applications, were used for the precipitation merging procedure in this study. Moreover, terrain elevation, which was reported to be a key physical variable with a strong influence on precipitation patterns in mountainous regions (Beck et al., 2020b; Bhuiyan et al., 2019; Chavez and Takahashi, 2017), was considered as an additional predictor variable.

Besides sparseness and uncertainty of rainfall observations in complex tropical mountain ranges, in some of those regions depositing fog and clouds may contribute significantly to precipitation, but cannot be recorded with conventional measurements. In páramos (grassland ecosystems extending from northern Peru to Venezuela and occurring between the tree line and glaciers) and tropical montane cloud forest (TMCF) such precipitation plays a key role in the water cycle as the cloud/fog interception by the páramos/forest constitutes an important water source to the system (Bruijnzeel et al., 2011; Cárdenas et al., 2017; Clark et al., 2014; Gomez-Peralta et al., 2008; Strauch et al., 2017). Modeled contributions of cloud water varying from less than 5% of total precipitation in wet areas to more than 75% in low-rainfall areas in TMCF were reported by Bruijnzeel et al. (2011). Fog water contribution of up to 30% of bulk precipitation (rainfall plus fog water) was estimated in tropical montane forests in the eastern Andes of Central Peru using fog gauges (Gomez-Peralta et al., 2008). Cloud water contribution of up to 15% of streamflow was reported for the montane Kosñypata catchment in the eastern Peruvian Andes using an isotopic mixing model (Clark et al., 2014). Fog water contribution of up to 28% of the total precipitation to páramos in the Colombian Andes was measured using fog gauges (Cárdenas et al., 2017). To correct the underestimation of precipitation by gridded precipitation products, adjustment of precipitation data for regions covered by cloud forests has been proposed (Strauch et al., 2017) with reported increases of up to 50% of the precipitation values in the WFDEI dataset (Weedon et al., 2014) required to improve streamflow simulation in the tropical montane watersheds.

However, the cloud/fog water component is not represented in the aforementioned precipitation data sources. This lacuna, together with the dearth of precipitation gauges, could explain some of the poor hydrologic model performances and problems with water budget closure reported in previous studies in páramo and/or montane catchments draining into the Amazon River (Aybar et al., 2020; Manz et al., 2016; Strauch et al., 2017; Zubieta et al., 2015, 2017; Zulkafli et al., 2014). Thus, for reliable and accurate estimation of precipitation in regions such as the TMCF and páramos, it is important to consider the contribution of cloud/fog water to the terrestrial hydrological system.

Correcting potential errors in gridded precipitation datasets for these areas requires the application of other types of observations and estimates. Corrected estimates of precipitation using satellite soil moisture products have been derived in recent years (Brocca et al., 2013; Brocca et al., 2019; Román-Cascón et al., 2017). However, the utility of these products could be limited due to their low accuracy in regions with dense forests (Brocca et al., 2020), such as TMCF and rainforest areas. Streamflow observations, which are spatially integrative and could be another source of data supplementing information from sparse rain gauges, offer an additional method to infer precipitation patterns and evaluate precipitation datasets (Henn et al., 2018; Le Moine et al., 2015). In this study, we applied regional streamflow observations inversely to infer or correct the precipitation input for the corresponding regional hydrological simulations. This approach has been termed "hydrology backwards" or "reverse hydrology" by Kirchner (2009) and has so far been applied in mountainous catchments like Rietholzbach in Switzerland (Teuling et al., 2010), Alzette in Luxembourg (Krier et al., 2012), Schliefau and Krems in Austria (Herrnegger et al., 2015), and the Sierra Nevada mountain range of California (Henn et al., 2015, 2018). These studies used a simple lumped hydrological model to do

reverse hydrology. In our case, we applied a process-based hydrological model to correct precipitation biases using streamflow data. We hypothesize that the correction of precipitation using streamflow data can improve closing the observed water budget gap over complex tropical mountainous catchments such as páramo and montane watersheds.

This study is the first attempt to generate a precipitation dataset for Peru and Ecuador by merging different sources of precipitation and correcting precipitation estimates through reverse hydrology. Furthermore, we evaluate the applicability of the precipitation dataset generated in this study, uncorrected precipitation datasets used for merging procedure (CHIRP and ERA5), and current state-of-the-art local (PISCO) and global (CHIRPS and MSWEP) merged precipitation products for hydrological modeling of Peruvian and Ecuadorian river catchments. This will demonstrate the effectiveness of the new methods combined here and will help illustrate the appropriateness of multiple precipitation datasets for countrywide hydrometeorological applications in both Peru and Ecuador. The objectives of this study are 1) to generate a high-spatial-resolution and hydrologically adjusted precipitation dataset for Peru and Ecuador and 2) to assess and compare the applicability of this precipitation data and the current state-of-the-art uncorrected and merged precipitation products for hydrological modeling.
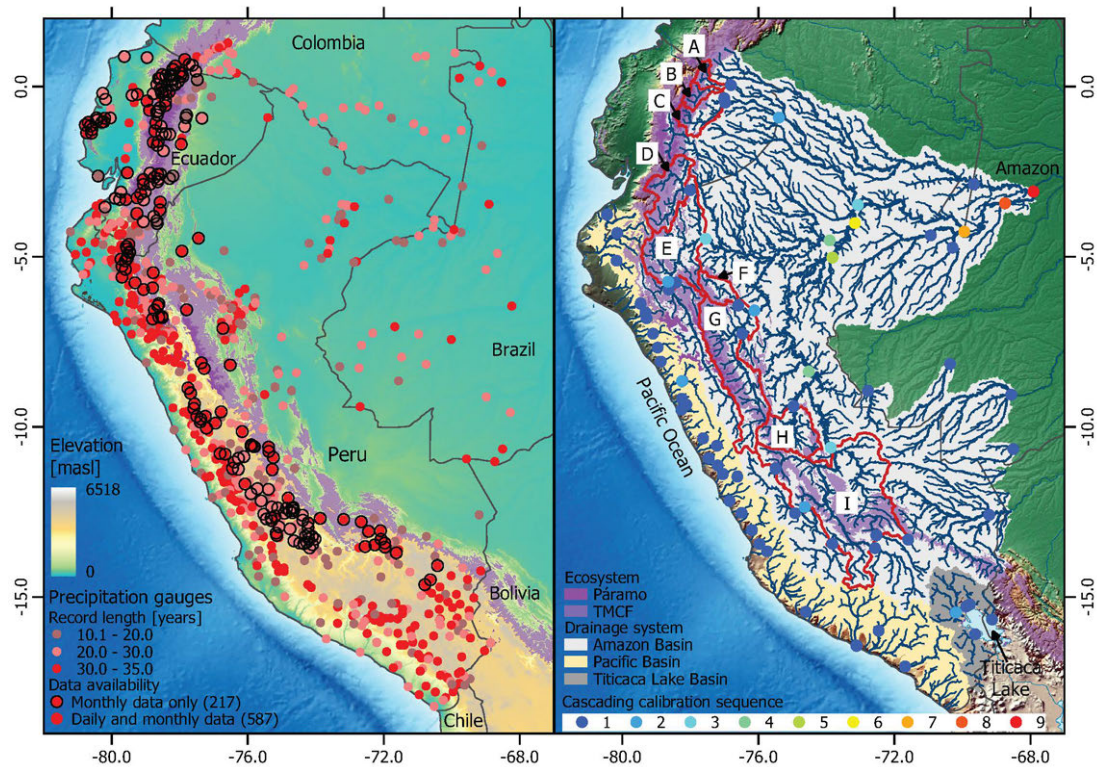
Figure 2.1: (left) Study area and spatial distribution of precipitation gauges with record length greater than 10 years for the 1981–2015 period used for the merging procedure. (right) Drainage systems, river networks, and streamflow stations used for hydrological model calibration based on the cascading calibration approach. Red polygons show the gauged catchments with water budget imbalance where gridded precipitation datasets are corrected using streamflow data through reverse hydrology. Nueva Loja station gauges the catchment "A", San Sebastian (B), Francisco De Orellana (C), Santiago (D), Borja (E), Shanao (F), Chazuta (G), Puerto Inca (H), and Lagarto (I). Boundaries of the páramo and tropical montane cloud forest (TMCF) ecosystems were obtained from Helmer et al. (2019).

2.2   Study area and data

2.2.1   Study area

The study area covers Peru and Ecuador with elevations ranging from 0 to 6518 m MSL (Fig. 2.1). The new precipitation dataset [Rain for Peru and Ecuador (RAIN4PE)] is generated for the terrestrial land surface between 19°S–2°N and 82°–67°W. The study area has complex hydroclimatic conditions related to its variable climate zones and the Andes Cordillera, which acts as a topographic barrier between the cold and dry eastern Pacific and the warm and moist Amazon region. The Andes divides the study area into three natural drainage basins (Fig. 2.1): (i) the Pacific basin (watersheds located on the western side of the Andes that convey water to the Pacific Ocean); (ii) Amazon basin (watersheds located on the eastern side of the Andes that drain to the Amazon River); and (iii) Titicaca Lake basin (catchments draining into Titicaca Lake).

In the region, the great spatial variability of precipitation patterns is modulated by the interplay among large-scale (e.g., latitudinal migration of Atlantic intertropical convergence zone, South American monsoon systems, Hadley, Walker cell, marine currents, Bolivian high) and local circulation patterns (e.g., upslope and downslope moisture transport) and the complex Andean orography (Espinoza et al., 2020; Laraque et al., 2007; Segura et al., 2019; Tobar and Wyseure, 2018). Furthermore, El Niño–Southern Oscillation (ENSO) is a major modulator of hydroclimatology at interannual time scales along the Andes (Poveda et al., 2020). The study area hosts a diversity of ecosystems such as deserts, punas (high mountain grasslands), páramos, glaciers, mountain forests, TMCFs, and rainforests. From these, páramo and TMCF (Fig. 2.1) are ecosystems where an important cloud/fog water input to the system was reported (Bruijnzeel et al., 2011; Cárdenas et al., 2017; Clark et al., 2014; Gomez-Peralta et al., 2008). This is an important precipitation source to consider in hydrological modeling of páramo and montane watersheds, as it was carried out herein.

2.2.2   Data

Ground-based precipitation data

The precipitation data of a total of 804 precipitation gauges with record length greater than ten years for the 1981–2015 period were used for this study (Fig. 2.1), out of which 587 (217) gauges have daily (only monthly) precipitation data. The data were collected from different sources such as national hydrometeorological institutions and previous studies in the region. The data for Peru were obtained from the Peruvian ANA (Autoridad Nacional del Agua) and Aybar et al. (2020); for Ecuador from Morán-Tejeda et al. (2016), Tamayo (2017), Tobar and Wyseure (2018); for Brazil from Xavier et al. (2016, 2017); and for Colombia from IDEAM (Instituto de Hidrología, Meteorología y Estudios Ambientales). We used 587 (804) precipitation gauges with daily (monthly) data for the merging of precipitation datasets at the daily (monthly) time step.

Table 2.1: List of gridded precipitation datasets used in this study. In uncorrected datasets, their temporal dynamics depend entirely on satellite (S) or reanalysis (R) data, while in gauge-corrected datasets, their temporal dynamics depend at least partly on gauge (G) data. In the spatial coverage column, "Global" means fully global coverage including oceans, while "Land" indicates that the coverage is limited to the terrestrial land surface.

Dataset (Version)	Data source(s)	Spatial resolution	Spatial coverage	Temporal resolution	Temporal coverage	Reference
			Non-gauge-corrected datasets			
CHIRP (V2.0)	S	0.05°	Land, 50° N/S	Daily	1981–present	Funk et al. (2015b)
ERA5	R	0.25°	Global	Hourly	1950–present	Hersbach et al. (2020)
			Gauge-corrected datasets			
CHIRPS (V2.0)	G, S	0.05°	Land, 50° N/S	Daily	1981–present	Funk et al. (2015a)
MSWEP (V2.2)	G, S, R	0.1°	Global	3-hourly	1979–present	Beck et al. (2017, 2019b)
PISCO (V2.1)	G, S	0.1°	Peru	Daily	1981–2016	Aybar et al. (2020)

Discharge data

Discharge data of 72 streamflow stations (Fig. 2.1) with record lengths ranging from one to 33 years for 1983–2015 were obtained from different sources, such as the Peruvian ANA and SENAMHI for catchments draining into the Pacific Ocean and located in the Andes. For the Amazon lowland, data were obtained from the Critical Zone Observatory HYBAM (Hydrogéochimie du Bassin Amazonien, `www.so-hybam.org`). This hydrological network has been operated by an international team from IRD (Institut de Recherche pour le Développement; France), SENAMHI (Peru), INAMHI (Instituto Nacional de Meteorología e Hidrología; Ecuador), and the Brazilian ANA (Agência Nacional de Águas; Brazil) since 2003 (Armijos et al., 2013; Santini et al., 2019).

Gridded precipitation data

Table 2.1 presents the five precipitation datasets used in this study. We used the non-gauge-corrected datasets (CHIRP and ERA5) for the merging procedure to generate RAIN4PE dataset. The satellite-based CHIRP precipitation dataset (Funk et al., 2015a) is obtained by considering infrared-based precipitation estimates and corresponding monthly precipitation climatology generated for Funk et al. (2015b). We selected CHIRP since it has high spatial resolution and long-term (from 1981 onward) daily precipitation data, which is appropriate for long-term hydrometeorological applications. ERA5 (Hersbach et al., 2020) is the latest climate reanalysis dataset produced by the European Centre for Medium Weather Forecasts (ECMWF). Compared with its predecessor ERA-Interim (Dee et al., 2011) that became operational in 2006, ERA5 is based on the ECMWF's Integrated Forecasting System Cycle 41r2 which was operational in 2016. ERA5 thus benefits from a decade worth of numerical weather prediction developments

Table 2.2: Data used for hydrological modeling.

Data type	Resolution	Description/source
Elevation	90 m	Surface elevation (m MSL) from Multi-Error-Removed Improved Terrain (MERIT; Yamazaki et al., 2017)
Land use	100 m	Land use classification representative for the year 2015 obtained from Copernicus Global Land Service (Buchhorn et al., 2019)
Soil	1000 m	Soil parameters for SWAT based on the Harmonized World Soil Database version 1.21 soil data (Abbaspour and Ashraf Vaghefi, 2019)
Soil thickness	1000 m	Soil thickness data (Pelletier et al., 2016) were used to implement variable soil thicknesses at hydrological response units (HRUs)
Groundwater table depth	1000 m	Groundwater table depth data (Fan et al., 2013) were used to constrain soil thickness in shallow water tables across the rain forest region
Temperature	Daily/10 km (1981–2016)	Gridded temperature (maximum and minimum) dataset for Peru (Huerta et al., 2018) as provided by SENAMHI (`ftp://publi_dgh2: 123456@ftp.senamhi.gob.pe/`)
Solar radiation	3-hourly/10 km (1983–2018)	Long-term monthly averages of solar radiation based on the global surface solar radiation data (Tang, 2019; Tang et al., 2019) were used
Evapotranspiration	Daily/0.25° (1980–2020)	Evapotranspiration data from the Global Land Evaporation Amsterdam Model (GLEAM v3.5a; Martens et al., 2017; Miralles et al., 2011)
Evapotranspiration	8-day/1 km (2000–14)	Evapotranspiration data from the Moderate Resolution Imaging Spectroradiometer Global Evaporation (MOD16; Mu et al., 2011)

in model physics, core dynamics, and data assimilation relative to ERA-Interim. Moreover, ERA5 has a much higher temporal and spatial resolution than previous global reanalyses. The hourly ERA5 precipitation data were downloaded and aggregated to obtain daily time step records matching the local gauge observations (from 0700 to 0700 local time).

To compare RAIN4PE against other gauge-corrected precipitation datasets besides the uncorrected ones (CHIRP and ERA5), we selected three merged products (CHIRPS, MSWEP, and PISCO) widely used in data evaluation and hydrometeorological applications in the region (Asurza-Véliz and Lavado-Casimiro, 2020; Baez-Villanueva et al., 2020; Bhuiyan et al., 2019; Espinoza et al., 2019; Fernandez-Palomino et al., 2020; Llauca et al., 2021; da Motta Paca et al., 2020; Paccini et al., 2018; Satgé et al., 2020, 2019; Wongchuig Correa et al., 2017). CHIRPS (Funk et al., 2015a) and PISCO (Aybar et al., 2020) are obtained by merging CHIRP and gauge estimates through deterministic and geostatistical interpolation methods. Finally, MSWEP is derived by optimally merging a range of gauge, satellite, and reanalysis precipitation estimates, where satellite and reanalysis datasets are merged using weights for each one based on the coefficient of determination between 3-day mean gauge- and grid-based precipitation time series (Beck et al., 2017, 2019b). The daily MSWEP precipitation data were provided for this study.

Additional data

In addition to various precipitation products, Table 2.2 presents other datasets that were used for the hydrological modeling process. The surface elevation data were used both for the merging procedure and setting up the hydrological model.

2.3   Methods

The framework of this study involves three main steps (Fig. 2.2): (i) merging procedure through a machine learning technique at the daily and monthly scales; (ii) calibration of model parameters and hydrological adjustment through the reverse hydrology concept; and (iii) evaluation of all precipitation products through hydrological modeling.

2.3.1   Merging procedure

In this section, the merging procedure to obtain RAIN4PE at 0.1° spatial resolution for the 1981–2015 period is described; see Fig. 2.2 for a scheme.

Covariates

For the merging procedure at the daily (monthly) scale, we used daily (monthly) precipitation estimates of CHIRP and reanalysis ERA5, surface elevation (Yamazaki et al., 2017), and buffer distances from observation points as covariates. The latter is to account for geographical proximity effects in the prediction process using the random forest (RF) method as suggested by Hengl et al. (2018). The elevation is taken into account because it is a key physical variable with a strong influence on precipitation patterns (Beck et al., 2020b; Chavez and Takahashi, 2017). We selected these covariates: satellite precipitation, reanalysis precipitation, and elevation, all of them based on recent studies (Baez-Villanueva et al., 2020; Beck et al., 2020b; Bhuiyan et al., 2019; Hong et al., 2021). To match the 0.1° spatial resolution of the final precipitation product, the covariates with grid cell size $< 0.1°$ ($> 0.1°$) were regridded to 0.1° spatial resolution applying the bilinear interpolation (nearest neighbor) method.

Random forest modeling to combine different data sources

In this study, the RF method (Breiman, 2001) was applied to produce a gridded precipitation dataset by merging multiple precipitation sources (gauge, satellite, and reanalysis). RF has been used and proved recently to have similar or superior performance in the interpolation of environmental variables such as precipitation, temperature, and evapotranspiration compared to traditional spatial interpolation techniques, e.g., regression kriging and inverse distance weighting (Hengl et al., 2018; Sekulić et al., 2020; da Silva Júnior et al., 2019). Last, RF-based methodologies (Baez-Villanueva et al., 2020; Bhuiyan et al., 2019) to merge precipitation

products with ground-based measurements were developed and applied successfully in data-scarce and complex terrain regions such as the Peruvian and Colombian Andes (Bhuiyan et al., 2019) and Chilean territory (Baez-Villanueva et al., 2020).

RF is a multivariate and nonparametric machine learning algorithm, in which the prediction is generated as an ensemble estimate from a number of regression trees (Breiman, 2001) as shown in Eq. (1.1):

$$\hat{f}(x) = \frac{1}{N} \sum_{b=1}^{N} T_b(x) \tag{2.1}$$

where $\hat{f}(x)$ is the final prediction, b is the individual bootstrap sample, N is the total number of trees, and T_b is the individual regression tree.

In RF, each tree is constructed from the random selection of covariates, which ensures that trees are decorrelated with each other, and a bootstrap sample of the observations (Breiman, 2001). The unsampled data, called out-of-bag, can be used to test the prediction accuracy and the importance of input variables, eliminating the need for an extra independent validation dataset (Breiman, 2001).

We implemented RF using the R package randomForest (Liaw and Wiener, 2002) and the following RF parameters: 1) the number of trees (set at 1000); 2) the number of predictor variables randomly selected at each node (set at one-third of the number of variables, default
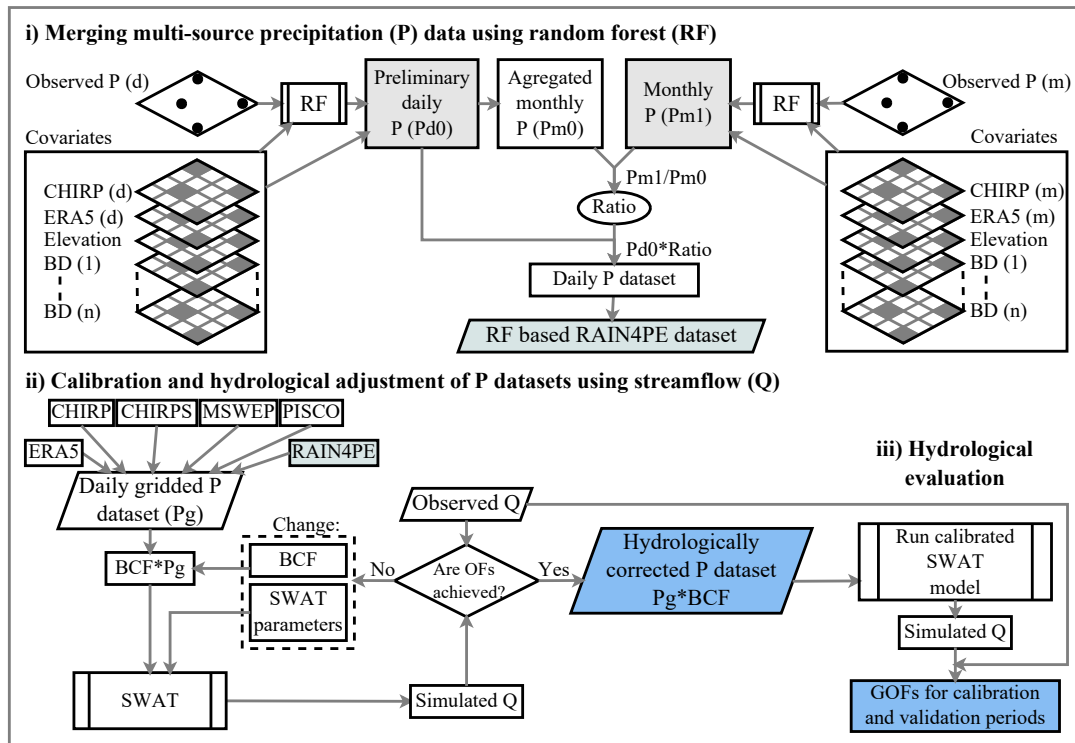
Figure 2.2: Flowchart for (i) the generation of gridded precipitation dataset, (ii) hydrological model calibration and adjustment of precipitation datasets, and (iii) hydrological evaluation. Here d (m) indicates the daily (monthly) time step, BD$_{(i),...,(n)}$ are buffer distances (distance from any point to all precipitation gauges), BCF is the bias correction factor, OFs are the objective functions for hydrological model calibration, and GOFs are the goodness of fit measures. BCF is optimized only over catchments with water budget imbalance. Note that for hydrological evaluation (step iii), the model was rerun using the respective corrected precipitation data and optimum model parameters values with BCF set to 1.

value); 3) the minimum number of observations in a tree's terminal node (set at 5, default value); and 4) the out-of-bag portion to test the accuracy of the predictions (set at one-third of the total number of observations). These parameter values were successfully used in other studies (Baez-Villanueva et al., 2020; Fox et al., 2020; Sekulić et al., 2020).

In the merging procedure (see Fig. 2.2), an RF model was trained using ground-based observations as the dependent variable and the selected covariates as predictor variables for each day and month in the 1981–2015 period. The trained RF models were then applied to covariates, yielding preliminary daily precipitation data (Pd0) and monthly precipitation data (Pm1). Finally, Pd0 was corrected to match Pm1. For that, the ratio of Pm1 over the monthly precipitation derived from Pd0 was computed on each grid cell for each month, and this ratio was then applied to multiply the Pd0 values on the grid for the month to generate the RF-based RAIN4PE dataset. This correction was because the interpolation of precipitation patterns at a monthly scale is more reliable and accurate than the daily interpolation (Aybar et al., 2020; He et al., 2020).

2.3.2   Hydrological modeling and adjustment of precipitation datasets

This section describes the approaches applied for hydrological model calibration and validation and hydrological adjustment of precipitation datasets using streamflow data through the reverse hydrology concept. The hydrological correction is applied only for nine catchments (Fig. 2.1) having a water budget imbalance due to underestimated streamflow in the simulations with uncorrected precipitation inputs, as reported in previous studies (Strauch et al., 2017; Zubieta et al., 2015, 2017; Zulkafli et al., 2014). We applied the reverse hydrology using the Soil and Water Assessment Tool (SWAT; Arnold et al., 1998) model in which both the bias correction factor (BCF) for precipitation fields and model parameters were calibrated jointly (Fig. 2.2).

SWAT model

Hydrological simulations were performed with the SWAT 2012 model (Arnold et al., 1998), updated for improved representation of tropical vegetation dynamics (Alemayehu et al., 2017). SWAT is one of the most widely used ecohydrological models in the world (Gassman et al., 2014; Tan et al., 2020), and had been applied successfully already for ecohydrological modeling of an Andean basin of Peru (Fernandez-Palomino et al., 2020). SWAT is a process-oriented, semidistributed and time-continuous river basin model used to simulate hydrological processes as well as vegetation dynamics, nutrients, pesticides, and sediment loads within a basin (Arnold et al., 1998; Neitsch et al., 2011). SWAT divides a basin into subbasins, which are then further subdivided into hydrological response units (HRUs) representing unique combinations of land use, soil type, and slope classes (Neitsch et al., 2011). The water balance computation is performed at the HRU level considering four water storage types (snow, soil profile, and shallow and deep aquifers), as follows:

$$\Delta S = \sum_{i=1}^{N}(\text{BCF} \times P - \text{WYLD} - \text{ET} - \text{GWL}) \tag{2.2}$$

where ΔS is the change in water storage (mm); N is the time in days; and P, WYLD, ET, and GWL are the amount of precipitation (mm), water yield (mm), evapotranspiration (mm), and groundwater losses (mm), respectively. BCF introduced herein is the bias correction factor to infer the precipitation fields from observed streamflow data.

In SWAT, flow routing in river channels can be computed using the Muskingum or the variable storage method, considering the flow velocity to be the same across the channel and floodplain section (Neitsch et al., 2011). This approach has been shown to be inefficient for flow routing in Amazon rivers (Santini, 2020), where flows are largely affected by floodplains that act as reservoirs, causing significant flood peak delay and attenuation (Paiva et al., 2011; Santini et al., 2015; Santini, 2020; Yamazaki et al., 2011). To exclude this limitation, Santini (2020) has implemented a new flow routing method for SWAT to consider the river–floodplain dynamics, where the associated floodplain of each river reach was treated as a simple storage model, as

Table 2.3: Parameters and their ranges for model calibration for evapotranspiration (ET), streamflow (Q), and precipitation (P). In the "Change type" column, R (V) refers to a relative (absolute) change of parameter values during the calibration. Parameter set 1 was applied for Andean catchments draining into the Pacific Ocean and Titicaca Lake and for Andean catchments upstream the montane watersheds. Montane watersheds having a water budget imbalance were calibrated using parameter set 2. Catchments downstream the montane watersheds were calibrated using parameter set 3. Note that BCF is applied only for catchments with water budget closure problems to infer precipitation from streamflow data. See Neitsch et al. (2011) for detailed parameter definitions.

Parameter	Description (unit)	Calibrated output	Range	Change type	Set 1	2	3
SOL_AWC	Soil available water capacity (mm H2O/mm soil)	ET	[−0.8, 0.8]	R	X		
GW_REVAP	Groundwater "revap" coefficient	ET	[0, 0.2]	V			X
SURLAG	Surface runoff delay coefficient	Q	[0.1, 2]	V	X	X	X
GW_DELAY	Groundwater delay time (days)	Q	[1, 100]	V	X	X	X
RCHRG_DP	Deep aquifer percolation fraction	Q	[0, 1]	V	X	X	X
GWQMN	Threshold for return flow from shallow aquifer (mm)	Q	[500, 1000]	V	X	X	X
ALPHA_BF	Baseflow recession constant	Q	[0.01, 1]	V	X	X	X
CH_K2	Hydraulic conductivity of main channel (mm h-1)	Q	[0, 50]	V			X
CHD	Main channel depth (m)	Q	[−0.1, 0.5]	R			X
FP_W_F	Ratio of floodplain width over bankfull width	Q	[1, 5]	V			X
BCF	Bias correction factor	P, Q	[0, 1]	R		X	

in other hydrological models (Paiva et al., 2011; Yamazaki et al., 2011). This approach was used in our study.

SWAT model setup, calibration, and validation

The SWAT model was set up for Peruvian and Ecuadorian catchments (total of 1,638,793 km^2) based on the input data listed in Table 2.2. The model includes 2,675 subcatchments and 6,843 HRUs. Channel cross-section parameters such as the bankfull width (B) and channel depth (CHD) were estimated using geomorphologic equations based on upstream drainage areas derived for Amazon rivers (Paiva et al., 2011). Floodplain width is estimated by multiplying the bankfull width by a factor (set at 5, default value). We assigned Manning's n values of 0.03 (0.10) for channels (floodplains). The modified Soil Conservation Service curve number, the Priestley–Taylor equation, and the variable storage methods were used to simulate surface runoff and infiltration, potential evapotranspiration, and river flow routing, respectively.

The simulation period was from 1981 to 2015. The first two years were considered for the model spinup. For the model calibration, all flow data were used for stations with a record lower than 10 years, and for those with longer, two-third of the data were used. In the latter case, the remaining flow data were used for model validation (53 out of 72 streamflow stations). The model calibration for each precipitation product was performed applying the multisite cascading calibration approach (Xue et al., 2016) in nine sequences (Fig. 2.1), where the calibrated discharge from the upstream catchments was used as input for the downstream. The model parameters and BCFs for each (sub)catchment were calibrated using the respective set of parameters defined in Table 2.3 for Andean, montane, and lower Amazon catchments. Moreover, plant parameters were adopted from our previous study (Fernandez-Palomino et al., 2020).

The optimum values of model parameters and BCFs were obtained through multiobjective calibration. For that, the model was calibrated against observed discharge using the Nash–Sutcliffe efficiency log (lNSE) and aggregated flow duration curve signature (FDC$_{sign}$) as objective functions (see Table 2.4). We selected lNSE and FDC$_{sign}$ since these have been shown sufficient to test the model for simulating all hydrograph aspects in the calibration (Fernandez-Palomino et al., 2020). Moreover, the application of FDC-based signatures provides more information about the hydrological behavior of the modeled basin (Hrachowitz et al., 2014; Yilmaz et al., 2008) and leads to better parameter identifiability, more accurate discharge simulation, and reduction of predictive uncertainty (Chilkoti et al., 2018; Fernandez-Palomino et al., 2020; Hrachowitz et al., 2014; Pfannerstill et al., 2017, 2014; Pokhrel and Yilmaz, 2012;

Sahraei et al., 2020; Yilmaz et al., 2008). Following Chilkoti et al. (2018) and Fernandez-Palomino et al. (2020), we estimated percent bias for four segments of the FDC [peak flow (0%–2%), high flow (2%–20%), midsegment (20%–70%), and low flow (70%–100%)], and then the absolute values of the bias percentages were averaged to obtain the FDC$_{sign}$ to take into consideration the hydrological signatures for model calibration. The respective FDC segmentation represents peak flow events occurring rarely, quick runoff (due to snowmelt and/or rainfall), the flashiness of a basin's response, and the streamflow's baseflow components. The Borg multiobjective evolutionary algorithm (Borg MOEA; Hadka and Reed, 2013) was used to optimize the objective functions (maximization of lNSE and minimization of FDC$_{sign}$) with 1000 iterations as the maximum. The Borg MOEA parameterization was the same as in Fernandez-Palomino et al. (2020). The parameters for ungauged catchments (at HRU level) were obtained applying the spatial proximity approach (Guo et al., 2021) using the inverse distance weighting (Shepard, 1968). For regionalization of parameters, donor catchments (gauged) within a radius of 150 km were used to avoid the influence of Amazonian catchments in the estimation of parameters for Andean basins draining into the Pacific Ocean and Titicaca Lake.

Hydrological adjustment of precipitation datasets

The optimum BCFs obtained for each catchment with water budget imbalance (Fig. 2.1) in the calibration procedure were applied to the respective daily gridded precipitation data to obtain the hydrologically corrected daily precipitation dataset (Fig. 2.2). For that, a continuous BCF map at 0.1° spatial resolution was produced where grid cells within the respective catchment retained the respective BCF, and for cells on the boundary, the area-weighted BCFs were estimated. It is noteworthy that applying the resulting BCF map to gridded precipitation data can result in spatial discontinuities of precipitation patterns at the border of the catchments. To reduce such discontinuities, we further applied a 5×5 mean filter to the BCF map. Finally, the corrected precipitation data were used as input to SWAT to run the model with the respective optimum parameters for the simulation period to compute the model performance measures for the hydrological evaluation of precipitation datasets.

2.3.3   Evaluation methods

Evaluation using out-of-bag sample

The prediction accuracy of preliminary daily precipitation data (Pd0) and monthly precipitation data (Pm1) produced by the RF method (see Fig. 2.2) was assessed using the mean absolute error (MAE) and determination coefficient (R^2) based on the out-of-bag sample.

Hydrological evaluation

We evaluated the accuracy of precipitation estimates through hydrological modeling for the three drainage systems in the study area. It is an adequate approach evaluating gauge-corrected precipitation datasets since streamflow observations are independent from ground precipitation observations that are used in these datasets (Beck et al., 2020a; Brocca et al., 2020; Satgé et al., 2020).

For hydrological evaluation, a multicriteria evaluation of SWAT-simulated streamflow using all precipitation products was carried out. For that, both hydrograph goodness of fit metrics and hydrological signatures (Table 2.4) were considered for both calibration and validation periods. The modified Kling–Gupta efficiency (KGE) and percent bias (PBIAS) were used for assessing model skills in representing general discharge dynamics and over or underestimation tendencies, respectively; lNSE and percent bias in FDC low segment volume (S_{low}) for low flows; Nash–Sutcliffe efficiency (NSE) and percent bias in FDC high segment volume (S_{high}) for high flows; and percent bias in FDC peak segment volume (S_{peak}) for extremely peak flow conditions. This multicriteria evaluation aims to assess model skills representing all aspects of the observed FDC and hydrographs, which is important for assessing the reliability of precipitation products for hydrometeorological applications such as the analysis of water budget and hydroclimatic extremes (floods and droughts). The hydrological model performance was ranked based on the rating performance criteria of Moriasi et al. (2007). Thus, for simplicity, the absolute values of PBIAS, S_{low}, S_{high}, and $S_{peak} < 10$ were considered as very good, (10–15) good, (15–25)

Table 2.4: Mathematical formulation of the goodness of fit metrics and hydrological signatures. Here, O and S are observed and simulated flow (m^3/s), respectively; EP is the exceedance probability; P, H, and L are the indices of the minimum flow of the peak flow, high flow, and low flow segments, respectively. In the optimization process for hydrological model calibration, lNSE was maximized, whereas FDC$_{sign}$ was minimized.

Criterion (reference)	Equation	Description
	Discharge-related performance measures	
Nash–Sutcliffe efficiency (Nash and Sutcliffe, 1970)	$\text{NSE} = 1 - \dfrac{\sum_{i=1}^{n}(S_i - O_i)^2}{\sum_{i=1}^{n}(O_i - O_a)^2}$	O_a is the average of the observed flow and n is the number of observations on evaluation
Nash–Sutcliffe efficiency log (Krause et al., 2005)	$\text{lNSE} = 1 - \dfrac{\sum_{i=1}^{n}(\ln(S_i) - \ln(O_i))^2}{\sum_{i=1}^{n}(\ln(O_i) - \ln(O_a))^2}$	
Percent bias (Gupta et al., 1999)	$\text{PBIAS} = \dfrac{\sum_{i=1}^{n}(S_i - O_i)}{\sum_{i=1}^{n} O_i} \times 100$	
Kling–Gupta efficiency (Gupta et al., 2009; Kling et al., 2012)	$\text{KGE} = \sqrt{(r-1)^2 + (\beta - 1)^2 + (\gamma - 1)^2}$	r is the Pearson product-moment correlation coefficient and beta (gamma) indicates the bias (relative dispersion) between observed and simulated flows
	Signature measures	
Percent bias in FDC peak segment volume (Yilmaz et al., 2008)	$S_{\text{peak}} = \dfrac{\sum_{p=1}^{P}(S_p - O_p) \times 100}{\sum_{p=1}^{P} O_P}$	$p = 1, 2, \ldots, P$ are flow indices located within the FDC peak flow segment (EP lower than 2%)
Percent bias in FDC high segment volume (Yilmaz et al., 2008)	$S_{\text{high}} = \dfrac{\sum_{h=1}^{H}(S_h - O_h) \times 100}{\sum_{h=1}^{H} O_h}$	$h = 1, 2, \ldots, H$ are flow indices located within the high flow segment (2%–20% flow EP)
Percent bias in FDC midsegment slope (van Werkhoven et al., 2009; Yilmaz et al., 2008)	$S_{\text{mid}} = \dfrac{((S_{m1} - S_{m2}) - (O_{m1} - O_{m2})) \times 100}{(O_{m1} - O_{m2})}$	$m1$ and $m2$ are the lowest and highest flow EP within the midsegment (20%–70%)
Percent bias in FDC low segment volume (Yilmaz et al., 2008)	$S_{\text{low}} = \dfrac{\sum_{l=1}^{L}(S_l - O_l) \times 100}{\sum_{l=1}^{L} O_l}$	$l = 1, 2, \ldots, L$ are flow indices located within the low flow segment (70%–100% flow EP)
FDC signature (Chilkoti et al., 2018)	$\text{FDC}_{\text{sign}} = \dfrac{1}{4}\left(|S_{\text{peak}}| + |S_{\text{high}}| + |S_{\text{mid}}| + |S_{\text{low}}|\right)$	FDC$_{\text{sign}}$ is the aggregated FDC signature

satisfactory, and ($>$25) unsatisfactory, and KGE, NSE, and lNSE $>$ 0.75 were considered very good, (0.65–0.75) good, (0.50–0.65) satisfactory, and ($<$0.50) unsatisfactory.

Furthermore, in this study, we analyzed the distribution of model parameters and compared the evapotranspiration (ET) simulated by SWAT with remotely sensed ET from Global Land Evaporation Amsterdam Model (GLEAM) and Moderate Resolution Imaging Spectroradiometer Global Evaporation (MOD16). The ET estimates from MOD16 and GLEAM are based on the Penman–Monteith and Priestly–Taylor equations, respectively. This comparison is to verify the plausibility of ET estimates which is one of the largest components of the water budget besides precipitation and difficult to estimate over complex terrain. Results of the analysis of parameter distribution and ET estimates are described in appendices 2.A.2 and 2.A.3.
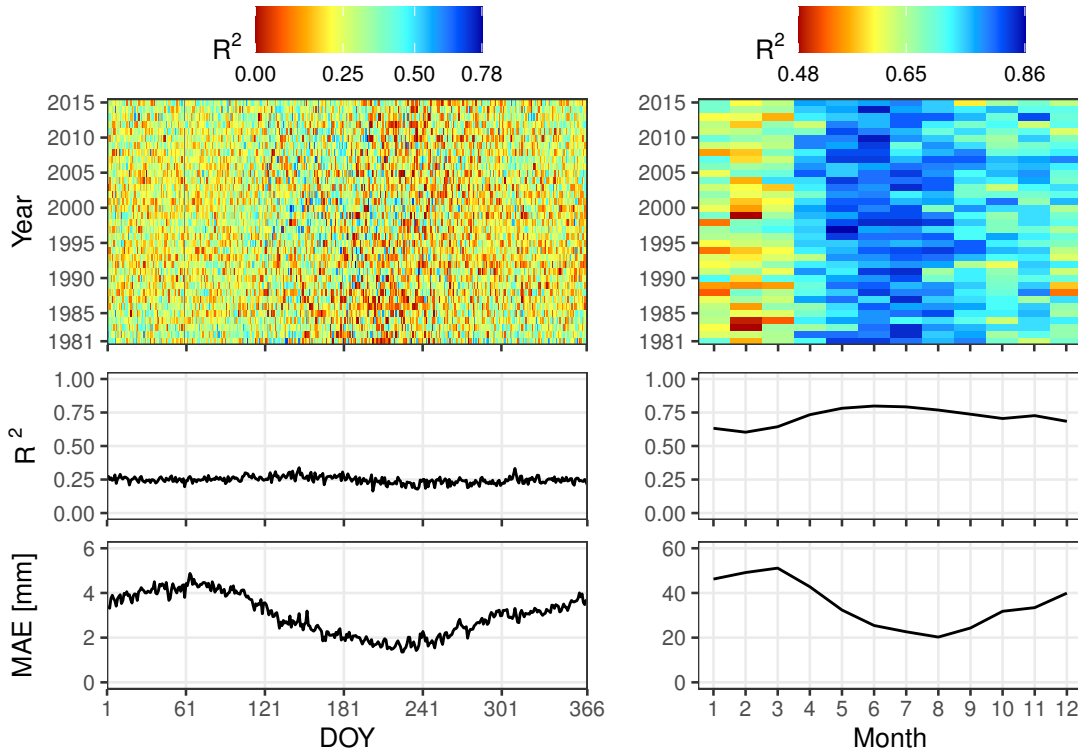
Figure 2.3: Performance of the random forest algorithm for spatial interpolation of (left) daily and (right) monthly precipitations. Here, R^2 is the coefficient of determination, and MAE is the mean absolute error. The middle and bottom graphs show the performance measures averaged for each day or month in the 1981–2015 period.

2.4 Results

2.4.1 Performance of the merging algorithm

The skill of the RF method for predicting daily and monthly precipitation patterns was evaluated using performance measures (R^2 and MAE) based on the out-of-bag sample. Figure 2.3 shows that based on the temporal distribution of R^2, the RF performance does not have a seasonal pattern for the daily precipitation prediction, whereas it exhibits better performance in the period from April to December for monthly prediction. Furthermore, R^2 shows that prediction is better for the monthly (mean R^2 = 0.72) than the daily (mean R^2 = 0.25) precipitation. This result supports the correction of daily-predicted precipitation values to match the monthly predictions performed in our study as described in the methods. MAE is much lower in the period June–September for both daily and monthly precipitation prediction, indicating that precipitation is more easily predictable when most of the study area experiences lower precipitation during the dry season. It is important to mention that satellite precipitation (CHIRP) was often the most important covariate in the merging procedure both at daily and monthly scale, followed by reanalysis precipitation (ERA5) and terrain elevation, while buffer distances were negligible (Fig. 2.13).

2.4.2 Hydrological correction of the gridded precipitation datasets

The spatial variation of the obtained bias correction factors (BCFs) for six precipitation datasets is shown in Fig. 2.4. This differs from the method of Strauch et al. (2017), who applied a unique correction factor to WFDEI (Weedon et al., 2014) dataset for all montane regions. The lower values of BCFs for ERA5 are related to significant precipitation overestimation along the Andes by ERA5 (Figs. 2.5 and 2.6). The results for the other datasets (Fig. 2.4) show that higher BCFs were the result for MSWEP (mean BCF = 1.66) and lower for RAIN4PE (mean BCF = 1.38). For a BCF of 1.38, on average, 28% of total precipitation is the precipitation underpredicted
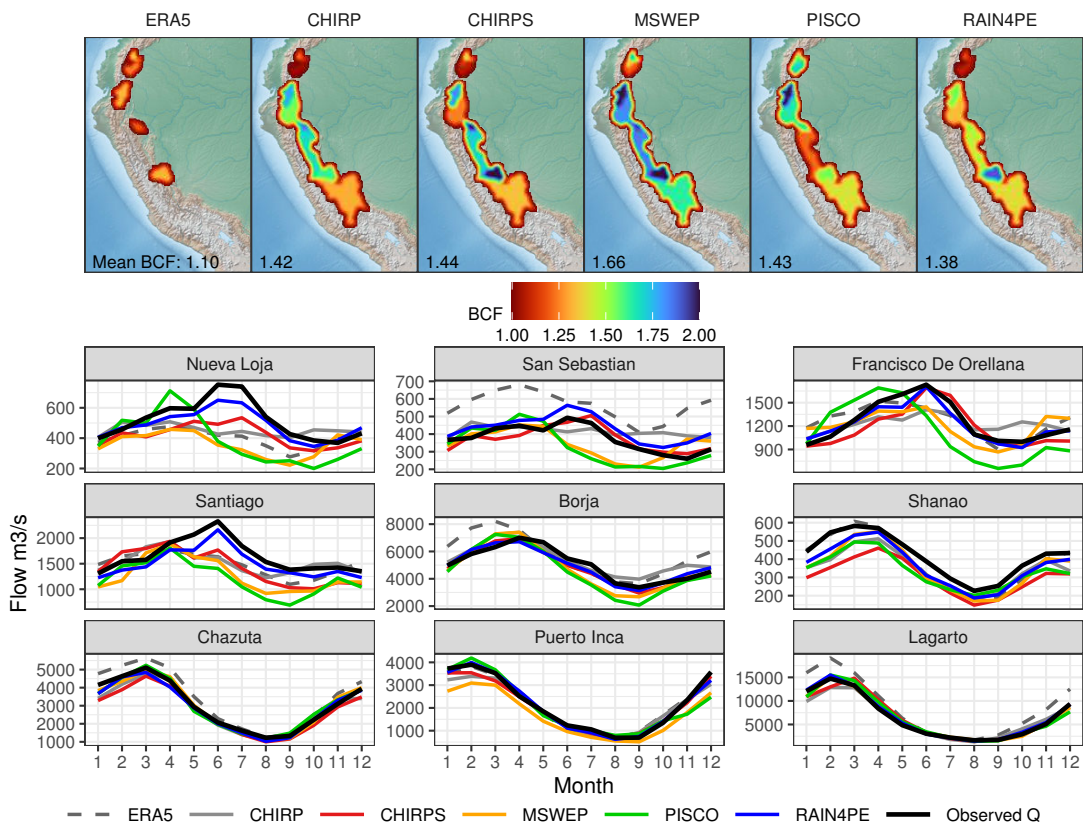
Figure 2.4: (top) Bias correction factors (BCFs) for six precipitation datasets and (bottom) long-term mean seasonal streamflow (Q) dynamics in the period 1983–2015 after SWAT model calibration over nine catchments with underestimation of precipitation amounts in comparison with the observed mean seasonal discharge. The mean BCF was computed using the catchment areas as weights. Note that both observed and seasonal streamflow were computed only for the months with available streamflow data.

in páramo and montane watersheds in the study area which falls in the range (0%–30%) of cloud/fog water contribution to total precipitation reported in previous studies of the region (Cárdenas et al., 2017; Gomez-Peralta et al., 2008). Figure 2.4 also shows that significant benefits of precipitation correction made for RAIN4PE are obvious in a good representation of streamflow seasonality for all nine catchments. The correction of CHIRPS also works relatively well in most of the catchments in terms of seasonal streamflow prediction, although it fails over the southern Ecuadorian Amazon (at Santiago station). The hydrological correction of the other datasets (CHIRP, ERA5, MSWEP, and PISCO) performs well for southern catchments (from Borja to Lagarto station) but not in Ecuadorian catchments (from Nueva Loja to Santiago station) since the streamflow seasonality change is underestimated, indicating a serious drawback of these datasets.

2.4.3 Spatial patterns of precipitation

In general, the spatial variability of the long-term average annual precipitation (1981–2015) portrayed by all precipitation datasets looks quite similar (Fig. 2.5), although PISCO shows distinct precipitation patterns and magnitudes in the rain forest regions. Figure 2.5 also shows the spatial patterns of the estimated precipitation underestimates for each precipitation dataset. As can be seen, these patterns look quite similar over the Peruvian Amazon for five datasets (CHIRP, CHIRPS, MSWEP, PISCO, and RAIN4PE) but vary over the northern Amazon basin in Ecuador. The substantial precipitation underestimation (ranging from 0 to 3369 mm, Fig. 2.5)
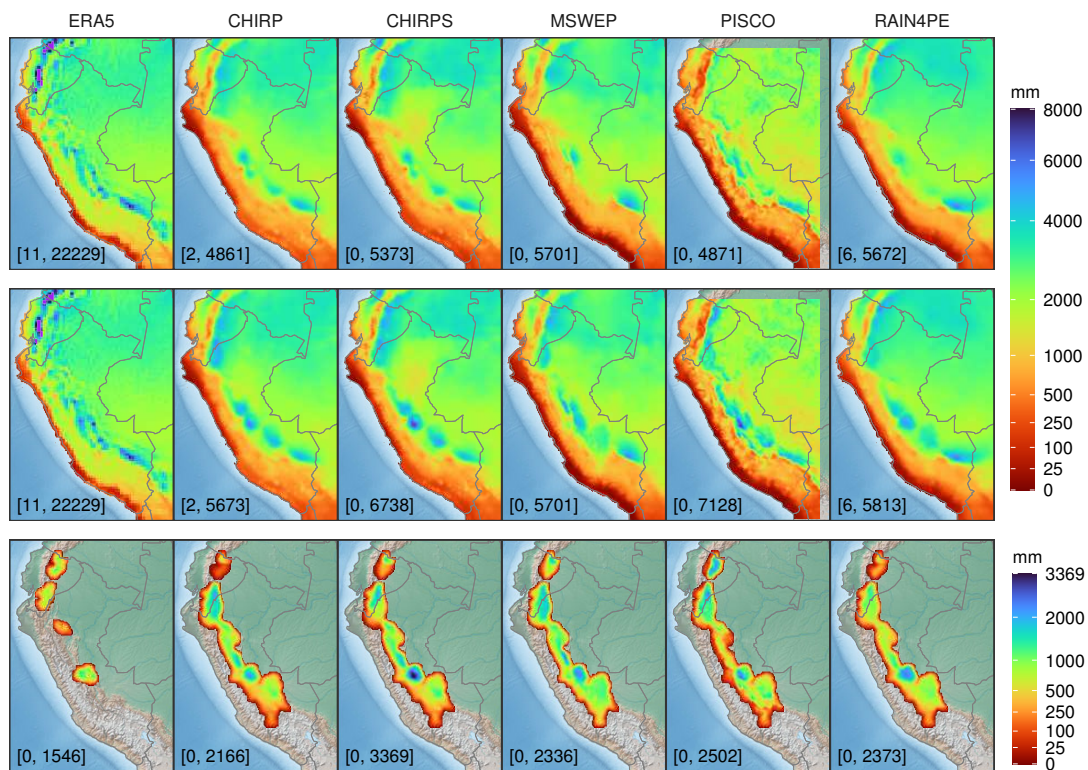
Figure 2.5: The spatial patterns of average annual precipitation for the period 1981–2015 based on (top) raw and (middle) hydrologically adjusted precipitation data of ERA5, CHIRP, CHIRPS, MSWEP, PISCO, and RAIN4PE. (bottom) The underestimated precipitation fields for each precipitation dataset. The numbers in brackets represent the precipitation ranges. In the case of ERA5, precipitation values exceeding 8000 mm are in purple (distributed over the Ecuadorian Andes mainly).

found here suggests that precipitation correction was necessary to achieve the closure of the water budget and appropriate hydrological modeling of the páramo and montane watersheds.

In addition, a comparison of the unadjusted precipitation data with gauge observation was done (Fig. 2.6) to assess precipitation datasets' reliability or critical shortcomings. It shows that ERA5 overestimates precipitation significantly over the Andes. CHIRP, CHIRPS, MSWEP, and PISCO (CHIRP and CHIRPS) underestimate (overestimate) precipitation over the northern (arid southern) Pacific coastal areas. Furthermore, ERA5, CHIRP, CHIRPS, MSWEP, and PISCO have inconsistent temporal distribution of precipitation over the northern Amazon, which is confirmed by low values of correlation and determination coefficients that result from comparing these products with gauge observations at a monthly scale (Fig. 2.6) and SWAT-simulated seasonal streamflow using these datasets (Fig. 2.4). Therefore, these datasets are less suitable for characterizing spatiotemporal variability of precipitation over the Ecuadorian Amazon than RAIN4PE. However, it should be kept in mind that the comparison measures in Fig. 2.6 could be biased toward datasets (CHIRPS, MSWEP, PISCO, and RAIN4PE) that used data from the assimilated precipitation gauges in their production (see Table 2.1).

2.4.4 Hydrological evaluation

In this section, we evaluate the performance of the SWAT model driven by the hydrologically adjusted CHIRP (CHIRP-SWAT), ERA5 (ERA5-SWAT), CHIRPS (CHIRPS-SWAT), MSWEP (MSWEP-SWAT), PISCO (PISCO-SWAT), and RAIN4PE (RAIN4PE-SWAT) for calibration and validation periods. For that, we used multiple performance measures to assess the model skills in representing discharge dynamics including all flow conditions (low, high, and peak flows). It
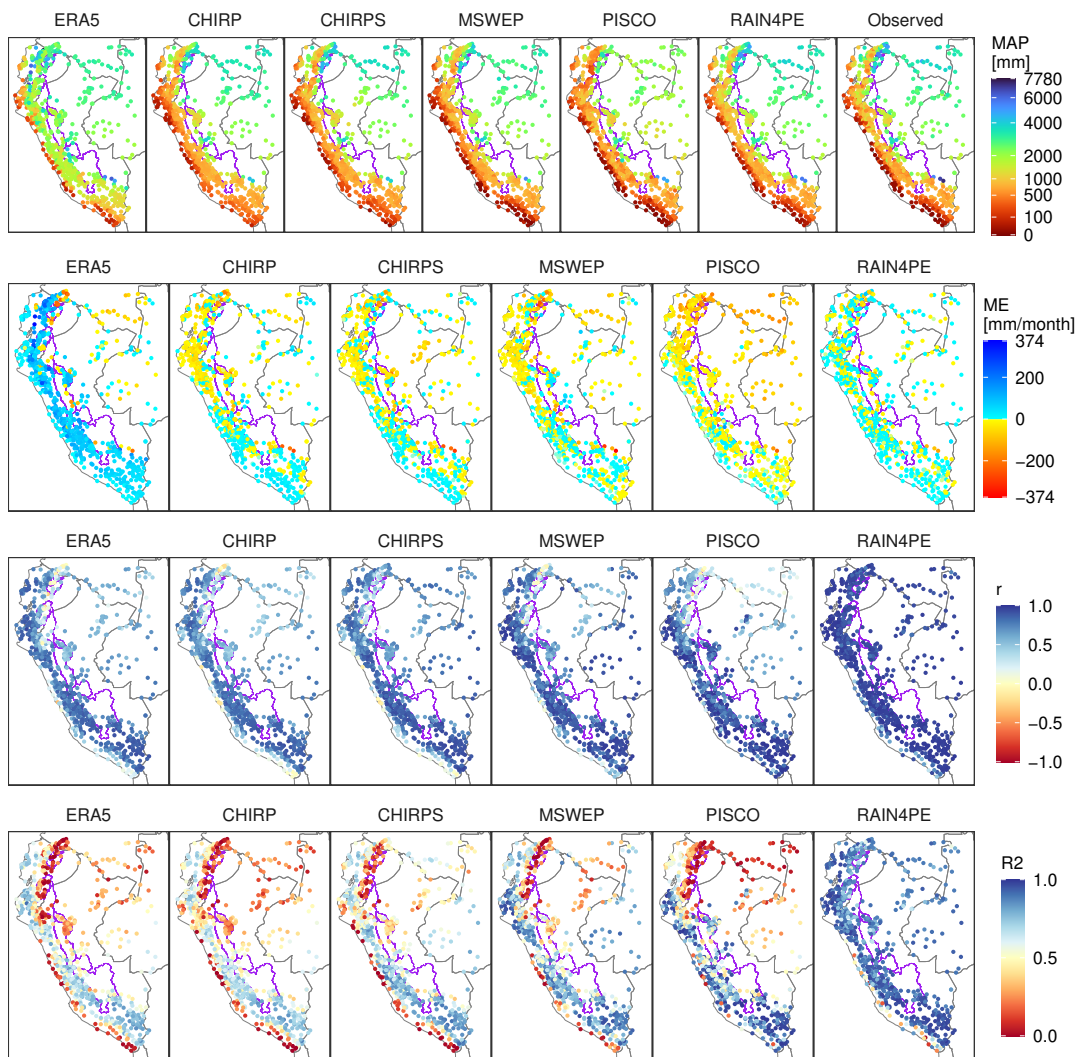
Figure 2.6: Performance of the unadjusted precipitation datasets in comparison with gauge observations: MAP is the mean annual precipitation, ME is the mean error, *r* is the Pearson's correlation coefficient, and R^2 is the coefficient of determination. The comparison measures (ME, *r*, and R^2) were computed using monthly precipitation time series for 1981–2015.

is important to mention that temporal mismatches in the daily precipitation accumulation may influence the model performance at the daily scale since CHIRP, CHIRPS, and MSWEP were delivered using different daily time window aggregation than the local one (from 0700 to 0700 local time). Furthermore, our analyses are based on the results of the only one hydrological model, SWAT, and the application of other hydrological models could be done in future to verify and refine the obtained results.

Performance evaluation for daily streamflow and extremes

We investigated the spatial variability of hydrological model performance for streamflow simulation forced by six precipitation products in calibration (Fig. 2.7, Table 2.6) and validation (Fig. 2.14, Table 2.7) periods. These figures present the Kling–Gupta efficiency spatial distribution and show results in terms of seven criteria for all streamflow stations and catchments draining into the Titicaca Lake, the Pacific Ocean, and the Amazon River as boxplots. Table 2.5 shows each criterion's median values for each drainage system and precipitation product for the simulation period (1981–2015). The results described in this section are based on the outputs
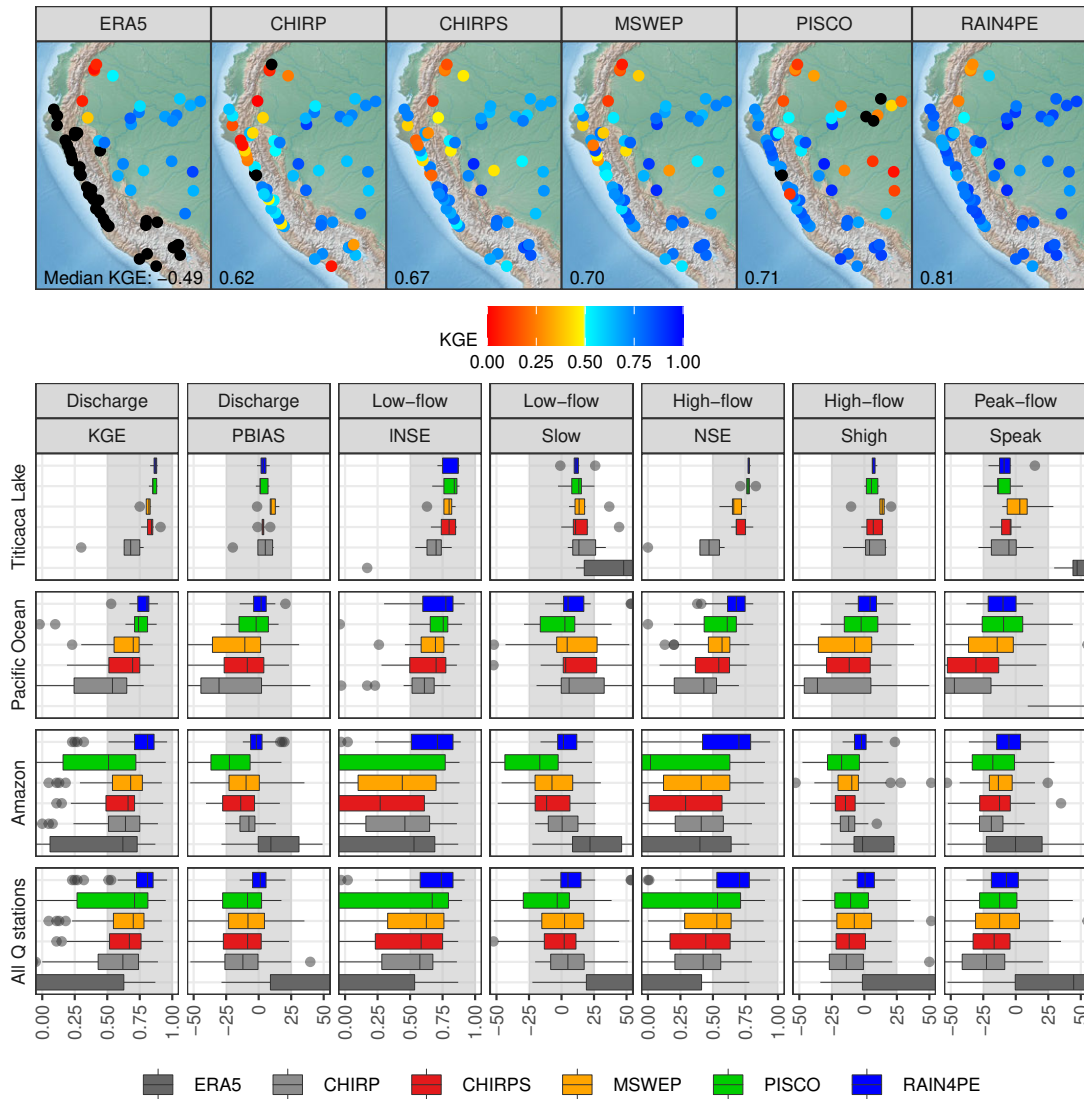
Figure 2.7: Hydrological model performance metrics for daily streamflow simulations by SWAT driven by six precipitation datasets in the calibration period: (top) spatial patterns of KGE and (bottom) boxplots showing seven criteria for all streamflow (Q) stations and stations located in catchments draining into the Amazon River, Pacific Ocean, and Titicaca Lake. The datasets are sorted in ascending order of the median KGE for all Q stations. Values exceeding 0.5 (between ±25%) for KGE, lNSE, and NSE (PBIAS, S_{low}, S_{high}, and S_{peak}) are considered skillful (marked by light gray background in boxplots). Black points in the upper part represent negative values of KGE. Note that the x axis starts at 0 for KGE, NSE, and lNSE to improve visualization, whereas PBIAS, S_{low}, S_{high}, and S_{peak} were constrained between ±50%.

for calibration period (Fig. 2.7) but they are also valid for the validation period (Fig. 2.14), as results for both periods are similar.

Results for catchments draining into Titicaca Lake show that SWAT driven by gauge-corrected precipitation datasets performs satisfactorily to very good for daily streamflow simulation (median KGE $\geq$ 0.79), including all flow conditions. The good performance of MSWEP and CHIRPS for hydrological modeling in the Titicaca Lake basin shown here coheres with the performance demonstrated in Satgé et al. (2020, 2019). However, RAIN4PE (median KGE = 0.86) was shown in our simulation to be the best choice for this drainage system. Regarding

Table 2.5: Median values of each performance measure for daily streamflow simulation for the period 1983–2015 (without the spinup period). Values in bold denote the best performing product in each drainage system and the study area according to the specific score on the left.

Basin	Product	KGE	NSE	INSE	|PBIAS|	|Slow|	|Shigh|	|Speak|
Titicaca Lake	ERA5	−1.1	−3.04	−0.07	205.9	47.8	197.5	44.5
Titicaca Lake	CHIRP	0.62	0.29	0.67	17.5	31.4	18.2	**7.2**
Titicaca Lake	CHIRPS	0.81	0.64	0.76	**6.1**	16	9	7.3
Titicaca Lake	MSWEP	0.79	0.67	0.8	14.6	20	15.2	8.8
Titicaca Lake	PISCO	0.84	0.74	0.82	7.2	18.5	7.6	13.9
Titicaca Lake	RAIN4PE	**0.86**	**0.77**	**0.86**	6.8	**14.3**	**6.7**	14.1
Pacific	ERA5	−2.29	−7.2	−1.47	325.6	238	293.9	117.9
Pacific	CHIRP	0.55	0.44	0.62	28.9	14.1	35.8	43.5
Pacific	CHIRPS	0.66	0.5	0.66	15.2	11.1	12.1	18.7
Pacific	MSWEP	0.68	0.55	0.66	17.4	14.8	21	27.5
Pacific	PISCO	0.74	0.57	0.73	10.2	11.4	10.7	17.3
Pacific	RAIN4PE	**0.78**	**0.67**	**0.74**	**5.2**	**6**	**7.5**	**7.7**
Amazon	ERA5	0.63	0.46	0.6	12.5	19.5	17.2	18.8
Amazon	CHIRP	0.63	0.4	0.45	7.7	12	9.6	12.6
Amazon	CHIRPS	0.67	0.31	0.38	13.7	15.3	14.5	14.6
Amazon	MSWEP	0.69	0.47	0.48	15.4	15.2	11.8	12.2
Amazon	PISCO	0.49	0	−0.11	21.9	23.9	18	18.9
Amazon	RAIN4PE	**0.8**	**0.7**	**0.73**	**6.2**	**10.8**	**7.3**	**10.7**
All watersheds	ERA5	−0.58	−2.26	−0.3	148.4	55	115.1	44.2
All watersheds	CHIRP	0.58	0.43	0.57	13.2	13.9	16.3	21.4
All watersheds	CHIRPS	0.67	0.41	0.58	13.6	15	13	15.8
All watersheds	MSWEP	0.7	0.53	0.63	15.3	16.5	15.2	15.1
All watersheds	PISCO	0.7	0.51	0.66	12.8	18.6	12.7	17.7
All watersheds	RAIN4PE	**0.8**	**0.7**	**0.74**	**5.9**	**9.7**	**7.3**	**9.6**

two non-gauge-corrected datasets, CHIRP-SWAT has unsatisfactory performances for high-flow dynamics, and ERA5-SWAT significantly overestimates streamflow (Fig. 2.16).

In the Pacific basin, CHIRPS-SWAT, MSWEP-SWAT, and even PISCO-SWAT have low KGE ($\leq$0.5), high biases, and poor performance for high and peak flows for some stations. The outcome for MSWEP and PISCO aligns with the findings of previous studies (Asurza-Véliz and Lavado-Casimiro, 2020; Bhuiyan et al., 2019; Derin et al., 2019). CHIRP-SWAT has more skill than ERA5-SWAT, which shows a significant overestimation of streamflow; however, they both are outperformed by the gauge-corrected precipitation datasets. The overall good performance of RAIN4PE-SWAT (median KGE = 0.78) allowed us to conclude that RAIN4PE is the most suitable precipitation product for daily streamflow simulation (including all flow conditions and water budget closure) in the catchments draining into the Pacific Ocean.

In the Amazon basin, among the six precipitation products driving SWAT, RAIN4PE (median KGE = 0.80) provided the best performance measures for daily streamflow simulation (including all flow conditions). PISCO (median KGE = 0.49) provided the worse measures, particularly over the lower Amazon catchments which is consistent with previous studies (Aybar et al., 2020; Llauca et al., 2021). Despite the fact that median KGE ($>$0.5) is satisfactory for CHIRP, CHIRPS, ERA5, and MSWEP, the other measures such as the INSE and NSE show that they tend to perform unsatisfactorily for the simulation of low- and high-flow dynamics. However, KGE patterns (Fig. 2.7) show unsatisfactory scores over the Ecuadorian Amazon catchments, showing the limitations of all products (including RAIN4PE) in portraying the actual daily precipitation variability there.

In general, SWAT performance for all streamflow stations (Fig. 2.7 and Fig. 2.14 and Table 2.5, Tables 2.6 and 2.7) suggests that RAIN4PE (e.g., median KGE = 0.80) is the most appropriate product for daily streamflow simulation, including all flow conditions in the study area.
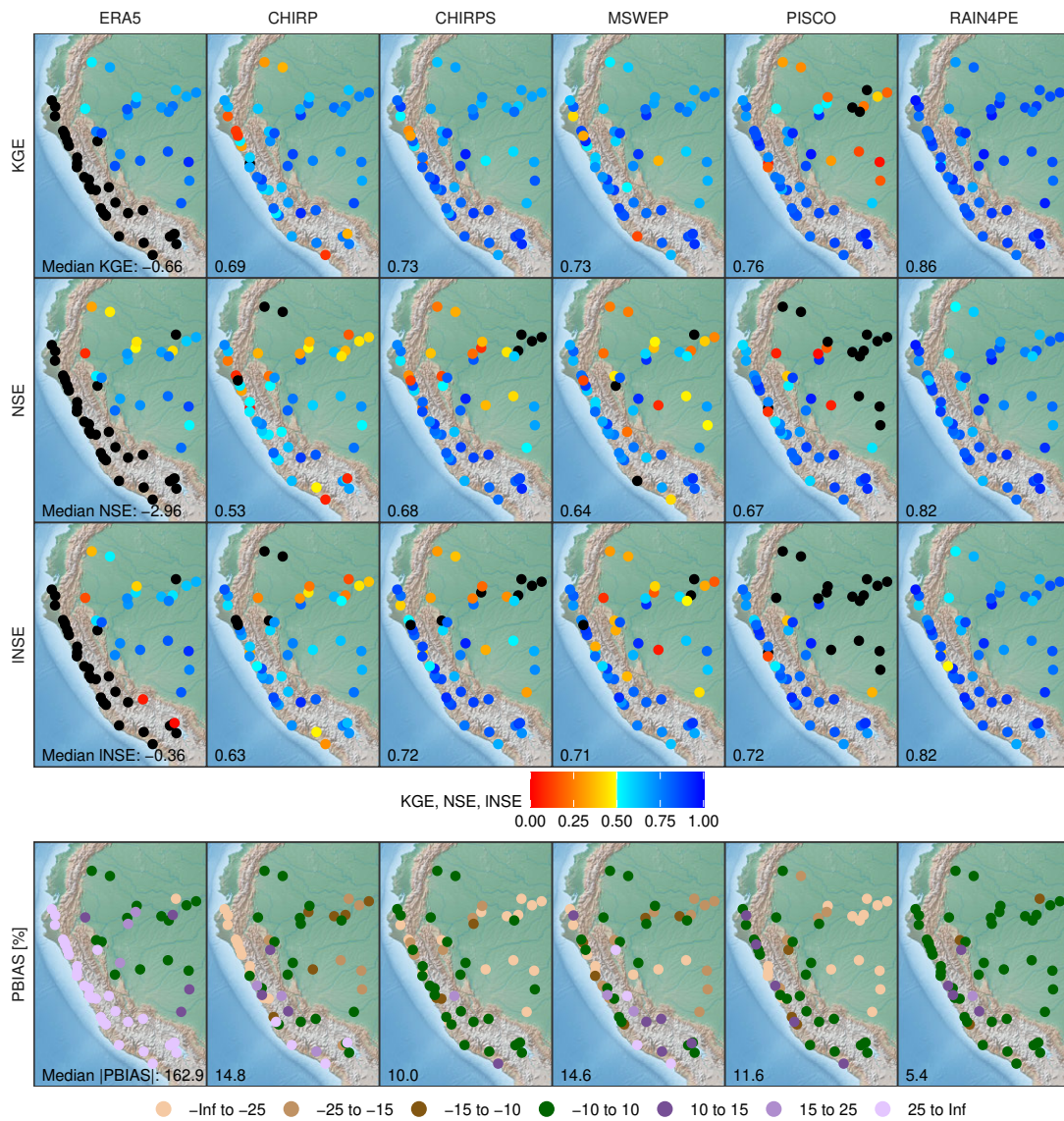
Figure 2.8: Hydrological model performance metrics KGE, NSE, lNSE, and PBIAS for monthly streamflow simulations by SWAT driven by six precipitation datasets in the validation period. Black points represent negative values of KGE, NSE, and lNSE.

Performance evaluation for monthly streamflow

Fig. 2.8 and Fig. 2.15 display the spatial distribution of KGE, NSE, lNSE, and PBIAS to assess the SWAT model skill for the monthly streamflow simulation in the calibration and validation periods. These figures show that results in both periods are quite similar, although the overall performance of PISCO-SWAT and MSWEP-SWAT is a bit lower in the validation period. Based on results of model performance in the validation period (Fig. 2.8), among the six precipitation products driving SWAT, overall RAIN4PE (median KGE = 0.86, NSE = 0.82, lNSE = 0.82, and |PBIAS| = 5.4%) provided the best performance measures for monthly streamflow simulation in all evaluated catchments. Despite the median KGE, NSE, and lNSE were satisfactory (>0.5, Fig. 2.8) for CHIRP, CHIRPS, MSWEP, and PISCO, the spatial patterns of these measures show the limitation (e.g., NSE < 0.5) of these products for hydrological modeling over the Ecuadorian Amazon, lower Amazon, and some catchments draining into the Pacific Ocean, which is in agreement with the results for the daily outputs. Otherwise, ERA5-SWAT was found to perform unsatisfactorily for Andean basins, although its performance improved for larger

catchments in the Amazon basin. The overall very good performance in accordance with criteria by Moriasi et al. (2007) obtained by RAIN4PE-SWAT highlights the increased utility of RAIN4PE for countrywide hydrometeorological applications in Peru and Ecuador.

2.5 Discussion

2.5.1 Advantages of the merging methodology

This study demonstrates a successful method for merging multiple precipitation sources (based on gauge, satellite, and reanalysis data) with surface elevation using the RF method to generate a spatially gridded precipitation dataset RAIN4PE. This is supported by the significant improvement of RAIN4PE for hydrological simulations compared to the non-gauge-corrected datasets (CHIRP and ERA5) used for the merging procedure. Furthermore, the superiority of RAIN4PE regarding the gauge-corrected datasets (CHIRPS, MSWEP, and PISCO) for hydrological simulations suggests that the methodology applied herein to generate RAIN4PE is much more robust than that of the other merged precipitation products. This means that the RF method is more effective in merging multiple precipitation data sources than deterministic and geostatistical interpolation methods (Aybar et al., 2020; Funk et al., 2015a) and merging approaches that use weights for each source (Beck et al., 2017, 2019b). Compared to the aforementioned merging approaches, RF has the flexibility to include multiple precipitation sources and environmental variables (e.g., surface elevation) that explain precipitation patterns. Besides this advantage, RF can capture nonlinear dependencies and interactions of variables, such as the nonlinear interactions among the precipitation and terrain elevation due to the complex Andes morphology (Figs. 2.1 and 2.5, Chavez and Takahashi, 2017), which could be challenging to model using geostatistical techniques. However, it is important to keep in mind the RF limitation for predicting value beyond the range in the training data (Hengl et al., 2018). Overall, the results of our study provide a reference for merging multisource precipitation data and environmental variables using RF in complex data-scarce regions.

2.5.2 Hydrological correction of the gridded precipitation datasets

The high BCF values (Fig. 2.4) obtained to correct gridded precipitation biases make evident that most of the datasets evaluated (CHIRP, CHIRPS, MSWEP, PISCO, and RAIN4PE) often have precipitation underestimation over the páramo and montane watersheds in the Amazon (Fig. 2.5). This underestimation, especially by gauge-corrected datasets, could be caused by the low number of precipitation gauges available (Fig. 2.1), which is further amplified by the fact that the gauges do not account for the important cloud/fog water input into the system (Cárdenas et al., 2017; Clark et al., 2014; Gomez-Peralta et al., 2008).

A substantial precipitation underestimation over the páramo and montane watersheds is critical since it might even lead to physically unrealistic runoff ratios above 1 in water budget estimates as reported in previous studies (Aybar et al., 2020; Builes-Jaramillo and Poveda, 2018; Manz et al., 2016; Strauch et al., 2017; Zubieta et al., 2015; Zulkafli et al., 2014). Furthermore, precipitation errors in the upstream catchments can negatively affect simulation results for downstream river catchments. For instance, the assignment of unrealistic model parameter values to counterbalance precipitation uncertainty can lead to misrepresentation of the basinwide water budget (see more details in appendix 2.A.2). To overcome these deficiencies, we used streamflow data to adjust precipitation biases.

Our results show that the hydrological correction of precipitation datasets was more efficient over the regions with the strongest rainfall seasonality such as the Peruvian catchments (Espinoza Villar et al., 2009b; Segura et al., 2019). This suggests that actual spatiotemporal precipitation fields over these regions are well depicted by the assessed datasets, whereas the correction efficiency over the Ecuadorian Amazon catchments, which experience precipitation throughout the year with high spatial regime variability (Laraque et al., 2007; Tobar and Wyseure, 2018), is more variable and depends more strongly on the precipitation product. For instance, the correction was not feasible for CHIRP, ERA5, MSWEP, PISCO, and even CHIRPS (at southern Ecuadorian Amazon) which led to the underrepresentation of the seasonal streamflow patterns and hence the true seasonal precipitation patterns as well (Figs. 2.4 and 2.6). This is a

critical drawback of these products, and our findings here could be helpful for their revision and improvement. Even though the hydrological correction of CHIRPS resulted in the improvement of the seasonal streamflow simulations for the northern Ecuadorian Amazon, CHIRPS-SWAT still performed unsatisfactorily for the daily and monthly discharge dynamics (Figs. 2.7, 2.8 and Figs. 2.14 and 2.15), indicating that CHIRPS does not represent well the actual precipitation patterns over the Ecuadorian Amazon catchments. In these catchments, other datasets such as gauge-based ORE HYBAM (Guimberteau et al., 2012), gauge-corrected WFDEI, reanalysis ERA-Interim, and satellite-based PERSIANN (Hsu et al., 1997), TMPA, CMORPH, and IMERG have also been reported to perform unsatisfactorily for streamflow simulation (Strauch et al., 2017; Towner et al., 2019; Zubieta et al., 2015, 2017; Zulkafli et al., 2014). Overall, when comparing RAIN4PE to CHIRP, ERA5, MSWEP, PISCO, CHIRPS, and other datasets mentioned above, we can see that it shows satisfactory performance for monthly (Fig. 2.8) and seasonal (Fig. 2.4) streamflow simulations with SWAT over the Ecuadorian Amazon. However, its performance for daily simulation is still unsatisfactory (Fig. 2.7), which highlights that estimation of precipitation at a daily resolution over data-scarce regions such as the equatorial Amazon region is very challenging. The exposed shortcomings of precipitation datasets suggest the urgent implementation and densification of precipitation and cloud/fog gauge networks over the Ecuadorian Amazon and Peruvian montane watersheds. These could help to improve the depiction of rainfall amounts and their spatiotemporal distribution and hence could be useful for improving streamflow simulations. It is important to keep in mind that the correction of the proposed precipitation product through the reverse hydrology concept was performed using the SWAT hydrological model, and therefore the performance of the RAIN4PE dataset may change if another hydrological model is used. Though, as SWAT is a widely used comprehensively verified model, we expect only minor deviation.

2.5.3   Implications for hydrological modeling

The results of the hydrological evaluation clearly show the advantages and shortcomings of each evaluated precipitation dataset for streamflow simulation, including low, high, and peak flows. Moreover, we presented the comparison of SWAT-simulated seasonal streamflow using all evaluated datasets against observed seasonal streamflow for the three drainage systems (Titicaca Lake basin, Pacific basin, and Amazon basin) in Figs. 2.16–2.18. These figures can assist practitioners in selecting the appropriate precipitation product for hydrological applications. In general, the hydrological evaluation highlighted RAIN4PE as the best precipitation dataset for hydrological modeling of the Peruvian and Ecuadorian watersheds. RAIN4PE is the only gridded precipitation product for Peru and Ecuador, which benefits from maximum available in situ observations, multiple precipitation sources, environmental variable (elevation data), and is supplemented by streamflow data to correct the precipitation underestimation over páramos and montane catchments. The exploitation of all these variables using state-of-the-practice methods to generate RAIN4PE proved that RAIN4PE-SWAT was capable of closing the (hitherto) observed water budget imbalance over Peruvian and Ecuadorian catchments which, eventually, makes the RAIN4PE a good candidate for hydrological applications in the region. Despite this, we consider that RAIN4PE is still subject to uncertainties, especially in regions where precipitation was inferred from the observed streamflow data. For these regions, precipitation estimates should be viewed with some care due to uncertainties in streamflow data, inferred evapotranspiration, gridded precipitation data, and hydrological model structure.

In this study, besides evaluating precipitation datasets for streamflow simulation, we show that uncertainties associated with precipitation estimates have implications in estimating hydrological model parameters (see appendix 2.A.2) and water budget components (e.g., evapotranspiration, see appendix 2.A.3). This is critical for the regionalization of parameters and reliable estimation of the water budget for water resources management. Furthermore, an aftermath verification of RAIN4PE-SWAT-simulated evapotranspiration with GLEAM and MOD16 estimates (appendix 2.A.3) shows that GLEAM and MOD16 return higher estimated values of evapotranspiration which would not allow the water budget closure and bring inconsistencies in the temporal evapotranspiration distribution over northern Amazon in Ecuador. This suggests that evapotranspiration estimation is still a challenge for remotely sensed based evapotranspiration products in the region.

It is important to highlight that this study is the first applying SWAT updated for improved representation of tropical vegetation dynamics (Alemayehu et al., 2017) and river–floodplain dynamics. These improvements are crucial to model the hydrological processes of Andean and Amazonian river catchments appropriately. The benefits of appropriate representation of tropical vegetation dynamics were demonstrated in previous studies (Alemayehu et al., 2017; Fernandez-Palomino et al., 2020; Strauch and Volk, 2013), while the benefit of flow water routing that considers river–floodplain dynamics can be observed in the good representation of discharge dynamics of the Amazonian rivers in this study. For instance, in the Ucayali River (a tributary of the Amazon River), the significant observed flood peak delay (on a scale of months) from Lagarto to Requena station is well reproduced by SWAT (see Fig. 2.18), which is consistent with the findings of Santini (2020).

It is also important to highlight that this study is the first applying SWAT at the country-level of Peru and performing a multiobjective calibration and validation using hydrograph goodness of fit and FDC signatures for large-domain modeling (1.6 million km^2) in a region with complex hydroclimatic conditions. Our results show the robustness of signature-based calibration guiding the model to reproduce not only one common objective function (e.g., high flows given by NSE) but all aspects of the hydrograph and FDC as supported by RAIN4PE-SWAT good performances reproducing all flow conditions. This is crucial for robust hydrometeorological applications including extremes such as droughts and floods as well as for the assessment of precipitation dataset reliability. Furthermore, our results reinforce previous study findings (Chilkoti et al., 2018; Fernandez-Palomino et al., 2020; Shafii and Tolson, 2015), which proved the robustness of a signature-based calibration approach in the hydrological modeling of small watersheds. We consider that our approaches can be helpful for future studies related to precipitation estimates as well as to hydrological model calibration, evaluation, and application.

2.5.4 Future development and application

Based on the experiences we gained, our future investigations will focus on applying RAIN4PE-SWAT to analyze the water budget at the national scale of Peru, as well as climate change impacts on water resources using RAIN4PE as the basis for bias adjustment, and trends in frequency and intensity of meteorological and hydrological droughts. The current RAIN4PE data availability (1981–2015) is planned to be extended in the future. Moreover, the methodology presented in the paper will also be extended to the entire Amazon basin.

2.6 Summary and conclusions

We developed a new hydrologically adjusted daily precipitation dataset (1981–2015, 0.1° resolution) called RAIN4PE by merging three existing datasets for a domain covering Peru and Ecuador. This dataset takes advantages of ground-, satellite-, and reanalysis-based precipitation datasets, including CHIRP and ERA5, which are merged with terrain elevation using the random forest (RF) method to provide precipitation estimates. Furthermore, streamflow data was used to correct precipitation estimates over catchments with water budget closure problems (e.g., the páramo and montane watersheds) through the reverse hydrology methods, for which the SWAT model was applied for the first time herein. Moreover, a comprehensive hydrological evaluation of RAIN4PE, CHIRP, ERA5, and the existing state-of-the-art gauge-corrected precipitation datasets—CHIRPS, MSWEP, and PISCO—in the Peruvian and Ecuadorian river catchments using a range of performance metrics was performed. For that, SWAT was calibrated and validated with each precipitation dataset in a number of catchments. We summarize our findings as follows.

- The good RAIN4PE-SWAT performance for streamflow simulation suggests the effectiveness of the RF method to merge multisource precipitation estimates with terrain elevation to develop a reliable spatially gridded precipitation dataset. As all datasets (CHIRP, ERA5, and terrain elevation) used to develop RAIN4PE are freely available, this approach can be used in other data-scarce regions.
- The utility of streamflow data to improve both precipitation and streamflow simulations over the páramo and montane watersheds with precipitation underestimation was demonstrated

herein. This highlights that the reverse hydrology approach offers a new effective way of understanding the hydrological processes of the Andean–Amazon catchments, which have a key role in the hydrological variability of the entire Amazon basin.

- The hydrological evaluation results from uncorrected precipitation datasets forcing SWAT for streamflow simulation revealed that CHIRP outperformed ERA5, which significantly overestimate precipitation along the Andes. However, these products were outperformed by the gauge-based precipitation datasets.
- Among the gauge-corrected precipitation datasets forcing SWAT for streamflow simulation, all products performed well in the catchments draining into the Titicaca Lake. For catchments draining into the Pacific Ocean and Amazon River, CHIRPS, MSWEP, and PISCO performed unsatisfactorily in several catchments, indicating the limitations of these products for hydrological modeling over these drainage systems. In contrast, RAIN4PE was the only product that provided consistently good performance for the daily and monthly streamflow simulations, including all discharge conditions (low, high, and peak flows) and water budget closure in almost all Peruvian and Ecuadorian river catchments.
- We found that CHIRP, CHIRPS, ERA5, MSWEP, and PISCO cannot represent the seasonal distribution of precipitation and hence the seasonal streamflow over the Ecuadorian Amazon. This is a critical drawback that can have implications in hydrometeorological applications in the Amazon basin.
- We found that uncertainties in precipitation data in existing datasets affect the estimation of model parameters and water budget components, suggesting the importance of developing high-quality meteorological forcing datasets in mountainous regions. Our contribution is in line with this and marks progress in developing precipitation datasets in the region.

The overall good performance of the RAIN4PE highlights its utility as an important new gridded precipitation dataset, which opens new possibilities for numerous hydrometeorological applications throughout Peru and Ecuador. Examples are streamflow simulations, estimation of the water budget and its evolution, water resources management, understanding spatiotemporal variations of droughts and floods, and exploring spatial variations and regimes of precipitation. We consider that RAIN4PE and our RAIN4PE-SWAT model can be adopted as a benchmark to evaluate precipitation datasets in Peru and Ecuador.

Acknowledgments

Data availability statement

The RAIN4PE data record is freely available at `https://doi.org/10.5880/pik.2020.010` (Fernandez-Palomino et al., 2021).

This paper was edited by Dr. Viviana Maggioni and reviewed by Dr. Liz Stephens, Dr. Oscar M. Baez-Villanueva and an anonymous referee.

2.A Appendix

2.A.1 Glossary

CHIRP: Climate Hazards Group InfraRed Precipitation
CHIRPS: CHIRP with Station data
CMORPH: Climate Prediction Center morphing technique
IMERG: Global Precipitation Measurement (GPM) Integrated Multi-satellite Retrievals
MSWEP: Multi-Source Weighted-Ensemble Precipitation
SENAMHI: Servicio Nacional de Meteorología e Hidrología del Perú
PISCO: Peruvian Interpolated data of SENAMHI's Climatological and Hydrological Observations
TMPA: Tropical Rainfall Measuring Mission (TRMM) Multisatellite Precipitation Analysis
WFDEI: WATCH Forcing Data methodology applied to ERA-Interim data
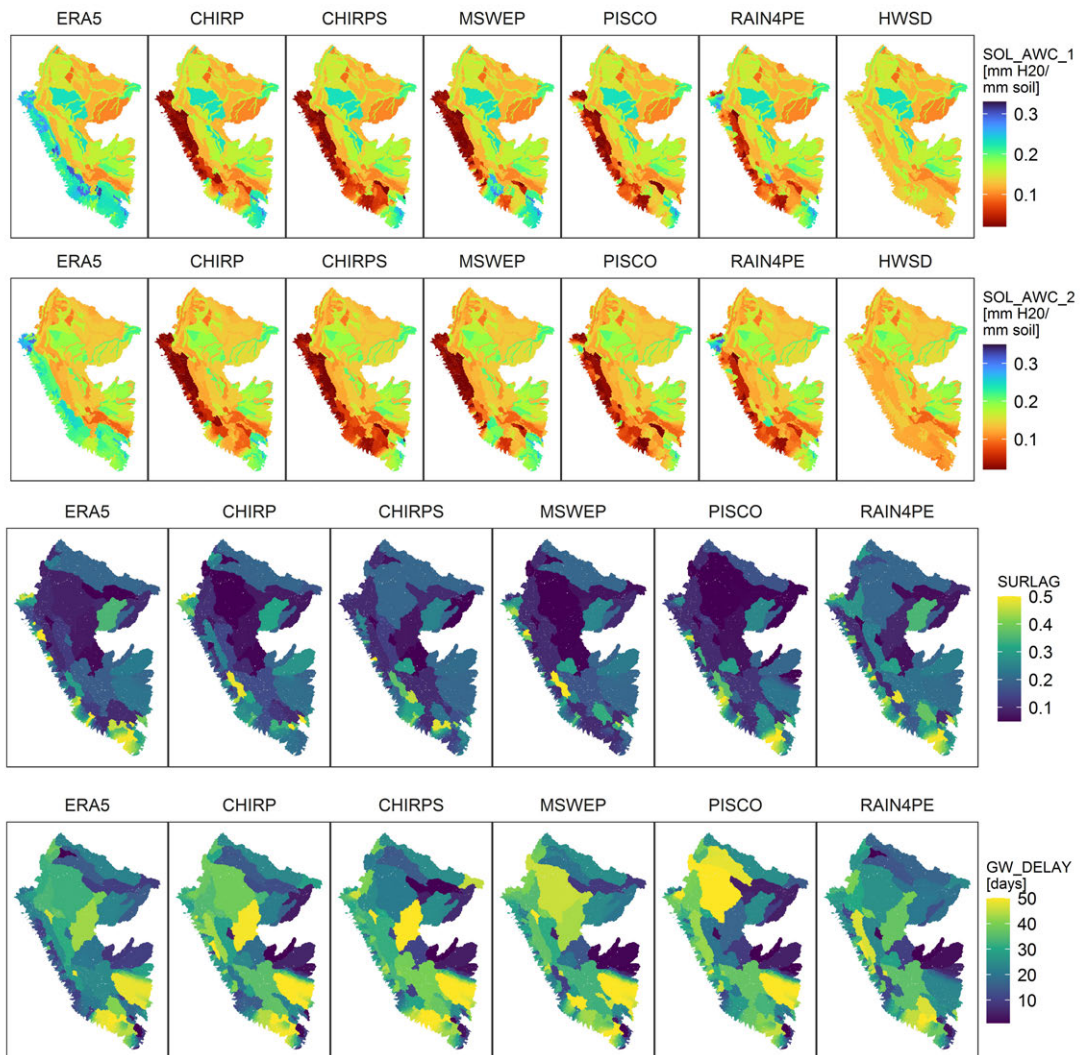
Figure 2.9: Calibrated parameter values for the soil available water capacity (SOL_AWC) for topsoil (1) and subsoil (2), the surface runoff delay coefficient (SURLAG), and the groundwater delay time (GW_DELAY). The HWSD map shows SOL_AWC values derived from the Harmonized World Soil Database, which were used for setting up the SWAT model.
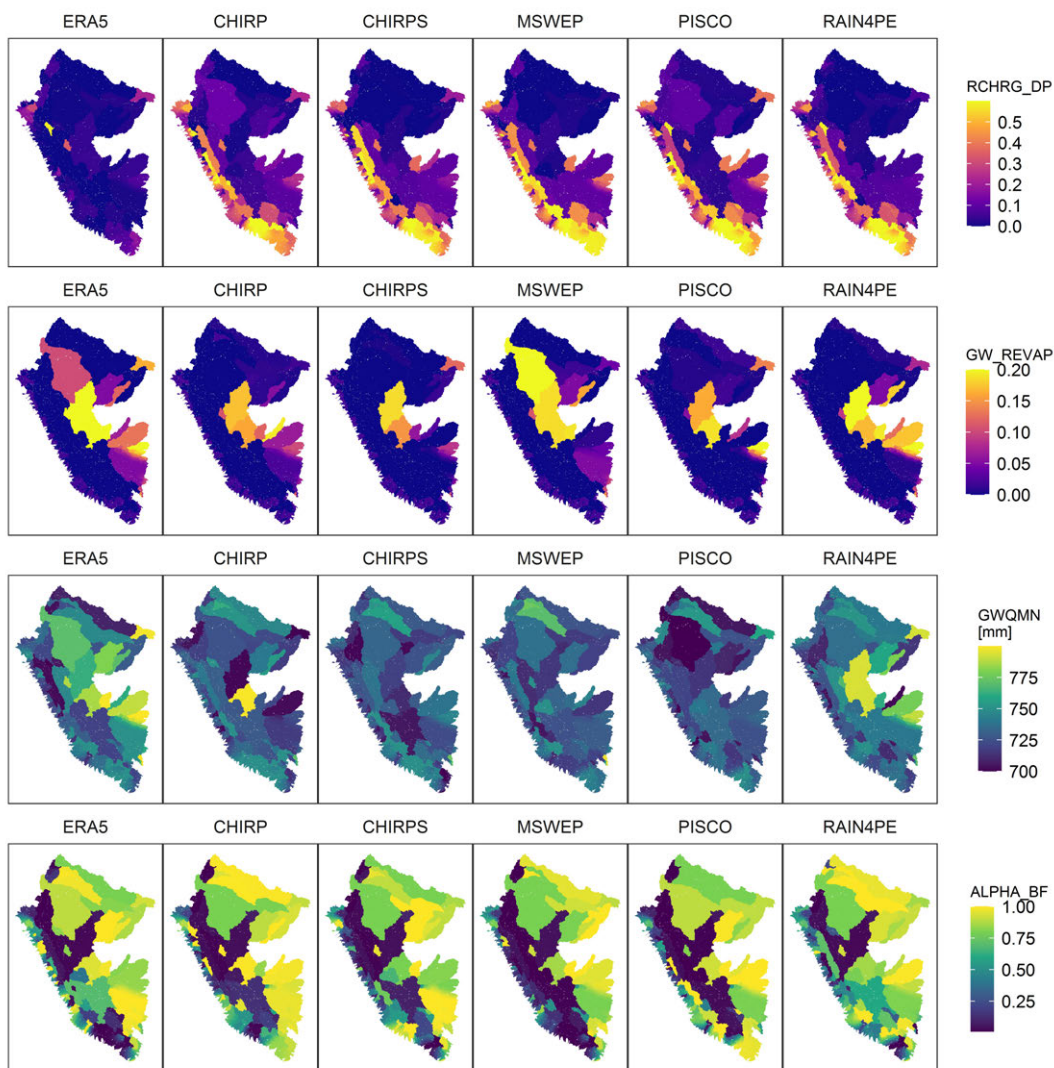
Figure 2.10: Calibrated parameter values for the deep aquifer percolation fraction (RCHRG_DP), the threshold for return flow from the shallow aquifer (GWQMN), the groundwater "revap" coefficient (GW_REVAP), and the baseflow recession constant (ALPHA_BF).

2.A.2   Evaluating the distribution of model parameters

In this section, we analyze the distribution of calibrated model parameters to see the regional parameter behavior and to elucidate potential input errors as they were identified to achieve the water budget closure using different precipitation datasets. Thus, unrealistic parameter values could be linked to input error. We advise readers to see Table 2.3 for the description of parameters and Neitsch et al. (2011) for detailed parameter definitions. Among the calibrated SWAT parameters, only two (SOL_AWC, GW_REVAP) can alter the water budget since they influence evapotranspiration and, subsequently, runoff estimation. The remaining parameters influence the surface runoff (SURLAG), groundwater (GW_DELAY, RCHRG_DP, GWQMN, ALPHA_BF), and flow routing (CH_K2, CHD, FP_W_F) not affecting water loss from the system. We illustrate in Figs. B1–B3 the spatial patterns of the calibrated parameters related to six precipitation datasets.

Figure B1 shows that the SOL_AWC, which constrains the maximum amount of plant available water a soil can provide and was derived from the Harmonized World Soil Database (HWSD; Abbaspour and Ashraf Vaghefi, 2019), was adjusted mainly for the Andean catchments. This is a critical parameter since higher values can lead to higher evapotranspiration and vice
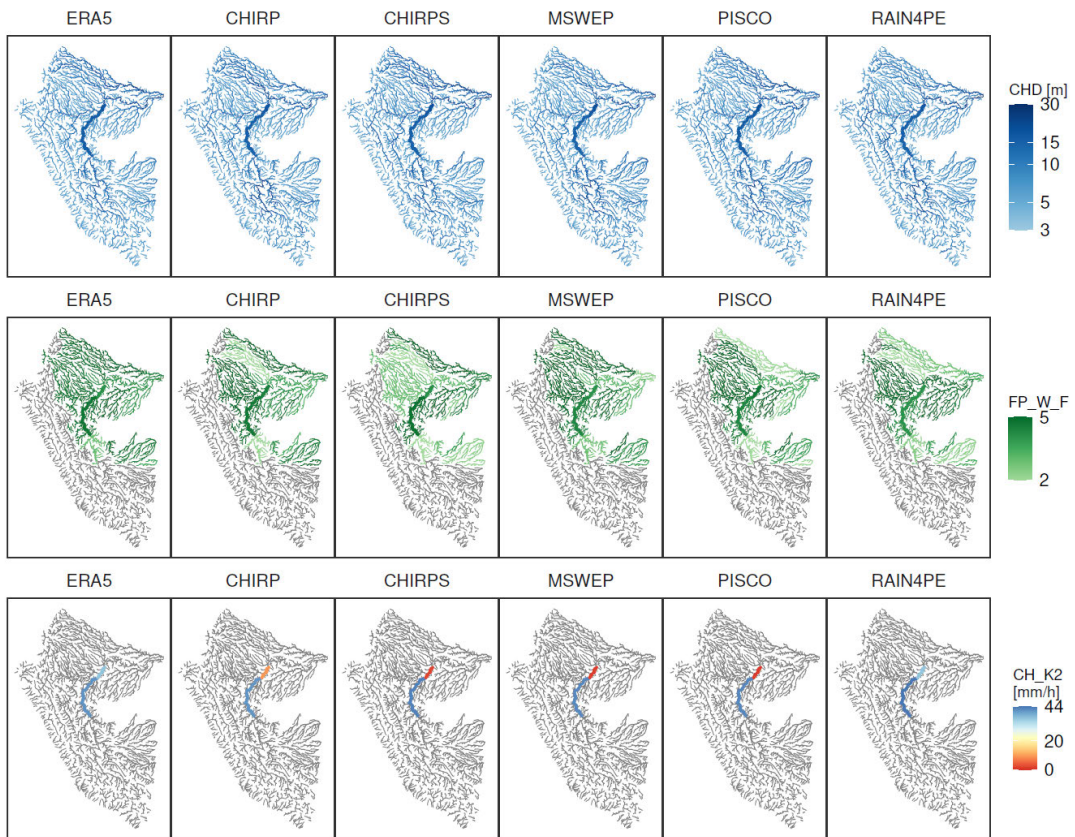
Figure 2.11: Calibrated parameter values for the main channel depth (CHD), the ratio of floodplain width over bankfull width (FP_W_F), and the hydraulic conductivity of main channel (CH_K2). Reaches in gray indicate that the parameter was not important in these reaches.

versa. The results show that high SOL_AWC values were identified for compensating the ERA5 precipitation overestimation (see positive errors in Fig. 6). However, despite this trade-off, discharge overestimation by ERA5-SWAT remains (see PBIAS in Fig. 8), suggesting that ERA5 precipitation estimates must be bias-corrected for the Andean regions prior to hydrological applications. Otherwise, unrealistic low SOL_AWC values ($\approx$0) and the prevalence of discharge underestimation (Fig. 8 and Fig. S5) over the northern pacific coastal catchments suggest that precipitation could be underestimated there, particularly by CHIRP, CHIRPS, MSWEP, and even PISCO (see negative errors in Fig. 6).

For the remaining parameters, we describe each one briefly based on the calibrated parameters for RAIN4PE-SWAT. Figure B1 shows overall low values (ranging from 0.05 to 0.5) for SURLAG in the study area, which is important for smoothing the simulated hydrograph due to the delay in surface runoff released from the HRUs (Neitsch et al., 2011) to match the peaks in the observed hydrograph. The GW_DELAY values (ranging from 1 to 50 days) reflect the lag in time that water in soil profile needs to enter shallow aquifer; high (low) values are usual for most of the Andean (Amazonian) catchments.

Figure B2 shows spatial distribution of the calibrated groundwater-related parameters. The RCHRG_DP parameter reflects the water volume percolated into the deep aquifer relative to the total recharge entering aquifers (both shallow and deep). Therefore, the calibrated RCHRG_DP values provide an insight into the important recharge entering deep aquifers in Peruvian Andean catchments, which subsequently sustain the prolonged dry season flow in these catchments (Clark et al., 2014; Fernandez-Palomino et al., 2020). The GW_REVAP values greater than zero reflect the areas (lower Amazon) where water is re-evaporated from the shallow aquifer (water entering the soil for evaporation and transpiration). In these areas,
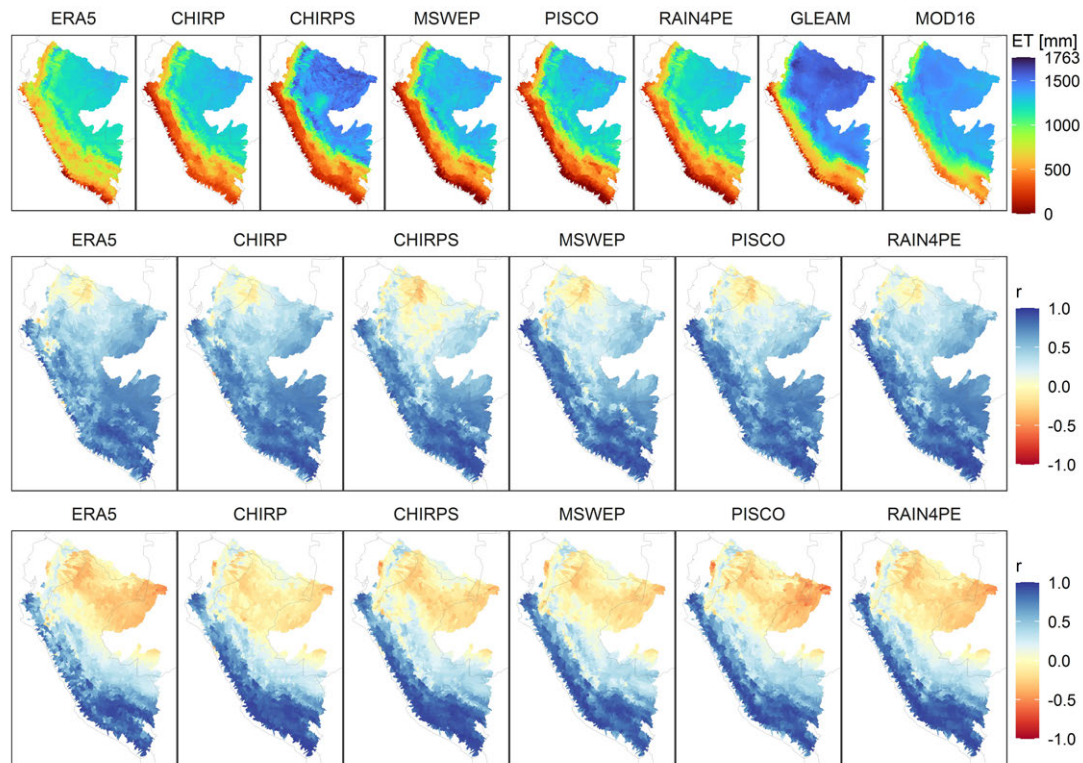
Figure 2.12: Comparison of evapotranspiration (ET) estimates from the calibrated SWAT model using different precipitation datasets as input with the remotely sensed based ET estimates from GLEAM and MOD16: (top) average annual ET for the period 2000–14 and Pearson's correlation coefficient (*r*) between SWAT-simulated ET and ET estimates from (middle) GLEAM and (bottom) MOD16. The comparison measure (r) was computed using monthly ET time series at the subcatchment scale for 2000–14.

deep-rooted evergreen forests can draw water from the shallow aquifer to meet their demands if available water in the soil profile is insufficient. All calibrated GWQMN values favor the return flow from aquifers and the re-evaporation from the shallow aquifer in areas (lower Amazon) where GWQMN values are greater than 750 mm (default water depth threshold in the shallow aquifer to allow re-evaporation). The high ALPHA_BF values (∼1) show shallow aquifers quickly contributing return flow to streams (e.g., lower Amazon catchments), whereas the low values (∼0) show those with slow contributions (e.g., most of the Andean catchments draining into the Pacific Ocean).

Figure B3 shows the calibrated reach and floodplain parameters (CHD, FP_W_F, and CH_K2). Among these parameters, the FP_W_F values can reflect the occurrence of flow over floodplains during the high discharge season in the lower Amazon rivers. The CH_K2 values greater than zero show reaches where water is infiltrated at the floodplain surface from floodplain flow or ponded water during overbank flood events. Then water stored at floodplain alluvium flows back to the channel when flood wave has passed and water levels in the channel have dropped, and the hydraulic gradient is reversed. This interaction between floodplains and reaches can explain the significant observed flood peak delay (on a scale of months) from Lagarto to Requena station (See Fig. S6), which is consistent with the findings of Santini (2020).

2.A.3 Comparison of SWAT and remotely sensed based evapotranspiration

Figure C1 compares evapotranspiration (ET) estimates from the calibrated SWAT model driven by different precipitation datasets with the GLEAM and MOD16 estimates. All ET estimates

show similar spatial patterns with increasing ET gradients from west to east. The differences in SWAT-simulated ET volumes can be attributed to inappropriate parameter estimation due to precipitation biases and uncertainties. The higher ET values for CHIRPS-SWAT are likely due to the prevalence of dry conditions in CHIRPS which affect the estimation of daily relative humidity and subsequently potential evapotranspiration, vapor stress on plant growth, and ET.

We compared GLEAM and MOD16 against the simulated ET by RAIN4PE-SWAT since it represents the water budget well (see PBIAS in Fig. 8). Figure C1 shows a general tendency for GLEAM and MOD16 to overestimate ET in the study area, and even their estimates are greater than precipitation along the Andes (see Figs. C1 and 6), which would not allow the water budget closure in the Andean catchments. The correlation coefficient (Fig. C1, middle panel) shows better agreement between GLEAM and SWAT-simulated ET, which are based on the same equation (Priestley–Taylor) for potential evapotranspiration estimation. Spatially, both GLEAM and MOD16 agree well with the SWAT-simulated ET in areas with strong seasonal precipitation variability, as the Peruvian Andes and southern region of the Peruvian Amazon. However, negative correlation values over the northern Amazon basin areas with a bimodal rainfall regime (Laraque et al., 2007) can indicate inconsistency in the temporal distribution in GLEAM and MOD16 ET estimates there. This is in line with the findings of Dile et al. (2020), who reported that remotely sensed based ET did not respond well to the rainfall in areas with a bimodal rainfall pattern in Ethiopia. Furthermore, the ET estimates could be affected by the inherent uncertainties in methods and input data. Our results demonstrate that the ET estimation by the remotely sensed ET products is still a challenge in the region, and the ground-based measurements are required for better understanding the ET spatiotemporal patterns and for a more reliable evaluation of the ET estimates.

2.B   Supporting information

Table 2.6: Median values of each performance measure for daily streamflow simulation for the calibration period. Values in bold denote the best performing product in each drainage system and the study area according to the specific score on the left.

Basin	Product	KGE	NSE	lNSE	|PBIAS|	|Slow|	|Shigh|	|Speak|
Titicaca Lake	ERA5	−1.05	−2.7	−0.07	201.7	47.8	192.4	47.2
Titicaca Lake	CHIRP	0.68	0.47	0.7	10.7	13.4	16.1	13.6
Titicaca Lake	CHIRPS	0.84	0.68	0.8	3.4	10.8	6.9	**4.3**
Titicaca Lake	MSWEP	0.82	0.66	0.8	9.6	13.5	13.7	8.8
Titicaca Lake	PISCO	0.85	0.77	0.84	**2.2**	13.3	**5.4**	13.5
Titicaca Lake	RAIN4PE	**0.87**	**0.78**	**0.87**	3.5	11.2	6.4	12.5
Pacific	ERA5	−2.34	−7.01	−1.52	330.6	285.3	292.4	113
Pacific	CHIRP	0.54	0.43	0.61	32.5	14.8	39.6	47.2
Pacific	CHIRPS	0.7	0.55	0.7	10.3	7.9	16.9	30.6
Pacific	MSWEP	0.7	0.57	0.7	17.5	16.3	19.8	25
Pacific	PISCO	0.74	0.61	0.76	9.9	14.6	12.8	20.1
Pacific	RAIN4PE	**0.8**	**0.68**	**0.78**	**4.4**	**5.3**	**6.8**	**11.1**
Amazon	ERA5	0.62	0.4	0.53	11.5	22.4	13.4	22.5
Amazon	CHIRP	0.64	0.41	0.46	10.6	11.5	12.1	18.8
Amazon	CHIRPS	0.66	0.29	0.27	15.1	15.8	15	14
Amazon	MSWEP	0.68	0.41	0.44	20.1	18.2	14.8	15.4
Amazon	PISCO	0.51	0.02	−0.26	22.5	22.1	18.6	18.2
Amazon	RAIN4PE	**0.81**	**0.7**	**0.71**	**5.8**	**7.4**	**5.4**	**10.1**
All watersheds	ERA5	−0.49	−2.16	−0.3	145.5	64.9	113	46
All watersheds	CHIRP	0.62	0.42	0.57	14.1	11.9	17.2	22.5
All watersheds	CHIRPS	0.67	0.44	0.58	10.5	12.5	14.5	18.4
All watersheds	MSWEP	0.7	0.53	0.62	15.7	17.2	15.1	15.9
All watersheds	PISCO	0.71	0.54	0.67	11.6	16.1	13.9	17.9
All watersheds	RAIN4PE	**0.81**	**0.7**	**0.74**	**5.6**	**7.8**	**6.5**	**10.2**

Table 2.7: Median values of each performance measure for daily streamflow simulation for the validation period. Values in bold denote the best performing product in each drainage system and the study area according to the specific score on the left.

Basin	Product	KGE	NSE	LNSE	|PBIAS|	|Slow|	|Shigh|	|Speak|
Titicaca Lake	ERA5	−1.08	−2.96	−0.11	205.1	39.5	230.9	56.7
Titicaca Lake	CHIRP	0.66	0.44	0.66	12.5	17.4	10.2	16.2
Titicaca Lake	CHIRPS	0.84	0.72	0.77	3.3	14.5	10.4	**7.6**
Titicaca Lake	MSWEP	0.82	0.69	0.79	9.2	12	12.8	8.5
Titicaca Lake	PISCO	0.86	**0.78**	0.8	**1.8**	**10.6**	**3.5**	9.5
Titicaca Lake	RAIN4PE	**0.88**	**0.78**	**0.81**	2.6	11.4	7.3	13.6
Pacific	ERA5	−2.23	−5.74	−1.57	320.4	263.4	308.5	104
Pacific	CHIRP	0.53	0.43	0.6	31.7	16.3	40.5	43.5
Pacific	CHIRPS	0.72	0.6	0.73	9.4	8.1	16.7	31.5
Pacific	MSWEP	0.71	0.6	0.72	20.3	25.3	18.7	16.2
Pacific	PISCO	0.74	0.62	0.73	9.9	19	14.8	19.1
Pacific	RAIN4PE	**0.81**	**0.69**	**0.78**	**4.3**	**5.1**	**6.5**	**14.8**
Amazon	ERA5	0.68	0.52	0.6	8.8	21.6	8.2	19.5
Amazon	CHIRP	0.66	0.42	0.46	8.6	10.9	12	20.1
Amazon	CHIRPS	0.66	0.29	0.26	17.2	16.5	18.2	16
Amazon	MSWEP	0.68	0.4	0.4	17.9	17.6	14.1	15.4
Amazon	PISCO	0.36	−0.08	−0.3	26.4	28.7	19.2	18.9
Amazon	RAIN4PE	**0.81**	**0.69**	**0.7**	**4.5**	**6.4**	**4.1**	**7.7**
All watersheds	ERA5	−0.36	−1.24	−0.07	120.4	53.1	82.4	37.3
All watersheds	CHIRP	0.62	0.42	0.57	14.6	11.8	16.7	23.6
All watersheds	CHIRPS	0.69	0.53	0.56	11.2	12.9	16.7	21.4
All watersheds	MSWEP	0.69	0.53	0.59	14.2	18.7	14.8	15.4
All watersheds	PISCO	0.71	0.47	0.65	11.5	22.1	14.8	18.2
All watersheds	RAIN4PE	**0.82**	**0.71**	**0.74**	**4.2**	**6.3**	**5.9**	**12.4**
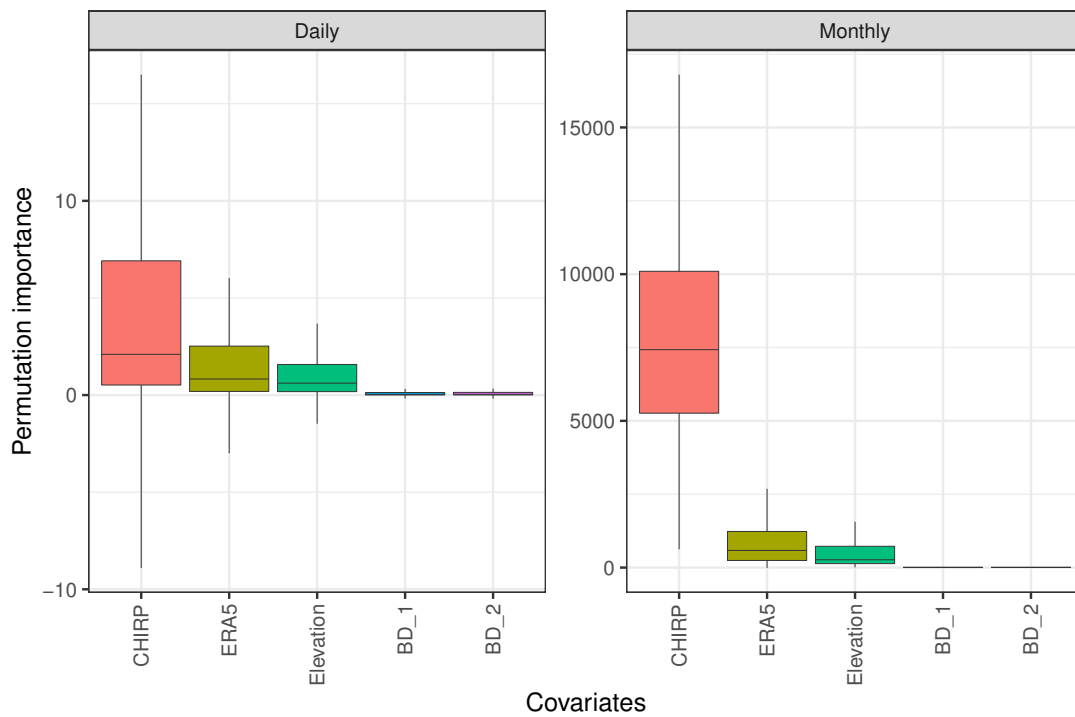
Figure 2.13: Distributions of the scaled permutation importance measure. Only the results for two buffer distances (BD) are shown in the figure. The most important predictor variable is CHIRP, followed by ERA5 and Elevation both for the daily and monthly merging procedures. Buffer distances are negligible. Negative values for permutation importance mean that there were some days when the covariate was not important for the prediction.
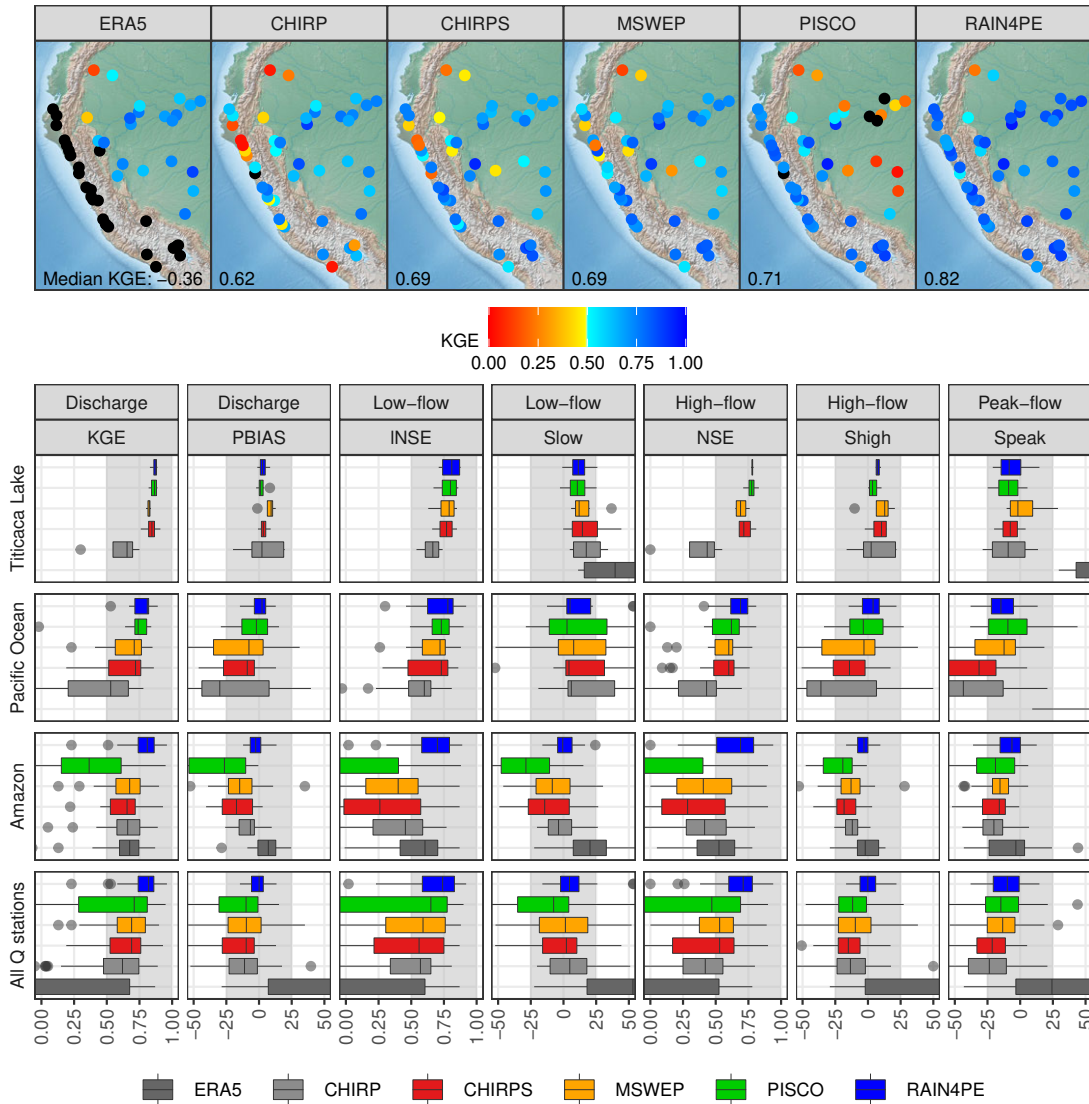
Figure 2.14: Hydrological model performance metrics for daily streamflow simulations by SWAT driven by 6 precipitation datasets in the validation period: spatial patterns of KGE (upper part) and boxplots showing seven criteria for all streamflow [Q] stations and stations located in catchments draining into the Amazon River, Pacific Ocean, and Titicaca Lake (lower part). The datasets are sorted in ascending order of the median KGE for all Q stations. Values exceeding 0.5 (between ±25%) for KGE, INSE, and NSE (PBIAS, S_{low}, S_{high}, and S_{peak}) are considered skillful (marked by light gray background in boxplots). Black points in the upper part represent negative values of KGE. Note that x-axis starts at 0 for KGE, NSE, and INSE to improve visualization, whereas PBIAS, S_{low}, S_{high}, and S_{peak} were constrained between ±50%.
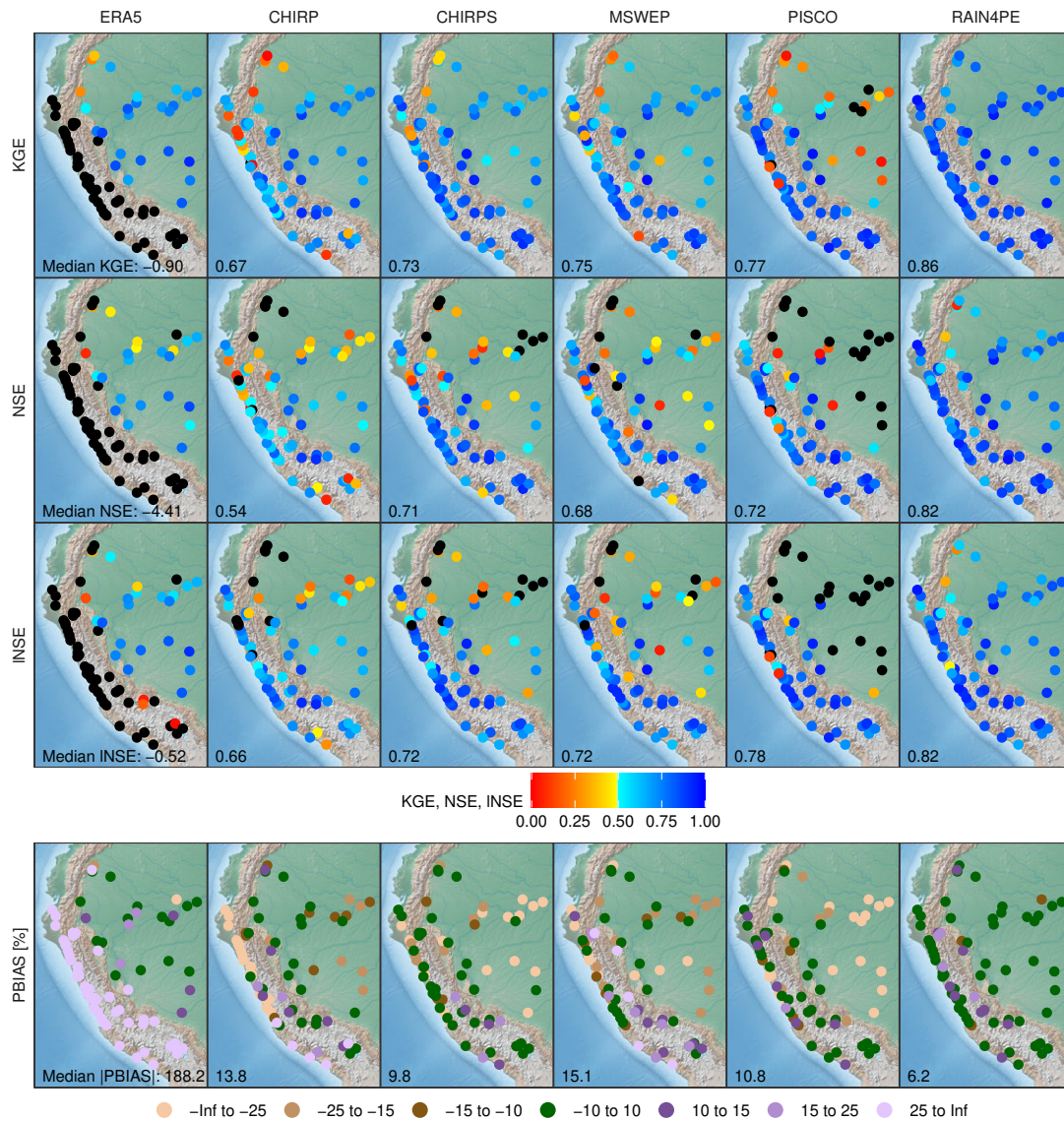
Figure 2.15: Hydrological model performance metrics KGE, NSE, INSE and PBIAS for monthly streamflow simulations by SWAT driven by 6 precipitation datasets in the calibration period. Black points represent negative values of KGE, NSE, and INSE.
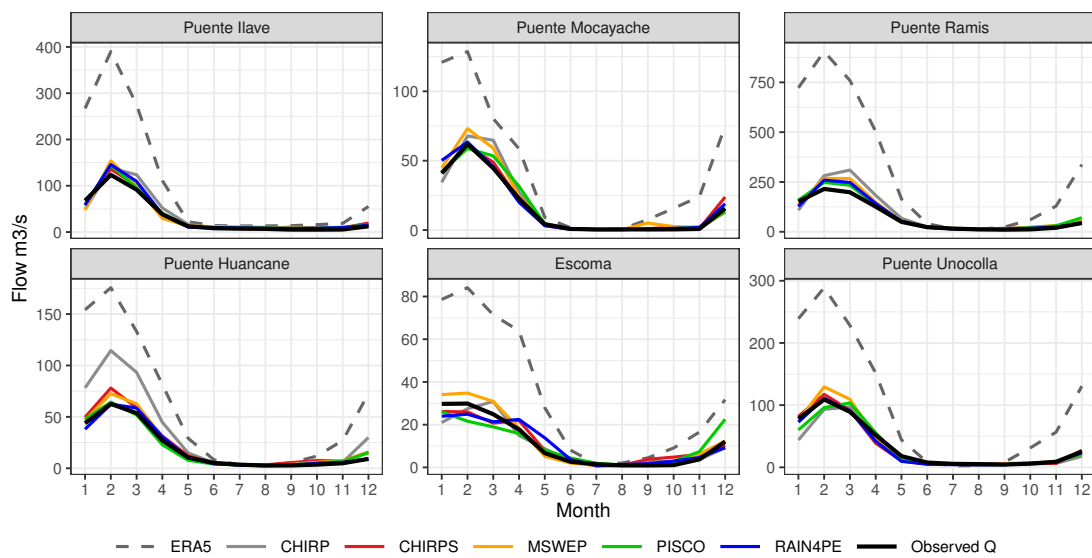
Figure 2.16: Mean seasonal streamflow (Q) simulated by SWAT in the period 1983–2015 driven by 6 precipitation datasets in comparison with the observed mean seasonal discharge in the same period for stations located in catchments draining into Titicaca Lake. The streamflow stations are ordered from south to north. Note that both observed and seasonal streamflow were computed only for the months with available streamflow data.
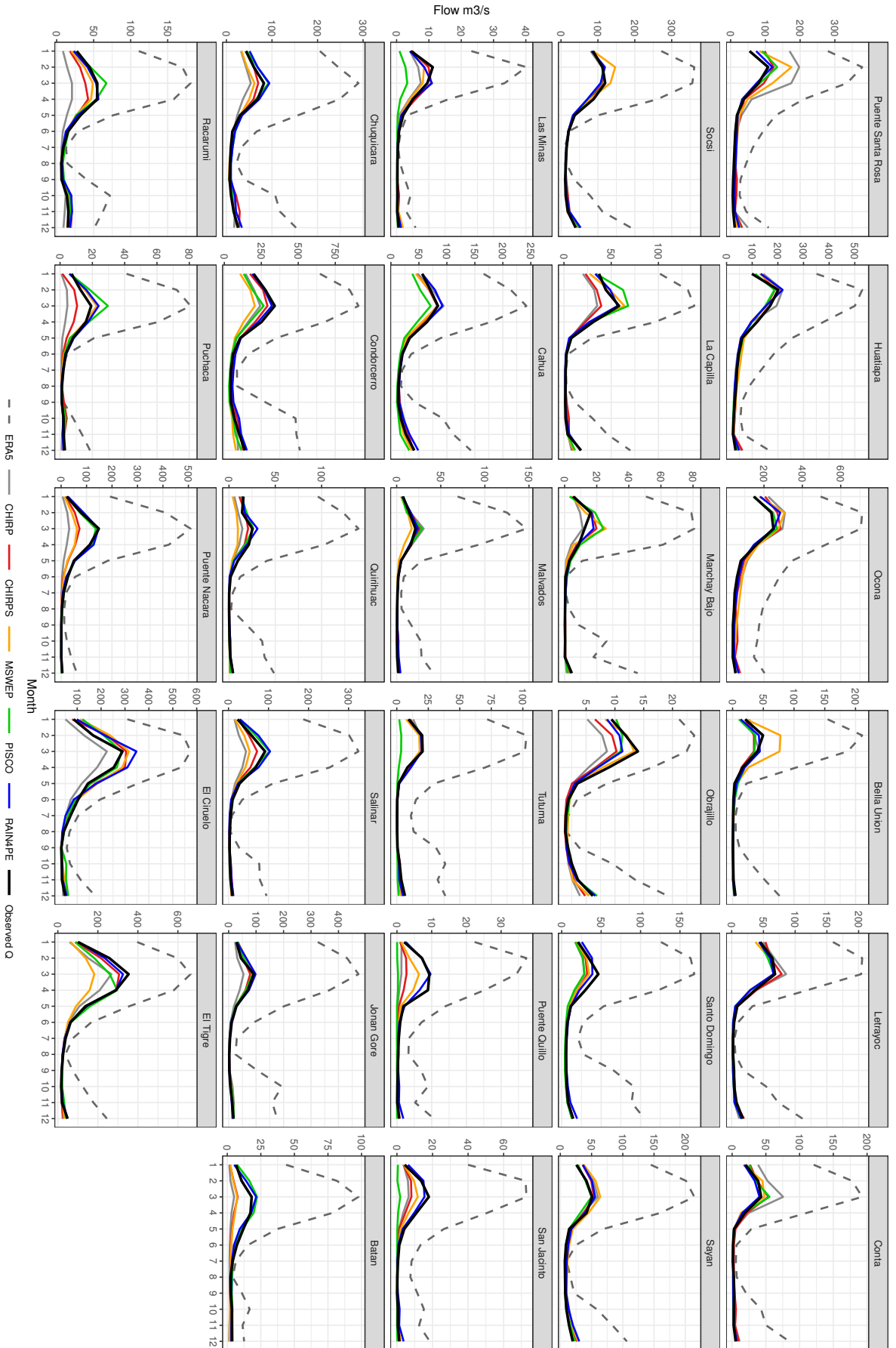
Figure 2.17: Mean seasonal streamflow (Q) simulated by SWAT in the period 1983–2015 driven by 6 precipitation datasets in comparison with the observed mean seasonal discharge in the same period for stations located in catchments draining into the Pacific Ocean. The streamflow stations are ordered from south to north. Note that both observed and seasonal streamflow were computed only for the months with available streamflow data
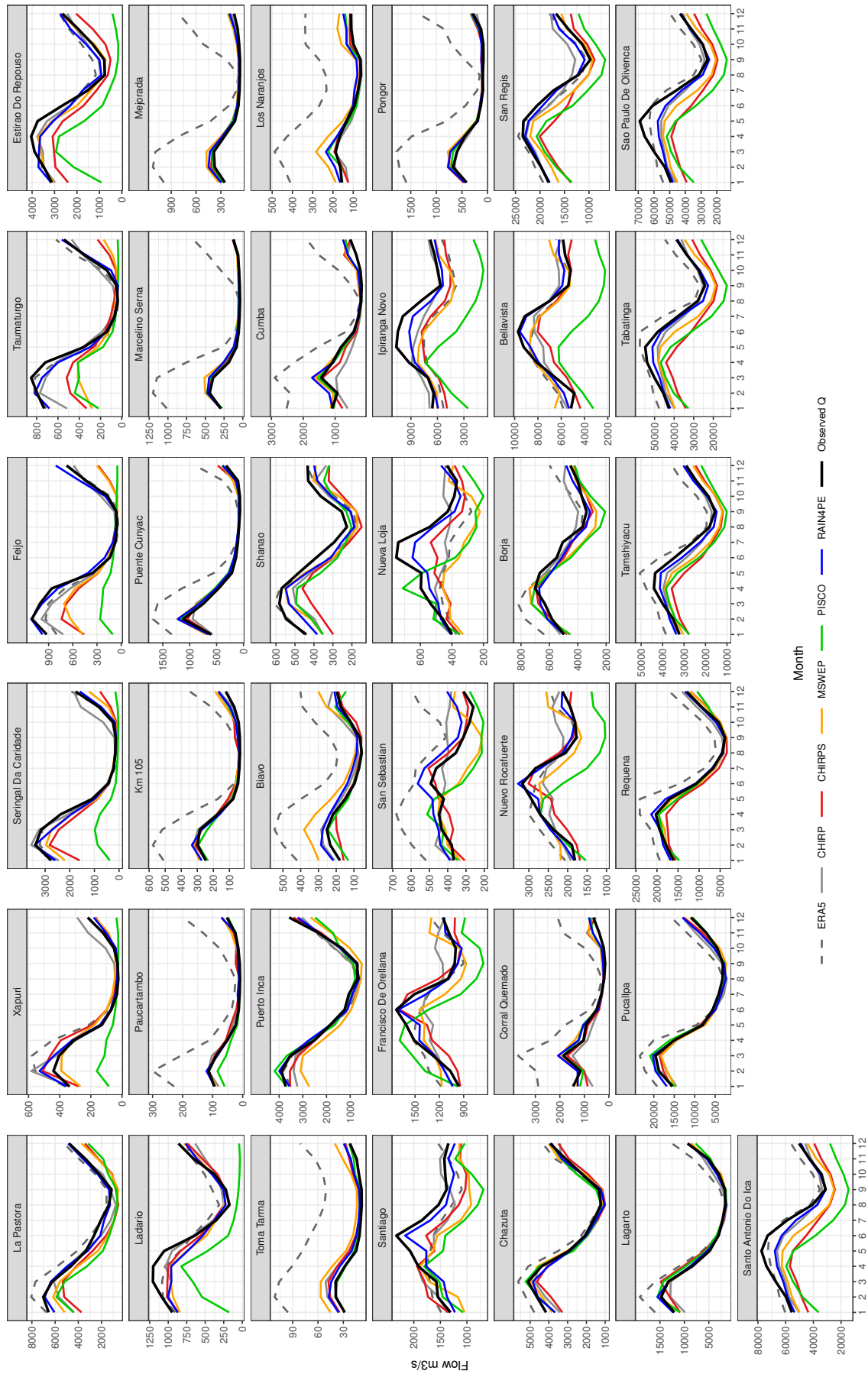
Figure 2.18: Mean seasonal streamflow (Q) simulated by SWAT in the period 1983–2015 driven by 6 precipitation datasets in comparison with the observed mean seasonal discharge in the same period for stations located in catchments draining into the Amazon River. The streamflow stations are ordered from upstream to downstream. Note that both observed and seasonal streamflow were computed only for the months with available streamflow data
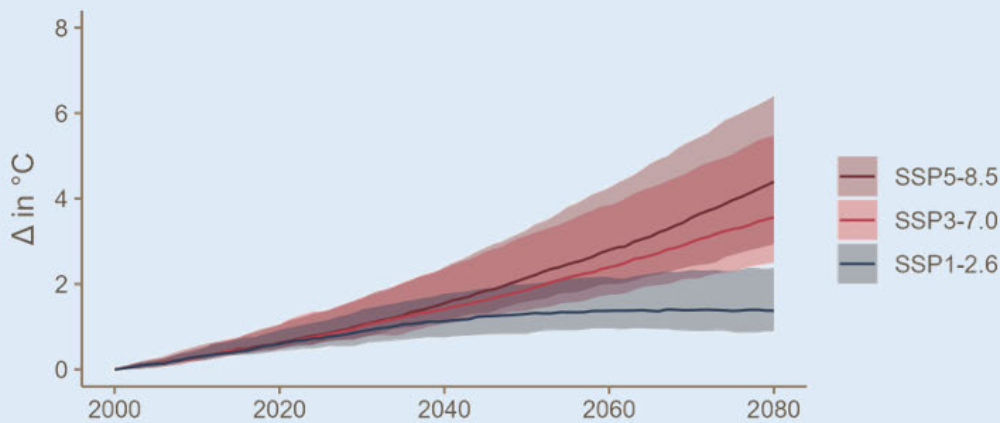
3. High-resolution climate projection dataset based on CMIP6 for Peru and Ecuador: BASD-CMIP6-PE

Abstract

Here, we present BASD-CMIP6-PE, a high-resolution (1d, 10 km) climate dataset for Peru and Ecuador based on the bias-adjusted and statistically downscaled CMIP6 climate projections of 10 GCMs. This dataset includes both historical simulations (1850–2014) and future projections (2015–2100) for precipitation and minimum, mean, and maximum temperature under three Shared Socioeconomic Pathways (SSP1-2.6, SSP3-7.0, and SSP5-8.5). The BASD-CMIP6-PE climate data were generated using the trend-preserving Bias Adjustment and Statistical Down-scaling (BASD) method. The BASD performance was evaluated using observational data and through hydrological modeling across Peruvian and Ecuadorian river basins in the historical period. Results demonstrated that BASD significantly reduced biases between CMIP6-GCM simulations and observational data, enhancing long-term statistical representations, including mean and extreme values, and seasonal patterns. Furthermore, the hydrological evaluation highlighted the appropriateness of adjusted GCM simulations for simulating streamflow, including mean, low, and high flows. These findings underscore the reliability of BASD-CMIP6-PE in assessing regional climate change impacts on agriculture, water resources, and hydrological extremes.

3.1 Background & summary

Reliable hydro-climate data are essential for understanding the effects of observed and projected climate change on social and natural systems and developing effective adaptation and mitigation strategies. Several global and regional observation datasets exist at different temporal and spatial resolutions (Aybar et al., 2020; Beck et al., 2017, 2019b; Fernandez-Palomino et al., 2021; Funk et al., 2015a,b; Harris et al., 2020; Hersbach et al., 2020; Huerta et al., 2018; Huerta et al., 2022). At the regional scale, the Servicio Nacional de Meteorología e Hidrología del Perú (SENAMHI) has developed the Peruvian Interpolated data of Climatological and Hydrological Observations (PISCO). The PISCO dataset includes precipitation (Aybar et al., 2020), maximum and minimum temperature (Huerta et al., 2018), and reference evapotranspiration (Huerta et al., 2022) data. SENAMHI uses this dataset for drought and flood monitoring at the countrywide level of Peru. Recently, a new hydrologically corrected daily precipitation dataset, called RAIN4PE (Rain for Peru and Ecuador), was developed and is available (Fernandez-Palomino et al., 2021, 2022). RAIN4PE has proved to be superior to other existing precipitation datasets such as CHIRP (Funk et al., 2015b), CHIRPS (Funk et al., 2015a), ERA5 (Hersbach et al., 2020), MSWEP (Beck et al., 2017, 2019b), and PISCO-precipitation (Aybar et al., 2020) for hydrometeorological applications and suggested to be a basis for bias adjustment of Global Climate Models (GCMs) output in Peru and Ecuador (Fernandez-Palomino et al., 2022).

GCMs have become important tools for historical climate simulation and future climate projection (IPCC, 2007). As part of the Coupled Model Intercomparison Project (CMIP) of the World Climate Research Programme (WCRP), GCMs' output has contributed to the assessment reports produced by the Intergovernmental Panel on Climate Change (IPCC) (IPCC, 2007, 2014, 2023c). Output from the latest generation of GCMs participating in the sixth phase of the CMIP (CMIP6) is now available (Eyring et al., 2016). CMIP6 models have better spatial resolution (100 km in the horizontal dimension) and physical process representation than earlier generations, as well as better simulation of recent mean climate compared to the previous CMIP phases (Eyring et al., 2021). Nevertheless, such resolution is still coarse for regional and local management decisions, which need more detailed climate information. Namely, such coarse-resolution data are useless for providing a reliable base for real-world water management, particularly related to extreme hydrological conditions (Bronstert et al., 2007). Moreover, even the latest generation of GCMs shows substantial biases (Arias et al., 2021b; Firpo et al., 2022; Monteverde et al., 2022). Therefore, it is important to bias-adjust and downscale the raw GCM outputs to produce reliable climate simulations and projections for finer-scale impact studies. To date, few studies have performed the bias adjustment and downscaling of the output of CMIP6 models, e.g., at a global scale (Lange and Büchner, 2021, 2022; Noël et al., 2022; Thrasher et al., 2022; Xu et al., 2021), for South Asia (Mishra et al., 2020), and for Brazil (Ballarin et al., 2023). To the best of our knowledge, there is currently no gridded dataset based on CMIP6 results bias-adjusted and downscaled for Peru and Ecuador using reliable reference data from the local observation datasets. To close this gap, we generated the new high-resolution climate dataset BASD-CMIP6-PE based on the bias-adjusted and statistically downscaled CMIP6 climate projections over Peru and Ecuador.

The BASD-CMIP6-PE dataset was generated using the trend-preserving Bias Adjustment and Statistical Downscaling (BASD) method (Lange, 2019, 2021b). BASD effectively reduced biases between CMIP6-GCM simulations and observational data, resulting in improved representations of long-term statistical properties, including mean and extreme values, as well as seasonal patterns. BASD also demonstrated its capability to approximately preserve the projected trends and the intermodel spreads of climate variables in future climate scenarios.

A hydrological evaluation, which compared raw and adjusted GCM simulations through hydrological modeling, provided additional support for the appropriateness of adjusted GCM simulations in simulating streamflow, including mean, low, and high flows.

These advantages underscore the dataset's reliability for assessing regional climate change impacts on agriculture, water resources, and hydrological extremes, thereby supporting the development of comprehensive adaptation strategies. Notably, the BASD-CMIP6-PE dataset has already played a pivotal role in conducting the first-ever investigation into projected future changes in various components of the regional hydrological cycle and hydrological extremes

across Peru, including the analysis of transboundary river catchments (Fernandez-Palomino et al., 2023a).

Table 3.1: List of the 10 CMIP6 models used in this study.

No.	Model	Resolution (lon. by lat.)	Member	Citation
1	CanESM5	2.8° × 2.8°	r1i1p1f1	Swart et al., 2019
2	IPSL–CM6A–LR	2.5° × 1.3°	r1i1p1f1	Boucher et al., 2020
3	UKESM1–0–LL	1.9° × 1.3°	r1i1p1f2	Sellar et al., 2019
4	CNRM–CM6–1	1.4° × 1.4°	r1i1p1f2	Voldoire et al., 2019
5	CNRM–ESM2–1	1.4° × 1.4°	r1i1p1f2	Séférian et al., 2019
6	MIROC6	1.4° × 1.4°	r1i1p1f1	Tatebe et al., 2019
7	GFDL–ESM4	1.3° × 1°	r1i1p1f1	Dunne et al., 2020
8	MRI–ESM2–0	1.1° × 1.1°	r1i1p1f1	Yukimoto et al., 2019
9	MPI–ESM1–2–HR	0.9° × 0.9°	r1i1p1f1	Müller et al., 2018
10	EC–Earth3	0.7° × 0.7°	r1i1p1f1	Döscher et al., 2022

Table 3.2: Climate observed data used in this study.

Variable	Resolution	Description and source
Precipitation	Daily/0.1°	Rain for Peru and Ecuador (RAIN4PE, Fernandez-Palomino et al., 2021, 2022)
Temperature	Daily/0.1°	Maximum and minimum temperature data for Peru (Huerta et al., 2018), as provided by SENAMHI (`ftp://publi_dgh2:123456@ftp.senamhi.gob.pe/`).

3.2 Methods

3.2.1 Study area

The study area encompasses Peru and Ecuador. The new BASD-CMIP6-PE dataset is generated for the land surface between 19°S–2°N and 82°–67°W, matching the observational data domain of the RAIN4PE and PISCO datasets. This region exhibits complex hydroclimatic patterns resulting from its diverse climate zones and the Andes Cordillera, acting as a topographic barrier that separates the cold, arid eastern Pacific from the warm, humid Amazon. These patterns arise from the interplay of large-scale factors (e.g., latitudinal migration of the Atlantic Intertropical Convergence Zone, South American Monsoon Systems, marine currents, Bolivian High) and local circulation patterns (e.g., upslope and downslope moisture transport), in conjunction with the complex Andean orography (Espinoza et al., 2020; Laraque et al., 2007; Segura et al., 2019; Tobar and Wyseure, 2018). El Niño-Southern Oscillation (ENSO) also significantly influences interannual hydroclimatic conditions in the Andes (Poveda et al., 2020).

3.2.2 Climate simulation data

Daily climate model output data for precipitation (pr) and minimum (tasmin), mean (tas), and maximum (tasmax) temperature were obtained from the CMIP6 ensemble (Eyring et al., 2016) for 10 GCMs (Table 3.1). Data were obtained for the historical simulation (1850–2014) and future projections (2015–2100), with projections run under SSP1-2.6, SSP3-7.0, and SSP5-8.5 scenarios (Riahi et al., 2017). These ten models were also used by phase 3b of the Inter-Sectoral Impact Model Intercomparison Project (ISIMIP3b) for climate impact assessment studies (Lange and Büchner, 2021, 2022). In terms of climate sensitivity (i.e., magnitude of the warming signal at the end of the century), the selected models are considered an appropriate choice since they approximately cover the full range of CMIP6 projections, including models with low (GFDL-ESM4, MPI-ESM1-2-HR, MRI-ESM2-0) and high (IPSL-CM6A-LR, UKESM1-0-LL) climate sensitivity Lange, 2021a. The selected three greenhouse gas emissions scenarios span
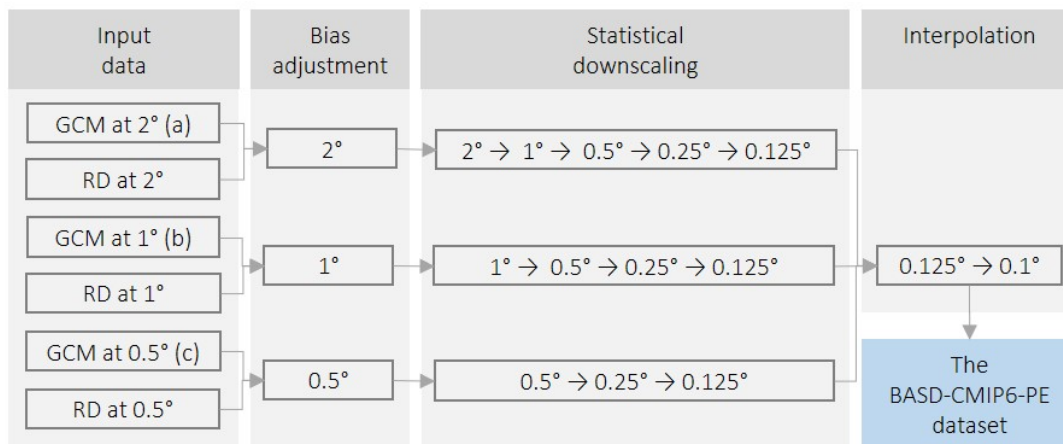
Figure 3.1: Flow chart for the BASD-CMIP6-PE dataset variables (pr, tasmin, tas, tasmax) for 10 GCMs. The bias adjustment was applied at: (a) 2° for CanESM5, IPSL-CM6A-LR, and UKESM1-0-LL; (b) 1° for CNRM-CM6-1, CNRM-ESM2-1, GFDL-ESM4, MIROC6, MPI-ESM1-2-HR, and MRI-ESM2-0; and (c) 0.5° for EC-Earth3. GCM (RD) is Global Climate Model (reference) data. Note that RD are aggregated observation data.

from one with mitigation policy (SSP1-2.6) to one without mitigation (SSP5-8.5) to sample future climate uncertainty from anthropogenic forcing. The SSP1-2.6 is close to the Paris Agreement goal, where global warming is limited to 2 °C above pre-industrial levels. The scenario is characterized by declining greenhouse gas (GHG) emissions to net zero until 2050, followed by varying levels of net negative CO_2 emissions. The SSP3-7.0 scenario is a high, and the SSP5-8.5 a high-end global warming scenario with continuing high fossil fuel development throughout the 21st century and consequently strong increases in GHG emissions. For a detailed description of SSPs scenarios, refer to the Sixth Assessment Report of the IPCC IPCC, 2023c.

3.2.3 Climate observation

The observational reference datasets used for the evaluation, bias adjustment, and statistical downscaling (BASD) of CMIP6 climate simulations are listed in Table 3.2. Data of precipitation (pr) were obtained from the RAIN4PE dataset (Fernandez-Palomino et al., 2021, 2022), minimum (tasmin) and maximum (tasmax) temperature from the SENAMHI-PISCO dataset (Huerta et al., 2018), and mean temperature (tas) was estimated as the average of tasmin and tasmax. RAIN4PE precipitation data (available for 1981-2015) are generated by merging multisource precipitation data (satellite, reanalysis, and ground-based precipitation from 804 gauges) with surface elevation using the random forest method. Additionally, total precipitation was adjusted using streamflow data through the reverse hydrology method for catchments influenced by fog/cloud water input, such as páramo and montane watersheds. The PISCO temperature data (available for 1981-2016) are generated by merging information from 178 observed climate stations, satellite-derived surface temperatures, and topographic variables. The data integrate spatially gridded estimates of normal climate (estimated using weighted regression Kriging) with daily anomalies (estimated using regression splines). These observational datasets have been validated by simulating streamflow through hydrological modeling for the Peruvian and Ecuadorian catchments (Fernandez-Palomino et al., 2022).

3.2.4 Bias adjustment and statistical downscaling

The software used for BASD is ISIMIP3BASD v2.5 (Lange, 2021b), which implements the BASD method described in Lange (Lange, 2019). In ISIMIP3, this method was applied to generate bias-adjusted and downscaled CMIP6 projections, utilizing the global observational dataset W5E5 (available at a spatial resolution of 0.5°) as reference data (Lange and Büchner,

Table 3.3: Statistical metrics and hydrological signatures. Here, R and S are the reference and simulated flow (m^3/s), respectively; EP is the exceedance probability; H, and L are the indices of the minimum flow of the high flow and low flow segments, respectively.

Criterion (reference)	Equation	Description
Discharge-related performance measures		
Kling–Gupta efficiency (Gupta et al., 2009; Kling et al., 2012)	$KGE = \sqrt{(r-1)^2 + (\beta-1)^2 + (\gamma-1)^2}$	r is the Pearson product-moment correlation coefficient and beta (gamma) indicates the bias (relative dispersion) between observed and simulated flows
Percent bias (Gupta et al., 1999)	$PBIAS = \dfrac{\sum_{i=1}^{n}(S_i - R_i)}{\sum_{i=1}^{n} R_i} \times 100$	n is the number of observations on evaluation
Signature measures based on the flow duration curve (FDC)		
Percent bias in FDC high segment volume (Yilmaz et al., 2008)	$S_{\text{high}} = \dfrac{\sum_{h=1}^{H}(S_h - R_h) \times 100}{\sum_{h=1}^{H} R_h}$	$h = 1, 2, \ldots, H$ are flow indices located within the high flow segment (0–5% flow EP)
Percent bias in FDC low segment volume (Yilmaz et al., 2008)	$S_{\text{low}} = \dfrac{\sum_{l=1}^{L}(S_l - R_l) \times 100}{\sum_{l=1}^{L} R_l}$	$l = 1, 2, \ldots, L$ are flow indices located within the low flow segment (95–100% flow EP)

2021, 2022; Lange et al., 2021). In our study, we adopted a different approach, employing highly reliable, region-specific, high-resolution datasets, namely PISCO-temperature and RAIN4PE precipitation, to develop BASD-CMIP6-PE. The BASD method uses 1) a trend-preserving quantile mapping approach to bias-adjust climate simulation data at their original spatial resolution using spatially aggregated climate observation data, and 2) a stochastic statistical downscaling approach to increase their spatial resolution using climate observation data, which consequently have to be available with the higher resolution. Note that bias adjustment (BA) and statistical downscaling (SD) are applied after one another and not together. Further details on the BASD method are given in Lange (Lange, 2019).

Figure 3.1 shows the bias adjustment and downscaling strategy to generate the BASD-CMIP6-PE dataset following the ISIMIP protocol (Lange, 2021a). This dataset includes both historical simulations (1850-2014) and future projections (2015-2100) for four variables (pr, tasmin, tas, tasmax) and three future CMIP6 scenarios (SSP1-2.6, SSP3-7.0, SSP5-8.5) for 10 GCMs. To apply the ISIMIP3BASD method, the original CMIP6 output (observational data) was interpolated (aggregated) onto regular latitude-longitude grids with 0.5°, 1.0°, or 2.0° resolutions using the first-order conservative remapping (Jones, 1999); Fig. 3.1 shows which resolution was used for each climate model. The interpolated CMIP6 data were bias-adjusted using the respective aggregated observational data and then downscaled in multiple steps. Finally, the downscaled data (0.125°) were interpolated onto 0.1° with the first-order conservative remapping method to match the spatial resolution of the observational data. This interpolation was carried out instead of downscaling due to the small resolution difference from 0.125° to 0.1°.

The training period used for bias adjustment and statistical downscaling was 1981-2014 (34 years), constrained by the availability of observed data and historical CMIP6 simulations. After training, we applied the bias adjustment and downscaling on the climate simulations over historical and future periods using contiguous 36-yr segments. This decomposition is recommended to keep a similar sample size in the training and application steps. Bias adjustment was applied using a running window with a width of 31 days and moved over the annual cycle in steps of 1 day, where results for the central day of each window constitute the overall result. This application pattern aimed to improve the annual cycle representation and reduce discontinuities at time window edges, as suggested in previous studies (Gennaretti et al., 2015; Grenier, 2018; Themeßl et al., 2012; Thrasher et al., 2012).

3.2.5 Evaluation approach

We conducted a comprehensive evaluation of the BASD method's performance and the reliability of the BASD-CMIP6-PE dataset for the historical period. This assessment included comparing the simulations from both unadjusted and adjusted CMIP6 models with observational data and employing hydrological modeling. Our primary focus was on the evaluation of the models' capability in representing long-term statistical aspects, including mean values, extreme values, and the mean annual cycle. Moreover, we examined whether the BASD method influenced the preservation or alteration of the projected GCM trends (or changes) and the inter-model spread.

Model simulations and observations were compared using widely applied climate modeling statistics (e.g., mean error, correlation coefficient) and the Taylor diagram (Taylor, 2001) for the overlapping time period 1981–2014. Mean error was used to show biases in GCM data, while the correlation coefficient assessed models' capability to represent the mean annual cycle of observations, a crucial aspect for hydrological modeling purposes. The Taylor diagram was used to summarize the performance of both unadjusted and adjusted CMIP6 models in simulating long-term climatological spatial fields, including mean and extreme values of precipitation and temperature across the entire study domain. According to the Taylor diagram, the closer the model points are to the reference point, the better the model performance is with relatively high correlation and low standard deviation and root-mean-square error (RMSE) values. Extreme values were determined by calculating the 95th percentile for precipitation and maximum temperature and the 5th percentile for minimum temperature. Note that simulations and reference data were conservatively interpolated to a $2° \times 2°$ latitude-longitude grid to facilitate the comparison.

The reliability of both raw GCM data and BASD-CMIP6-PE dataset for describing the climatology of climate variables (pr, tas, tasmax, and tasmin) was also evaluated through hydrological modeling since the response of the watershed's flow is primarily driven by the variations in precipitation and temperatures. This approach was used in recent years to evaluate gauge-corrected precipitation datasets in data-scarce regions (Beck et al., 2020a; Brocca et al., 2020; Fernandez-Palomino et al., 2022; Satgé et al., 2020), as well as raw and bias-adjusted GCM simulation data (Hakala et al., 2018).

Hydrological simulations were performed using the Soil and Water Assessment Tool (SWAT) model (Arnold et al., 1998). SWAT is one of the world's most widely used ecohydrological models (Gassman et al., 2014; Tan et al., 2020), and it has been successfully applied for ecohydrological modeling of Andean and Amazonian catchments in Peru and Ecuador (Fernandez-Palomino et al., 2022, 2020). SWAT is a process-oriented, semi-distributed, and time-continuous river basin model applied to simulate hydrological processes as well as vegetation dynamics, nutrients, pesticides, and sediment loads within a basin (Arnold et al., 1998; Neitsch et al., 2011). We used the SWAT model that was set up for the Peruvian and Ecuadorian watersheds (total of 1,638,793 km², including 2675 river segments), calibrated and validated over 72 stream gauges in our previous study (Fernandez-Palomino et al., 2022). It was forced by the observational reference climate data listed in Table 3.2 and was proven to represent well the water budget closure of catchments as well as discharge dynamics, including mean, low, and high flows (Fernandez-Palomino et al., 2022). In this study, the SWAT model was run for 1981-2014 to derive the following streamflow series for the hydrological evaluation for a selected period (1984-2014):

- Qref, streamflow simulated by SWAT driven by the reference climate data listed in Table 3.2,
- Qgcm, the ensemble mean of the streamflow series simulated by SWAT employing raw GCM data (pr, tasmin, and tasmax) from 10 models.
- Qbasd, the ensemble mean of the streamflow series simulated by SWAT using BASD-CMIP6-PE climate data (pr, tasmin, and tasmax) from 10 models.

The comparison between Qgcm (Qbasd) and Qref reflects the reliability of the raw GCM data (BASD-CMIP6-PE dataset). For that, we used various comparison metrics based on hydrological signatures and hydrograph goodness of fit (Table 3.3), which were calculated using the daily values of the seasonal streamflow for the 1984-2014 period. The modified Kling-Gupta
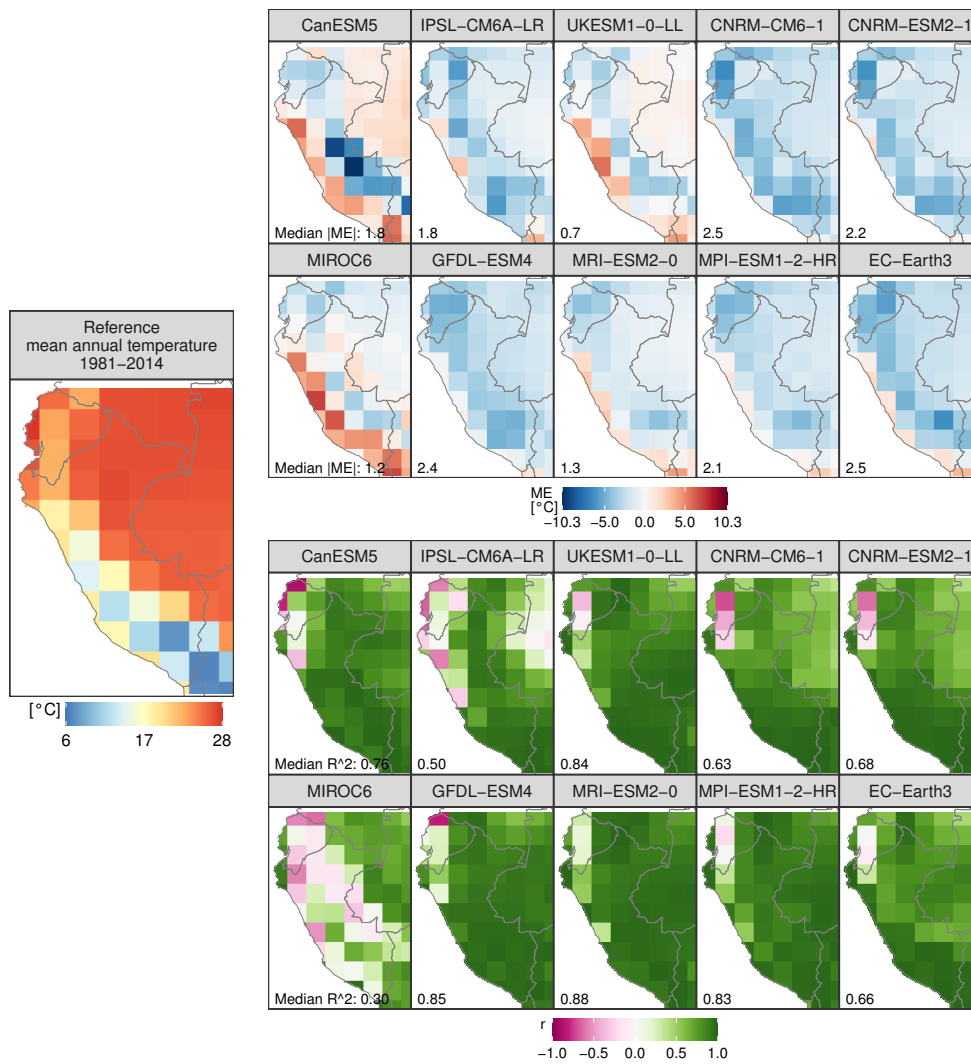
Figure 3.2: Performance of the unadjusted CMIP6 models in simulating mean temperature was compared with reference temperature data from PISCO-temperature for the 1981–2014 period. ME is the mean error, r is Pearson's correlation coefficient, and R^2 is the coefficient of determination. r and R^2 show the agreement between the simulated and observed mean annual temperature cycle.

efficiency (KGE) and percent bias (PBIAS) were used for assessing model skills in representing general discharge dynamics and over or underestimation tendencies, respectively; and percent biases in flow duration curve (FDC) low segment volume (S_{low}) and FDC high segment volume (S_{high}) for low flows and high flows, respectively. In this multicriteria evaluation, all aspects of the FDC and hydrographs are assessed, which is important for assessing the reliability of climate simulation data for hydroclimatic applications, including extremes (floods and low flows). The best-fit value for PBIAS, S_{low}, and S_{high} is 0, and the best fit for KGE is 1.

3.3 Data records

The BASD-CMIP6-PE dataset (Fernandez-Palomino et al., 2023b) is freely available under the CC BY 4.0 license at https://doi.org/10.5880/pik.2023.001. BASD-CMIP6-PE provides bias-adjusted and statistically downscaled CMIP6 climate projections, encompassing four meteorological variables: precipitation (pr), minimum temperature (tasmin), mean temperature (tas), and maximum temperature (tasmax). These data cover both the historical period (1850-
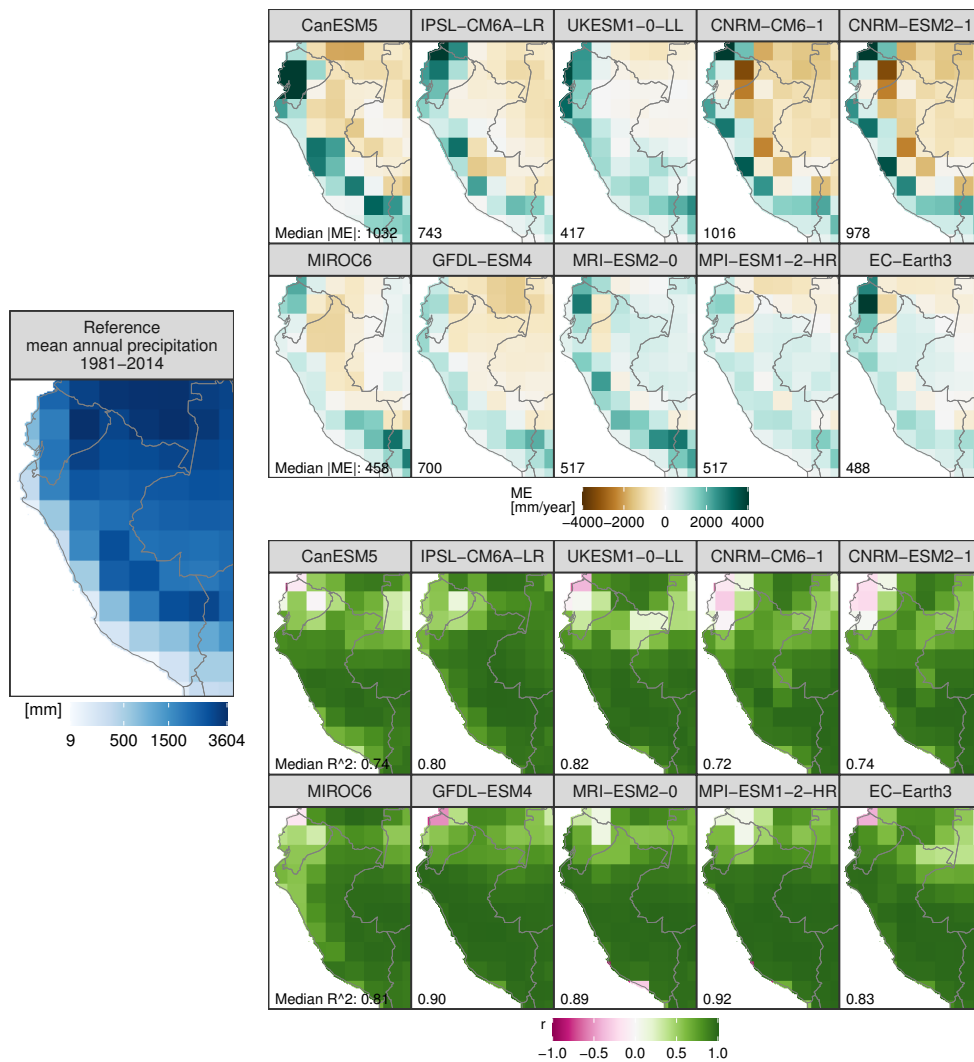
Figure 3.3: Performance of the unadjusted CMIP6 models in simulating precipitation is compared with reference precipitation data from RAIN4PE for the 1981–2014 period. ME is the mean error, r is Pearson's correlation coefficient, and R^2 is the coefficient of determination. r and R^2 show the agreement between the simulated and observed mean annual precipitation cycle.

2014) and future projections (2015-2100) under three different CMIP6 experiments (SSP1-2.6, SSP3-7.0, and SSP5-8.5) for 10 CMIP6-GCMs. Precipitation data is reported in millimeters (mm), while temperature data is presented in degrees Celsius (°C). The total size of the dataset is 374 GB.

The BASD-CMIP6-PE dataset is organized within a "daily" folder, denoting its availability at a daily temporal resolution. Within this directory, four subfolders are present: "historical" containing historical data, "ssp126" for SSP1-2.6, "ssp370" for SSP3-7.0, and "ssp585" for SSP5-8.5. Each of these subfolders further includes ten distinct folders, corresponding to different GCMs: CanESM5, IPSL–CM6A–LR, UKESM1–0–LL, CNRM–CM6–1, CNRM–ESM2–1, MIROC6, GFDL–ESM4, MRI–ESM2–0, MPI–ESM1–2–HR, and EC–Earth3. These folders store the data in the NetCDF format arranged by model, model member, experiment, variable, temporal resolution, and subset period, resulting in file names like "canesm5_r1i1p1f1_ssp126_pr_daily_2015_2020.nc".
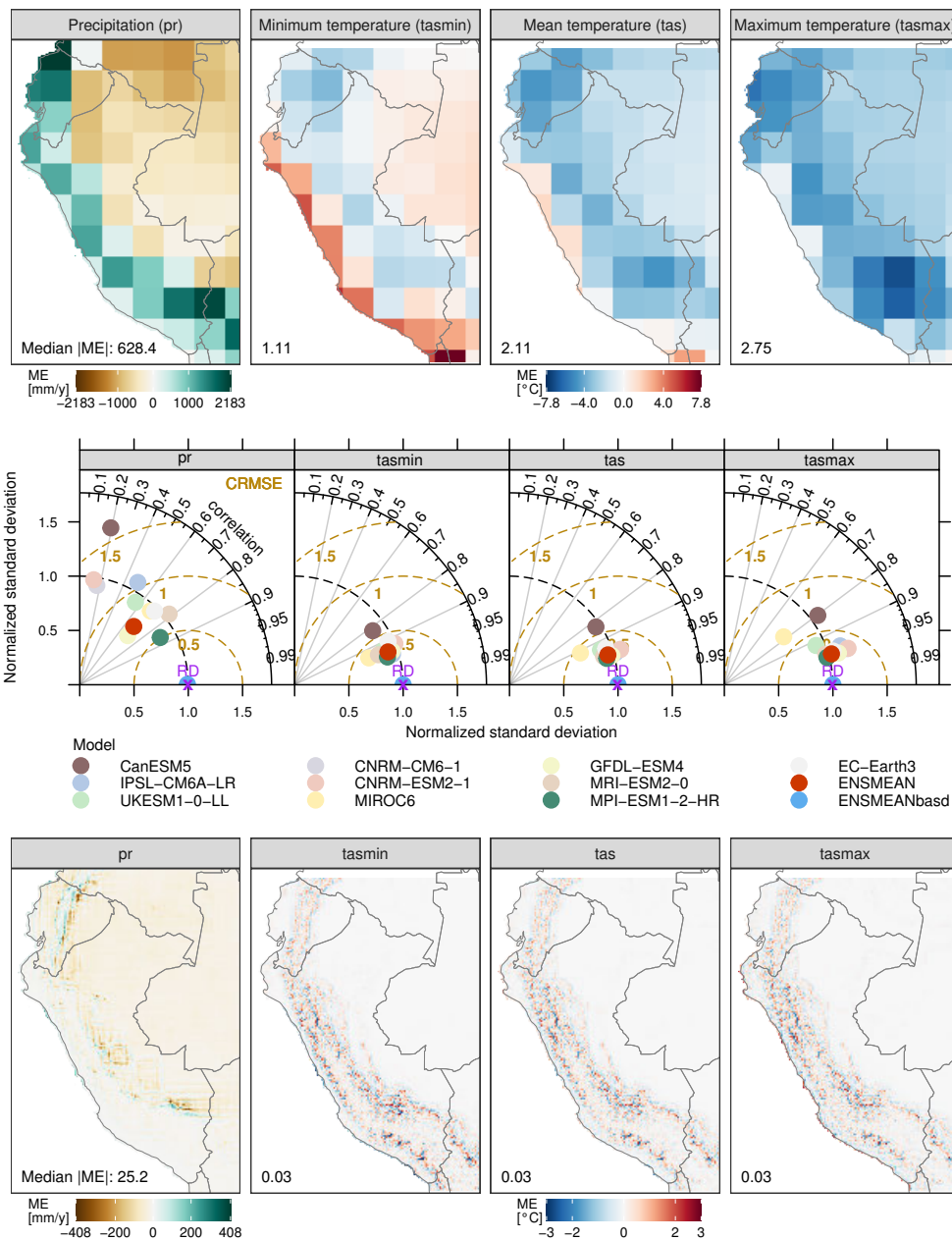
Figure 3.4: Mean Errors [ME] in (Top) unadjusted [ENSMEAN] and (Bottom) adjusted [ENS-MEANbasd] CMIP6 multimodel ensemble means, and (Middle) Taylor diagrams, both comparing simulated and reference climate means for 1981–2014. Adjusted models were excluded from the Taylor diagrams as they closely match ENSMEANbasd and the reference data. The bottom panel displays ME in ENSMEANbasd, computed by comparing BASD-CMIP6-PE and observational data at a 0.1° spatial resolution.

3.4 Technical validation

3.4.1 Comparison of unadjusted and adjusted CMIP6 models for the historical period

Mean climate and seasonality

Outputs of the atmospheric variables (pr, tasmin, tas, and tasmax) obtained from CMIP6-GCMs exhibit biases (Figs. 3.2-3.4) and limitations in capturing the mean annual cycle (Figs. 3.2, 3.3). Figure 3.4 (top panel) shows that CMIP6 models are generally biased cold (warm) for tas and tasmax (tasmin) over the Andes (Peruvian coastal areas) and tend to overestimate (under-
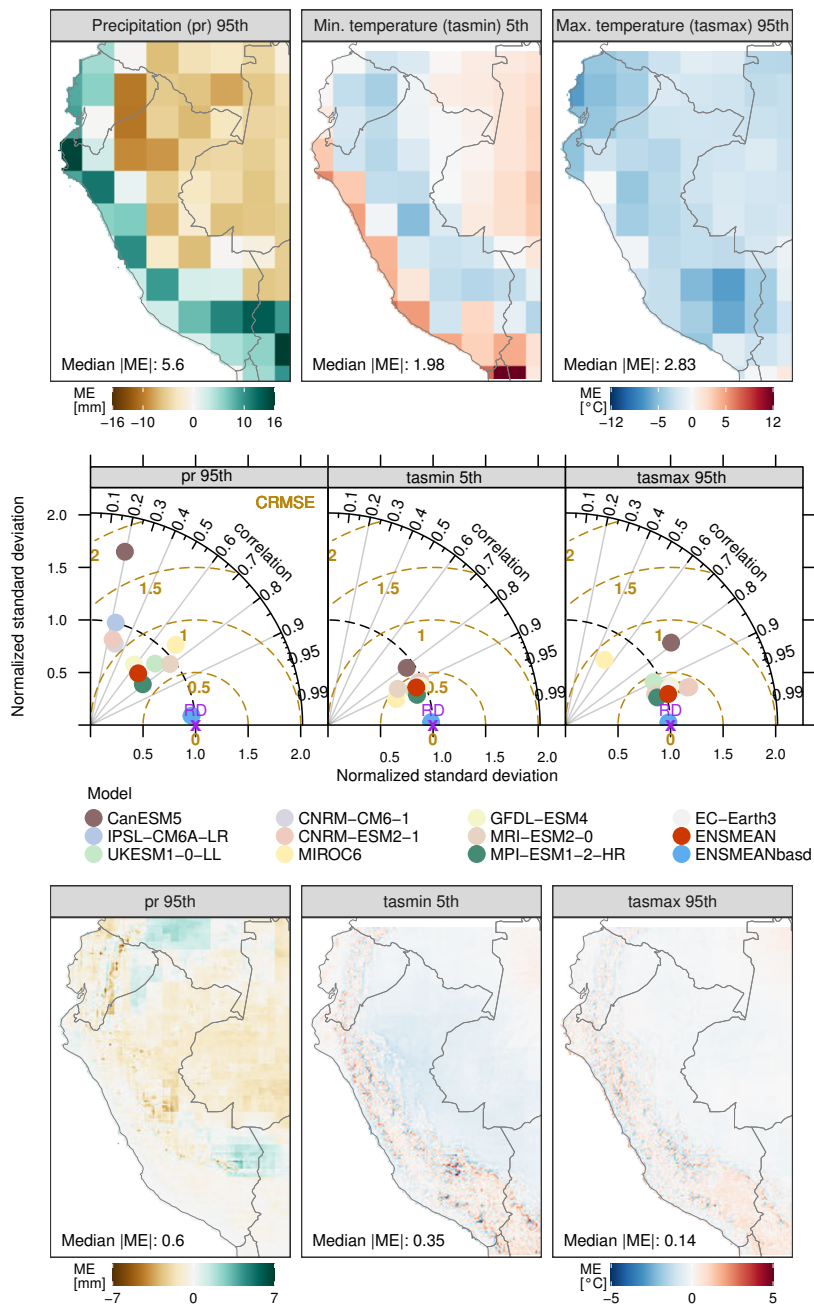
Figure 3.5: Mean Errors [ME] in (Top) unadjusted [ENSMEAN] and (Bottom) adjusted [ENSMEANbasd] CMIP6 multimodel ensemble means, and (Middle) Taylor diagrams, both comparing simulated and reference climate extremes for 1981–2014. Adjusted models were excluded from the Taylor diagrams as they closely match ENSMEANbasd and the reference data. The bottom panel displays ME in ENSMEANbasd, computed by comparing BASD-CMIP6-PE and observational data at a 0.1° spatial resolution.

estimate) pr over the Andes (Amazon lowlands). Models simulate better the annual cycle of precipitation (Fig. 3.3) than temperature (Fig. 3.2). However, models cannot capture the annual cycle of pr over Ecuador and northwest Amazon (Fig. 3.3). This is critical as unadjusted data from models are useless, for example, for evaluating the hydrological impact of Peruvian and Ecuadorian catchments under climate change. The Taylor diagrams (Fig. 3.4, middle panel) show that the GCMs simulate the spatial patterns of temperature (tasmin, tas, and tasmax)

better than the precipitation patterns. The models simulate a realistic spatial variability (standard deviation similar to that of reference) of precipitation, but the correlation between the spatial patterns is weak for most models (between 0.13 and 0.86). In the same Fig. 3.4 (middle panel), the Taylor diagram component values (correlation, standard deviation, and RMSE) indicate that the MPI-ESM1-2-HR (CanESM5) model has the best (worst) performance in simulating all atmospheric variables analyzed in this study. This distinction is emphasized by the general proximity of MPI-ESM1-2-HR points to the reference point, while CanESM5 points are situated farther away.

Overall, our results reveal that CMIP6 simulations (pr, tas, tasmin, and tasmax) are biased when compared to reference datasets over Peru and Ecuador, with larger biases over the Andes (Figs. 3.2-3.4). Such CMIP6 biases were also reported in previous studies (Almazroui et al., 2021; Arias et al., 2021b; Fiedler et al., 2020; Ortega et al., 2021). The precipitation overestimation is likely related to the too-pronounced double ITCZ in the models, a complex error in models produced by anomalous warming over the southern tropical Pacific in association with a misrepresentation of ocean-atmosphere couplings (Li and Xie, 2014; Ortega et al., 2021). Our results also reveal the limitation of CMIP6 models to reproducing the annual cycle of temperature and precipitation (Figs. 3.2, 3.3). CMIP6 models simulate the annual precipitation cycle better over regions with the strongest rainfall seasonality, such as the Peruvian Andes and lowlands, and poorly over equatorial regions, such as Ecuador and the northwest Amazon (Fig. 3.3). Poor representation of the annual precipitation cycle by CMIP6 models was also reported over Colombia (Arias et al., 2021b) and Northern Amazon (Firpo et al., 2022; Monteverde et al., 2022). Our results show significant limitations of CMIP6 models in reproducing regional climate features over equatorial regions and terrains with complex topography, such as the Andes. Further improvements of these models are necessary to permit their usage in impact studies.

To exclude the aforementioned limitations in climate model outputs, we applied the BASD method in order to adjust biases, increase spatial resolution, and improve representation of the annual cycle of atmospheric variables. The comparison of the ensemble mean of unadjusted (ENSMEAN) and adjusted (ENSMEANbasd) outputs of 10 GCMs shows that the BASD method largely reduced the biases in the GCM data for all climate variables (pr, tasmin, tas, and tasmax) as shown in Fig. 3.4 (middle panel). However, biases remain after the application of BASD at the spatial resolution of the reference datasets at 0.1° (Fig. 3.4, bottom panel). Small biases of precipitation remain over precipitation hotspots and small temperature biases (tasmin, tas, and tasmax) along the Andes. These results indicate that the application of BASD to the output of CMIP6 models is challenging in terrains with complex topography, such as the Andes. Despite some remaining biases, the purpose of the method - to create a dataset suitable for hydrological modeling - has been achieved, as the following hydrological section demonstrates.

Extreme values

The assessment of the models' performance in simulating precipitation and temperature extremes, both before and after applying BASD, is shown in Fig. 3.5. In this figure, Taylor diagrams compare the degree of similarity in spatial patterns of extremes, considering their correlation, RMSE, and standard deviation.

Results show that CMIP6 models, particularly CanESM5, exhibit poor performance in simulating extreme values, as indicated by Taylor diagrams (Fig. 3.5, middle panel). Figure 3.5 (top panel) shows notable biases in the unadjusted multimodel ensemble (ENSMEAN), with distinct spatial patterns. ENSMEAN tends to overestimate extreme precipitation along the Andes while underestimating it over the Amazon lowland regions. Moreover, it exhibits a warm bias in extreme minimum temperatures in coastal areas and the Brazilian lowlands, while concurrently revealing a cold bias in the transitional zone between the Andes and the Amazon. A cold bias is also observed in extreme maximum temperatures across the entire study area.

These biases are substantially reduced by the adjusted multimodel ensemble (ENSMEAN-basd) for all extreme climatic variables assessed herein, as demonstrated by Taylor diagrams (Fig. 3.5, middle panel) and the adjusted CMIP6 multimodel mean errors (Fig. 3.5, bottom panel). The results clearly show that the BASD method improves the variability and extremes of precipitation and temperature, thereby establishing the reliability of the BASD-CMIP6-PE dataset for studying the impacts of climate change on extreme events.
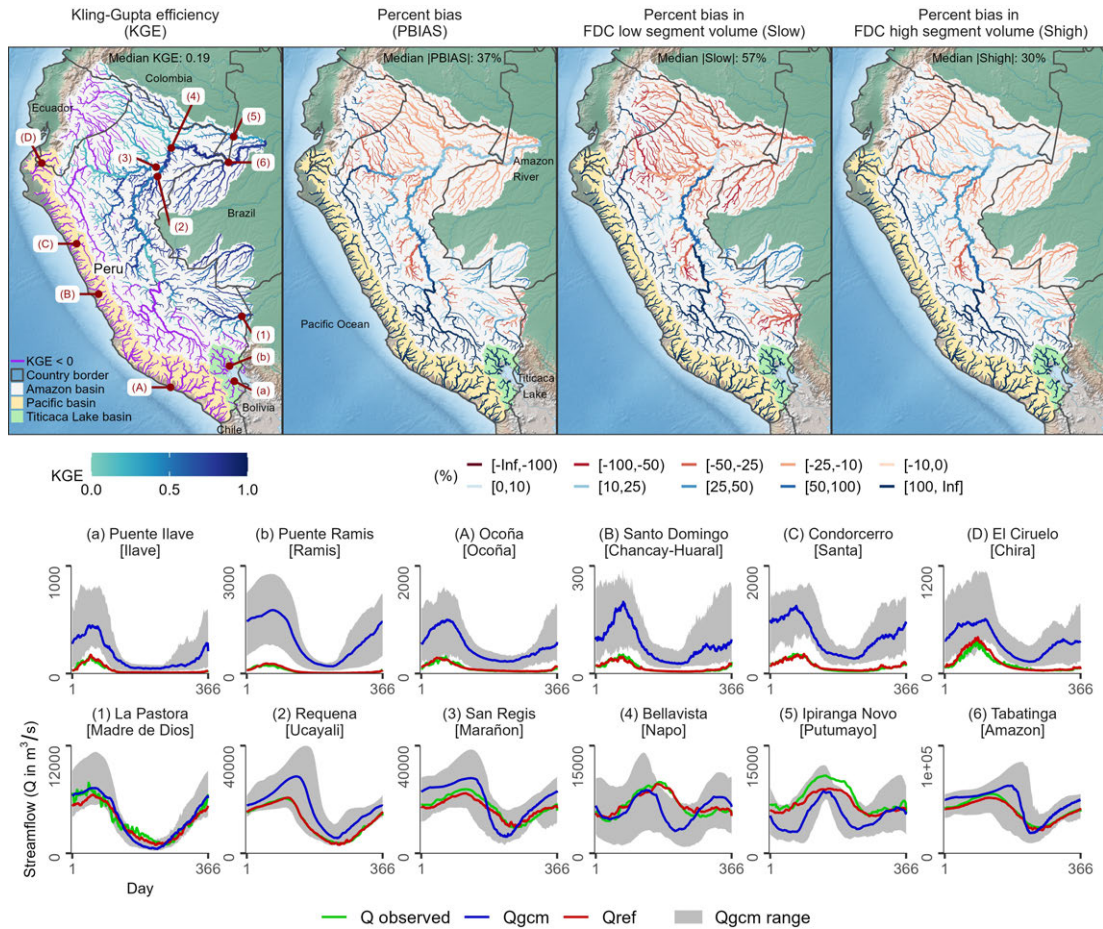
Figure 3.6: Comparison of simulated streamflow dynamics, including extreme events of both low flows (S_{low}) and high flows (S_{high}), from raw GCM simulations (Qgcm) and reference climate-based simulated streamflow (Qref). (top) Statistical metrics and hydrological signatures and (bottom) daily values of climatological seasonal streamflow (Q) in the period 1984–2014 for representative river catchments draining into the Titicaca Lake (a,b), the Pacific Ocean (A:D), and the Amazon River (1:6). Note that observed seasonal streamflow was computed only using the days with available streamflow data.

3.4.2 Hydrological evaluation of unadjusted and adjusted CMIP6 models for the historical period

In Fig. 3.6 (or Fig. 3.7), a comparison is presented between the long-term mean annual streamflow cycle at a daily resolution derived from Qgcm (or Qbasd) and that derived from Qref. The comparison is made through statistical metrics (KGE and PBIAS) and hydrological signatures (S_{low} and S_{high}). These figures also show climatological seasonal streamflow plots for representative river catchments draining into the Titicaca Lake, the Pacific Ocean, and the Amazon River.

In Fig. 3.6, the comparison metrics (with median values of KGE = 0.19, |PBIAS| = 37%, $|S_{low}|$ = 57%, and $|S_{high}|$ = 30%) alongside seasonal streamflow plots reveal significant discrepancies in the mean annual streamflow cycle between Qgcm and Qref. These disparities indicate that hydrological model simulations using raw GCM data tend to overestimate mean, low, and high flows along the Andean rivers while underestimating them over Amazonian lowland tributaries, especially in the northern Peruvian Amazon and Ecuadorian Amazon. Additionally, these simulations underrepresent seasonal streamflow in these regions, as evidenced by the seasonal plots for the Marañón, Napo, and Putumayo rivers. These issues underscore how biases and regional seasonal underrepresentation in GCM simulations impact the accurate
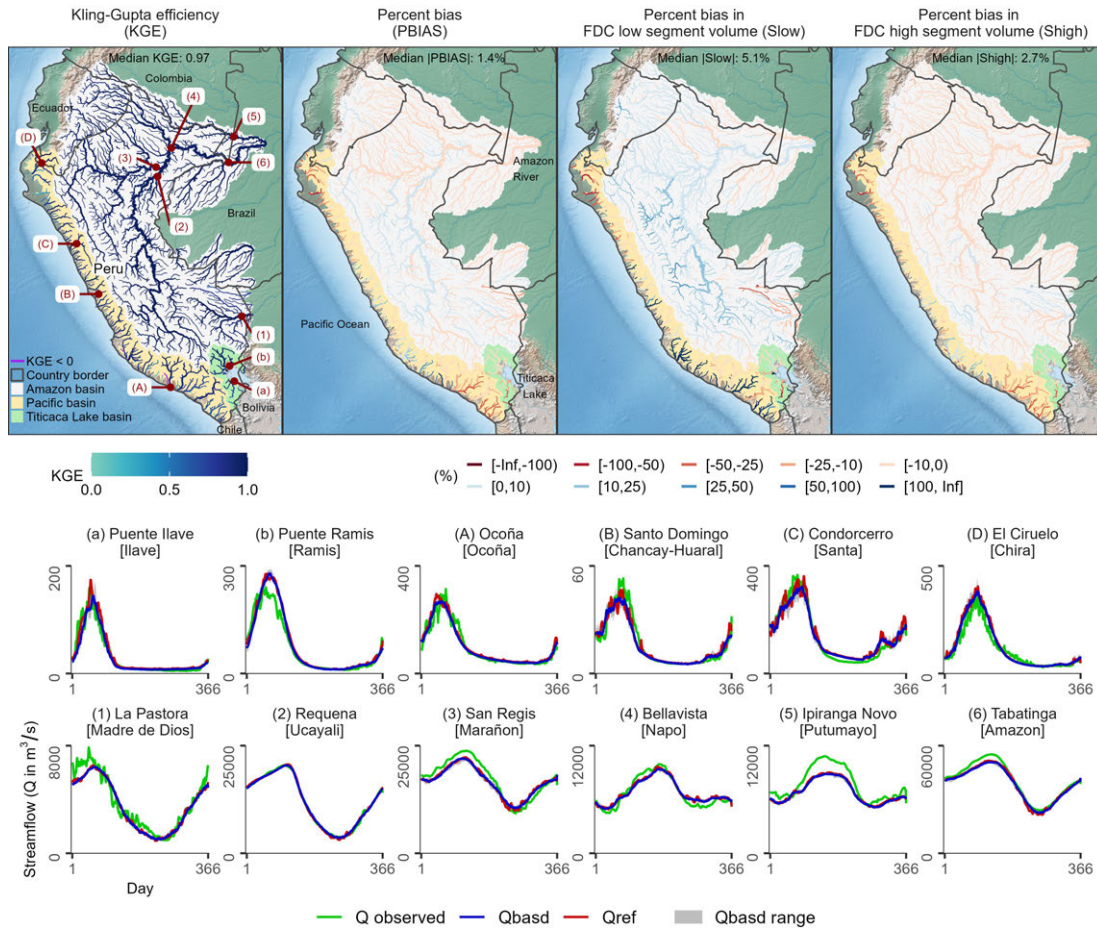
Figure 3.7: Comparison of simulated streamflow dynamics, including extreme events of both low flows (S_{low}) and high flows (S_{high}), from adjusted GCM simulations (Qbasd) and reference climate-based simulated streamflow (Qref). (top) Statistical metrics and hydrological signatures and (bottom) daily values of climatological seasonal streamflow (Q) in the period 1984–2014 for representative river catchments draining into the Titicaca Lake (a,b), the Pacific Ocean (A:D), and the Amazon River (1:6). Note that observed seasonal streamflow was computed only using the days with available streamflow data.

representation of hydrological processes, rendering them unsuitable for hydrological impact assessments.

In Fig. 3.7, median KGE = 0.97 and median |PBIAS| = 1.4% demonstrate good agreement between Qbasd and Qref. This agreement is further supported by long-term mean seasonal streamflow plots for representative rivers across the three drainage systems. Low KGE ($<$ 0.5) and large negative |PBIAS| values ($< -25\%$) indicate relatively poor BASD performance over northern and southern Peruvian arid coastal areas in the Pacific drainage system. It is worth noting that these areas have mean annual precipitation of less than 15 mm and are not relevant for runoff processes. Median $|S_{low}|$ = 5.1% and median $|S_{high}|$ = 2.7% also indicate that overall low and high flows are well represented, suggesting that the BASD method is able to represent also precipitation extremes to some extent. However, there is a tendency to overestimate low flows over river segments in the eastern slopes of the Peruvian Andes, especially over mountainous catchments.

Overall, the hydrological comparisons reveal much better agreement between Qbasd and Qref (median KGE = 0.97) compared to Qgcm and Qref (median KGE = 0.19) across different hydroclimate regimes in Peru and Ecuador. This indicates that the BASD method is effective, and the BASD-CMIP6-PE dataset is reliable for hydroclimatic applications, including extremes
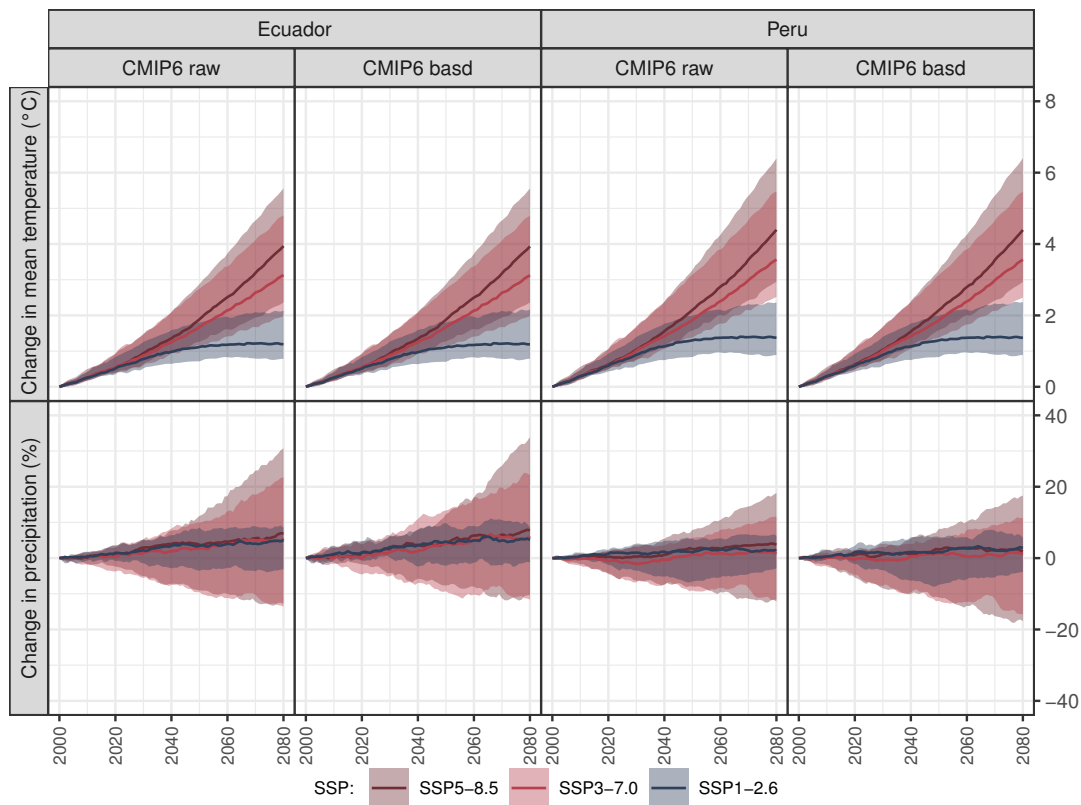
Figure 3.8: Comparison of projected multimodel median changes and spreads in precipitation and mean temperature for Ecuador and Peru using raw (CMIP6 raw) and adjusted (CMIP6 basd) GCM simulations.

such as floods and droughts. However, it is important to keep in mind that the hydrological evaluation was performed for the period where the BASD method was trained, and our evaluation results could be overconfident. Nevertheless, we believe that our hydrological evaluation is still plausible in the study area featured by data scarcity and lack of long-term time series.

3.4.3 Projected changes and inter-model spread

The assessment of the BASD method's impact on preserving or altering the projected GCM trends and the inter-model spread is presented in Fig. 3.8. This figure presents the projected multimodel median changes and spreads in precipitation and mean temperature for both Ecuador and Peru, using both unadjusted and adjusted CMIP6 data.

Results show that temperature trends and spreads show a significant degree of similarity between the two datasets in each country, highlighting the effectiveness of the BASD method in preserving future temperature trends. For Ecuador, the projected changes in mean temperature for the end of the century (2065-2095) relative to the reference period of 1985-2015, based on both raw and adjusted multimodel median data, are 1.2 °C (SSP1-2.6), 3.1 °C (SSP3-7.0), and 3.9 °C (SSP5-8.5). For Peru, these values are 1.4 °C (SSP1-2.6), 3.6 °C (SSP3-7.0), and 4.4 °C (SSP5-8.5).

However, the projected multimodel median changes and spreads for precipitation undergo minor modifications. The differences in projected changes for the end of the century, based on raw and adjusted CMIP6 data, are less than 2% across all SSPs for both Ecuador and Peru. These small differences suggest that the BASD method alters precipitation patterns without adversely affecting the ensemble median. Projected multimodel median changes in precipitation can range up to 8% in Ecuador and 3% in Peru, with variations within these countries.

It is noteworthy that intermodel spread increases towards the distant future, with low uncertainty under SSP1-2.6 and high uncertainty under SSP5-8.5.

In summary, our analysis indicates that the BASD method effectively preserves projected temperature trends while making only minor adjustments to precipitation patterns. This underscores the reliability of the BASD-CMIP6-PE dataset for evaluating regional and local hydrological impacts of climate change.

3.5 Code availability

The software used for bias adjustment and statistical downscaling is ISIMIP3BASD v2.5 (Lange, 2021b).

Author contributions

C.A.F.P. conceived the study and wrote the first version of the manuscript with inputs from all co-authors, and all authors contributed significantly to further revisions.
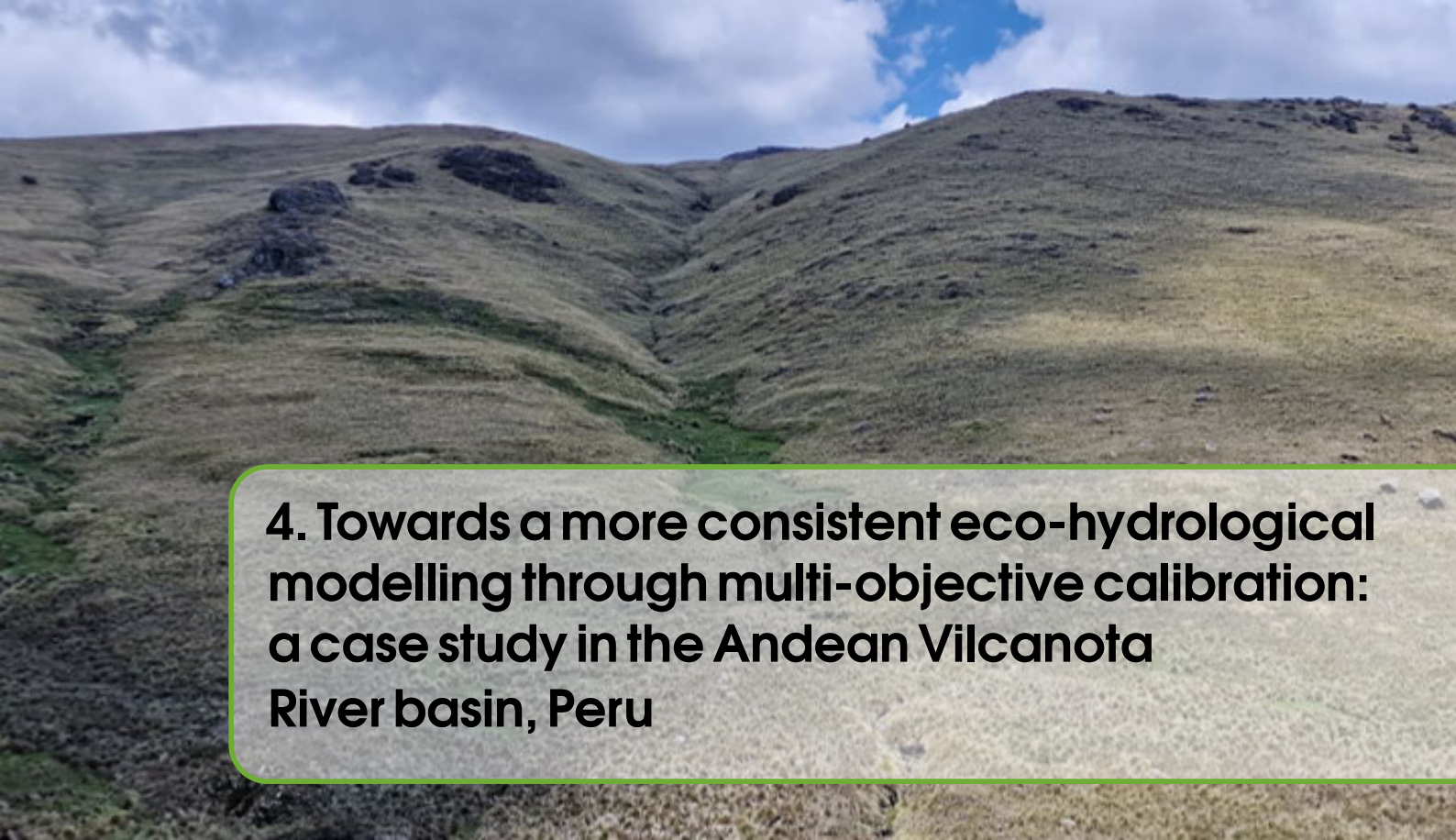
Competing interests

The authors declare no competing interests.

This paper was edited by Dr. Elizabeth Miller and reviewed by three anonymous referees.

4. Towards a more consistent eco-hydrological modelling through multi-objective calibration: a case study in the Andean Vilcanota River basin, Peru

Abstract

Most hydrological studies rely on a model calibrated using discharge alone. However, judging the model reliability based on such calibration is problematic, as it does not guarantee the correct representation of internal hydrological processes. This study aims (a) to develop a comprehensive multi-objective calibration framework using remote sensing vegetation data and hydrological signatures (flow duration curve – FDC, and baseflow index) in addition to discharge, and (b) to apply this framework for calibration of the Soil and Water Assessment Tool (SWAT) in a typical Andean catchment. Overall, our calibration approach outperformed traditional discharge-based and FDC signature-based calibration strategies in terms of vegetation, streamflow, and flow partitioning simulation. New hydrological insights for the region are the following: baseflow is the main component of the streamflow sustaining the long dry-season flow, and pasture areas offer higher water yield and baseflow than other land-cover types. The proposed approach could be used in other data-scarce regions with complex topography.

4.1 Introduction

The understanding of hydrological processes and vegetation dynamics within a basin is crucial for better water resources management. For this purpose, hydrological models that integrate hydrological processes, vegetation, and biogeochemical cycles (carbon, nitrogen, and phosphorus) have been used, often called eco-hydrological river basin models (Krysanova and Arnold, 2008). Examples of well-supported models are the Soil and Water Assessment Tool (SWAT, Arnold et al., 1998), Soil and Water Integrated Model (SWIM, Krysanova et al., 1998), Variable Infiltration Capacity (VIC, Liang et al., 1994), and Hydrological Predictions for the Environment (HYPE, Lindström et al., 2010). In this study, SWAT is applied since it is internationally accepted as a robust tool for interdisciplinary modeling of basin water resources (Abbaspour et al., 2017; Gassman et al., 2007) and ecosystem services (Francesconi et al., 2016). It has been applied and evaluated in diverse climates from arid and semi-arid regions (Brouziyne et al., 2017; Jajarmizadeh et al., 2017) to wet and tropical areas (Alemayehu et al., 2017; Strauch and Volk, 2013).

Regardless of the choice of hydrologic model, one primary task in any hydrological modeling is the determination of model parameters during the model calibration procedure, owing to the mismatch between model complexity and available data (Devak and Dhanya, 2017; Razmkhah et al., 2017). Estimation of model parameters is commonly performed using manual and automatic calibration approaches, with discharge-related measures (e.g., Nash–Sutcliffe efficiency, NSE) most commonly used as the objective function because discharge at the basin outlet integrates all hydrological processes upstream. However, it has been argued that model calibration based solely on discharge does not guarantee the credibility of a hydrological model since the water balance components can be misrepresented despite the performance statistics being accurate (Acero Triana et al., 2019; Guse et al., 2016; Hattermann et al., 2005; Larabi et al., 2018; Pfannerstill et al., 2017; Pokhrel and Yilmaz, 2012). Recognizing this deficiency, other strategies have focused on improving the calibration to better represent hydrological processes and system dynamics. For this, hydrological signatures mostly derived from streamflow time series, e.g., the flow duration curve (FDC), have been used. The application of signatures related to FDC provides more information about the hydrological behaviors of the modeled basin (Hrachowitz et al., 2014) and their underlying processes (Gupta et al., 2009; Yilmaz et al., 2008). FDC has often been used for model evaluation (Hrachowitz et al., 2014; Pfannerstill et al., 2017; Pokhrel and Yilmaz, 2012; Yilmaz et al., 2008) and lately as an objective in model calibration (Chilkoti et al., 2018; Sahraei et al., 2020; Shafii and Tolson, 2015). These studies have demonstrated that signature-based calibration approaches (using discharge and FDC) lead to a more accurate discharge simulation and the reduction of predictive uncertainty. However, Shafii et al. (2017) argued that these approaches do not necessarily guarantee correct flow partitioning among the different flowpaths, which is critical when modeling hydrology-related processes like solute transport, erosion, surface runoff, and baseflow contribution. Therefore, to properly reproduce flow partitioning, the inclusion of another hydrological signature such as the baseflow index (the ratio of long-term mean base flow to total streamflow) in the multi-objective calibration framework is proposed in this study. The baseflow index represents the baseflow component of streamflow, which is critical for regulating seasonal distribution of river flows and is associated with climatic and physiographic characteristics of the basin (Beck et al., 2013; Mohammed and Scholz, 2018; Singh et al., 2019). Baseflow, or the baseflow index, is crucial to develop appropriate water resources management strategies, such as aquatic ecosystem preservation, hydropower generation, and low-flow forecasting (Beck et al., 2013; Singh et al., 2019). Previously mentioned and proposed calibration approaches have focused mainly on the identification of physical parameters related to streamflow, evapotranspiration, and flow components. However, additional identification of vegetation parameters is crucial for models integrating vegetation dynamics. Indeed, leaf area index (LAI) is a key driver of the water balance of a landscape and is considered in SWAT for subsequent estimation of other processes, such as evapotranspiration, biomass accumulation, sediment, baseflow, and surface runoff (Ma et al., 2019). Only a few hydrological studies in general and SWAT-related publications in particular have considered the combined model calibration of LAI and streamflow dynamics and proved that this calibration leads to improved streamflow and evapotranspiration

simulations (Alemayehu et al., 2017; Ha et al., 2018; Rajib et al., 2018; Strauch and Volk, 2013). These studies also showed the utility of remotely sensed LAI data to calibrate the SWAT LAI-related parameters (i.e., plant parameters) in data-scarce basins. It is important to mention that the SWAT LAI estimation is based on heat units (Neitsch et al., 2011), and for that, the total number of heat units needed to bring the plant to maturity (PHU_PLT) must be estimated by the user for the vegetation growth simulation. Previous studies have used satellite-based LAI to identify SWAT plant parameters considering a constant PHU_PLT value for each plant type throughout the basin. However, this could be critical, especially in basins with complex topography – in particular high altitudinal differences – since the air temperature (biophysical variable) that controls the PHU_PLT (Neitsch et al., 2011) depends on the altitude. To overcome this, we used the satellite-based LAI data to identify not only plant parameters but also PHU_PLT for each plant in each hydrological response unit (HRU). Moreover, we investigated the relationship between the elevation and PHU_PLT, which could be useful for application in other data-scarce regions with complex topography.

In general, some previous studies have reported the benefits of incorporating hydrological signatures (e.g., FDC signatures) and remote sensing data (e.g., LAI) in the calibration of hydrological models (Chilkoti et al., 2018; Ha et al., 2018; Rajib et al., 2018; Sahraei et al., 2020; Shafii and Tolson, 2015). However, to the best of our knowledge, no previous study has taken into account both datasets for hydrological model calibration. We consider that inclusion of these variables, in addition to streamflow, in the calibration can improve the model reliability in representing the hydrological system. Hence, one of the objectives of this study is to develop a multi-objective calibration framework that exploits the benefits of using both hydrological signatures and satellite-based LAI data for eco-hydrological models. This study is the first of its kind considering these benefits for a more realistic hydrological modeling not only of streamflow but also of vegetation dynamics and flow partitioning. As such, we hope to contribute to hydrological modeling science with a new way of understanding the eco-hydrological processes of basins with complex topography for efficient water resource management.

We conducted our study in the tropical Andes of Peru where there is a paucity of research. Most existing studies related to Andes hydrology have focused mainly on Andean basins dominated by páramo ecosystems, which span the Andean region of Venezuela, Colombia, Ecuador, and northern Peru (Buytaert et al., 2007; Carrillo-Rojas et al., 2019; Guzmán et al., 2015; Hill et al., 2018; Mosquera et al., 2015). Only a few studies have focused on the hydrology of Peruvian Andean basins, and most of these in small catchments dominated by a glacier (Somers et al., 2019), forest (Clark et al., 2014), páramo and puna biome (Ochoa-Tocachi et al., 2016). Therefore, another objective of this study is to contribute to the basic understanding of hydrological processes of the tropical Andes of Peru. To this end, we selected the Vilcanota River basin (VRB), which is dominated by land uses such as pasture of the puna biome, forest, and agriculture, to better understand its hydrology (e.g., water budget) and to analyze the hydrological services offered by each land-use type regarding the water yield and baseflow.

For this purpose, our proposed novel multi-objective calibration framework for eco-hydrological models such as SWAT, and for basins with complex terrain such as the VRB, consists of a step-wise calibration scheme. First, SWAT LAI-related parameters are calibrated using satellite LAI data. In the second step, parameters related to streamflow, evapotranspiration, and flow components are calibrated. For the latter step, we propose the inclusion of the baseflow index in addition to discharge-related performance metrics and signatures based on FDC within a multi-objective calibration approach to better constrain the flow partitioning during the calibration process. This approach is compared to conventional discharge-based and signature-based calibration approaches in order to test the model's ability to simulate vegetation dynamics, streamflow, and flow partitioning in the Andean VRB. Furthermore, we address how streamflow calibration strategies impact parameter identifiability and equifinality.
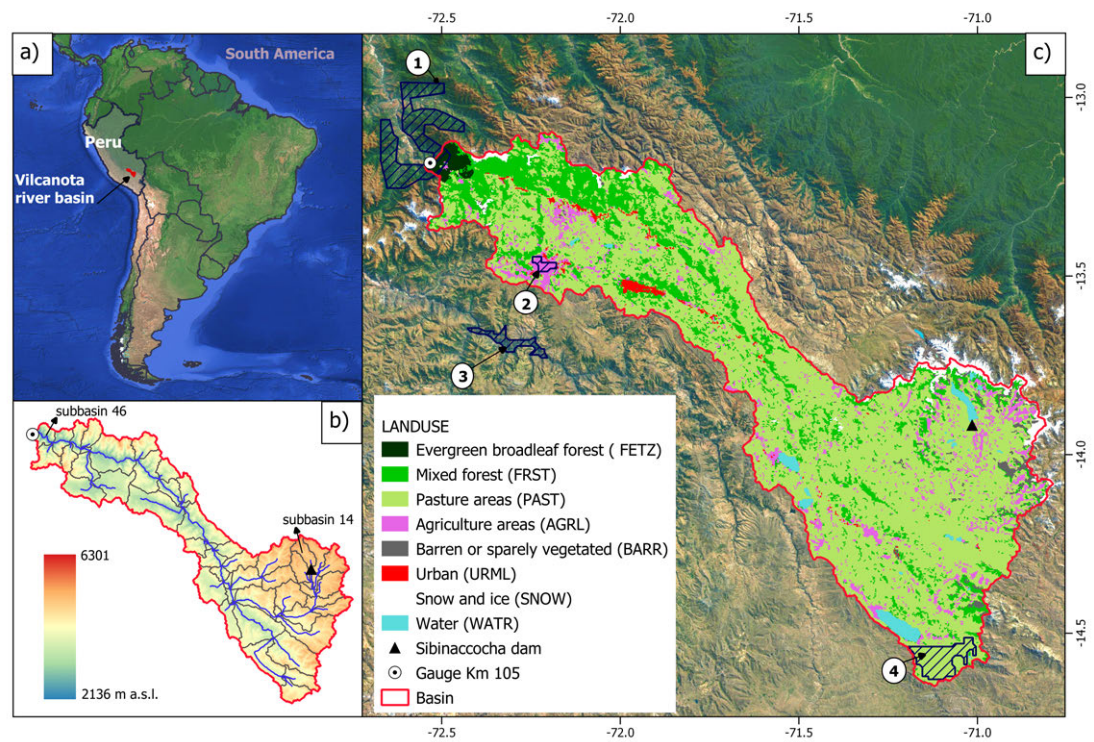
Figure 4.1: (a) Location of the Vilcanota River Basin (VRB); (b) Terrain elevation, sub-basins, and river network ; and (c) land-use map. Dashed areas represent sample site locations for the major vegetation classes (1: FETZ, 2: AGRL, 3: FRST and 4:PAST) which were used to mask the MODIS (Moderate Resolution Imaging Spectroradiometer) LAI.

4.2   Materials and methods

4.2.1   Study area

The VRB is located in the southern Andes of Peru in the Cuzco region (Fig. 4.1). Its drainage area is 9617 km^2, and the topography within the basin is characterized by a terrain with steep slopes and elevations that range from 2136 to 6301 m a.s.l. Predominant soils are Lithosols (67%) and Kastanozems (23%) (FAO-UNESCO, 1988). The land use is dominated by natural pasture (68%) with a minor contribution of mixed forest (15%), agriculture (8%), and evergreen forest (4%). The latter mainly spans the area which is close to the basin outlet (Fig. 4.1) and experiences higher amounts of precipitation. The annual mean precipitation is 748.5 mm/year (1985–2015), with more than 80% of the rainfall occurring during the rainy season (October–March). Hydrologically, VRB shows high variability of daily discharge, ranging from 20 m^3/s in the dry season to 1100 m^3/s in the rainy season, and an average daily discharge of 120 m^3/s (1985–2015 period). In VRB, there are several natural lakes, but since 1996, Lake Sibinaccocha (Fig. 4.1) has been dammed for water storage during the wet season and to supply water to the Machu Picchu Hydroelectric Power Plant (EGEMSA company) during the dry season (Catacora-Acevedo, 2008). This dam has 120 hm^3 active storage volume with a small sub-drainage basin surface (137 km^2 being 1.4% of the VRB area). The Vilcanota River provides water for drinking, irrigation, and energy production, hence understanding the hydrologic system and accurate simulation of streamflow are important for appropriate water resources management.

4.2.2   SWAT model

The SWAT model is a process-oriented, semi-distributed, and time-continuous river basin model used to simulate hydrological processes as well as vegetation dynamics, nutrients, pesticides, and sediment loads within a basin (Arnold et al., 1998; Neitsch et al., 2011). It is also possible to

include water management activities such as reservoirs for hydrological simulation of managed basins (Neitsch et al., 2011). SWAT divides a basin into sub-basins, which are then further subdivided into HRUs representing unique combinations of land use, soil type, and slope classes (Neitsch et al., 2011). SWAT differentiates between the land phase that controls the water, sediment, and solute loads to the main channel in each sub-basin and the routing phase that defines water, solute, and sediment movement through the channel network to the basin outlet (Arnold et al., 1998; Neitsch et al., 2011).

The water balance computation is performed at the HRU level considering four water storage types (snow, soil profile, and shallow and deep aquifers), as follows:

$$\Delta S = \sum_{i=1}^{N} (P - \text{WYLD} - \text{ET} - \text{losses}) \tag{4.1}$$

where ΔS is the change in water storage (mm), N is the time in days, and P, WYLD, ET, and losses are the amounts of precipitation (mm), water yield (mm), evapotranspiration (mm), and groundwater losses (mm), respectively. Water yield (WYLD) is given by the contribution of surface runoff (Qsurf), lateral flow (Qlat), and return flow (Qgw) from the aquifers (shallow and deep).

In SWAT, the vegetation dynamics (e.g., LAI) are simulated based on the simplified version of the Environmental Policy Integrated Climate (EPIC) plant growth model (Neitsch et al., 2011). The vegetation growth is simulated based on daily cumulative heat units (plant heat requirements) reflecting the fact that plant growth only occurs on the days when the daily mean temperature exceeds the base temperature for growth (Neitsch et al., 2011). This means that temperature is the main vegetation growth controlling factor in SWAT but is restricted by temperature, water, and nitrogen or phosphorus stress (Neitsch et al., 2011). For a detailed description of the SWAT vegetation module, readers are advised to read Neitsch et al. (2011).

In this study, we used SWAT-T (Alemayehu et al., 2017), a modified SWAT version based on SWAT 2012 (Rev. 627), which provides an improved vegetation growth module for a better simulation of plant growth dynamics in tropical regions. SWAT-T uses the soil moisture index – a quotient of rainfall and potential evapotranspiration – as an indicator to initiate a new growth cycle within a predefined period, such as the months when the rainy season starts, e.g., October to November for Andean basins. This SWAT-T feature was introduced to overcome SWAT's shortcomings in simulating the seasonal growth cycles for trees and perennials in the tropics, where rainfall rather than temperature is the dominant plant growth controlling factor (Alemayehu et al., 2017; Strauch and Volk, 2013). Moreover, SWAT-T uses a logistic function to simulate the LAI curve during the senescence stage (Strauch and Volk, 2013), instead of the linear decreasing LAI curve which could underestimate evapotranspiration (Wei et al., 2018). SWAT-T is referred to as SWAT in this paper.

4.2.3 Input data

The inputs (e.g., topography, land use, soil, and meteorology) and their sources are summarized in Table 4.1. As geographical input data, a digital elevation model (DEM) of 90 m resolution, a land-use map obtained from the European Space Agency and Climate Change Initiative – Land Cover Project (ESA CCI-LC), and a soil map from the Harmonized World Soil Database (HWSD) that includes soil properties were used for the hydrological model. The daily gridded PISCO (Peruvian Interpolated data of SENAMHI's Climatological and Hydrological Observations) meteorological forcing data (precipitation, and maximum and minimum temperature) for driving SWAT model simulations was used, as provided by the National Service of Meteorology and Hydrology of Peru (SENAMHI). Controlled outflow data from the Sibinaccocha Dam was used to consider its impact on downstream runoff since 1996.

4.2.4 Reference data for model calibration and verification

The leaf area index

The satellite-based Moderate Resolution Imaging Spectroradiometer (MODIS) LAI product (Yuan et al., 2011) was used as a reference to calibrate LAI dynamics of perennial plants.

Table 4.1: Data type, resolution, and data source.

Data type	Resolution	Description/source
Topography	90 m	Digital elevation of the Shuttle Radar Topography Mission (SRTM V4.1) product (Jarvis et al., 2008) (`http://srtm.csi.cgiar.org/`)
Land use	300 m	Land-use classification representative for the year 2010 obtained from ESA CCI-LC (`http://maps.elie.ucl.ac.be/CCI/viewer/`)
Soil	1000 m	Horizon-specific soil properties for each soil type based on the HWSD (Abbaspour and Ashraf Vaghefi, 2019)
Soil thickness	1000 m	Gridded global data of soil thickness (Pelletier et al., 2016) used to implement variable soil thicknesses at HRUs
Hydrologic soil group	250 m	Global gridded hydrologic soil group data (Ross et al., 2018) used to update the curve number (CN) parameter at HRUs after the model creation. This step helped to identify appropriate CN values, mainly in current urban areas
Temperature	Daily/10 km (1981–2016)	Gridded temperature (maximum and minimum) dataset for Peru (PISCO temperature V1.1, Huerta et al., 2018) provided by SENAMHI (`ftp://publi_dgh2:123456@ftp.senamhi.gob.pe/`)
Precipitation	Daily/10 km (1981–2016)	Gridded rainfall dataset for Peru (PISCO precipitation V2.1, Aybar et al., 2020) provided by SENAMHI (`ftp://publi_dgh2:123456@ftp.senamhi.gob.pe/`)
Reservoir	Daily (1996–2015)	Controlled outflow data from Sibinaccocha Dam obtained from Electricity Generation Company of Machupicchu (EGEMSA)
Discharge	Daily (1958–2015)	Flow data at Km-105 hydrological station (EGEMSA)
LAI	8 d/1000m (2000–2016)	Improved MODIS LAI data based on the MODIS collection 5 LAI product (MOD15A2) (Yuan et al., 2011) (`http://globalchange.bnu.edu.cn/research/lai`)

MODIS LAI has been proven capable of reproducing vegetation timely and accurately (Ma et al., 2019; Yuan et al., 2011) and has been used successfully in the calibration and/or validation of SWAT plant parameters (Alemayehu et al., 2017; Ha et al., 2018; Rajib et al., 2018; Strauch and Volk, 2013).

To derive the reference LAI data, we selected 200 pixels for pasture, 100 for the mixed forest, 405 for the evergreen forest, and 35 for agriculture, using as a mask the corresponding representative area (polygon) defined in Fig. 4.1 with the help of the land-use map and Google Earth images. Then, from these subsets, we derived the 8-day median LAI time series for each of the land-use types. Note that the identified representative areas for evergreen forest and mixed forest span areas outside of the basin (Fig. 4.1). This was necessary to obtain MODIS LAI pixels with better LAI temporal patterns because forest areas located inside the basin mostly present noisy LAI time series with breaks, which could be attributed to the cloud contamination of the MODIS LAI in those areas.

Streamflow

Daily observed discharge series (1958–2015) at the km-105 gauging station located at the VRB basin outlet was used (Fig. 4.1) for model calibration and validation of streamflow simulation.

4.2.5 SWAT model setup

The SWAT model was set up for the VRB based on the available input data listed in Table 4.1. The model includes one reservoir, 53 sub-basins, and 320 HRUs (Fig. 4.1). The modified Soil Conservation Service Curve Number method, the Hargreaves method, and the variable storage

method were used to simulate surface runoff and infiltration, potential evapotranspiration, and river flow routing, respectively. The Sibinaccocha Reservoir outflow was simulated using a predefined daily outflow option in SWAT to account for the effects of this dam on downstream runoff. For more details about the SWAT model configuration, see Neitsch et al. (2011).

The periods considered for model warm-up, calibration, and validation for simulation of LAI were 2001–2004, 2005–2010, and 2011–2015, and those for streamflow were 1981–1984, 1985–1990, and 1991–2015, respectively. Note that the model calibration for streamflow was carried out in the pre-damming period of the river, while the LAI calibration and validation periods were constrained based on LAI data availability.
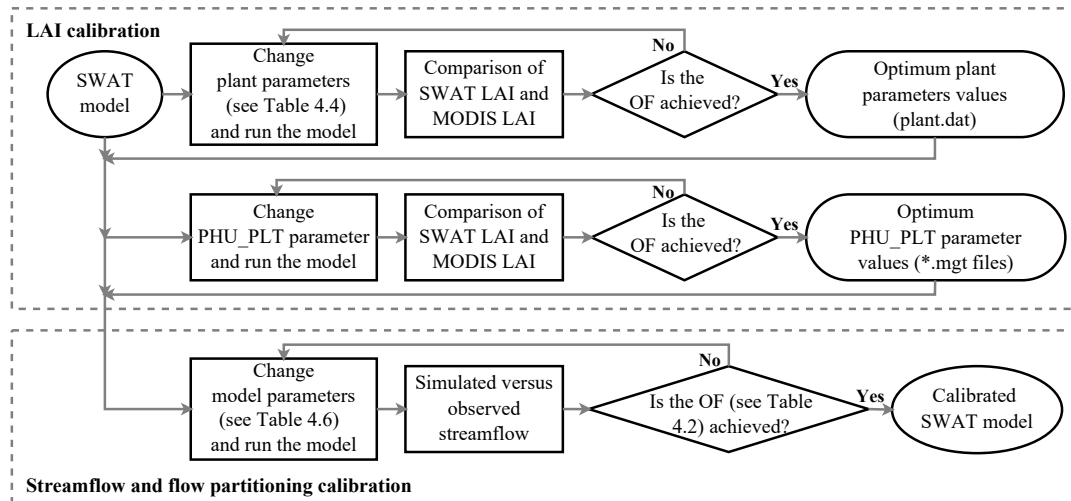
Figure 4.2: Flowchart of the SWAT model calibration framework. OF: objective function, PHU_PLT: total number of heat units needed to bring the plant to maturity. In the case of LAI calibration, the Nash-Sutcliffe efficiency (NSE) is the OF. The OF for streamflow and flow partitioning calibration is defined in Table 4.2 for each calibration strategy applied in this study.

4.2.6 SWAT calibration and evaluation framework

We propose the following step-wise framework for SWAT model calibration for basins with complex terrain (Fig. 4.2).

First, SWAT LAI-related parameters are calibrated using 8-day MODIS LAI as a reference for each perennial tropical vegetation type (e.g., pasture, mixed forest, forest evergreen, and agriculture) at the HRU level. To do so:

(a) The simulated LAI is calibrated against MODIS LAI to identify SWAT LAI-related parameters (see Section 4.3.2) for a specific HRU. This procedure helps to build a SWAT plant database (plant.dat) for the study area, which is used for the next steps.
(b) The total number of heat units needed to bring the plant to maturity parameter (PHU_PLT) depends on temperature data (Neitsch et al., 2011). PHU_PLT is calibrated for each HRU using MODIS LAI as a reference since the temperature varies with height in mountainous regions. This step is important for better modeling of vegetation LAI dynamics in HRUs defined by trees and perennials.

In this study, NSE is used as the objective function for LAI and PHU_PLT calibration.

The second part of the calibration strategy deals with the calibration of the SWAT parameters that mainly control streamflow, evapotranspiration, and discharge components. For this purpose, we propose a multi-objective calibration approach that includes the baseflow index to constrain the model calibration in addition to discharge-related performance metrics and hydrological signatures related to FDC (Flow Duration Curve). This approach is compared to approaches applied before, where only hydrograph goodness-of-fit metrics (e.g., NSE or the log NSE, lNSE)

Table 4.2: Optimization problems. In the optimization process, NSE and lNSE (log NSE) were maximized while the absolute values of FDC$_{sign}$ (FDC signature) and BIAS_BFI (bias of baseflow index) were minimized.

Number	Approach	Formulation	Optimization problem
1	Applied before	Single-objective	NSE
2	Applied before	Single-objective	lNSE
3	Applied before	Bi-objective	lNSE, FDC$_{sign}$
4	Proposed in this study	Multi-objective	lNSE, FDC$_{sign}$, BIAS_BFI

and signatures related to FDC were used. Table 4.2 shows the single- and multi-objective optimization approaches tested in this study, and Table 4.3 shows the objective metrics.

In the formulation of multi-objective calibration approaches, we selected lNSE instead of NSE as part of the objectives for flow timing and magnitude to avoid overfitting discharge peaks since NSE is more sensitive to larger errors that often occur in high-flow periods (Gupta et al., 2009; Krause et al., 2005). To quantify catchment overall behavior and flashiness, several aspects of FDC were considered to evaluate the model performance in emulating the FDC. Following Chilkoti et al. (2018), FDC is divided into four segments, of peak flow volume (0–2%), high flow volume (2–20%), mid-segment slope (20–70%), and low flow volume (70–100%). The respective FDC partitioning represents peak flow events occurring rarely, quick runoff (due to snowmelt and/or rainfall), the quickness of a basin's response, and baseflow components of the streamflow (Chilkoti et al., 2018; McMillan et al., 2017; van Werkhoven et al., 2009; Yilmaz et al., 2008). To properly reproduce flow partitioning, the baseflow index is used to constrain the slow-flow component.

For the model evaluation, discharge statistics and individual hydrological signatures defined in Table 4.3 are used. The conventional hydrograph goodness-of-fit metrics (NSE, lNSE, and Percent bias (PBIAS)) are used to evaluate the model performance in streamflow simulation (Krause et al., 2005; Moriasi et al., 2007). Note that in this study, PBIAS is not included as an objective function for model calibration but is only used to evaluate model performance. PBIAS measures the average tendency of the simulated discharge, which can be larger or smaller than the measured values. The optimal value of PBIAS is 0.0, with low values indicating accurate model simulation. A positive (negative) value of this measure indicates overestimation (underestimation). FDC signatures (S_{peak}, S_{high}, S_{mid}, and S_{low}) are used to assess the model performance through biases in the flow distributional response (Chilkoti et al., 2019). PBIAS_BFI (introduced in this study) is used to evaluate the model capability in the simulation of flow partitioning in terms of the baseflow index. The overall goal of this multi-criteria evaluation design is to assess how realistically the model represents the hydrologic system response, which is crucial both for hydrological models intended to operate in a predictive mode and for projecting climate change impacts (Krysanova et al., 2018).

4.2.7   Baseflow index estimation

The reference baseflow index (BFI) was estimated from streamflow using two baseflow separation techniques. The baseflow filter program (BFLOW, `http://swat.tamu.edu/`) (Arnold and Allen, 1999) and the Eckhardt filter using the Web GIS-based Hydrograph Analysis Tool system were applied (WHAT, `https://engineering.purdue.edu/mapserve/WHAT/`) (Lim et al., 2005). For a detailed description of filter methods, the reader is referred to Arnold et al. (1995), Arnold and Allen (1999), and Lim et al. (2005). BFLOW and WHAT have been used successfully in many studies related to the SWAT model (e.g. Jang et al., 2018; Luo et al., 2012; Meaurio et al., 2015; Yesuf et al., 2016).
Following Jang et al. (2018), the simulated baseflow index (SWAT_BFI) was computed as follows:

$$\text{SWAT\_BFI} = \frac{\text{Qlat} + \text{Qgws} + \text{Qgwd}}{\text{Qsurf} + \text{Qlat} + \text{Qgws} + \text{Qgwd}} \qquad (4.2)$$

Table 4.3: Mathematical formulation of goodness-of-fit metrics and hydrological signatures. *O* and *S* are observed and simulated flow, respectively (in m³/s). EP is the exceedance probability, while *P*, *H*, and *L* are the indices of the minimum flow of the peak-flow, high-flow, and low-flow segments, respectively.

Criterion (reference)	Equation	Description
	Discharge-related performance measures	
Nash–Sutcliffe efficiency (Nash and Sutcliffe, 1970)	$\mathrm{NSE} = 1 - \dfrac{\sum_{i=1}^{n} (S_i - O_i)^2}{\sum_{i=1}^{n} (O_i - O_a)^2}$	O_a is the average of the observed flow and n is the number of observations on evaluation
Nash–Sutcliffe efficiency log (Krause et al., 2005)	$\mathrm{lNSE} = 1 - \dfrac{\sum_{i=1}^{n} (\ln(S_i) - \ln(O_i))^2}{\sum_{i=1}^{n} (\ln(O_i) - \ln(O_a))^2}$	
Percent bias (Gupta et al., 1999)	$\mathrm{PBIAS} = \dfrac{\sum_{i=1}^{n} (S_i - O_i)}{\sum_{i=1}^{n} O_i} \times 100$	
	Signature measures	
Percent bias in FDC peak-segment volume (Yilmaz et al., 2008)	$S_{\mathrm{peak}} = \dfrac{\sum_{p=1}^{P} (S_p - O_p) \times 100}{\sum_{p=1}^{P} O_P}$	$p = 1, 2, \ldots, P$ are flow indices located within the FDC peak-flow segment (EP lower than 2%)
Percent bias in FDC high-segment volume (Yilmaz et al., 2008)	$S_{\mathrm{high}} = \dfrac{\sum_{h=1}^{H} (S_h - O_h) \times 100}{\sum_{h=1}^{H} O_h}$	$h = 1, 2, \ldots, H$ are flow indices located within the high-flow segment (2–20% flow EP)
Percent bias in FDC mid-segment slope (van Werkhoven et al., 2009; Yilmaz et al., 2008)	$S_{\mathrm{mid}} = \dfrac{((S_{m1} - S_{m2}) - (O_{m1} - O_{m2})) \times 100}{(O_{m1} - O_{m2})}$	$m1$ and $m2$ are the lowest and highest flow EP within the mid-segment (20–70%)
Percent bias in FDC low-segment volume (Yilmaz et al., 2008)	$S_{\mathrm{low}} = \dfrac{\sum_{l=1}^{L} (S_l - O_l) \times 100}{\sum_{l=1}^{L} O_l}$	$l = 1, 2, \ldots, L$ are flow indices located within the low-flow segment (70–100% flow EP)
FDC signature (Chilkoti et al., 2018)	$\mathrm{FDC}_{\mathrm{sign}} = \dfrac{1}{4} \left(|S_{\mathrm{peak}}| + |S_{\mathrm{high}}| + |S_{\mathrm{mid}}| + |S_{\mathrm{low}}| \right)$	$\mathrm{FDC}_{\mathrm{sign}}$ is the aggregated FDC signature
Bias of baseflow index	$\mathrm{BIAS\_BFI} = \mathrm{SWAT\_BFI} - \mathrm{BFI}$	SWAT_BFI is the simulated baseflow index and BFI the reference

where Qsurf is the surface runoff, Qlat is the lateral flow, Qgws is the return flow from the shallow aquifer, and Qgwd is the return flow from the deep aquifer.

4.2.8 Multi-objective optimization algorithm

We applied the Borg Multi-Objective Evolutionary Algorithm (Borg MOEA) (Hadka and Reed, 2013) to achieve the optimum solutions of SWAT parameters based on the calibration strategies defined in Section 4.2.6, as Borg MOEA has superior performance when compared with a range of state-of-the-art multi-objective algorithms (Hadka and Reed, 2012, 2013). Moreover, it was applied successfully in the calibration of SWAT in which hydrograph goodness-of-fit metrics and signatures related to FDC were included in the objective function (Chilkoti et al., 2018). The Borg MOEA is an auto-adaptive optimization algorithm that uses a population-based search to find the archived non-dominated solutions (Pareto approximate set) at the end of the optimization. The Borg MOEA parameterization was based on its default recommended parameter values (Hadka and Reed, 2013). The initial population size was set to 100, generated based on random parameter sampling. To achieve a reasonable trade-off between objectives, the ε-precision level was set to 0.01 for the NSE family and a difference of 1% for $\mathrm{FDC}_{\mathrm{sign}}$ and

BIAS_BFI. The total number of objectives for the evaluation was set to 500 for LAI calibration, 500 for PHU_PLT, and 1000 for streamflow. For more details on Borg MOEA theory and features, readers are advised to see Hadka and Reed (2013).

4.3 Results and discussion

4.3.1 BFI estimation

Baseflow index estimation (the ratio of long-term mean baseflow to total streamflow) was conducted from daily streamflow data recorded at the km-105 hydrological station for 1964–1990 since this period does not include the potential effects of the Sibinaccocha Dam on runoff (from 1996 onwards). The baseflow indices estimated by BFLOW and WHAT were 0.76 and 0.78, respectively. The mean of these values was considered the reference baseflow index (BFI = 0.77); it means that around 77% of the river discharge at gauge km-105 can be attributed to baseflow. The latter is consistent with the baseflow index reported for the neighbouring Andean Kosñypata basin with similar geology, topography, and vegetation, where 77% of annual flow was attributed to baseflow (Clark et al., 2014). In addition, BFLOW estimated the flow recession constant from the shallow aquifer (ALPHA_BF equal to 0.0351) which was used to replace the default ALPHA_BF value of the model.

4.3.2 Performance of LAI simulation

Table 4.4 presents the optimized plant parameter values for mixed forest (FRST), evergreen broadleaf forest (FETZ), pasture (PAST), and agricultural areas (AGRL). Using these optimal parameter values, the PHU_PLT (head unit) parameter was calibrated for all HRUs covered by perennial plants so that the SWAT-simulated LAI mimics the MODIS 8-day LAI as close as possible. Note that AGRL was considered perennial in this study to simulate the LAI decline during senescence using a logistic function (a feature of the SWAT version used here), since the

Table 4.4: Calibrated SWAT plant parameter values for HRUs with perennial plants: mixed forest (FRST), evergreen broadleaf forest (FETZ), pasture (PAST), and agricultural areas (AGRL).

Parameter	Parameter description	Calibrated values			
		PAST	AGRL	FRST	FETZ
BIO_E	Radiation-use efficiency ((kg/ha)/(MJ/m^2))	17.04	13.92	1.10	0.56
BLAI	Maximum potential leaf area index (m^2/m^2)	1.10	2.74	1.70	5.30
FRGRW1	Fraction of PHU corresponding to the first point on the optimal leaf area development curve	0.06	0.07	0.02	0.10
LAIMX1	Fraction of BLAI corresponding to the first point on the optimal leaf area development curve	0.02	0.17	0.10	0.20
FRGRW2	Fraction of PHU corresponding to the second point on the optimal leaf area development curve	0.49	0.38	0.44	0.50
LAIMX2	Fraction of BLAI corresponding to the second point on the optimal leaf area development curve	0.90	0.92	0.98	0.90
DLAI	Fraction of total PHU when leaf area begins to decline	0.48	0.59	0.40	0.48
ALAI_MIN	Minimum leaf area index for plant during dormant period (m^2/m^2)	0.31	0.58	0.32	0.90
T_BASE	Minimum temperature for plant growth (°C)	2.07	3.46	2.00	0.05
T_OPT	Optimal temperature for plant growth (°C)	18.16	10.00	14.50	13.18
PHU_PLT	Total number of heat units needed to bring plant to maturity	Variable for each HRU			
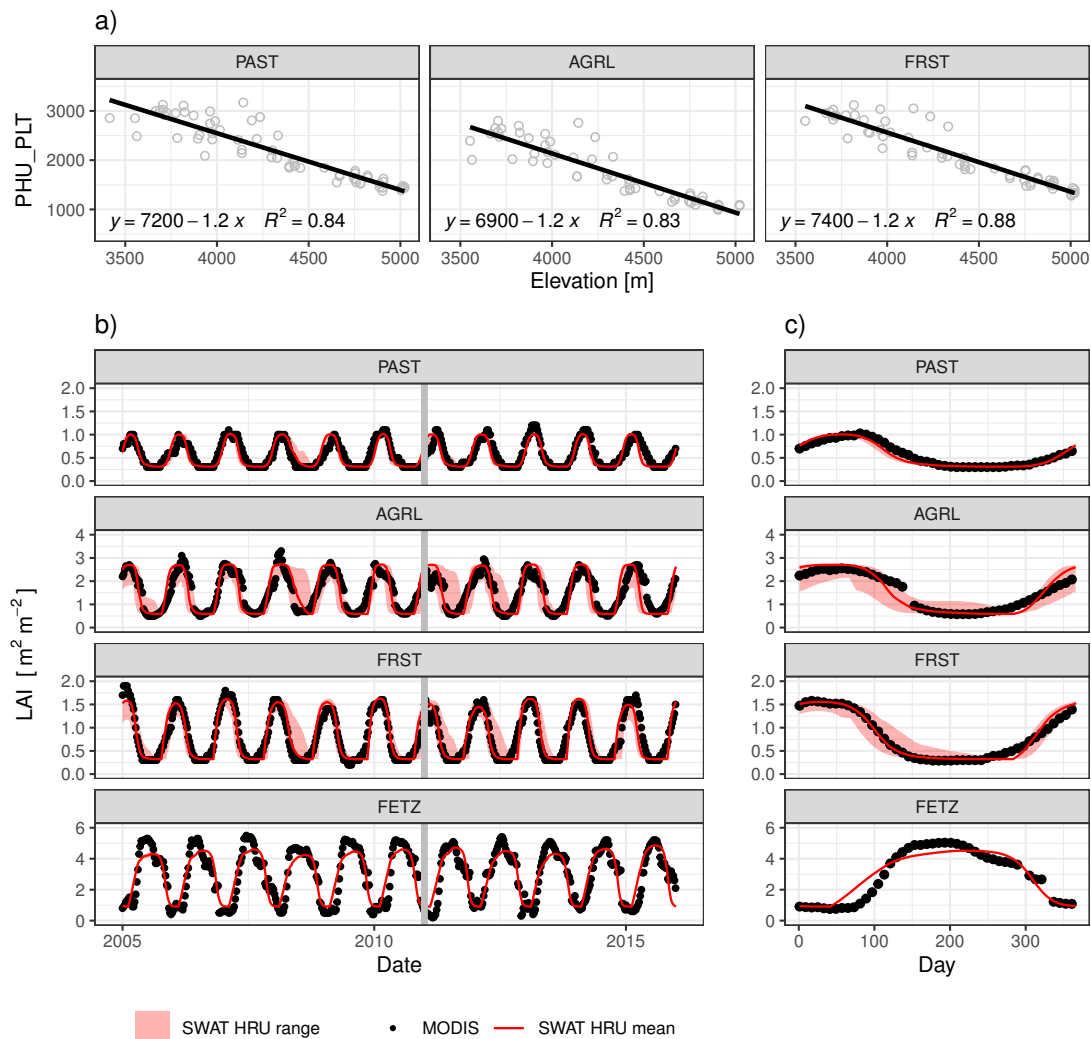
Figure 4.3: (a) Scatterplot of PHU_PLT against elevation. (b) Simulated daily LAI (range over HRUs and area weighted HRU mean) and the 8-day MODIS LAI. (c) Long-term (2005–2015) average daily (8-day) LAI based on SWAT (MODIS). The vertical grey line marks the end of the calibration period and the beginning of the validation period. R^2 is the coefficient of determination.

AGRL MODIS LAI curve follows a logistic curve instead of a linear curve during the senescence stage (Fig. 4.3(b,c)). This is in agreement with Wei et al. (2018), who recommended the use of the logistic LAI curve during senescence for agricultural crops.

Figure 4.3(a) shows the strong negative relationship ($R^2 \geq 0.83$) between calibrated PHU_PLT values and elevation for PAST, AGRL, and FRST. This means that the total number of heat units required for a plant to reach maturity (PHU_PLT) decreases with altitude, and this can be used as a descriptor variable to estimate PHU_PLT in basins showing high elevation gradients. As a result, the plant parameters and the relationship between PHU_PLT and elevation derived in this study can be used in other Andean basins.

Comparing the temporal variation of LAI dynamics (Fig. 4.3(b)), in general, SWAT-simulated LAI corresponds well with MODIS LAI data during both calibration and validation periods for all perennial plants. This observation is supported by good model performance statistics (NSE ≥ 0.63, $R^2 \geq 0.76$, and PBIAS within reasonable limits $\pm 15\%$) in simulating LAI dynamics for both evaluation periods as shown in Table 4.5. In addition, Figs 4.3(c) and 4.8 (see Appendix) show that the spatio-temporal variability of the seasonal LAI simulated by SWAT agrees well with MODIS LAI for all perennials. Since LAI in SWAT influences the simulation of hydrological

Table 4.5: Performance metrics for the SWAT for simulating LAI in the calibration (validation) period. Note that performance refers to 8-day aggregated data. R^2 is the coefficient of determination.

	PAST	AGRL	FRST	FETZ
NSE	0.78 (0.72)	0.77 (0.63)	0.91 (0.83)	0.81 (0.81)
R^2	0.79 (0.76)	0.81 (0.76)	0.91 (0.85)	0.82 (0.81)
PBIAS %	−0.90 (−6.20)	0.20 (−1.10)	1.90 (0.00)	1.00 (2.20)

and vegetation processes such as evapotranspiration, biomass accumulation, streamflow, and sediments (Alemayehu et al., 2017; Ha et al., 2018; Ma et al., 2019; Rajib et al., 2018; Strauch and Volk, 2013), the good model performance in LAI simulation found here increases the quality of the simulation of these processes.

Figure 4.3(c) shows a similar seasonal LAI pattern for PAST, FRST, and AGRL, and it follows the seasonal rainfall pattern of the Andes. However, the onset/end (February–March/October–November) of LAI development for FETZ is delayed regarding the onset/end (October/March) of the rainy season in the rainforest area. This behavior was also observed in other tropical regions with natural ecosystems (e.g. Alemayehu et al., 2017).

We found in the literature that only a few SWAT-related studies have reported the calibration of plant parameters, and most of these have only considered a constant PHU_PLT value for each plant type. To simulate appropriately the vegetation dynamics and hydrological processes that depend on LAI, however, the calibration of plant parameters is crucial, particularly the parameter that controls plant development such as the PHU_PLT, which varies with altitude in mountain basins, as demonstrated in this study. We believe that our results and proposed LAI calibration strategy can support modelers for a better simulation of vegetation dynamics.

4.3.3 Model performance in streamflow simulation

The Borg MOEA approach (see Section 4.2.8) was used to calibrate the SWAT model according to the aforementioned calibration strategies (see Table 4.2), and the parameters obtained are shown in Table 4.6. These model parameters were chosen to correct the deficiencies of the uncalibrated model (e.g., systematic flow underestimation being higher during low-flow periods, strong simulated peak discharges, etc.), for which the authors' knowledge about basin characteristics, model structure, and how each model parameter influences the hydrological processes was important.

For single-objective, bi-objective, and multi-objective calibration, the Pareto front solution consisting of one, three, and six sets of parameters were obtained, respectively. Figure 4.4 summarizes the results of different calibration strategies. Furthermore, the hydrographs, the

Table 4.6: Selected parameters and their ranges for model calibration for streamflow. In the "Change type" column, R refers to a relative change of parameter values during the calibration, and V to absolute change. "Adjusted value" refers to the parameter mean values associated with the Pareto set obtained in the multi-objective scenario.

Parameter	Description	Range	Change type	Adjusted value
CN2	Runoff curve number for moisture condition II	[−0.15, 0.15]	R	0.06
SURLAG	Surface runoff delay coefficient	[0.1, 2]	V	0.11
SOL_BD	Wet bulk density	[−0.25, 0.25]	R	0.09
SOL_K	Soil hydraulic conductivity	[−0.25, 0.25]	R	−0.15
SOL_AWC	Available water capacity of the soil layer	[−0.5, 0.25]	R	−0.31
GW_DELAY	Groundwater delay time	[1, 100]	V	42.16
RCHRG_DP	Deep aquifer percolation fraction	[0.05, 1]	V	0.52
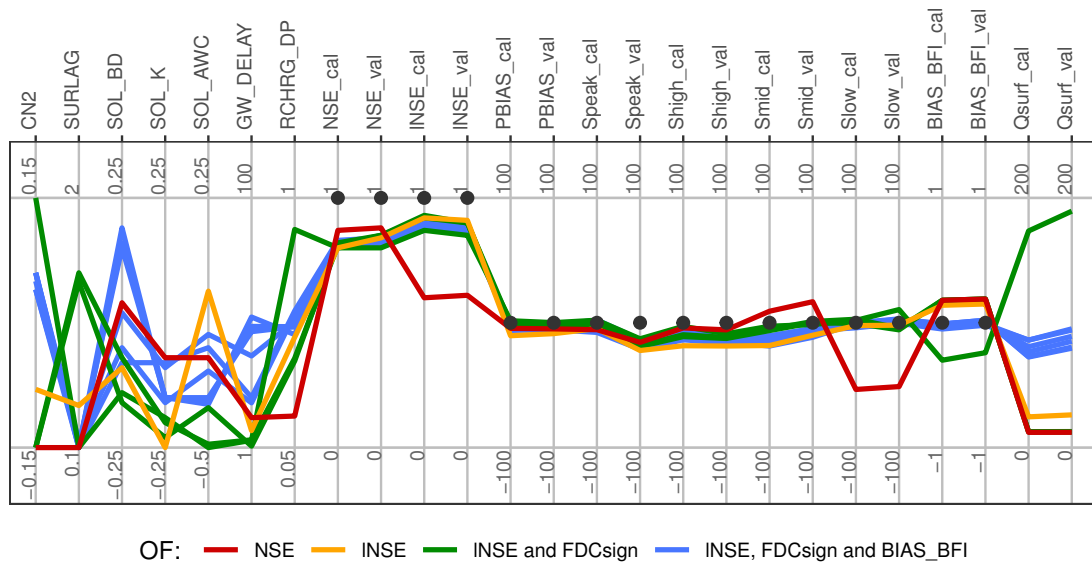
Figure 4.4: Parallel coordinates plot of the Pareto front optimal solutions obtained by different calibration strategies. For each solution, optimal parameter values, discharge-based performance measures (NSE, lNSE, and PBIAS), and hydrological signatures (S_{peak}, S_{high}, S_{mid}, S_{low}, and BIAS_BFI) are displayed. _cal (_val) indicates the measurements for the calibration (validation) period. Qsurf is the mean surface runoff in mm. A description of the SWAT parameters is provided in Table 4.6. A description of objective functions (OFs) is provided in Table 4.3.

FDCs, and the mean seasonal flow dynamics of the different objective calibrated simulations are shown in Figs 4.5(a,b), and 4.6, respectively.

In terms of the temporal variation of discharge dynamics (Fig. 4.5(a)), FDCs (Fig. 4.5(b)), and seasonal discharge dynamics (Fig. 4.6), the NSE calibrated simulation corresponds well with observed daily discharge during high discharge season but fails (flow underestimation) during the low discharge season. This observation is supported by the higher (lower) performance value for NSE (lNSE) as shown in Fig. 4.4. Moreover, hydrological signatures based on FDC (Fig. 4.4) show that this calibration approach is primarily focused on the peak, high, and mid flows at the expense of improvements to the low-flow predictions. This finding is congruent with previous studies (Chen et al., 2018; Krause et al., 2005; Zhang et al., 2018b).

Nevertheless, lNSE calibrated simulations match well with observed discharge in all aspects of the hydrograph (Fig. 4.5) although discharges are moderately underestimated during high-discharge season (Fig. 4.6). Hence, lNSE is used in this study as part of the multi-objective calibration approaches to drive the model in simulating all hydrograph aspects in the calibration.

The results for bi-objective and multi-objective approaches show that the observed and simulated hydrographs match each other to a high degree (Fig. 4.5), and all performance measures (goodness of fit and FDC signature metrics; Fig. 4.4) show that these formulations are superior to the results of single-objective approaches. This finding demonstrates that the inclusion of FDC signatures in addition to discharge-based performance measures within a multi-objective calibration leads to improved discharge simulation, which is in agreement with previous studies (Chilkoti et al., 2018; Hrachowitz et al., 2014; Pfannerstill et al., 2017, 2014; Pokhrel and Yilmaz, 2012; Sahraei et al., 2020; Shafii and Tolson, 2015).

Regarding the model performance in simulating the flow components, Fig. 4.4 shows the smaller values of PBIAS_BFI for the multi-objective calibration approach, which demonstrates that our approach leads to a more accurate representation of the flow partitioning into surface runoff and baseflow. Whereas approaches applied before (single-objective and bi-objective approaches) fail in simulating the partitioning into flow components according to the baseflow index, this agrees with the findings of Shafii et al. (2017), who reported that traditional signature-based calibration (using discharge and FDC) does not necessarily guarantee correct flow partitioning in a Hydrologic Model (HYMOD) hydrology model application.
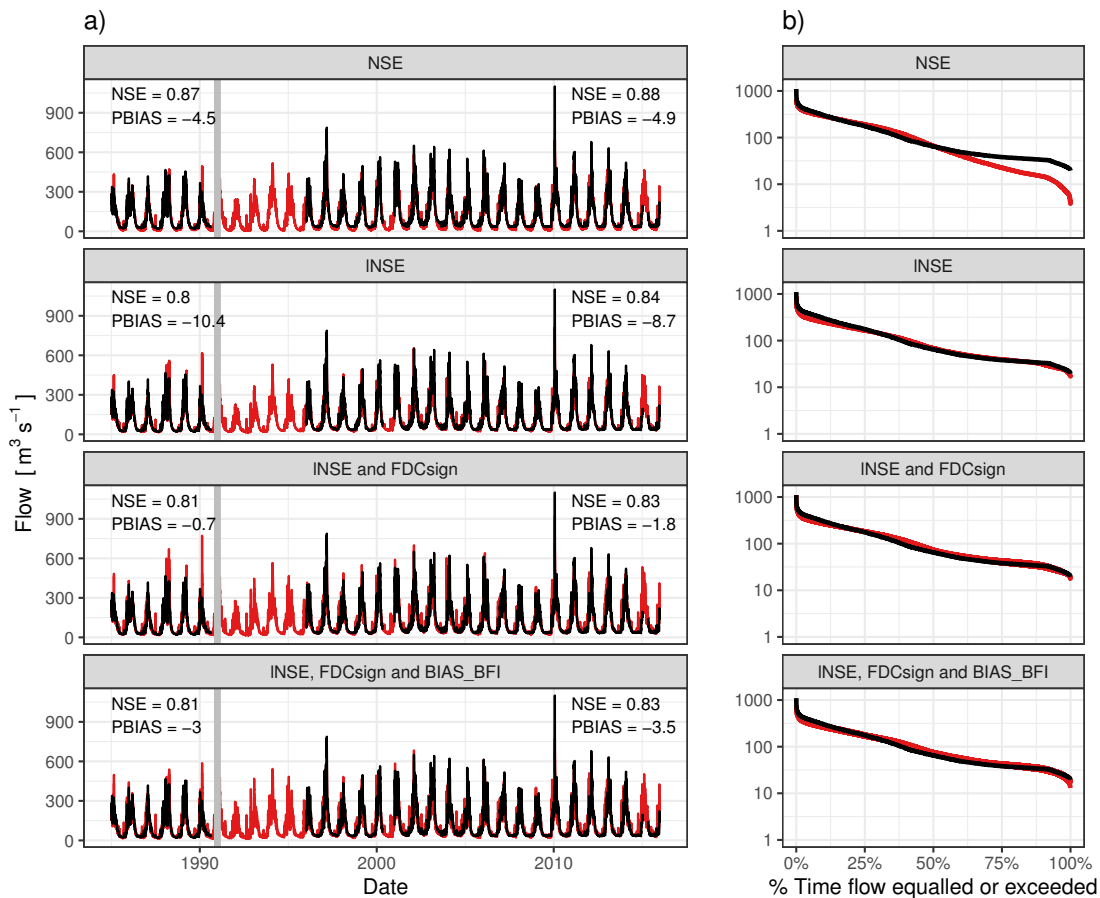
Figure 4.5: Comparison of the observed (black line) and simulated (red line/area) (a) daily discharges and (b) simulated and observed FDC for four calibration strategies. In the case of the bi-objective (INSE and FDC$_{sign}$) and multi-objective (INSE, FDC$_{sign}$, and BIAS_BFI) optimization, the red area indicates optimal Pareto solutions and NSE and PBIAS are the mean of Pareto solutions. The grey line marks the end of the calibration period and the beginning of the validation period.

Considering the rating performance criteria of Moriasi et al. (2007), NSE greater than 0.75 and PBIAS less than 10% are indicative of very good model performance for streamflow simulation; therefore, model performance was very good in both calibration (NSE $\geq$ 0.8, |PBIAS| $\leq$ 10%) and validation (NSE $\geq$ 0.8, |PBIAS| $\leq$ 8.7%) for daily streamflow simulation in all calibration strategies performed in this study. The results of this study (Fig. 4.4), however, clearly demonstrate that practitioners must be careful judging model credibility using only these discharge-based metrics, since good model performance for streamflow and FDC simulation does not guarantee internal consistency of all simulated processes (e.g. surface runoff and baseflow).

In this study, additional calibration strategies (Appendix Fig. 4.9) that do not include FDC signatures were performed, and their results suggest that our proposed multi-objective approach is much more robust.

4.3.4 Parameter identifiability

The identification of physically plausible, representative, and robust model parameter sets for the basin under investigation is an important task in hydrologic modelling (Shafii and De Smedt, 2009; Wagener et al., 2001). For this purpose, we focused on the range of parameter values associated with the Pareto optimal solutions, as suggested by Gupta et al. (1998), and particularly on the parameters retained by bi-objective and multi-objective calibration strategies.
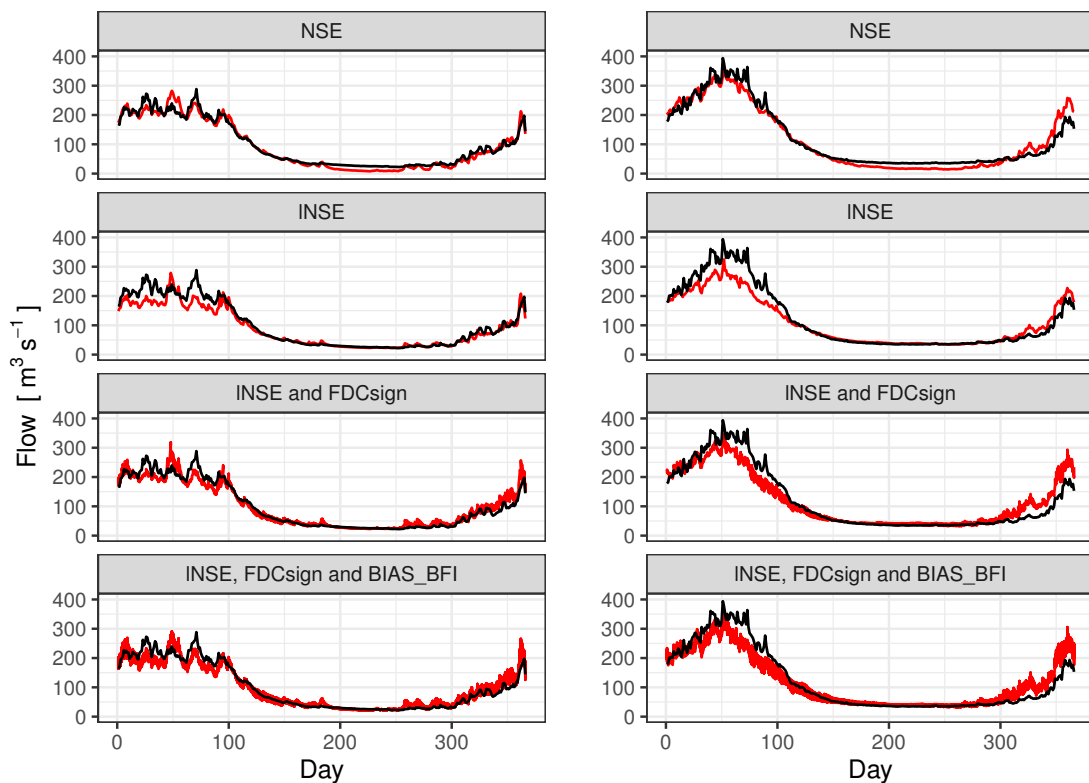
Figure 4.6: The mean seasonal dynamics of simulated discharge (red line/area) and observed discharge (black line) for each calibration strategy in the calibration period (left) and validation period (right).

A parameter becomes more identifiable when the parameter range is narrower and/or its optimum values are located in a particular region of the feasible range.

Figure 4.4 shows that in the bi-objective calibration scenario, four parameters (Wet bulk density (SOL_BD), Soil hydraulic conductivity (SOL_K), Available water capacity of the soil layer (SOL_AWC), and Groundwater delay time (GW_DELAY)) are identifiable and three parameters (Runoff curve number for moisture condition II (CN2), Surface runoff delay coefficient (SURLAG), and Deep aquifer percolation fraction (RCHRG_DP)) are barely or not identifiable, since different values of these parameters give similar results in combination with the other parameters. Otherwise, six parameters (CN2, SURLAG, SOL_K, SOL_AWC, GW_DELAY, and RCHRG_DP) – influencing main hydrologic processes such as surface runoff, lateral flow, evapotranspiration, and return flow from aquifers – are well identifiable, and only the parameter SOL_BD is hardly identifiable in the multi-objective calibration strategy. The larger number of identifiable parameters in the latter approach is due to the inclusion of the baseflow index in the multi-objective calibration, which guides the optimization algorithm to identify parameters related to processes that impact the baseflow index. Therefore, when more information (objectives) is fed (required) into model calibration, the number of identifiable parameters will also increase.

Comparing the robustness of parameter sets obtained by each calibration strategy, the parameter sets of models calibrated based on single-objective and bi-objective optimization performed satisfactorily in simulating streamflow but for the unrealistic representation of surface runoff (Fig. 4.4) as well as of the basin baseflow index. On the contrary, the parameter sets obtained by a multi-objective strategy led to appropriate representation of the baseflow index as well as streamflow and FDC simulation, and hence these parameter sets can be catalogued as representative for the study basin. The superiority of the multi-objective strategy in simulating flow partitioning is related to the better identification of the CN2 parameter, which directly impacts surface runoff and infiltration partition and alters water balance components (Arnold et al., 2012; Qi et al., 2020). Here, only representative parameters are described, and the

narrower ranges of CN2, SURLAG, and RCHRG_DP obtained by the multi-objective approach indicate that the basin response is very sensitive to surface runoff and deep aquifer contribution. The obtained optimum values for CN2 (Fig. 4.4) must lead to the increase of surface runoff, and consequently to simulated high peaks. Hence, SURLAG values contributed to smoothing the simulated hydrograph in the channel due to the delay in surface runoff release from the HRUs (Neitsch et al., 2011). The resulting optimal values of SOL_K (SOL_AWC) were identified to overcome the initial issue of the fast water movement through the soil (flow underestimation). Optimal values of RCHRG_DP (mean value 0.52) indicate that from the total water for aquifer recharge, approximately 52% (48%) recharges the deep aquifer (shallow aquifer). The high percentage of water reaching the deep aquifer is important for return flow from this aquifer to improve the streamflow simulation in the low-flow period. This agrees with the finding of Clark et al. (2014), who demonstrated the importance of return flow from deep aquifers to explain the sustained dry season flow in the neighbouring Andean Kosñypata basin.

4.3.5   Equifinality

Figure 4.4 shows that each calibration strategy produces a model or several models with good performance in streamflow simulation despite each model having a different set of parameters. This result demonstrates that model outputs are subjected to the effects of equifinality or the non-uniqueness issue (different sets of parameters in the calibration procedure resulting in similar simulations – see Beven, 2006). This issue is common in complex nonlinear models such as SWAT (Ficklin and Barnhart, 2014; Her and Chaubey, 2015; Shen et al., 2012; Zhang et al., 2018a), which presents interactions among its parameters as reported by Zhang et al. (2018a).

Controlling the equifinality to arrive at meaningful parameter sets and solutions is a challenge. For instance, Fig. 4.4 shows that conventional calibration strategies based on hydrograph goodness-of-fit optimization (approaches 1 and 2 with NSE or lNSE only) produce pseudo-accurate models (with unrealistic parameter values), showing accurate performance statistics in streamflow simulation while incorrectly representing some internal basins processes. This study also reveals that even the bi-objective calibration strategy including FDC signature as criterion in addition to lNSE does not improve the equifinality. However, our proposed multi-objective calibration strategy improves parameter identifiability and reduces the equifinality because the inclusion of the baseflow index as part of the objective function leads to better identification of the CN parameter, which controls the flow partitioning into surface runoff and baseflow.

Overall, model calibration using only discharge is not sufficient to judge the validity of a model in representing the hydrologic system. Therefore, we suggest including more variables (e.g. LAI, evapotranspiration, snow, baseflow, and hydrological signatures) to better constrain the calibration process (which was also suggested by Krysanova et al., 2018). Likewise, we suggest the use of multi-objective evolutionary algorithms that search for acceptable trade-offs between objectives, since these methods can help to mitigate the parameter uncertainty partly due to equifinality during the calibration. Otherwise, practitioners must be careful using single-objective optimization algorithms, since no sampling design schemes used in these algorithms consider the interactions among the parameters (Devak and Dhanya, 2017; Razmkhah et al., 2017; Song et al., 2015), and hence the solution can be subjected to equifinality.

4.3.6   Basin water balance and vegetation response

For a better understanding of the water budget for VRB, Table 4.7 shows the long-term average annual values (1985–2015 period) for the most relevant water balance and flow components. The results show that annual precipitation in the basin is 748 mm, of which about 50% is lost from the system by evapotranspiration (ET = 375 mm), and 50% is the water yield of the basin (WYLD = 373 mm). Similar ratios (44.6–51%) of ET over precipitation in Ecuadorian Andean basins were reported (Carrillo-Rojas et al., 2019; Guzmán et al., 2015; Mosquera et al., 2015). Regarding the WYLD components, the contribution of baseflow (BF = 291 mm, 78%) is higher than that of surface runoff (Qsurf = 82 mm, 22%). The main component of baseflow is the lateral flow (Qlat = 137 mm, 47%), followed by return flow from the deep aquifer (Qgwd = 79 mm, 27%) and the return flow from the shallow aquifer (Qgws = 75 mm, 26%). Our results

Table 4.7: Long-term average annual water balance (1985–2015 period) for the VRB

Water balance components	Value
Precipitation, P (mm)	748
Evapotranspiration, ET (mm)	375
Water yield, WYLD (mm)	373
Surface runoff, Qsurf (mm)	82
Baseflow, BF = Qlat + Qgws + Qgwd (mm)	291
Lateral flow, Qlat (mm)	137
Return flow from the shallow aquifer, Qgws (mm)	75
Return flow from the deep aquifer, Qgwd (mm)	79
Checks	
BFI	0.77
SWAT_BFI	0.79
BIAS_BFI	0.02
ET/P	0.50

indicate that the large baseflow contribution plays a key role in modulating the flow regime of VRB, and the important groundwater contribution explains the dry-season baseflow. This outcome is consistent with the findings for Peruvian Andean basins draining into the Amazon River, such as the Kosñypata (Clark et al., 2014) and upper Marañon River basin (Hill et al., 2018), where the substantial dry-season discharge was attributed to return flow from deep aquifers.

To assess the role of tropical Andean vegetation on water yields and baseflow, we examined the variability of the ratio of water yield over precipitation (Fig. 4.7b,d) and the SWAT-estimated baseflow index (SWAT_BFI; Fig. 4.7c,e) across HRUs and different land-use types. The results show that the greatest ratio (∼0.63) of water yield over precipitation is produced in pasture (PAST) areas which span the middle and upper part of the basin mainly (Fig. 4.1). Urban (URML) and barren (BARR) areas can produce water yields of ∼43% and ∼52% of precipitation, respectively, contributed by surface runoff mainly, as the baseflow index (SWAT_BFI) values are very low in these land uses. Although the evergreen broadleaf forest (FETZ) areas located around the basin outlet experience the greatest amount of precipitation, the water yield in those areas is lower (<37% of precipitation), as for example in agricultural areas (AGRL) and mixed forest (FRST).

Figure 4.7(e) shows lower values of baseflow indices for agricultural areas, compared to pasture for instance, which may indicate the poor hydrological regulation capacity of cultivated areas. Otherwise, mixed forest, evergreen broadleaf forest, and pasture exhibit higher rates (>∼0.89) of baseflow to water yield, which highlights the features of these land uses in improving the infiltration and subsurface processes. We observed, however, that pasture presents important hydrological services such as greater water yields and higher rates of baseflow simultaneously in comparison to forest, which shows higher baseflow but poor water yields in VRB. The negative impacts of forest on water yield are consistent with the findings of previous studies in Andean basins (e.g. Buytaert et al., 2007; Ochoa-Tocachi et al., 2016).

Finally, the verification of BIAS_BFI being equal to 0.02 (2%; Table 4.7) highlights the SWAT model's capability in simulating surface runoff and baseflow, which is essential to help the local water resources management including water supply services, identification of critical areas for soil conservation intervention, hydroelectric energy production, and preventing floods and droughts.

4.3.7 Limitations and perspectives

Despite the efforts of this study to reduce parameter uncertainty during the calibration procedure, we note that our results are still subject to uncertainties in the input data (e.g. climate, soil, and land use), data used for model calibration (e.g. discharge, BFI, and LAI), and model structure due to the simplification of hydrologic processes as well as to uncertainties in remaining model parameters. For instance, despite the utility of the climate data used in this study to
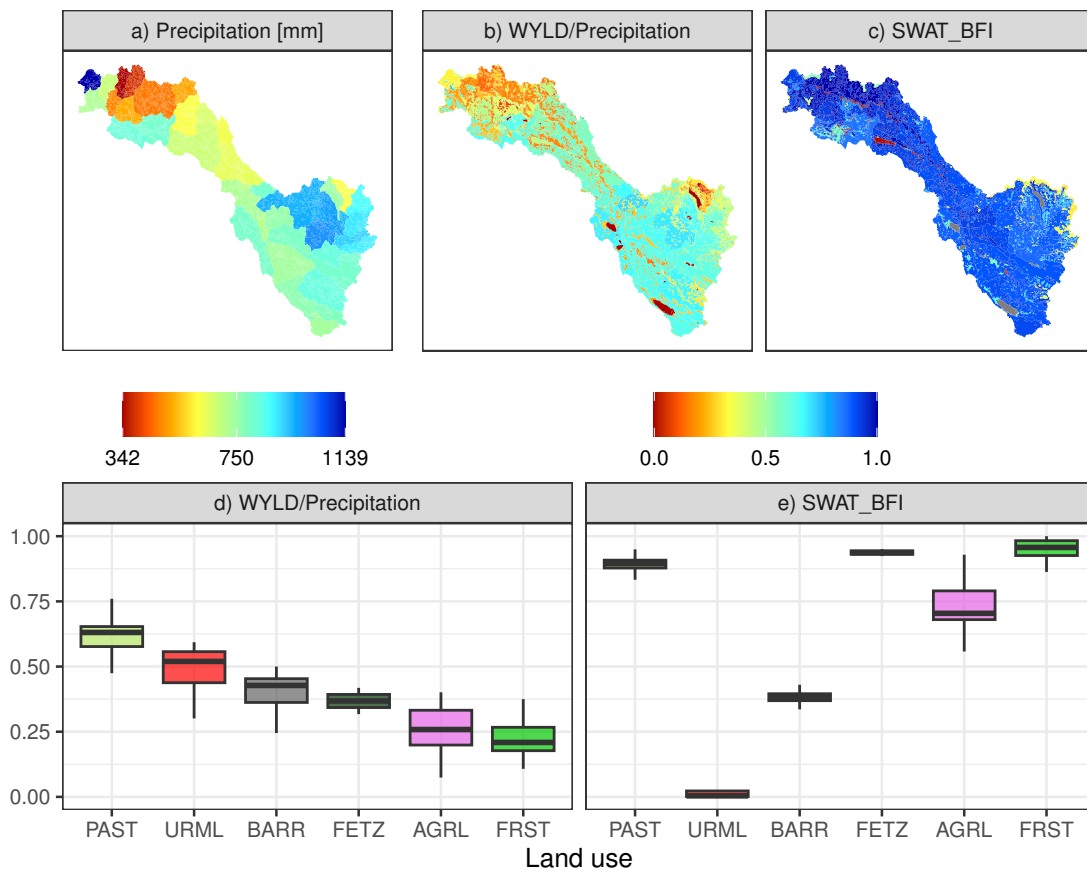
Figure 4.7: Above is (a) the spatial variability at HRU level of precipitation, (b) ratio of water yield (WYLD) over precipitation, and (c) simulated baseflow index (SWAT_BFI). Below is (d) the ratio of WYLD over precipitation and (e) SWAT_BFI for each land-use type.

drive hydrologic model in a basin with data scarcity, such as VRB, gridded climate data are subject to uncertainties in the observed data and spatial interpolation procedures. In particular, precipitation may have systematic bias caused by wind, which is inherent in precipitation measurements and introduces an unquantified error (Pollock et al., 2018). We assumed that BFI, which was estimated using digital filter methods based on daily discharge and used to constrain the flow partitioning, gives a physically plausible result. However, future work should involve the use of tracers and/or stable isotopes to estimate BFI and validate the indirect methods used in this study. We rely on discharge data from the km-105 hydrometric station for model calibration and validation. However, discharge data may have errors because of inherent uncertainties in flow measurement and rating curves (Tomkins, 2014). Uncertainties up to ±20% in flow measurement using the traditional area-velocity method and the current meter were reported in Andean basins of Colombia (Parra et al., 2016). Hence, future studies are needed to quantify uncertainties in hydrologic modelling owing to errors in observed discharge data in Andean basins. Finally, in this study, only one streamgauge was used for model calibration and validation because of data scarcity, but we are confident in the robustness of our methodology which can be used in instrumented basins to perform the calibration/validation at multiple sites within the catchment, and even in ungauged basins where FDC and baseflow index can be obtained through regionalization approaches (e.g. Atieh et al., 2017; Beck et al., 2013).

4.4 Summary and conclusions

This study developed a step-wise, multi-objective calibration framework applied to the SWAT model for the simulation of vegetation dynamics, streamflow, and flow partitioning. The first part

of the framework deals with model calibration of leaf area index dynamics, for which the SWAT LAI-related parameters of perennial plants were calibrated using MODIS LAI data as a reference and following the LAI calibration scheme proposed in this study (see Section 4.2.6). The second part of the calibration strategy deals with model calibration of streamflow and flow partitioning, for which the inclusion of the baseflow index as well as discharge and FDC signatures within a multi-objective calibration approach is proposed. This approach is compared to discharge-based (single-objective, e.g. NSE) and signature-based (bi-objective, which includes criterion for discharge and FDC signatures) calibration strategies. The data-scarce Vilcanota River basin located in the Peruvian Andes served as a case study to demonstrate the advantages of the proposed model calibration framework, with a view to providing a better understanding of the basin's internal hydrological processes. The following conclusions can be drawn from the study:

- The LAI calibration scheme led to good model performance in the simulation of LAI when compared to MODIS LAI. Moreover, our findings shed light on the fact that in basins with high elevation gradients, heat units change with altitude; therefore, the SWAT parameter that controls the plant growth (PHU_PLT) decreases with height, and its calibration is crucial for correct LAI simulation in mountainous regions.
- Our results also show that better model performance in streamflow, FDC, and flow partitioning simulation is achieved when the model is calibrated using the proposed multi-objective calibration approach, whereas calibration approaches applied previously led to an unrealistic representation of flow partitioning even though good model performance for streamflow simulation is achieved with these strategies.
- The proposed methodology was observed to increase the identifiability of SWAT parameters related to evapotranspiration, streamflow, and flow partitioning, whereas the parameter values obtained by previous calibration approaches were unrealistic.
- This study shows that the solution of the SWAT model, which presents interactions among its parameters (Zhang et al., 2018a), using previous calibration approaches is subjected to equifinality since these approaches produced pseudo-accurate models, showing good model performance for streamflow simulation while incorrectly representing some internal basin processes. In contrast, the proposed multi-objective calibration, which includes the baseflow index, was observed to reduce the parameter equifinality.
- Regarding the eco-hydrology of the Andean Vilcanota River basin, it was found that evapotranspiration represents 50% of the average annual precipitation. The baseflow is the main component of the long-term streamflow (78% of it, on average) with an important contribution from deep aquifers that sustains the dry-season baseflow. Our findings further illustrate that areas covered by pasture offer better hydrological services regarding the water yield and baseflow in comparison to other land uses. The ability of the SWAT model to realistically simulate vegetation dynamics, streamflow, and baseflow can contribute to improving water resources management of the VRB and similar water catchments.

Overall, our proposed calibration and validation framework for hydrologic models such as SWAT increases the chances of obtaining the right answer for the right reason in hydrologic modelling, which is a crucial step toward more realistic hydrological applications. Examples include a better understanding of basin hydrology and water resources and an evaluation of the impacts of land-use changes and climate change. The proposed calibration framework can be applied in any mountain basin and can be adapted to the calibration of other physically or process-based hydrological models.

Acknowledgements

Disclosure statement

No potential conflict of interest was reported by the authors.

4.A Appendix
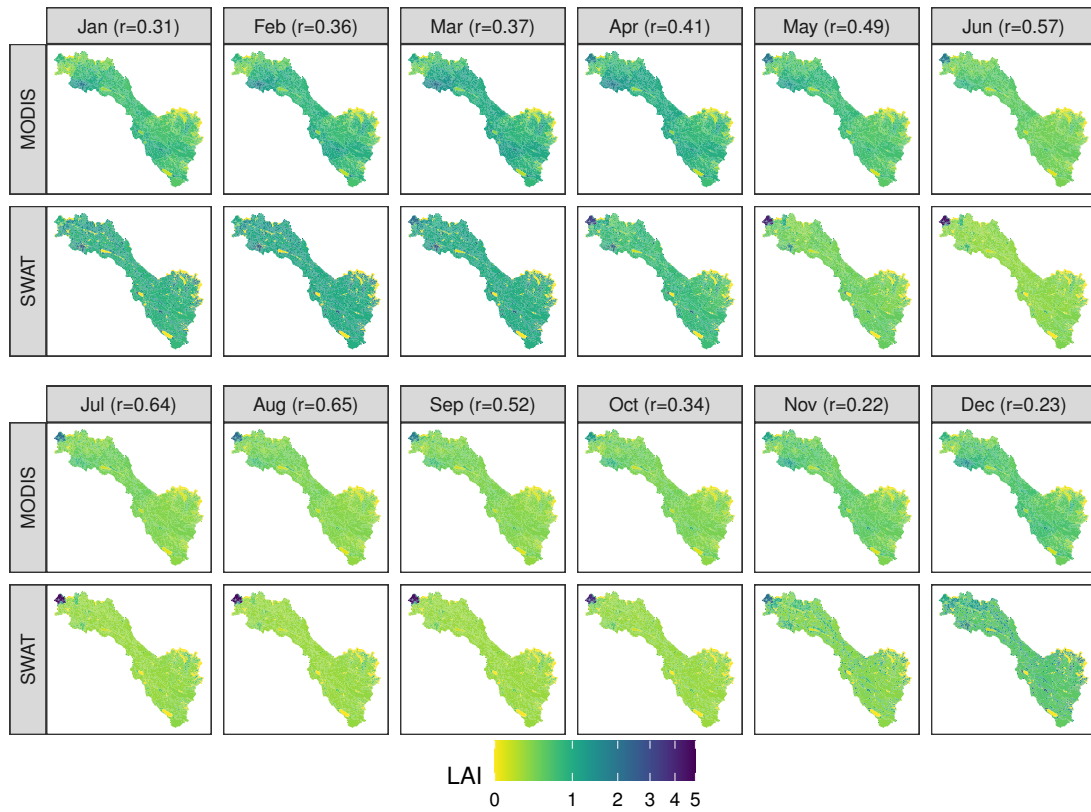
Figure 4.8: Spatio-temporal variability of average monthly LAI values for the period 2005–2015 estimated by MODIS and SWAT at HRU level. The spatial correlation (r) between MODIS and SWAT LAI is shown in parentheses.
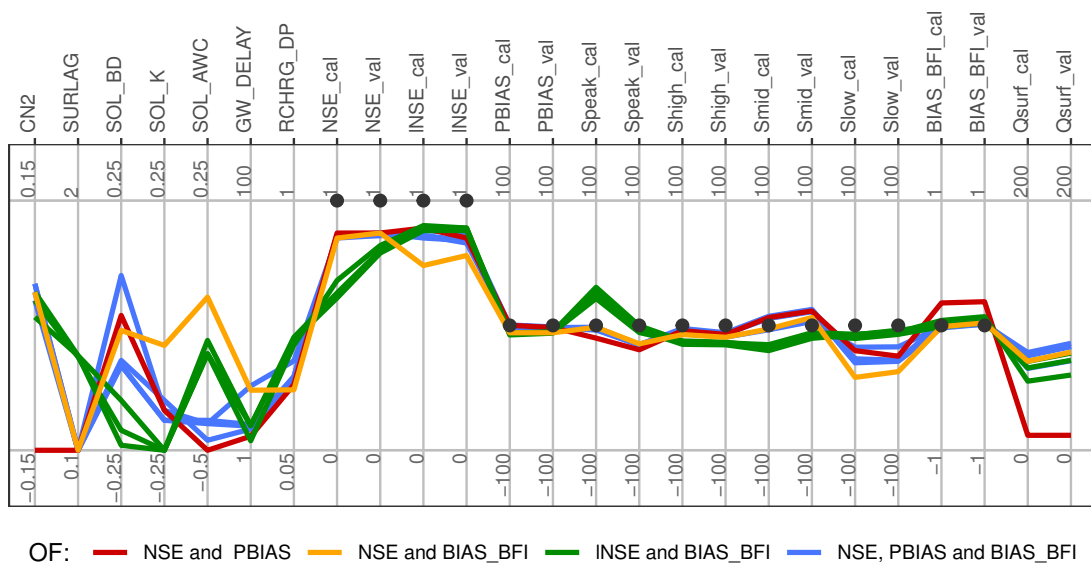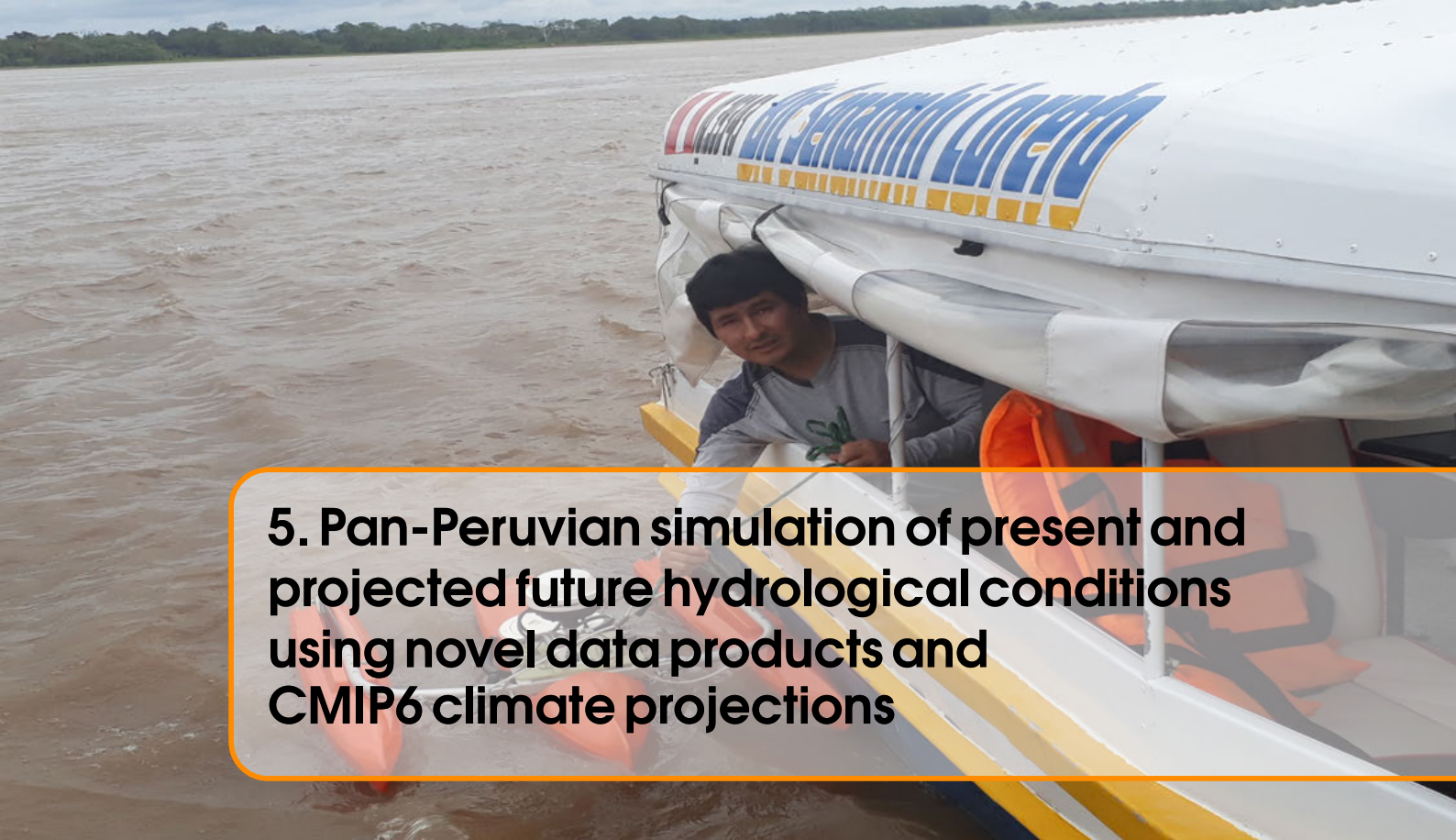
Figure 4.9: Parallel coordinates plot of the Pareto front optimal solutions obtained by additional calibration strategies: the traditional biobjective function based on discharge only (NSE and PBIAS) and the objectives defined by discharge measures and baseflow index, such as "NSE and BIAS_BFI," "lNSE and BIAS_BFI," and "NSE, PBIAS, and BIAS_BFI." For each solution, optimal parameter values, discharge-based performance measures (NSE, lNSE and PBIAS), and hydrological signatures (S_{peak}, S_{high}, S_{mid}, S_{low}, and BIAS_BFI) are displayed. _cal (_val) indicates the measurements for the calibration (validation) period. Qsurf is the mean surface runoff in mm. A description of SWAT parameters is provided in Table 4.6. A description of objective functions (OFs) is provided in Table 4.3. All calibration strategies shown in this figure perform worse than those calibration strategies that include lNSE, FDC signatures, and baseflow index within a multiobjective calibration framework as shown in Fig. 4.4.

5. Pan-Peruvian simulation of present and projected future hydrological conditions using novel data products and CMIP6 climate projections

Abstract

Peru faces climate change, and its consequences include retreating glaciers and more frequent severe droughts and floods. This study intends to analyze current and projected hydrological conditions in Peruvian and transboundary river catchments using novel hydrometeorological datasets and state-of-the-art regional climate projections. The objective is to investigate the various components of the regional terrestrial hydrological cycle and hydrological extremes under current conditions and scenarios for the mid (2035-2065) and end (2065-2095) of the century. The study utilizes novel observational data and bias-adjusted CMIP6 projections for sustainable (SSP1-2.6) and fossil fuel-based (SSP5-8.5) development scenarios, employing a well-calibrated and regionally adapted and extended regional-scale hydrological model.

Key findings reveal the Amazon-Andes transition region as a significant hotspot for water yield, driven by abundant rainfall and lower atmospheric water demand/evapotranspiration. Subsurface hydrological pathways, particularly baseflow from aquifers, strongly influence water yield in lowland and Andean catchments. The Pacific Basin exhibits an elevation- and latitude-dependent increase in water yield, while the Amazon Basin follows an unimodal curve peaking in the Amazon-Andes transition region. The study emphasizes the importance of floodplains in the Ucayali River in mitigating flood peaks.

Climate change projections indicate spatiotemporal and elevation-dependent shifts in the dynamics of hydrological variables and extremes. Andean regions are expected to experience amplified precipitation, water yield, and streamflow year-round, whereas Peruvian Amazon lowland catchments may see reductions in these variables during the wet season onset, particularly in central and southern regions. Additionally, there is an anticipated decrease in low flows in the Amazon lowlands and an increase in high flows in the Andean and northern Amazon catchments. These findings have crucial implications for water resource management, climate change adaptation, and the development of strategies to mitigate the risks associated with hydrological extremes.

Highlights

1. State-of-the-art simulations of current and projected hydrological conditions across Peru.
2. The Amazon-Andes transition region is highly relevant for South American water yield.

3. Floodplains in the Ucayali River play a vital role in mitigating flood peaks.
4. Water yield is projected to increase in Andean basins and decrease in Amazon lowlands.
5. Projections suggest more floods in Andean basins and more droughts in Amazon lowlands.

5.1 Introduction

Peru heavily relies on the available water resources for agriculture, energy, human well-being, and natural ecosystems. However, water availability is unevenly distributed across its three natural drainage basins (the Amazon basin, the Pacific basin, and the Titicaca Lake basin; Fig. 5.1), with climate change exacerbating this situation. In the Pacific basin, home to 66% of the population, only 2% of the total water resources are available, posing a risk of water scarcity for major coastal cities like Lima, which has over 10 million inhabitants (ANA, 2012; Bergmann et al., 2021). Climate change-induced rising temperatures and altered precipitation patterns are accelerating the hydrological cycle, leading to intensified floods, droughts, changes in river flow regimes, and limiting the operational capabilities of water infrastructure (Gloor et al., 2015; Marengo and Espinoza, 2016; Pabón-Caicedo et al., 2020; Rosas et al., 2020). To address these challenges, comprehensive knowledge of current and projected future hydroclimatic conditions at a national scale is crucial for sustainable water management, long-term planning, and successful adaptation. However, obtaining such knowledge in the tropical Andes is challenging due to the region's complex, highly variable, and changing hydrological and climatic conditions (Espinoza et al., 2020; Pabón-Caicedo et al., 2020; Russell et al., 2017), sparse and poor-quality hydrometeorological measurements (Condom et al., 2020), and particular uncertain precipitation datasets (Fernandez-Palomino et al., 2022). Moreover, global hydrological and even more global climate models (GCMs) have shown that their capabilities in simulating regional-scale processes in these terrains are too limited to base meaningful and responsible water resources management actions on Fernandez-Palomino et al., 2024; Towner et al., 2019.

Peru's hydroclimatic conditions, influenced by the Andes and various large-scale and local factors, are complex and crucial for regulating the country's climate. The Andes act as an orographic barrier, separating the comparatively cold and dry eastern Pacific region from the warm and moist Amazon region. These conditions are further modulated by large-scale factors (e.g., Atlantic intertropical convergence zone, South American monsoon systems, marine currents, Bolivian high) and local circulation patterns (e.g., upslope and downslope moisture transport) as well as the complex Andean orography (Espinoza et al., 2020). The El Niño-Southern Oscillation significantly impacts hydroclimate at the interannual timescale (Poveda et al., 2020). This intricate interplay of factors has resulted in Peru's remarkable ecological diversity, with diverse ecosystems like deserts, punas, páramos, glaciers, mountain forests, tropical montane cloud forests, and rainforests, which reflect the country's unique characteristics Espinoza et al., 2020; Fernandez-Palomino et al., 2022. Importantly, these hydroclimatic conditions are currently changing (see below), affecting Peru's ecological diversity and calling for increased attention and understanding of these changes.

Peru is already experiencing hydroclimatic intensification due to warming and changes in precipitation patterns. Since the mid-20th century, significant warming has been observed, particularly in higher elevations and the southern Peruvian Andes, with a trend of up to 0.3°C per decade (Aguilar-Lome et al., 2019; Bergmann et al., 2021; Imfeld et al., 2021; Lavado Casimiro et al., 2013; Pabón-Caicedo et al., 2020; Vicente-Serrano et al., 2018; Vuille et al., 2015). This warming, along with other factors such as increased El Niño events and local conditions (slope, aspect, altitude, and albedo), has significantly impacted Peru's glaciers (Cai et al., 2023; Juřicová and Fratianni, 2018; Rabatel et al., 2013; Veettil and Kamp, 2019; Vuille et al., 2018). From 1962 to 2016, Peruvian glaciers have rapidly reduced in area, shrinking by 54% (INAIGEM, 2018; Masiokas et al., 2020). The shrinking glaciers initially lead to increased runoff but eventually reach a 'peak water' turning point, after which runoff declines. Peak water has already been reached in 82-95% of the tropical Andes glacier area (Hock et al., 2019; Huss and Hock, 2018), indicating a rise in water stress during the dry season in glaciated catchments (Buytaert et al., 2017; Vuille et al., 2018).

Several studies show changes in precipitation and discharge patterns, with noticeable regional and seasonal variations. While mean and maximum precipitation and discharge in the Pacific and Titicaca Lake basins show no significant trends under current conditions, there has been an increase in minimum discharge, attributed to glacier melting or water regulation infrastructures (Fernández-Palomino and Lavado-Casimiro, 2017; Lavado Casimiro et al., 2012; Rau et al., 2019; Vega-Jácome et al., 2018). Southern Peruvian Andes have experienced

increased summer precipitation and shortened rainy season duration, with the wet season beginning later and ending earlier (Imfeld et al., 2021; Segura et al., 2020; Torres-Batlló and Martí-Cardona, 2020). In the Peruvian Amazon basin, the northern region (north of 8°S) has experienced an increase in precipitation, discharge, and wet-day frequency, while the southern region has seen a decrease in these variables, along with an increase in dry-day frequency and a month-longer dry season since the 1970s (Espinoza et al., 2019, 2016; Espinoza Villar et al., 2009a; Gloor et al., 2013; Lavado Casimiro et al., 2012; Marengo et al., 2018; da Motta Paca et al., 2020; Pabón-Caicedo et al., 2020). Furthermore, floods and droughts have intensified in the Amazon River basin in recent decades (Marengo and Espinoza, 2016). These findings highlight the ongoing intensification of Peru's hydroclimatic conditions, with the potential for further amplification in the future.

Climate projections based on CMIP Phase 3, 5, and 6 models indicate that Peru will likely face more severe hydro-climatic conditions due to climate change. These models suggest a temperature increase throughout the 21st century in Peru, with seasonal and regional variations (Bradley et al., 2006; Fernandez-Palomino et al., 2024; Pabón-Caicedo et al., 2020; Seiler et al., 2013; Vuille et al., 2018). By the end of the century, temperatures are expected to rise by 1.4°C to 4.4°C under low and high-end CMIP6 scenarios, reaching up to 7°C during September-November in the Peruvian Amazon lowlands (Fernandez-Palomino et al., 2024). This is a matter of concern, as temperature increase exceeding 4°C in the Amazon will likely disrupt the forest-climate equilibrium and may cause significant loss of tropical forests (Lenton, 2011; Nobre et al., 2016; Salazar and Nobre, 2010). Even in the most optimistic climate scenario, the Peruvian tropical glaciers are projected to disappear or shrink substantially by the end of the century (see Masiokas et al., 2020 and references therein). Precipitation projections vary by region and CMIP class, with notable changes under high-warming scenarios. CMIP3, 5, and 6 models project a drier lowland and wetter Andes response, but CMIP3 models anticipate a reduction in precipitation in the southern Peruvian Andes (Altiplano) during the 21st century (Fernandez-Palomino et al., 2024; Pabón-Caicedo et al., 2020; Seiler et al., 2013). Further investigation is needed to reduce uncertainties in precipitation projections over Altiplano.

The hydrological projections for limited Andean catchments, including Llanganuco, Vilcanota, Chancay-Huaral, and Santa River, indicate increased wet-season streamflow attributed to higher precipitation under high-emission scenarios, and reduced dry-season flow resulting from diminishing glaciers and rising water demand for various water uses (Andres et al., 2014; Juen et al., 2007; Motschmann et al., 2022; Olsson et al., 2017). These changes raise concerns regarding water scarcity during the dry season due to anticipated future increases in water demand in the Andean catchments. Marañón, the main tributary of the Amazon River, including the Huallaga River, is expected to experience increased river flow under high-warming scenarios (Lavado Casimiro et al., 2011; Zulkafli et al., 2016), while the Purus catchment in the southern lowlands is likely to have a decrease in discharge (Dalagnol et al., 2017). Hydrological projections for extremes indicate a higher risk of wet-season floods in the Marañón river basin and increased drought frequency, intensity, and duration in the Titicaca Lake basin (Zubieta et al., 2021; Zulkafli et al., 2016) as well as in the glaciated Santa and Vilcanota-Urubamba river catchments (Potter et al., 2023). These hydroclimatic projections suggest that the acceleration of the hydrological cycle will continue in the future.

To effectively address the challenges posed by climate change, reliable hydrometeorological data is crucial. However, the only coarse observational network and unreliable gridded meteorological datasets, particularly for precipitation—a critical factor in the water cycle and hydrological studies—hinder progress (Condom et al., 2020; Fernandez-Palomino et al., 2022). Regional studies consistently report biases and inaccuracies in global precipitation datasets derived from various sources for Peru, including satellite data, reanalysis, and merging procedures (see Fernandez-Palomino et al., 2022 and references therein). These uncertainties significantly affect the estimation of hydrological model parameters and water balance components, emphasizing the need for improved data quality (Fernandez-Palomino et al., 2022; Wang et al., 2023; Ye et al., 2012).

The Peru's National Meteorology and Hydrology Service (SENAMHI) has recently developed the Peruvian Interpolated data of SENAMHI's Climatological and Hydrological Observations (PISCO) dataset, which provides gridded meteorological data, including precipitation, maximum

and minimum temperature (Aybar et al., 2020; Huerta et al., 2018). PISCO has been used for hydrological modeling at various scales, ranging from specific catchments like the Andean Vilcanota River catchment and those draining into the Pacific Ocean to the national level (Asurza-Véliz and Lavado-Casimiro, 2020; Fernandez-Palomino et al., 2020; Llauca et al., 2021, 2023). SENAMHI evaluated the current and future national water balance using climate data from PISCO and three CMIP5-GCMs (Lavado-Casimiro et al., 2021). However, our understanding of countrywide hydrological conditions remains incomplete due to the primary reliability of PISCO precipitation data limited to Peruvian Andean catchments (Aybar et al., 2020; Fernandez-Palomino et al., 2022). Additionally, relying on a few climate models restricts the robustness of hydroclimatic projections, potentially overlooking significant variations and uncertainties.

To bridge this gap, Fernandez-Palomino et al. (2022) successfully developed the 'Rain for Peru and Ecuador (RAIN4PE)' dataset, providing the most reliable and accurate precipitation data for countrywide hydrological applications. In addition, Fernandez-Palomino et al. (2023b, 2024) introduced the BASD-CMIP6-PE dataset, offering bias-adjusted and statistically downscaled climate projection data based on the latest CMIP6 climate models. This dataset utilizes PISCO-temperature and RAIN4PE precipitation as its foundation, enabling reliable climate impact assessments in Peru and Ecuador.

Building upon state-of-the-art and reliable climate datasets, our study intends to comprehensively analyze current and projected hydrological conditions in the Peruvian and transboundary river catchments for the first time. The objective is to investigate the different components of the regional hydrological cycle and hydrological extremes for current conditions and for scenarios of the mid (2035-2065) and end (2065-2095) of the century addressing the following research questions:

1. What is the current spatial distribution and pattern of water balance components?
2. How does the distribution between water yield components vary?
3. How does the current seasonal water yield vary?
4. What is the relationship between water yield and elevation across different basins?
5. How does streamflow vary seasonally, and how do floodplains influence this variation?
6. How do projected changes in precipitation, evapotranspiration, and water yield vary spatially and with elevation?
7. How do projected precipitation, evapotranspiration, and water yield vary throughout the seasons?
8. How does projected streamflow vary spatially and seasonally?
9. How will climate change impact extreme hydrological conditions in Peru?

By evaluating the present situation (points 1-5) and future projections (points 6-9) for low and high warming scenarios, we believe that our findings will provide valuable insights for regional and national water resource management, climate change adaptation, and the development of effective strategies to mitigate the risks associated with hydrological extremes such as floods and droughts.

5.2 Methods

5.2.1 Hydrological model and observation-based driving data

We employed the process-based, semi-distributed, continuous, and widely-used hydrological model Soil and Water Assessment Tool (SWAT 2012 Rev. 664; Arnold et al., 1998) with recent improvements to better represent tropical vegetation and river-floodplain dynamics (Alemayehu et al., 2017; Fernandez-Palomino et al., 2022; Santini, 2020). SWAT has been successfully applied in Peru for ecohydrological modeling, assessing and improving precipitation data through reverse hydrology, and evaluating various precipitation datasets and bias-adjusted GCM outputs (Fernandez-Palomino et al., 2022, 2020, 2024). The basin is divided into subbasins and further into hydrological response units (HRUs) based on land use, soil type, and slope classes (Neitsch et al., 2011). Water balance computations are performed at the HRU level considering four water storage types (snow, soil profile, shallow aquifers, and deep aquifers).
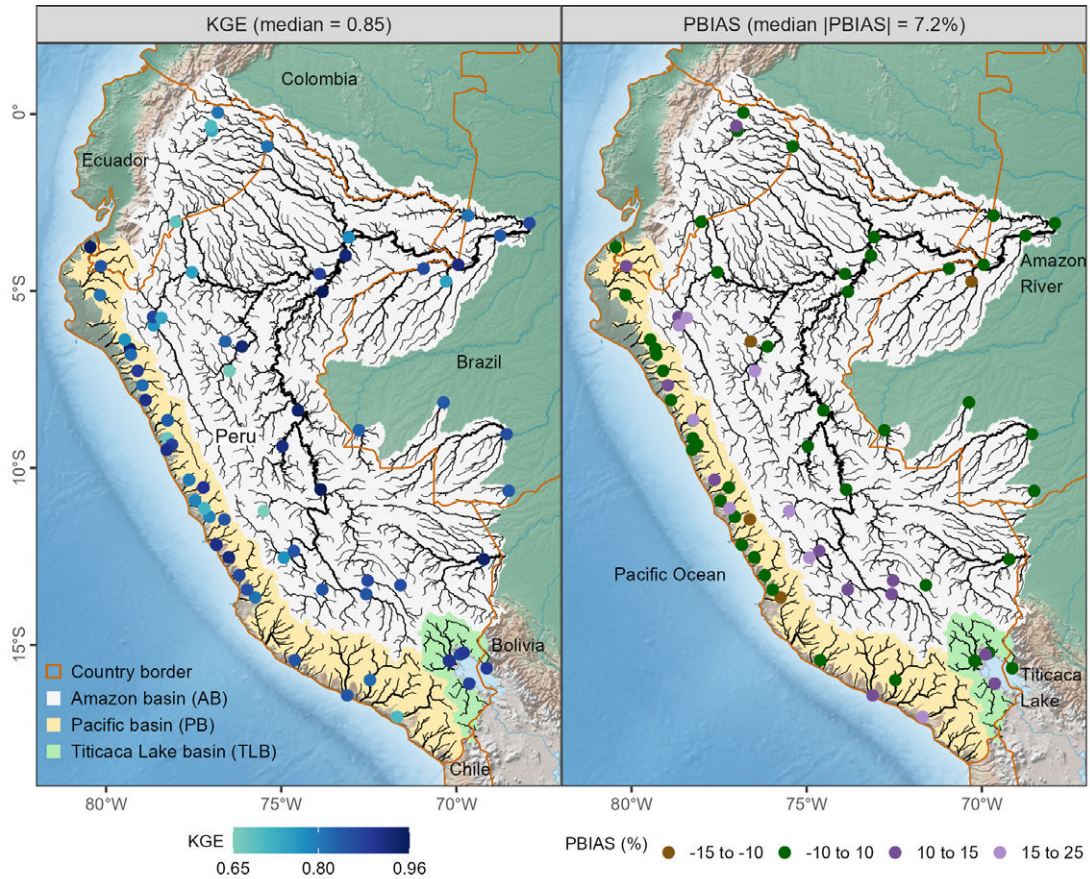
Figure 5.1: SWAT model performance in simulating monthly streamflow for 72 gauges in Peru in terms of Kling-Gupta efficiency (KGE) and percent bias (PBIAS) for the 1983-2015 period, based on Fernandez-Palomino et al. (2022). The figure also depicts the three natural drainage basins: (i) the Pacific basin (located on the western side of the Andes and draining water to the Pacific Ocean); (ii) the Amazon basin (located on the eastern side of the Andes and draining into the Amazon River); and (iii) the Titicaca Lake basin (catchments draining into Titicaca Lake).

$$\Delta S = \sum_{i=1}^{N}(P - \text{WYLD} - \text{ET} - \text{GWL}) \tag{5.1}$$

where ΔS is the change in water storage (mm); N is the time in days; and P, WYLD, ET, and GWL are the amount of precipitation (mm), water yield (mm), evapotranspiration (mm), and deep groundwater losses (mm), respectively.

Water yield (WYLD) is considered to be the sum of the following components of the hydrological cycle: surface runoff (Qsurf), lateral flow (Qlat), and return flow from shallow (Qgws) and deep (Qgwd) aquifers.

$$\text{WYLD} = \text{Qsurf} + \text{Qlat} + \text{Qgws} + \text{Qgwd} \tag{5.2}$$

In this study, we used the calibrated and validated SWAT model by Fernandez-Palomino et al. (2022) for Peruvian and transboundary river catchments, covering a total area of 1,638,793 km^2, comprising 2,675 subbasins and river segments and 6,843 HRUs.

The model was driven by high-resolution (1d, 10km) observation-derived novel data, including daily precipitation from the RAIN4PE dataset (Fernandez-Palomino et al., 2021, 2022) and

minimum and maximum temperature from the PISCO dataset (Huerta et al., 2018). Figure 5.1 presents the model's performance in simulating streamflow during the historical period (calibration and validation) in terms of modified Kling-Gupta efficiency (KGE, Kling et al., 2012) and percent bias (PBIAS, Gupta et al., 1999) for 72 gauges. The KGE values range from 0.65 to 0.96, and 89% of the gauges show PBIAS between -15% to 15%. Overall, the model exhibited very good performance according to the criteria set by Moriasi et al. (2007), with a median KGE of 0.85 and a median |PBIAS| of 7.2% for simulating streamflow and achieving water balance closure across most of the streamflow stations. The model was also verified for high and low flows and showed good performance as well (Fernandez-Palomino et al., 2022). For a better understanding of the SWAT model's application for Peruvian catchments, including details on its setup, calibration, validation, and parameter regionalization, we refer to Fernandez-Palomino et al. (2022).

5.2.2 Driving climate model data

We utilized meteorological forcing data (precipitation, minimum and maximum temperature) from the BASD-CMIP6-PE dataset (Fernandez-Palomino et al., 2023b, 2024). This dataset, tailored for the region, incorporates historical and projected climate data from 10 CMIP6-GCMs. Employing Lange's trend-preserving method for bias adjustment and statistical downscaling (Lange, 2019, 2021b), the dataset achieves a high-resolution representation (1d, 10km) that aligns and optimizes with observational data.

The BASD-CMIP6-PE climate data, designed for assessing climate impacts in Peru and Ecuador, reliably captures spatial patterns of atmospheric variables and streamflow dynamics, including mean, low, and high flows (Fernandez-Palomino et al., 2024). The dataset includes regional data from the following GCMs: CanESM5 (Swart et al., 2019), CNRM–CM6–1 (Voldoire et al., 2019), CNRM–ESM2–1 (Séférian et al., 2019), GFDL–ESM4 (Dunne et al., 2020), IPSL–CM6A–LR (Boucher et al., 2020), MIROC6 (Tatebe et al., 2019), MPI–ESM1–2–HR (Müller et al., 2018), MRI–ESM2–0 (Yukimoto et al., 2019), and UKESM1–0–LL (Sellar et al., 2019).

The hydrological simulations in this article incorporate data from all 10 CMIP6-GCMs, considering historical and future scenarios based on two Shared Socioeconomic Pathways (SSPs): SSP1-2.6 (sustainable, 2.6 W/m^2 by 2100) and SSP5-8.5 (fossil fuel-based, 8.5 W/m^2 by 2100). This approach addresses model uncertainty by utilizing the multimodel median and spread, exploring future, model-based climate uncertainty from anthropogenic forcing through the selected CMIP6 scenarios.

5.2.3 Analysis of current hydrological dynamics and projected hydrological changes

We analyzed current hydrological conditions using the calibrated SWAT model driven by observational climate data and projected future conditions using the aforementioned 10 GCMs and subsequent bias-adjustment of the climate data. To assess the impact of climate change on hydrological processes and extremes, we computed the multimodel median changes in water balance components and river flows (average, low, and high) for two future time slices (2035–2065, the 2050s, and 2065–2095, the 2080s) under SSP1-2.6 and SSP5-8.5, relative to the reference period of 1985-2015 (the 2000s). These future periods represent projected hydroclimatic conditions for the mid-century (2050s) and end-of-century (2080s). High and low flows were determined using Q5 and Q95, respectively, representing flows exceeding the 5% and 95% thresholds of the analysis period. These indices were computed based on simulated daily mean flows.

Our analysis defines the Amazon-Andes transition region as encompassing areas above 500 meters above sea level (m a.s.l.) within the Amazon basin, and Amazon lowland refers to lower elevations. Within the transition region is a tropical montane forest zone known as the 'montane zone/catchments,' spanning elevations ranging from 500 to 3000 m a.s.l.. These catchments are characterized by tropical montane cloud forests and páramo ecosystems, which receive a significant proportion, up to 30%, of their precipitation from cloud and fog water sources (Cárdenas et al., 2017; Fernandez-Palomino et al., 2022; Gomez-Peralta et al., 2008).

Table 5.1: SWAT-simulated average annual water balance (1985–2015) for Peru and three drainage systems, including transboundary basins

Component	Amazon basin	Pacific basin	Titicaca Lake basin	Peru
Area (km^2)	1361958	234824	42011	1638793
Precipitation, P (mm)	2491	414	693	2147
Evapotranspiration, ET (mm)	1075	252	528	943
Water yield, WYLD (mm)	1416	162	165	1204
Streamflow, Q (m^3/s)	60967	1212	220	62399
Ratios				
ET/P (%)	43	61	76	44
WYLD/P, Q/P (%)	57	39	24	56
Q basin/Q Peru (%)	97.7	1.9	0.4	100

In general, the basins located in the Amazon-Andes transition region, the Pacific basin, and the Lake Titicaca basin are considered Andean regions/basins in the literature.

5.3 Results and discussion

5.3.1 What is the current spatial distribution and pattern of water balance components?

The simulated water balance for Peru, including its transboundary basins, provides information about the country's water resources and its distribution for the different large basins (Table 5.1). They show that Peru receives an average annual precipitation of 2,147 mm, with water yield (evapotranspiration) accounting for 56% (44%) of the total precipitation. The Amazon basin exhibits the highest water yield among the basins, representing 57% of the precipitation, while the Pacific and Lake Titicaca basins have lower percentages of 39% and 24%, respectively. These lower percentages indicate a larger share of evapotranspiration in the Pacific and Titicaca Lake basins. The runoff ratios in each drainage system were similar to the water yield values over precipitation, indicating minimal long-term water storage and a balanced regional water cycle.

Regarding total freshwater resources, Peru has a combined discharge of 62,399 m^3/s leaving Peruvian catchments, underlining its importance as a water tower in the region. The Amazon basin contributes 97.7% (60,967 m^3/s) of this total, followed by the Pacific basin accounting for 1.9% (1,212 m^3/s), and the Titicaca Lake basin contributing 0.4% (220 m^3/s). These findings align with the observation-based (river gauging data) estimation of water availability in Peru by the National Water Authority of Peru (ANA, 2012), which reported 54,535 m^3/s in the Amazon basin, 1,140 m^3/s in the Pacific basin, and 222 m^3/s in the Titicaca Lake basin. In contrast, our findings differ from the previous countrywide simulation-based study conducted by Lavado-Casimiro et al. (2021). They reported lower water supply in the Pacific basin (1,010 m^3/s) and the Amazon basin (40,538 m^3/s), and higher water supply in the Titicaca basin (285 m^3/s).

Other local studies have also reported a similar lower water supply in the Pacific basin. For instance, Rau et al. (2019) estimated a value of 747 m^3/s, while Asurza-Véliz and Lavado-Casimiro (2020) estimated 990 m^3/s. These differences can be partly attributed to the exclusion of transboundary catchments between Peru and Ecuador, such as the Tumbes and Chira, in the study by Rau et al. (2019). It is possible that both Asurza-Véliz and Lavado-Casimiro (2020) and Lavado-Casimiro et al. (2021) underestimated streamflow in the Pacific basin due to the underestimation of precipitation over the northern Andean region when using the PISCO-precipitation product as a driver for hydrological modeling, as demonstrated in Fernandez-Palomino et al. (2022). Additionally, the PISCO-precipitation product substantially underestimates precipitation over the Amazon lowlands (Fernandez-Palomino et al., 2022), which can explain the significant underestimation of water supply in the Amazon basin by Lavado-Casimiro et al. (2021). Despite these differences, our estimated water availability for Peru and across the three drainage systems is consistent with observation-based estimations,

enhancing the reliability of our water balance estimations and providing valuable information for effective water resource management.

The spatial pattern of water balance components in Peru shows an increasing trend for all hydrological components from west to east, with notable concentration areas (hotspots) of precipitation (P) and water yield ($WYLD$) in the montane zone (Fig. 5.2a,d). In this zone and the northern Amazon lowlands, water yield exceeds evapotranspiration ($WYLD/P > 0.5$). Conversely, in the highlands of the Amazon basin ($>$3000 m a.s.l.), as well as in the Pacific and Titicaca Lake basins and the southern Amazon lowlands, evapotranspiration dominates ($WYLD/P < 0.5$), signifying less available water for runoff and potential anthropogenic water use.

Mean annual streamflow shows a wide range (Fig. 5.3a, left panel), ranging from low values in the dry catchments of the Pacific basin to high values of approximately 52,000 m^3/s in the Amazon River at Santo Antonio Do Ica hydrological station downstream of the Peru-Colombia-Brazil border. Specific streamflow (Fig. 5.3a, center panel), which accounts for streamflow per unit area, highlights the Amazon basin catchments as nearly ten times more productive on average (with a median value of about 43 l/s/km^2) compared to the Pacific (4 l/s/km^2) and Titicaca Lake (6 l/s/km^2) basins. Montane catchments generally have high specific streamflow values, up to 143 l/s/km^2.

Previous studies have emphasized the Amazon-Andes transition region as the wettest area (Chavez and Takahashi, 2017; Espinoza et al., 2015), with higher runoff compared to the Amazon lowland (Builes-Jaramillo and Poveda, 2018). In this study, we show, for the first time, that the montane zone (500-3000 m a.s.l.) in the Amazon-Andes transition region also exhibits the highest water yield and streamflow per unit area. This is attributed to abundant precipitation (up to 5700 mm/year) from rainfall and cloud/fog water, along with reduced evapotranspiration resulting from persistent low-level cloud cover and cooler temperatures compared to the surrounding lowlands. These wet atmospheric conditions minimize evaporative losses and contribute to a higher water yield and streamflow. Overall, our findings emphasize the significant role of the montane catchments in shaping the hydrological variability of the entire Amazon basin.

5.3.2 How does the distribution between water yield components vary?

The simulated water yield components highlight the dominant influence of subsurface hydrological pathways over surface runoff in determining water yield in Peruvian and Ecuadorian catchments (Fig. 5.2b). Baseflow, primarily driven by return flow from the shallow aquifer (Qqws), emerges – according to our model results – as the primary contributor to water yield in Amazon lowland catchments. In contrast, Andean catchments exhibit a complex system with multiple sources, including lateral flow (Qlat) and return flows from both shallow (Qqws) and deep (Qgwd) aquifers. The return flow from deep aquifers plays a crucial role in regulating the baseflow regime in Andean catchments, ensuring substantial discharge even during the extended dry seasons. Previous studies conducted in Peruvian Andean basins, such as Kosñypata (Clark et al., 2014), upper Marañon (Hill et al., 2018), and Vilcanota River basin (Fernandez-Palomino et al., 2020; Wunderlich et al., 2023), have also highlighted the importance of this flow. Although there is uncertainty in quantifying water yield components due to the inability to directly verify or compare these flows with measurements, these results provide valuable information for improved water resource management and sustainable use by recognizing the significance of subsurface hydrological flows.

5.3.3 How does the current seasonal water yield vary?

The simulated seasonal distribution of water yield shows spatial variations across the study area, with different timing of water yield peaks from south to north (Fig. 5.2c). In the Ecuadorian and northern Peruvian Amazon, water yield follows a weak annual cycle (with small differences in water yield between seasons), while the southern catchments, including both Andean and lowland areas, experience a strong annual cycle, with high (low) yields during December-May (June-November). The timing of water yield peaks varies spatially, occurring in December-February over southern catchments, March-May over northern Andean catchments draining
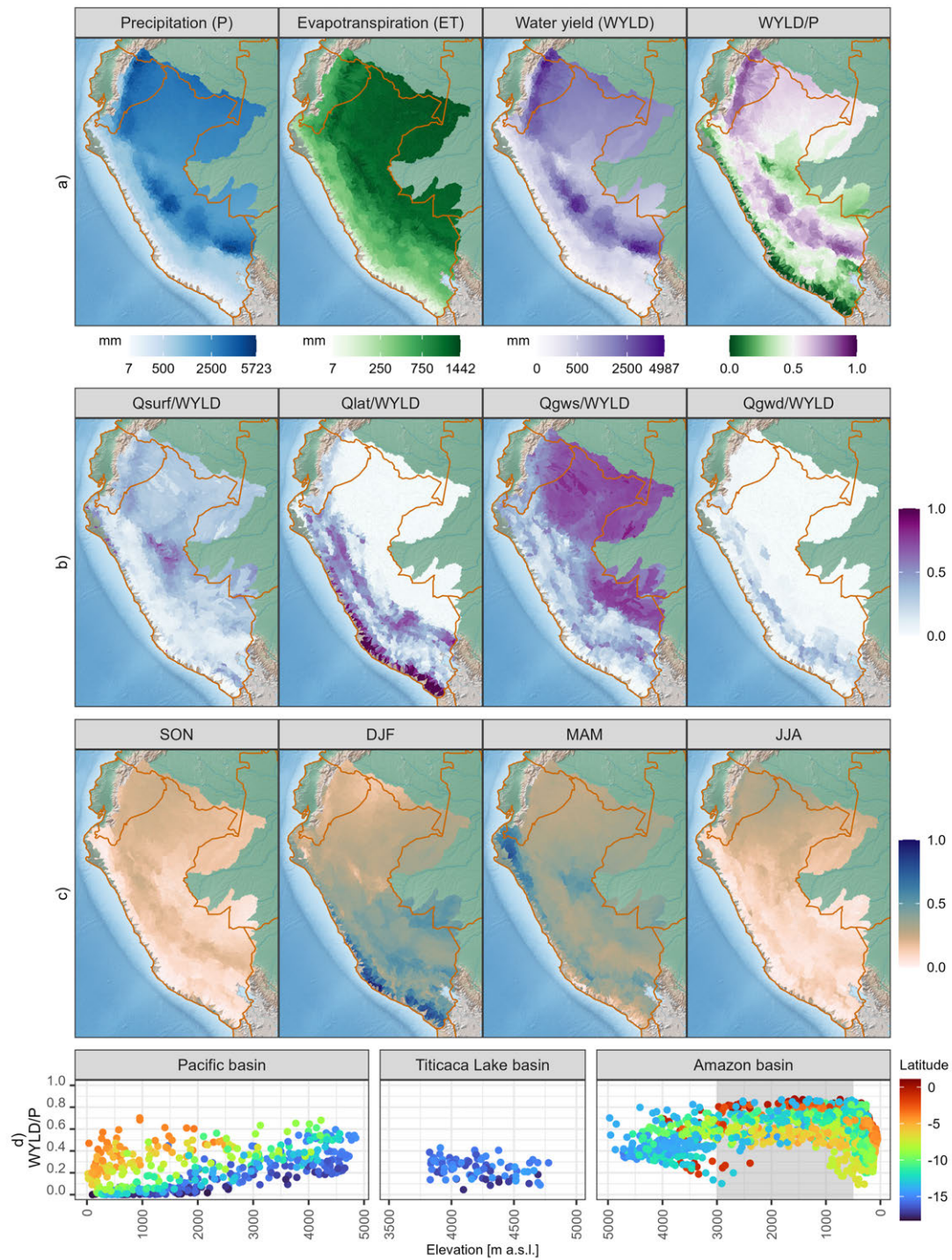
Figure 5.2: (a) The distribution of water budget components, including precipitation (P), evapo-transpiration (ET), water yield (WYLD), and the WYLD/P ratio; (b) the ratio of WYLD components, such as surface runoff (Qsurf), lateral flow (Qlat), and return flow from shallow (Qgws) and deep (Qgwd) aquifers, relative to the total WYLD; (c) the seasonal-to-annual WYLD ratio; and (d) the elevation-dependent distribution of WYLD/P, with the shaded region (gray) representing the montane zone and the x-axis showing increasing (decreasing) elevation values for the Pacific and Titicaca Lake basins (Amazon basin), mirroring the western and eastern slopes of the Andes.
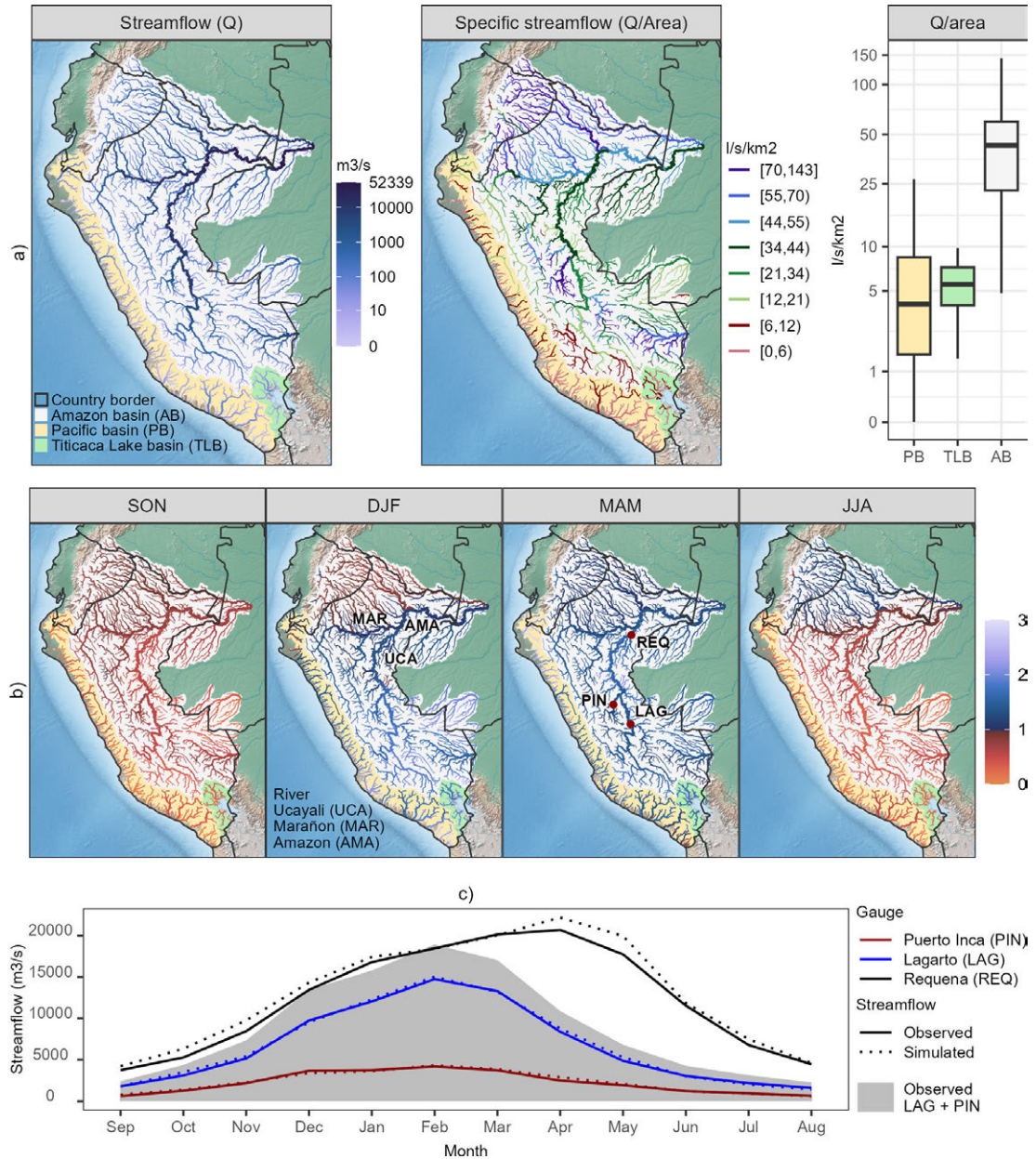
Figure 5.3: (a) Distribution of mean annual streamflow (Q) and specific streamflow (per unit area) for 1985-2015 period, (b) seasonal distribution of streamflow, represented by the ratio of seasonal mean streamflow to annual mean streamflow, and (c) streamflow seasonality in Ucayali River for 2009-2015 (common period with available observed data). The specific streamflow map shows intervals containing 12.5% of the total river segments. The LAG + PIN represents the combined streamflow observed at the Lagarto and Puerto Inca hydrological stations.

into the Pacific, and March-August over the Ecuadorian and northern Peruvian Amazon. These variations in peak timing are influenced by precipitation fluctuations associated with the latitudinal migration of the Intertropical Convergence Zone, the mature phase of the South American Monsoon system, and the influence of the Andes topography on precipitation (Arias et al., 2021a; Espinoza et al., 2020). These results highlight the complexity of water availability dynamics and emphasize the importance of considering seasonal dynamics in water resource management, infrastructure development, and planning efforts.

5.3.4 What is the relationship between water yield and elevation across different basins?

Water yield distribution exhibits diverse patterns related to elevation across different basins (Fig. 5.2d). In the Pacific Basin, there is a gradual increase in WYLD/P with elevation for similar latitudes, and water yield generally increases from south to north, which is consistent with the findings of Asurza-Véliz and Lavado-Casimiro (2020). Conversely, no clear pattern emerges in the Titicaca Lake basin. In the Amazon Basin, WYLD/P and elevation follow an unimodal curve, with a peak occurring at 1000-1500 m a.s.l. (mean WYLD/P = 0.68) in the Amazon-Andes transition region. These findings highlight the complex relationship between water yield distribution and elevation in different basins.

5.3.5 How does streamflow vary seasonally, and how do floodplains influence this variation?

Simulated streamflow exhibits seasonal variations, following a pattern of water yield from south to north and from summer (December-February) to winter (June-August) (Figs. 5.2c, 5.3b). The annual seasonal streamflow variation in the Ecuadorian and northern Peruvian Amazon is relatively attenuated but more pronounced in southern catchments.

In the Amazonian rivers of the Amazon lowlands, the floodplain (a landscape that is periodically inundated by water from an adjacent river) plays a crucial role in attenuating peak discharge due to the water connection between the channel and floodplain (De Paiva et al., 2013; Opperman et al., 2010; Yamazaki et al., 2011). We observed in measured discharge data that the Ucayali River, a tributary of the Amazon River, exhibits the most pronounced delay in peak flows during the high discharge season (Fig. 5.3b,c). Upstream at the Lagarto and Puerto Inca hydrological stations, peak flow occurs during summer (February), while downstream at the Requena hydrological station, it is observed in autumn (April). This two-month delay could be attributed to floodplains acting as reservoirs, causing significant delays and attenuations of flood peaks (Fernandez-Palomino et al., 2022; Santini et al., 2015; Santini, 2020).

Previous studies have modeled this phenomenon by considering floodplains as surface reservoirs connected to the main river channel (De Paiva et al., 2013; Yamazaki et al., 2011; Zulkafli et al., 2016). However, this approach could not fully explain the delay from Lagarto to the Requena station, which can last several months.

Fernandez-Palomino et al. (2022) and Santini (2020) have incorporated additional interactions between floodplains and reaches into the SWAT model. These interactions encompass factors such as water infiltration from floodplain flow or ponded water during overbank flood events, storage of water in floodplain alluvium, and subsequent backflow into the channel as the flood wave subsides and water levels decrease. Incorporating these additional processes into the SWAT model has shown improvement in the agreement between the observed and simulated streamflow, as depicted in Fig. 5.3c.

One has to acknowledge the significant influence of floodplains on the delay and attenuation of flood peaks in the Ucayali River. Neglecting this aspect in hydrological modeling can have significant negative implications (e.g., misrepresentation of flood peak magnitude and timing) for flow simulation in the Amazon River. Therefore, incorporating these processes into the hydrological models is essential for proper modeling and predicting the river system's behavior.

5.3.6 How do projected changes in precipitation, evapotranspiration, and water yield vary spatially and with elevation?

Projected changes in precipitation, evapotranspiration, and water yield exhibit spatial variability and are influenced by elevation across the study area (Figs. 5.4a,b). The Andean regions are expected to experience increased precipitation, while a decrease is projected over the Amazon lowlands, especially noticeable under the high warming scenario towards the end of the century. In the Pacific basin, precipitation is anticipated to increase by 6-11% (2035-2065) and 6-23% (2065-2095) under the SSP1-2.6 and SSP5-8.5 scenarios, with greater increases towards lower elevations. Caution is advised when interpreting percentage changes over coastal and arid regions (<2000 m a.s.l.), as small changes in precipitation can lead to significant percentage variations in precipitation, evapotranspiration, and water yield (Fig. 5.4b). In the Titicaca Lake basin, precipitation is projected to increase by 5% (2035-2065) under both scenarios, with a persistent increase of 4% (SSP1-2.6) or an amplified increase of 14% (SSP5-8.5) for 2065-2095.

a) Spatial variation of projected changes in water budget components

b) Projected changes in water budget components along elevation for each drainage system
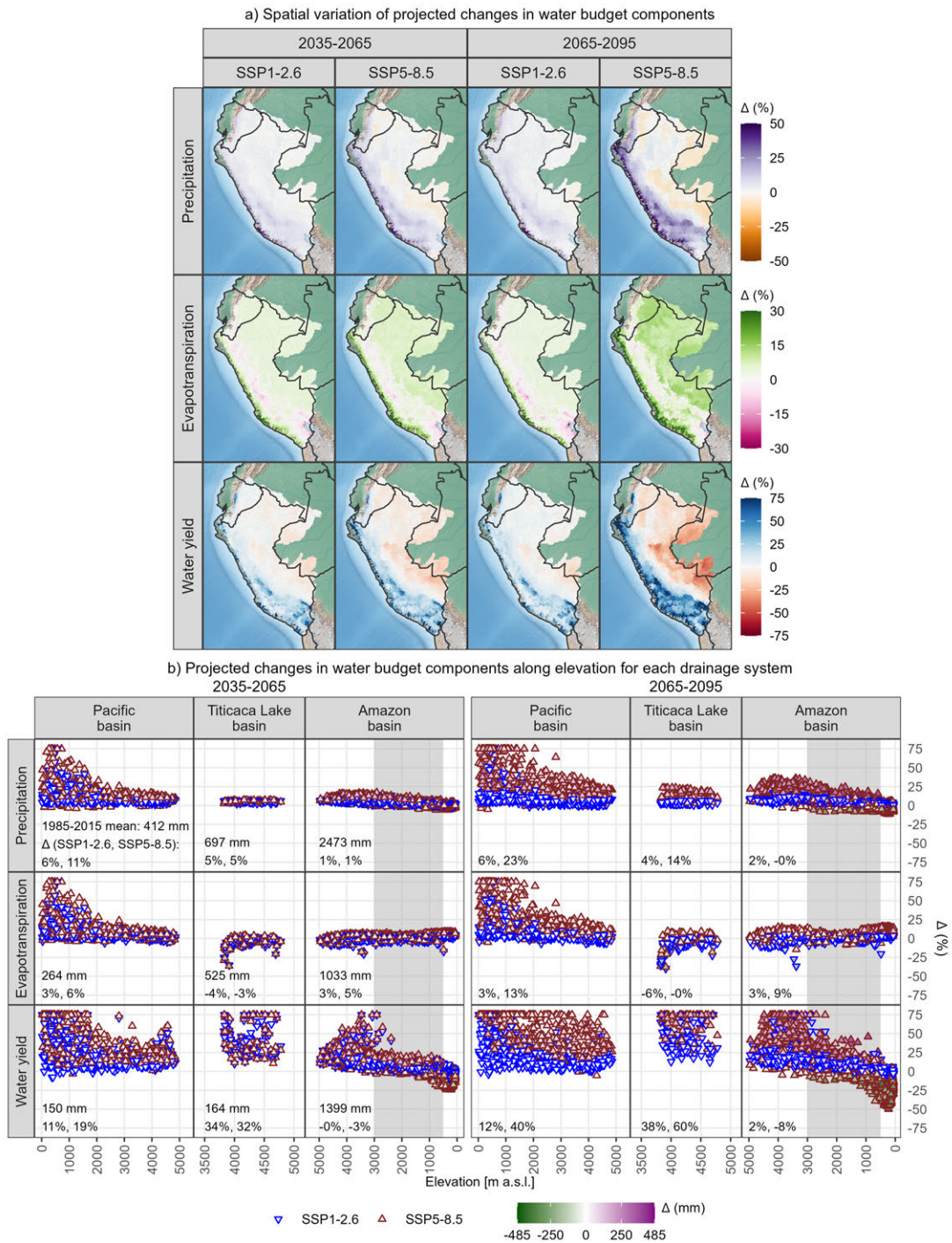
Figure 5.4: (a) Spatial and (b) elevation distribution of projected multimodel median changes in water budget components under SSP1-2.6 and SSP5-8.5 scenarios for 2035–2065 and 2065-2095, relative to the reference period (1985–2015). The shaded region (gray) represents the montane zone, and the x-axis shows increasing (decreasing) elevation values for the Pacific and Titicaca Lake basins (Amazon basin), mirroring the western and eastern slopes of the Andes. Note that multimodel median values of water balance components for 1985-2015 are similar to those derived from SWAT driven by observational data.

The greater precipitation changes (up to 24%) are expected in lower elevations in the northern areas of Titicaca Lake. In the Amazon basin, overall changes in precipitation are negligible, but

they vary with elevation, with an increase (of up to 36%) in the Andean region and a decrease (of up to -12%) in the lowlands, particularly in central and southern areas.

Projected evapotranspiration changes indicate that the Amazon lowlands are expected to experience a more significant increase than the Andean region, except for the Altiplano region in the Titicaca Lake basin, where a decrease is anticipated. In the Pacific basin, evapotranspiration is projected to increase by 3-6% (2035-2065) and 3-13% (2065-2095) under SSP1-2.6 and SSP5-8.5 scenarios, with greater increases towards lower elevations. Conversely, the Titicaca Lake basin is anticipated to experience a decrease in evapotranspiration of -4% to -3% (2035-2065) and -6% to 0% (2065-2095), with greater reductions (of up to -40%) in lower elevations surrounding Titicaca Lake. This paradoxical evapotranspiration reduction can be linked to the projected rise in humidity and cloud cover due to projected increased rainfall and wet days. Ground measurements also suggest that evaporation decreases with higher rainfall in the Titicaca Lake region (Delclaux et al., 2007). In the Amazon basin, evapotranspiration is expected to increase by 3-5% (2035-2065) and 3-9% (2065-2095), with the montane zone between 1000-3000 m a.s.l. showing lower increases compared to 500-1000 m a.s.l., as well as the lowlands (<500 m a.s.l.) and highlands (>3000 m a.s.l.).

Projected water yield changes expose regional variations in response to shifts in precipitation and evapotranspiration. The Pacific basin is expected to experience a water yield increase of 11-19% (2035-2065) and 12-40% (2065-2095) under SSP1-2.6 and SSP5-8.5 scenarios, with some sub-catchments showing even higher than 75% increase. Also, for the Titicaca Lake basin, the model projects a rise of 34-32% (2035-2065) and 38-60% (2065-2095). In the Amazon basin, the high Andean basins (>3000 m a.s.l.) may even see water yield increases exceeding 75%, while lowland areas (<500 m a.s.l.) could experience a decline of up to -50% by the end of the century under SSP5-8.5. Although the montane zone (500-3000 m a.s.l.) is expected to undergo less pronounced changes, the significant reduction in water yield (under future drier conditions) below 1000 m a.s.l. (see Fig. 5.4b) could lead to an upward shift in the minimum elevations of tropical montane cloud forests. This aligns with a previous report by Helmer et al. (2019), highlighting the shrinking of these forest habitats due to climate change.

The simulated overall increased (decreased) water yield over the Andean regions (Amazon lowland) in the future, as presented in this study, aligns with the findings of Brêda et al. (2020). Their study, based on an ensemble of 25 CMIP5-GCMs at the South American level, also reported similar patterns of water yield over the tropical Andes under medium and high warming scenarios. Additionally, Lavado-Casimiro et al. (2021) observed similar patterns over northern Andean catchments (>8°S) draining into the Pacific Ocean, using three CMIP5-GCMs. However, their projections suggest a negative change signal towards the southern Andean catchments. This discrepancy may be attributed to the use of a limited number of climate models, which could potentially limit the robustness of hydroclimate projections.

We consider that the use of 10 CMIP6-GCMs in this study and the agreement of our results with the findings of Brêda et al. (2020) enhances the plausibility of the projected hydroclimatic changes.

5.3.7   How do projected precipitation, evapotranspiration, and water yield vary throughout the seasons?

Projected changes in seasonal precipitation (Fig. 5.10), evapotranspiration (Fig. 5.11), and water yield (Fig. 5.5) reveal distinct patterns in the study area, with pronounced changes, particularly under fossil fuel based development (SSP5-8.5) towards the end of the century. Precipitation decreases in the Amazon lowlands at the beginning (September-November) and end (June-August) of the hydrological year, with no significant changes during the wet seasons (December-March). In contrast, Andean regions would experience increased precipitation almost year-round. Evapotranspiration shows consistent increases in the lowlands and minimal changes in the Andean regions year-round. These changes in precipitation and evapotranspiration have significant implications for water yield across the study area. The Amazon lowlands witness a decrease in projected water yield throughout the year, except during the wet season (June-August) in the Ecuadorian and northern Peruvian Amazon. In contrast, Andean regions exhibit increased water yield year-round, with only minor changes in the montane zone. These projections underscore the seasonal variability of water yield in response to changes
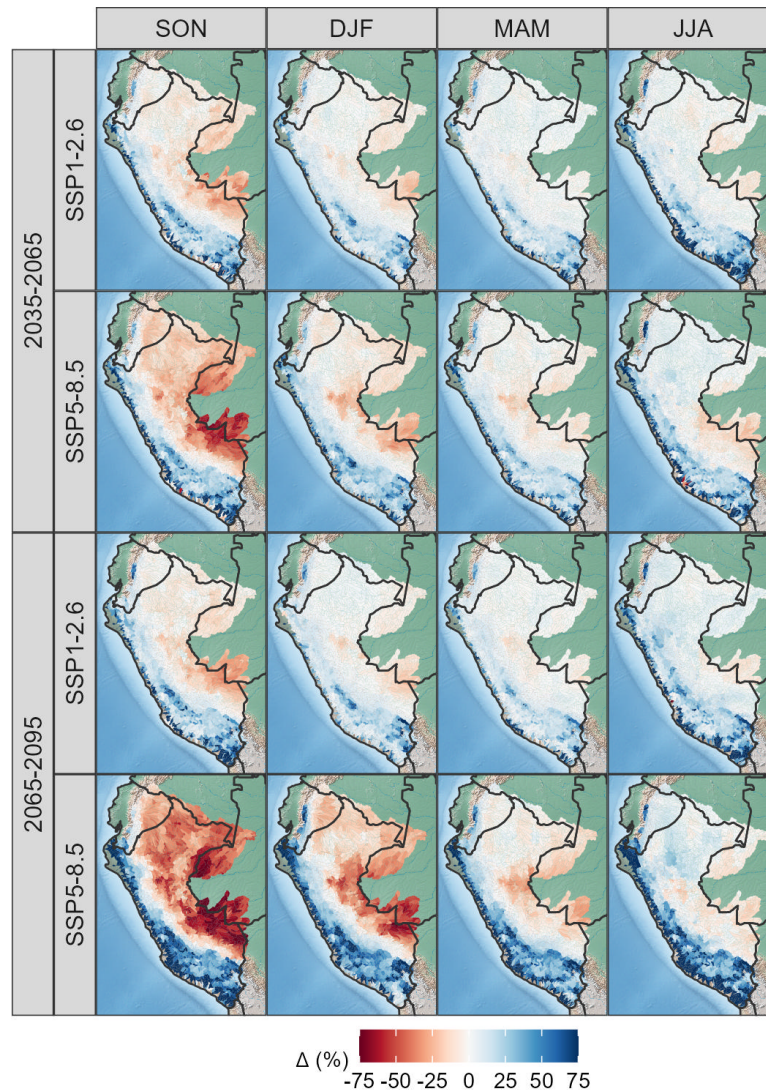
Figure 5.5: Projected seasonal multimodel median changes in water yield under SSP1-2.6 and SSP5-8.5 scenarios for 2035–2065 and 2065-2095, relative to the reference period (1985–2015).

in precipitation and evapotranspiration, emphasizing the importance of understanding water resources in the study area.

5.3.8 How does projected streamflow vary spatially and seasonally?

The projected changes in mean annual and seasonal flow show spatiotemporal variations that align with projected patterns in water yield, with notable impacts, particularly under fossil fuel intense development (Figs. 5.6, 5.7, 5.8, 5.9, 5.12). Figs. 5.6 and 5.12 illustrate the spatial distribution of annual and seasonal streamflow changes. Fig. 5.7 presents the seasonal streamflow projections and annual changes for specific river catchments across the three drainage systems, ordered from south to north. Similarly, Figs. 5.8 and 5.9 display the results for other river catchments. These figures (Figs. 5.7, 5.8, and 5.9) may be valuable resources for users interested in examining specific river catchments and comparing past and future studies.

   The projections show an increase in streamflow in Andean rivers year-round, with significant rises in the wet season and minor increases in the dry season (Figs. 5.6, 5.12). This positive trend is evident in the Andean rivers of the Pacific basin (e.g., Ocoña, Chancay-Huaral, Santa, and Chira rivers, see Figs. 5.7, 5.8), the Titicaca Lake basin (Ilave, Ramis, Coata, Huancane,
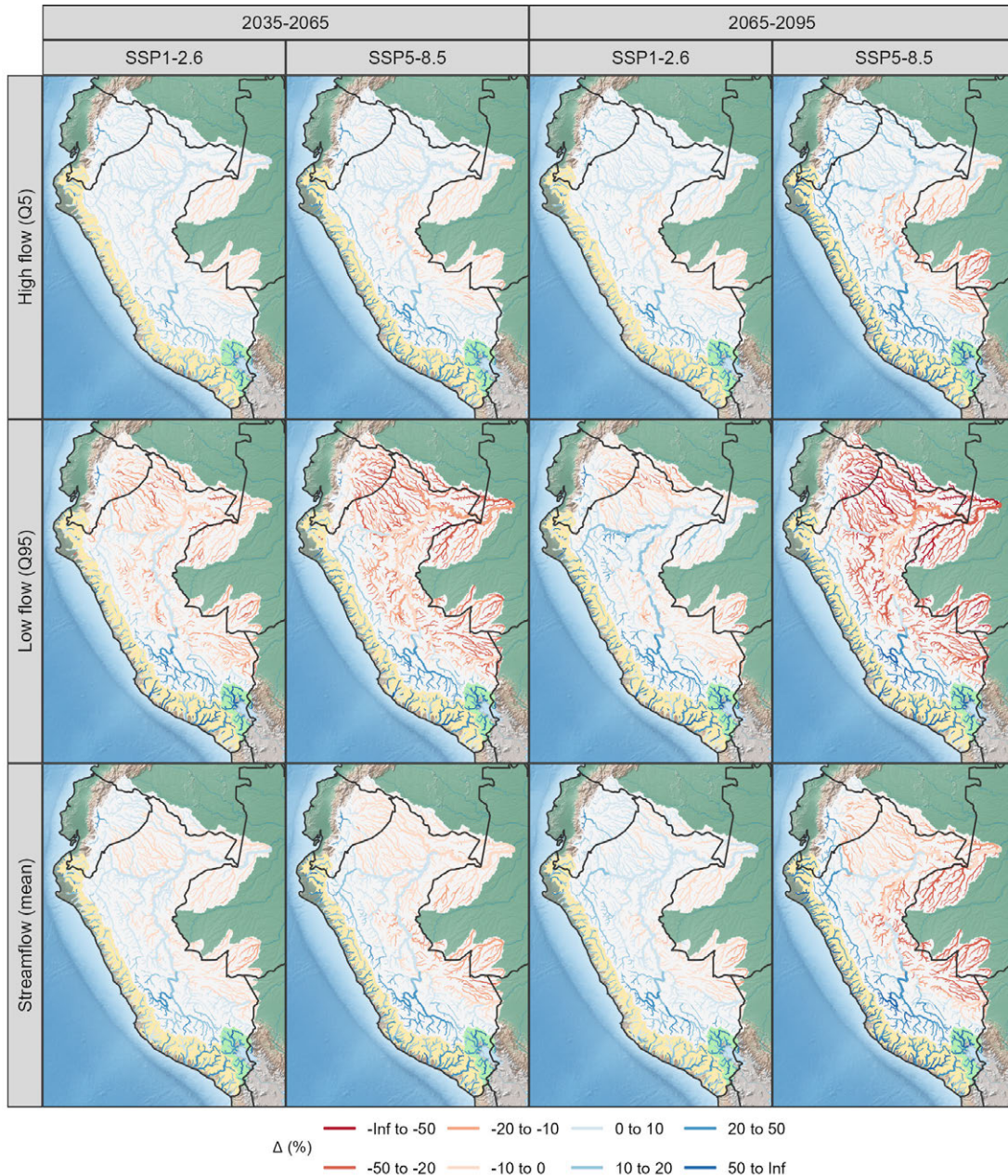
Figure 5.6: Spatial distribution of projected multimodel median changes in mean, high (Q5), and low (Q95) flows under SSP1-2.6 and SSP5-8.5 scenarios for the periods 2035–2065 and 2065–2095, relative to the reference period (1985–2015).

see Figs. 5.7, 5.8), and the Amazon basin (e.g., Upper Marañon at Borja station, Mantaro, Pampas, Vilcanota, Apurimac, see Fig. 5.9). The multimodel projections indicate that median changes in streamflow can reach up to 70% in Andean rivers, especially in the Titicaca Lake catchments under the SSP5-8.5 scenario. Among the Andean catchments, the montane catchments, including Mayo and Pachitea rivers (Fig. 5.9), are projected to have minimal streamflow changes (less than 7%) throughout the year under both warming scenarios (SSP1-2.6 and SSP5-8.5).

The positive change in streamflow in Andean catchments aligns with previous research (Andres et al., 2014; Juen et al., 2007; Lavado Casimiro et al., 2011; Motschmann et al., 2022; Olsson et al., 2017), which consistently indicated increased wet-season streamflow under high
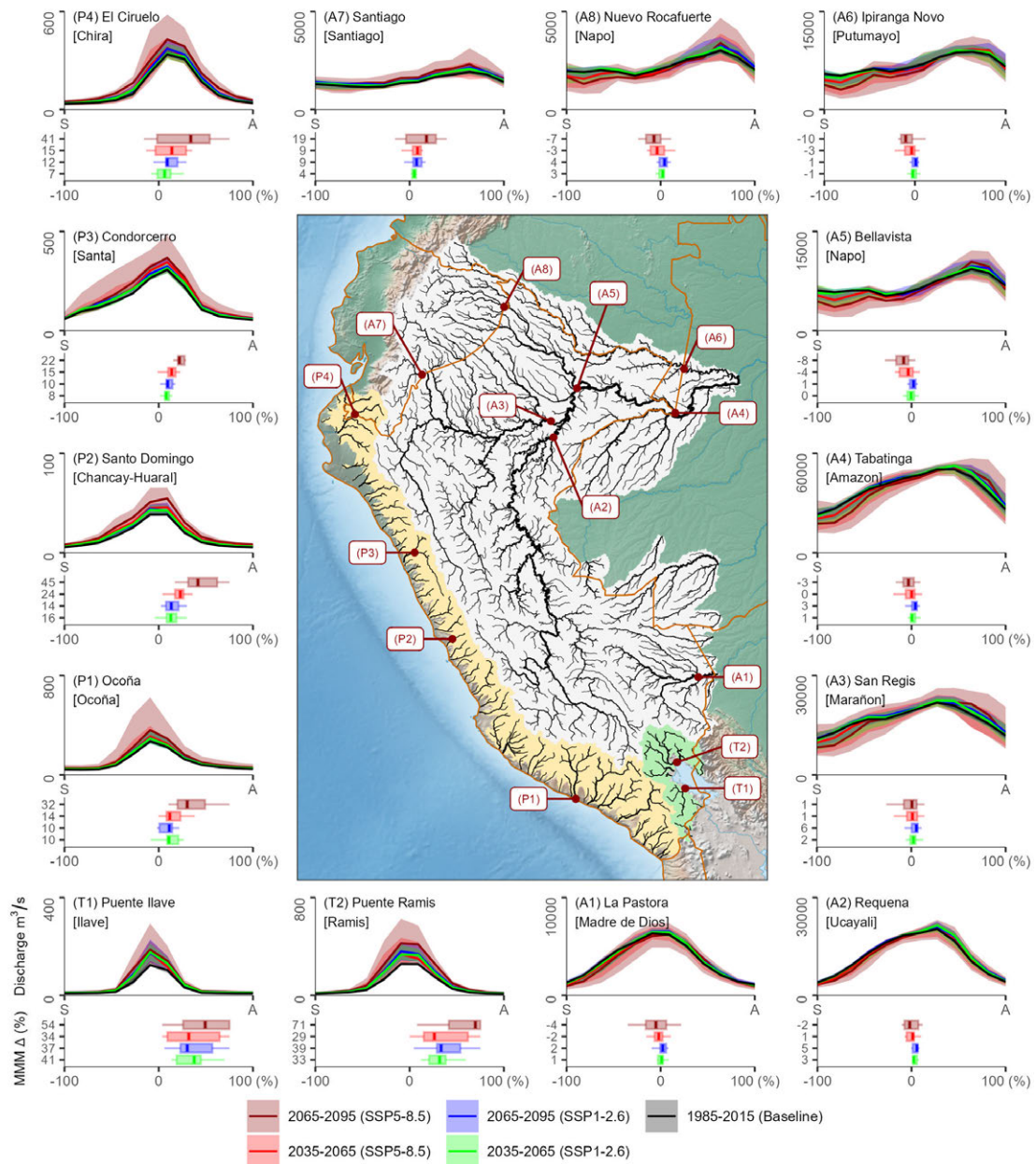
Figure 5.7: Seasonal streamflow projections for 2035–2065 and 2065–2095 under SSP1-2.6 and SSP5-8.5 scenarios in representative river catchments draining into the Pacific Ocean (P1:P4), the Titicaca Lake (T1:T2), and the Amazon River (A1:A8), arranged from south to north. Boxplots display mean streamflow changes with multimodel median values relative to the reference period (1985–2015). River catchments (indicated by gauges specified in numbers) are shown in brackets.

emissions scenarios in catchments such as Llanganuco, Mantaro, Vilcanota, Chancay-Huaral, and Santa River. However, the minor increase in water availability during the dry season will be insufficient due to anticipated future increases in water demand in Andean catchments (Goyburo et al., 2023; Motschmann et al., 2022). Therefore, to mitigate potential water shortages during dry periods, it is recommended to focus on adaptation strategies that enhance both natural and artificial water storage and regulation capacity.

The Amazon lowland tributaries generally experience a decrease in projected streamflow throughout the year, except during the wet season (June-August) in the Ecuadorian and northern

Peruvian Amazon (Figs. 5.6 and 5.12). Specifically, those near the Brazilian border (e.g., Purus, Jurua, Javari, see Fig. 5.9) are projected to have significant year-round reductions, with expected decreases of up to 28%. These findings align with the negative anomalies reported for these tributaries by Brêda et al. (2020). Additionally, Dalagnol et al. (2017) projected a decrease in discharge in the Purus catchment, further supporting the evidence of declining streamflow in the region.

Our projections indicate that the overall streamflow of the upper Amazon River will remain relatively stable during the 21st century, except for its northern tributaries under the worst-case scenario (Fig. 5.7). Specifically, we anticipate significant annual streamflow reductions of up to -10% in the transboundary rivers such as Napo and Putumayo in the north, primarily occurring between September and February. The Marañón River will exhibit minimal fluctuations, ranging from 1% to 6%, with a decrease observed from September to November. Conversely, the southern tributaries, such as the Ucayali and Madre de Dios rivers, are projected to experience negligible changes throughout the year, with streamflow anomalies ranging from -4% to 5%. Similarly, at the Tabatinga hydrological station, the Amazon River is projected to undergo marginal variations, ranging from -3% to 1%, with a decrease from September to November. These projections align with similar future anomalies reported for the upper Amazon River, ranging from -5% to 5%, by Brêda et al. (2020), further supporting our projections of the future streamflow dynamics in the upper Amazon River system.

Our projections also show significant changes in the Ecuadorian Amazon under SSP5-8.5 (Fig. 5.7). The northern Napo river at the Nuevo Rocafuerte station is expected to experience a streamflow decrease of up to -7% between September and November, while the southern Santiago river will undergo a substantial increase of up to 19% in streamflow. These projections provide valuable insights into the future streamflow dynamics in the Ecuadorian Amazon which is crucial for transboundary water management.

5.3.9   How will climate change impact extreme hydrological conditions in Peru?

Projected changes show significant alterations in extreme hydrological conditions, especially under fossil-fueled development, towards the end of the century (Fig. 5.6). These changes exhibit spatial variability across Peru. Low flows (Q95) are projected to decrease further over the Amazon lowlands but increase in the Andean catchments. On the other hand, high flows (Q5) are expected to decrease in the central and southern Peruvian Amazon lowlands while increasing in the Andean and northern Amazon catchments, which agree with the projected higher risk of wet-season floods in the Marañón river basin (Zulkafli et al., 2016). These projections indicate the potential for increased water exposure during flood events in the Andean catchments and water scarcity during droughts in the lowlands. The projected changes in hydrological extremes emphasize the urgent need for developing adaptation measures to mitigate the impacts of floods and droughts. Under the sustainable pathway (SSP1-2.6), the future impacts on hydrological extremes are relatively minor, highlighting the benefits of climate adaptation and mitigation efforts.

5.3.10   Limitations and perspectives

We conducted an analysis of current and projected hydrological conditions in Peruvian and transboundary river catchments, utilizing reliable observational and projected climate datasets for Peru and Ecuador that were generated in our previous studies (Fernandez-Palomino et al., 2021, 2022, 2023b, 2024). The SWAT model, adapted for Andean and Amazonian regions, was carefully calibrated and validated in our previous study by Fernandez-Palomino et al. (2022) to simulate streamflow effectively, including both low and high flows.

Despite the overall good performance of SWAT in simulating streamflow, uncertainties persist in the results of water balance components (e.g., evapotranspiration, water yield, surface runoff, lateral flow and return flows from both shallow and deep aquifers) due to the lack of direct observations to verify these variables. These uncertainties are influenced by factors such as the quality of input data (e.g., climate, soil, and land use) and data used for model calibration (e.g., discharge). We used discharge data from stations located upstream of the largest dams and reservoirs (primarily situated in the Pacific basin), which have also been

used in previous studies to simulate natural hydrological processes (Asurza-Véliz and Lavado-Casimiro, 2020; Llauca et al., 2021; Rau et al., 2019). However, these discharge data might incorporate influences from water management infrastructures (e.g., small man-made reservoirs and irrigation) not accounted for in our hydrological modeling. Additionally, the simplification of hydrologic processes in the model structure and uncertainties in model parameters and parameter regionalization contribute to overall uncertainties in the results.

Furthermore, it's crucial to recognize that projected changes in hydrological variables are also subject to future climate uncertainty incorporated in GCMs, anthropogenic forcing scenarios (Hattermann et al., 2018), and bias adjustment and downscaling of GCM outputs. These additional sources of uncertainty must be considered when interpreting the study's findings and implications. To compare and verify the projected hydrological changes in this study—derived from bias-adjusted and statistically downscaled CMIP6-GCM simulations for Peru—we recommend future studies incorporating simulations from regional climate models. These models dynamically downscale GCM outputs, enhancing the depiction of complex terrain-related processes, like precipitation (Dereczynski et al., 2020; Lloyd et al., 2021). Naturally, these regional model simulations should undergo bias adjustment using dependable local observational climate datasets before their incorporation into climate impact assessments.

Additionally, our study was conducted at the national scale, and certain small-scale hydrological processes, particularly in glaciated catchments, may not have been fully accounted for in the modeling. To better understand these specific areas and their contributions to the overall hydrology of Peru, future studies should focus on improving hydrological modeling at smaller scales.

In this study, we showed the potential impacts of climate change on hydrological variables. To gain deeper insights, future research should explore how changes in land use might affect these water processes.

5.4 Summary and conclusions

We comprehensively analyzed current and projected hydrological conditions in Peruvian and transboundary river catchments using observational data and bias-adjusted CMIP6 projections for sustainable (SSP1-2.6) and fossil fuel-based development (SSP5-8.5) pathways. Our findings can be summarized as follows:

1. Peru's total renewable freshwater resource, including total river runoff, is estimated at around 62,399 m^3/s, with the Amazon basin contributing 97.7%, the Pacific basin 1.9%, and the Titicaca Lake basin 0.4%. The montane zone (500-3000 m a.s.l.) in the Amazon-Andes transition region has the highest water yield and streamflow per unit area (up to 143 l/s/km^2), playing a significant role in shaping the hydrological variability of the entire Amazon basin.

2. The distribution of water yield components highlights the dominant influence of subsurface hydrological pathways in determining water yield. Baseflow, driven by return flow from aquifers, is crucial in water yield in lowland and Andean catchments.

3. In the study area, seasonal water yield patterns show an attenuated annual cycle in the Ecuadorian and northern Peruvian Amazon and a strong varying annual cycle in southern catchments. The timing of peak water yields differs spatially and temporally, emphasizing the significance of considering these variations in water resource management and planning efforts.

4. The relationship between water yield and elevation differs across different basins. In the Pacific Basin, water yield increases with elevation and latitude. The Titicaca Lake basin does not show a clear pattern, while in the Amazon Basin, water yield follows an unimodal curve with a peak in the montane zone, highlighting the complex relationship between water yield and elevation.

5. Floodplains significantly impact streamflow seasonality in the Ucayali River, attenuating and delaying peak flows for up to two months during the high discharge season. Considering the impact of floodplains is crucial for managing and predicting river behavior in the Ucayali River and downstream in the Amazon River.

6. Projected changes in hydrological variables exhibit spatial and elevation-dependent variations, particularly by the end of the century under the high-end scenario (SSP5-8.5). Andean regions are expected to receive increased precipitation, whereas the Amazon lowlands, particularly in central and southern areas, may experience a decrease. Evapotranspiration is projected to increase throughout the study area, except in the Altiplano region, where a decrease is anticipated. Water yield changes align with precipitation patterns, resulting in significant increases in high Andean basins and potential declines in lowland areas.

7. Projected changes in water balance components show distinct seasonal patterns. In the Amazon lowlands, precipitation is projected to decrease at the beginning and end of the hydrological year (during the dry seasons), while Andean regions would experience increased precipitation year-round. Evapotranspiration consistently may increase in the lowlands and minimally changes in the Andean regions year-round. Consequently, water yield may increase in the Andean regions and decrease in the Amazon lowlands throughout the year, except for the northern Amazon, where an increase is projected during the wet season.

8. Projected streamflow changes show spatial and seasonal variability. Andean rivers are expected to have increased streamflow throughout the year, while Amazon lowland tributaries may experience a decrease in river flow, especially during the wet season onset (September-February). Despite these regional differences, the overall streamflow of the upper Amazon River is expected to remain relatively stable over the course of the 21st century.

9. Climate change is projected to have significant impacts on extreme hydrological conditions. Low flows are projected to decrease further in the Amazon lowlands but increase in the Andean catchments. High flows are expected to decrease in the central and southern Amazon lowlands while increasing in the Andean and northern Amazon catchments. These changes call for adaptation measures to mitigate flood and drought risks.

10. In conclusion, the projected increase in precipitation, water yield, and low flows anticipates greater water availability for Andean ecosystems and water usage within Andean catchments. Nevertheless, the projected rise in precipitation and high flows could lead to increased flooding and sediment load, potentially causing economic and human impacts, as well as shortening the lifespan of water reservoirs, as highlighted by Potter et al. (2023) and Rosas et al. (2020). Conversely, within Amazon lowland catchments, the anticipated decrease in precipitation, water yield, and low flows, particularly during dry seasons, points to heightened dry season water stress in the future. This could significantly impact Amazon rainforest ecosystems, exacerbating the currently marked loss of rainforest resilience (Boulton et al., 2022), and affecting fluvial transportation and food supplies.

11. It is crucial to highlight that the projected changes in hydrological variables (precipitation, evapotranspiration, water yield, and streamflow) and hydrological extremes (high and low flows) are more pronounced in the SSP5-8.5 pathway than in SSP1-2.6, especially toward the end of the century. This highlights the urgent need to implement robust climate policies to promote sustainable development and address the impacts posed by fossil fuel-based development.

The study has clearly shown the high level of spatiotemporal details and variations in the regional-scale/meso-scale hydrological cycle. Understanding such nuances is crucial for adequate water management and precautionary adaptation to expected hydrological changes driven by global climate change. This also emphasizes the necessity for hydro-climate change projections tailored to the region, as highlighted by studies such as Bronstert et al. (2007) and Vormoor et al. (2015). When considering potential water management and adaptation measures for such a region, global-scale analysis can hardly provide the required level of detail (Hattermann et al., 2017).

Author contributions

Carlos Antonio Fernandez Palomino conceived the study, conducted the hydrological modeling and analysis, and wrote the original manuscript with inputs from all co-authors, and all authors contributed significantly to further revisions.

Declaration of competing interest

The authors declare that they have no known competing financial interests or personal relationships that could have appeared to influence the work reported in this paper.

Acknowledgments

Data availability

Simulated data of current and projected future hydrological conditions will be available upon request.

5.A Appendix
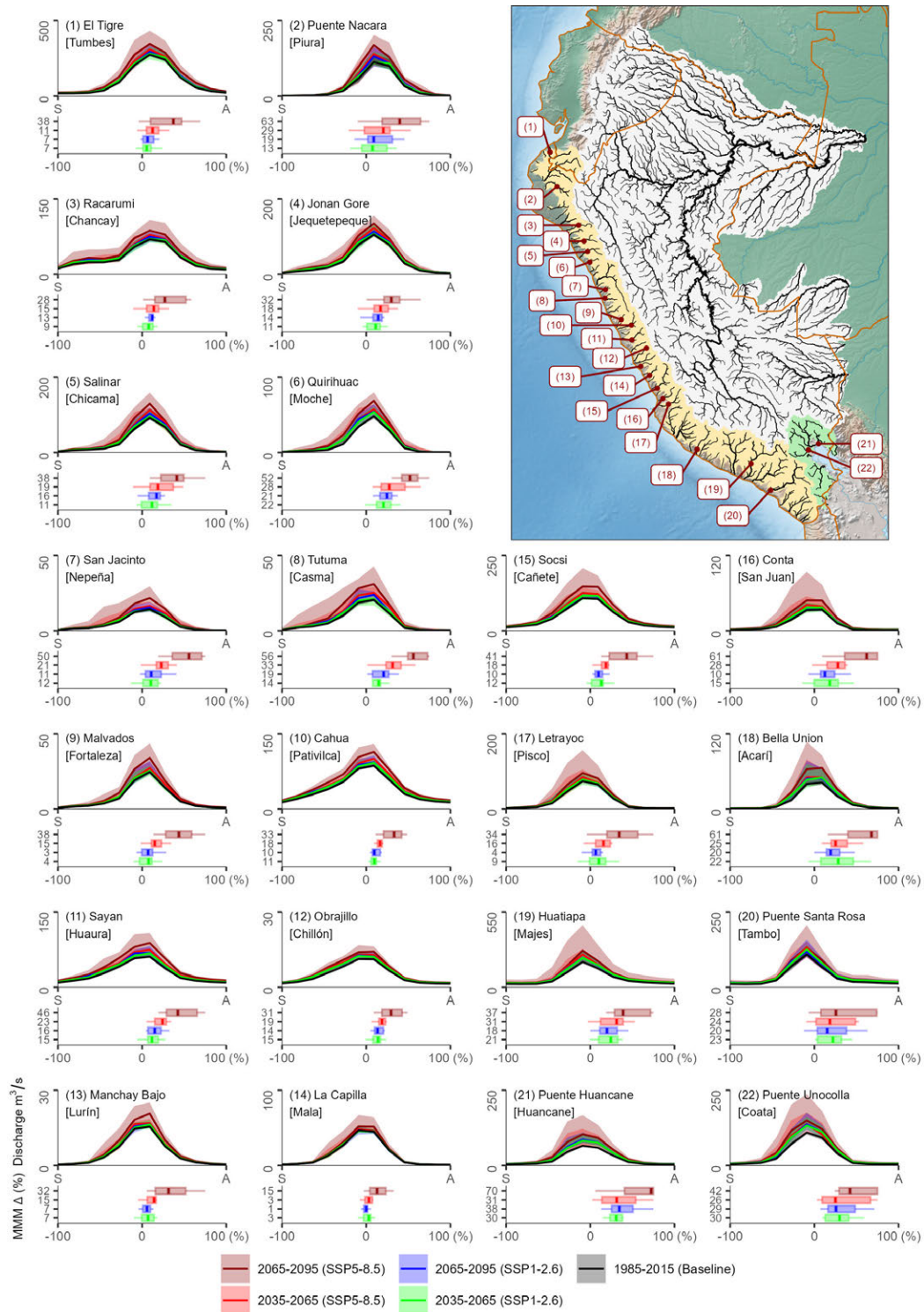
Figure 5.8: Seasonal streamflow projections for catchments draining into the Pacific Ocean (1:20) and Titicaca Lake (21:22). Boxplots show mean streamflow changes with multimodel median values. River catchments (indicated by gauges specified in numbers) are shown in brackets.
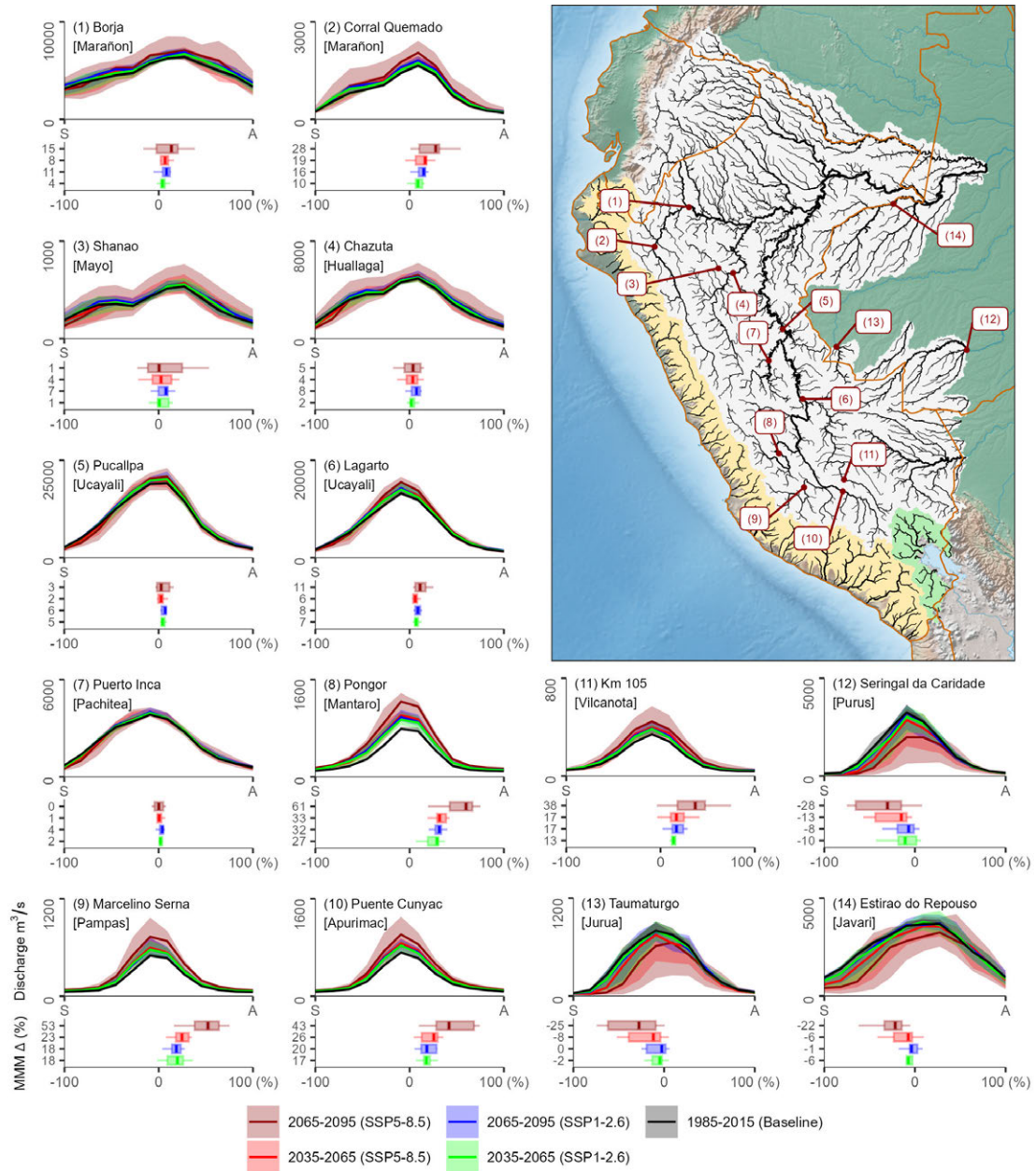
Figure 5.9: Seasonal streamflow projections for catchments draining into the Amazon River. Boxplots show mean streamflow changes with multimodel median values. River catchments (indicated by gauges specified in numbers) are shown in brackets.

5.B Supporting information
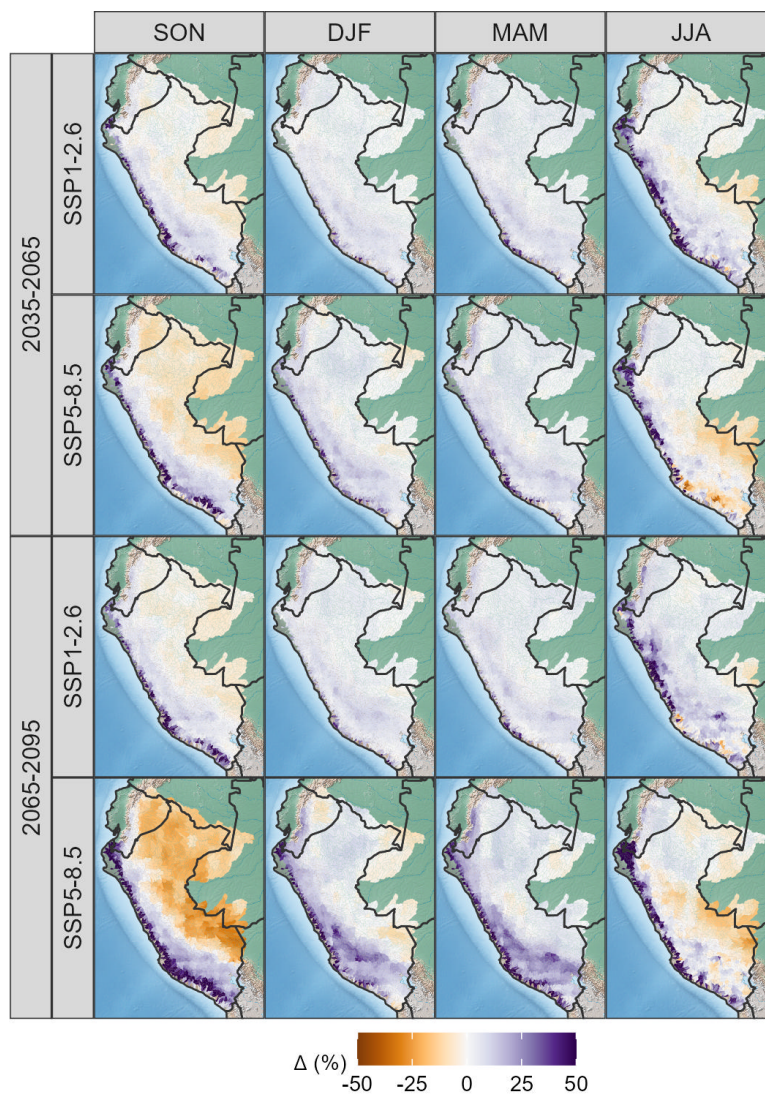
Figure 5.10: Projected seasonal multimodel median changes in precipitation under SSP1-2.6 and SSP5-8.5 scenarios for 2035–2065 and 2065-2095, relative to the reference period (1985–2015).
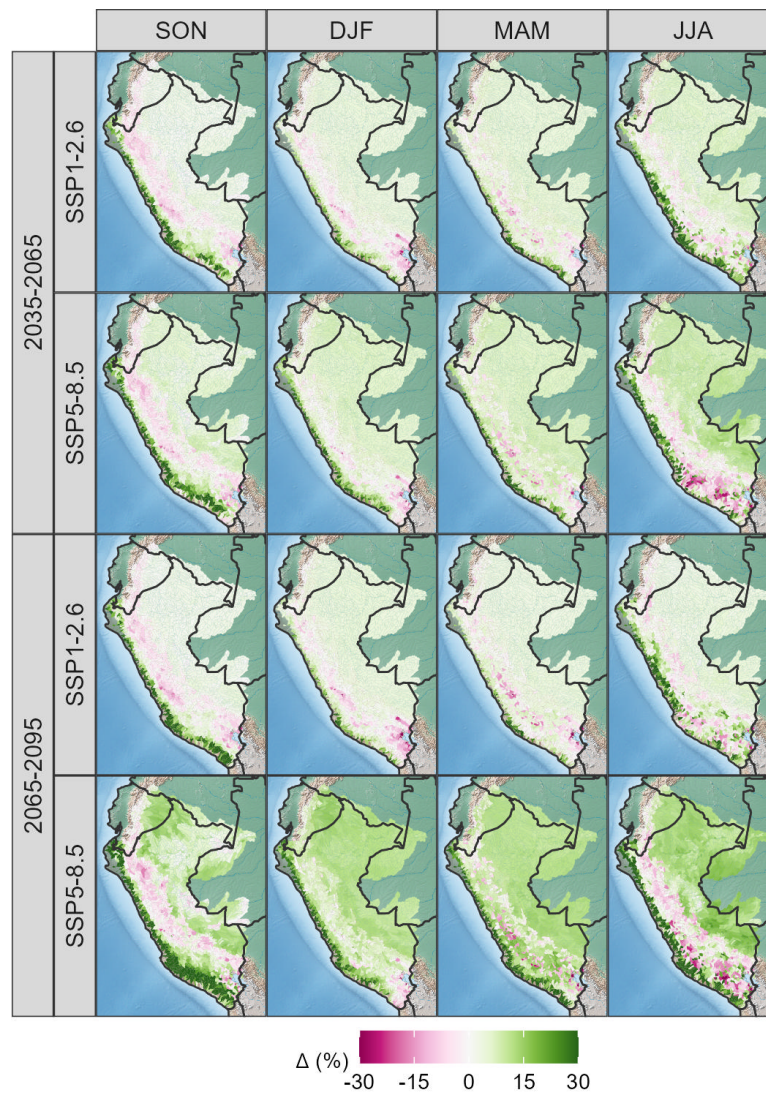
Figure 5.11: Projected seasonal multimodel median changes in evapotranspiration under SSP1-2.6 and SSP5-8.5 scenarios for 2035–2065 and 2065-2095, relative to the reference period (1985–2015).
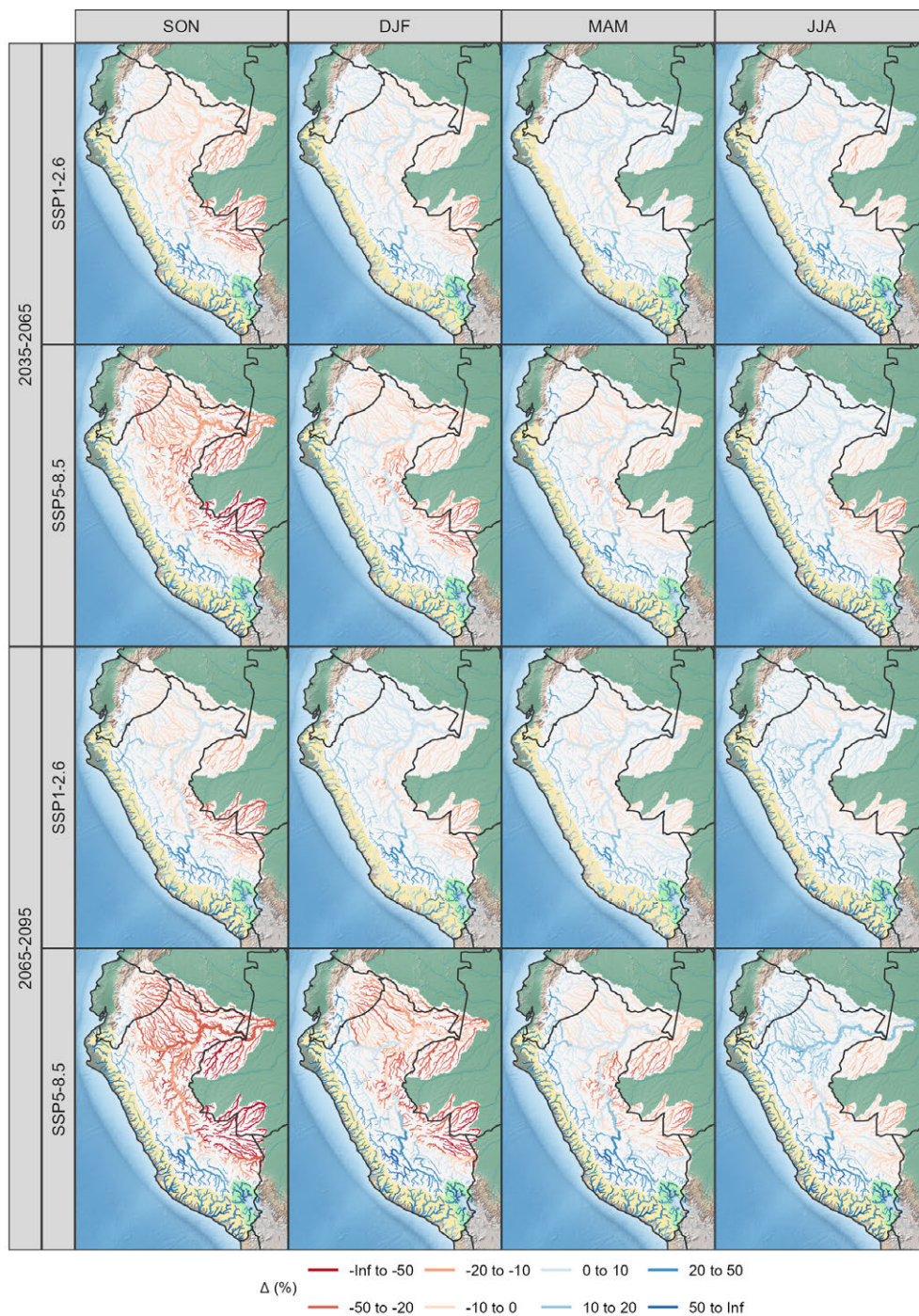
Figure 5.12: Projected seasonal multimodel median changes in streamflow relative to the baseline (1985-2015)

6. Synthesis, conclusion, and outlook

6.1 Synthesis and conclusion

This thesis aimed to enhance the understanding of the hydrological dynamics in the tropical Andes of Peru and Ecuador with a specific emphasis on their responses to climate change. To achieve this, existing research gaps have been identified and analyzed in more detail. This section summarizes and discusses the main findings and conclusions related to the specific research questions.

How well do state-of-the-art regional and global precipitation datasets perform in the tropical Andes for hydrometeorological applications?

The developed novel high-resolution (1d, 10km) precipitation dataset for Peru and Ecuador, called RAIN4PE, emerges as the most reliable precipitation product in the region for hydrometeorological applications (Chapter 2). RAIN4PE was created by integrating multisource precipitation data (satellite, reanalysis, and ground-based precipitation) with surface elevation using the random forest method. Furthermore, precipitation estimates underwent adjustments using streamflow data through the reverse hydrology method for catchments influenced by fog/cloud water input, such as páramo and montane watersheds on the eastern side of the Andes.

The assessment of the reliability and accuracy of RAIN4PE, alongside other precipitation products (CHIRP, ERA5, CHIRPS, MSWEP, and PISCO), utilizing observed precipitation data and hydrological modeling, reveals that the latter products exhibit greater biases and inadequately represent the temporal dynamics (seasonality) of precipitation, especially in equatorial regions such as the Ecuadorian Amazon (Fig. 2.6). It is demonstrated that these errors propagate in streamflow simulations, resulting in the poor performance of the hydrological model (Figs. 2.7,2.8).

Contrarily, RAIN4PE proves to be more reliable and accurate when compared to precipitation gauge data and when used as a forcing input for hydrological modeling. This is evidenced by the satisfactory performance of the hydrological model in simulating mean, low, and high streamflows in most Peruvian and Ecuadorian watersheds (Figs. 2.7,2.8). Furthermore, RAIN4PE is the only product ensuring the closure of the water balance in most simulated basins (Fig. 2.8). These results underscore that the precipitation product generated as part of this thesis is currently the most suitable in the tropical Andes for hydrometeorological applications, including hydrological extremes.

Indeed, RAIN4PE has been utilized in several research studies. For example, it has been employed as a reference dataset to evaluate the effectiveness of regional climate simulations in reproducing historical rainfall patterns across the Andes-Amazon transition region (Gutierrez et al., 2024). Additionally, it has been instrumental in simulating discharges in the San Pedro River catchment in Quito, Ecuador (Núñez Mejía et al., 2023).

What is the performance of raw and regionally adapted global climate model simulations over the tropical Andes?

Chapter 3 comprehensively evaluates raw and regionalized global climate model (GCM) simulations, focusing on their performance over the tropical Andes. The regionalized climate simulations belong to the developed BASD-CMIP6-PE dataset, presenting results derived from applying the bias adjustment and statistical downscaling method to the CMIP6-GCM simulations at high resolution (1d, 10km) tailored to the region of Peru and Ecuador. It is worth mentioning that the adjusted simulations were derived using reliable regional observational datasets, such as RAIN4PE, as reference data.

Significant shortcomings were identified in the performance of raw GCM simulations when evaluated using observation-based data and hydrological modeling. Raw simulations exhibit notable biases and limitations in capturing the mean annual cycle of atmospheric variables, particularly falling short in representing the annual precipitation cycle over the equatorial region (refer to Figs. 3.2-3.5). These errors are critical as they propagate in streamflow simulations, making raw GCM data unsuitable for hydrological impact assessments (refer to Fig. 3.6).

In contrast, results from the BASD-CMIP6-PE dataset showed substantial improvements. The regionalized outputs demonstrated improved representations of long-term observed climate statistical properties, including mean and extreme values and seasonal patterns (Figs. 3.4,3.5,3.7). Hydrological simulations utilizing the regionalized GCM outputs underscored the appropriateness of regionalized GCM simulations in accurately depicting streamflow, including mean, low, and high flows (Fig. 3.7). These findings highlight the reliability of the BASD-CMIP6-PE dataset in assessing regional climate change impacts on agriculture, water resources, and hydrological extremes. In fact, BASD-CMIP6-PE has been utilized in local-scale projects within river catchments, such as Mantaro and Piura, to examine historical and potential future changes in climate and water resources.

In summary, the findings expose challenges GCMs face in accurately representing key hydro-climatic variables, such as precipitation and temperature, within the present-day climate of the tropical Andes, emphasizing the significance of regionalization for reliable impact assessments at the regional level.

How does hydrological model calibration influence the model's reliability regarding vegetation, streamflow, and flow partitioning simulations?

This research question is addressed in Chapter 4 by employing various calibration strategies for the Soil and Water Assessment Tool (SWAT) eco-hydrological model within a typical Andean catchment, the Vilcanota River catchment. The evaluation includes traditional single-objective calibration approaches, relying on discharge data metrics like Nash-Sutcliffe Efficiency (NSE or log NSE), and bi-objective approaches that incorporate flow duration curve (FDC) signatures in addition to discharge metrics (log NSE). Additionally, a newly developed multiobjective calibration framework integrates remote sensing vegetation data, baseflow index, discharge metrics, and FDC signatures.

The NSE-calibrated simulation matches observed daily discharge well during high discharge seasons but underestimates flow during low discharge seasons, suggesting that this calibration approach prioritizes mid and high flows, reducing accuracy in low-flow predictions (Figs. 4.4-4.6). These findings support previous studies by Chen et al. (2018), Krause et al. (2005), and Zhang et al. (2018b). Log NSE calibrated simulations match well with observed discharge in all aspects of the hydrograph and FDC, although moderate underestimations exist during the high-discharge season (Figs. 4.4-4.6).

Including FDC signatures in bi-objective calibration improves discharge (hydrograph and FDC) simulation compared to single-objective approaches (Figs. 4.4-4.6). However, both

strategies fail to simulate the partitioning of precipitation between surface runoff and baseflow (Fig. 4.4).

The developed multiobjective calibration framework enhances the simulation of vegetation, streamflow, and flow partitioning into surface runoff and baseflow (Figs. 4.4-4.6). Furthermore, it improves the identification of model parameters, mitigating parameter uncertainty partly due to equifinality during the calibration (Fig. 4.4). I consider these outcomes a crucial progress in understanding catchment hydrological responses and the underlying hydrological processes.

In conclusion, incorporating more variables (e.g., vegetation, evapotranspiration, soil moisture, snow, and hydrological signatures) is crucial for better constraining the calibration process. However, using remotely sensed data, such as evapotranspiration, should be approached with care, as these sources are biased and may lead to overestimation of SWAT-simulated evapotranspiration and precipitation along the Andes (Chapter 2, Fig. 2.6,2.12), potentially hindering water budget closure in Andean catchments.

How does the current spatiotemporal distribution of water balance components look like across Peru?

For the first time, the current hydrological conditions across Peru and transboundary river catchments were investigated through hydrological modeling using the most reliable developed climate input data, such as RAIN4PE, as outlined in Chapter 5 (Table 5.1 and Figs. 5.2,5.3). The results of this investigation improve understanding how water sources behave and provide insights that can be important for managing water resources.

Peru's total renewable freshwater resource (total river runoff) is estimated at approximately 62,399 m^3/s. The Amazon basin is the predominant contributor, constituting 97.7%, while the Pacific and Titicaca Lake basins contribute 1.9% and 0.4%, respectively. Notably, the montane zone in the Amazon-Andes transition region stands out with the highest water yield and streamflow per unit area (up to 143 l/s/km^2), playing a pivotal role in shaping the hydrological variability of the entire Amazon basin.

A thorough analysis of water yield components underscores the significant influence of subsurface hydrological pathways. Baseflow, attributed to aquifer return flow, is a critical determinant of water yield, particularly in Amazon lowland and Andean catchments.

Distinct seasonal water yield patterns characterize the study area. The Ecuadorian and northern Peruvian Amazon exhibit an attenuated annual cycle, contrasting with strongly varying annual cycles in southern Peruvian catchments.

The intricate relationship between water yield and elevation unfolds uniquely across the basins (drainage systems). In the Pacific Basin, water yield increases with elevation and latitude. Conversely, the Titicaca Lake basin lacks a clear pattern, while the Amazon Basin features a complex unimodal curve, emphasizing the nuanced connection between water yield and elevation.

In the Amazon lowlands, floodplains substantially impact streamflow seasonality, as observed in the Ucayali River. They attenuate and delay peak flows for up to two months during high discharge seasons, underscoring their crucial role in managing and predicting river behavior in the Ucayali River and downstream in the Amazon River.

In conclusion, these research outcomes provide distinct insights into the hydrological dynamics in the tropical Andes. The findings underscore the need for sophisticated water resource management approaches to address spatial and temporal variations, elevation-related complexities, and the influence of key factors such as baseflow and floodplains. This study enhances our understanding of sustainable water resource planning, particularly in the context of climate change and varying development pathways.

How do hydrological responses vary across areas with different land use types in the tropical Andes?

This study investigated hydrological responses, including evapotranspiration, water yield, and baseflow, across various land use categories—urban, barren, pasture, agricultural areas, and high mountain forests (mixed forest)—within a typical high Andean catchment, the Vilcanota River basin (Chapter 4, Fig. 4.7). Chapter 5 (Fig. 5.2) extended the analysis to water yields across elevational gradients in Peru, providing insights into hydrological responses in tropical

montane cloud forests (Amazon-Andes transition region, 500-3000 m a.s.l.) and rainforests (Amazon lowlands, <500 m a.s.l.).

In high Andean catchments, pasture areas exhibited the highest ratio (~0.63) of water yield over precipitation, driven predominantly by baseflow. Urban and barren areas contributed approximately 43%-52% of precipitation to water yield, primarily through surface runoff. Agricultural areas and mountain forests exhibited the lowest water yields (<~25% of precipitation), suggesting significant evapotranspiration in these land use types. Agricultural areas also exhibited lower baseflow indices than pasture and mountain forests, indicating reduced hydrological regulation capacity.

Despite the hydrological benefits of mountain forests in enhancing infiltration and subsurface processes, their high evapotranspiration demand negatively impacted water yield. Therefore, introducing new mountain forest ecosystems for soil conservation and climate change adaptation may adversely affect downstream water yield, as also reported in other regional studies. In contrast, pastures provided higher water yields and baseflow rates than forests in Andean catchments, underscoring the importance of conserving puna ecosystems to address climate impacts.

In the Peruvian and Ecuadorian Amazon, the Amazon-Andes transition zone, dominated by montane forest ecosystems, exhibited the highest water yields at 1000-1500 m a.s.l. (mean water yield over precipitation = 0.68). Abundant precipitation (up to 5700 mm/year), including rainfall and cloud/fog water, combined with reduced evapotranspiration due to persistent low-level cloud cover and lower temperatures, contributes to elevated water yields in this transition region. Meanwhile, water yields were lower in the Amazon lowland rainforest than in the montane forest, decreasing towards the low latitudes.

In conclusion, puna ecosystems, such as pastures and páramos, play a crucial role in regulating natural storage and distributing flow during extended dry periods in the region. A recent observation-based study has emphasized the significance of these ecosystems and bofedales (peat-forming wetlands) in natural hydrological regulation in high Andean catchments (Wunderlich et al., 2023). Additionally, this thesis underscores, for the first time, that the highest water yields in the region are observed in the Amazon-Andes transition zone, dominated by montane forests, highlighting the importance of this ecosystem in the overall hydrological regulation of the Amazon basin.

How do projected changes in water balance components vary spatially, along elevation, and over the seasons?

Chapter 5 (Figs. 5.4-5.12) analyzes projected hydrologic trajectories in Peruvian and transboundary river catchments, considering sustainable (low warming, SSP1-2.6) and fossil fuel-based development (high-end warming, SSP5-8.5) scenarios for the mid (2035-2065) and end (2065-2095) of the century.

The projected changes reveal distinct spatial and elevational patterns, notably amplified under high-end warming, especially towards the century's end. Projections indicate increased precipitation in the Andean regions, contrasting with potential decreases in the Amazon lowlands, especially in central and southern areas. Evapotranspiration is projected to increase throughout the study area, except in the Altiplano region, where a decrease is anticipated. Water yield changes closely align with precipitation patterns, resulting in substantial increases in high Andean basins and potential declines in the Amazon lowlands, with minimal changes in the Amazon-Andes transition region (500-3000 m a.s.l.).

Seasonal changes further emphasize hydrological complexity in the tropical Andes region. In the Amazon lowlands, a decrease in precipitation is projected at the hydrological year's onset and end, suggesting dry season amplification. Conversely, Andean regions anticipate increased year-round precipitation. Evapotranspiration consistently rises in the lowlands throughout the year, with minimal changes in the Andean regions. Water yield is expected to increase in the Andean regions and decrease in the Amazon lowlands across all seasons, except for the northern Amazon, where an increase is projected during the wet season. Similarly, Andean rivers could expect year-round increased streamflow, while Amazon lowland tributaries may undergo a decrease, especially during the onset of the wet season (September-February).

Despite these regional differences, the upper Amazon River streamflow is expected to remain relatively stable over the 21st century.

In conclusion, this research offers valuable insights for addressing future water balance challenges. The spatial and seasonal variation in water yield and streamflow shifts highlight the need for tailored water management strategies. The amplification of changes, particularly under high-end warming scenarios, underscores the urgency for emissions mitigation and adaptation measures to address negative impacts on water resources.

What is the potential impact of climate change on extreme hydrological conditions in the region?
Chapter 5 (Fig. 5.6) presents the projected changes in hydrological extremes, including low and high flows, considering sustainable and fossil fuel-based development scenarios for the mid (2035-2065) and end (2065-2095) of the century. High and low flows were determined using Q5 and Q95, respectively, representing flows exceeding the analysis period's 5% and 95% thresholds.

Projections show significant changes in extreme hydrological conditions, with more severe impact under high-end warming and towards the century's end. The magnitude of low flows is projected to decrease in the Amazon lowlands but increase in the Andean catchments. High flows are expected to decrease in the central and southern Amazon lowlands while increasing in the Andean and northern Amazon catchments. These changes call for adaptation measures to mitigate flood and drought risks.

6.2 Outlook

This thesis represents a significant advancement to enhance the reliability of data and hydrological models, deepening our understanding of current and potential future hydrological trends in the tropical Andes. Although some progress has been made, future investigations are crucial for further improving climate data, understanding hydrological extremes (such as droughts and floods) and local hydrological processes, and assessing the impact of land use changes. Additionally, it is imperative to focus on implementing effective mitigation and adaptation measures to address the impacts of climate change.

6.2.1 Improvement of meteorological data

Improving the representation of precipitation patterns and other meteorological variables involves assimilating all available data from hydrometeorological services and private sector entities. Specifically, daily data from numerous rain gauge stations in Ecuador and the private sector (e.g., electricity company of ELECTROPERU) were not incorporated into the generation of RAIN4PE due to difficulties in accessing the data. Their inclusion can further enhance the product. Additionally, the next step is to extend the RAIN4PE product to make it available over a longer time period for monitoring droughts and floods in the region, taking into account that RAIN4PE data are currently available only for the period 1981-2015. Furthermore, hydrometeorological services and agencies should expand the station network in areas with low station density, such as the Amazon lowlands, the Amazon-Andes transition region, and the highlands. This expansion will enable future studies to assimilate these data, improving the representation of meteorological patterns in the region. Constructing new and improved gridded observational datasets will also enhance the regionalization of climate model simulations and understanding local hydrological processes.

6.2.2 New opportunities in research

The climatic products developed as part of this thesis (RAIN4PE and BASD-CMIP6-PE) have proven to be the most reliable in the region, opening up new avenues for research. For instance, future investigations could comprehensively analyze the spatiotemporal variability of meteorological droughts in historical periods and under climate change scenarios. Similarly, the hydrological model implemented for the region can be applied to comprehend hydrological droughts, including future scenarios. Given their impact on agriculture and the economy of Peru and Ecuador, these hydrological extremes deserve heightened attention. Undoubtedly, the data

generated here presents numerous research opportunities in hydrometeorological applications in the region, which have been hindered by the scarcity of observational data and the poor reliability of existing local and global gridded climate datasets.

This study concentrated on the regional-scale/meso-scale in the tropical Andes. However, certain small-scale hydrological processes may not have been reflected thoroughly in the modeling, especially in glaciated catchments. Future research should focus on refining water process modeling at a smaller scale to enhance our understanding of these specific catchments.

In this study, we highlighted the potential effects of climate change on hydrological variables of such a tropical mountain region. To gain a deeper understanding, future research should investigate how land-use changes could additionally impact these water processes.

6.2.3   Climate change adaptation measures

Anticipated changes in water availability and extreme hydrological conditions underscore the need for a comprehensive set of adaptation measures. This is particularly crucial given the heightened impact of climate change, especially under high-end warming scenarios towards the end of the century. Here are potential adaptation measures for decision-makers:

- **Conservation and restoration of natural ecosystems:** In regions with projected decreases in water yield, streamflow, and low flows, priority should be the conservation and restoration of primary rainforests in the Amazon lowlands. These rainforests contribute significantly to moisture recycling, providing up to 50% of regional rainfall and serving as a vital moisture source for South America (Staal et al., 2018). Conversely, scenarios involving a 30% to 50% reduction in the Amazon rainforest may lead to a 40% reduction in rainfall in non-deforested parts of the western Amazon (Boers et al., 2017). Similarly, conservation and restoration efforts should extend to puna ecosystems (pastures, páramos, and bofedales) in Andean catchments. These initiatives can reduce greenhouse gas emissions, enhance overall ecosystem health, and promote groundwater recharge, a crucial water source during the extended dry season when water availability is limited due to the anticipated rise in anthropogenic water uses.
- **Water storage and reservoir management:** Enhancing water storage capacity through reservoirs and sustainable water management practices is crucial to counteract the projected decrease in streamflow and low flows in the Amazon lowlands. This approach also applies to Andean catchments to buffer water for the dry season and mitigate floods, ensuring a more reliable water supply during periods of reduced flow.
- **Climate-resilient agriculture practices:** In regions facing changes in water availability, promoting climate-resilient agricultural practices is crucial. This involves encouraging water-efficient irrigation systems, adopting drought-resistant crop varieties, and implementing sustainable land management practices to adapt to altered hydrological conditions.
- **Floodplain management and infrastructure:** In areas projected to experience increased high flows, effective floodplain management is crucial. This involves planning, regulation, and the implementation of strategies to mitigate the impacts of flooding. Measures may include the development of sustainable land-use planning, zoning regulations, as well as the implementation of levee systems and construction of flood barriers.
- **Community engagement and early warning systems:** Developing robust community engagement programs and early warning systems are essential for enhancing preparedness and response to increased high flows and decreased low flows. This includes educating communities on adaptive practices and providing timely information to facilitate effective decision-making.
- **Integrated water resource management:** Adopting an integrated approach to water resource management that considers surface and groundwater sources is essential. This involves coordinated planning and governance to ensure sustainable water use across different sectors.
- **International collaboration:** Given the transboundary nature of many river catchments, fostering international collaboration is vital. Shared strategies for adapting to changing hydrological conditions can enhance the effectiveness of adaptation measures and promote regional resilience.

These adaptations, tailored to the specific challenges presented by changing hydrological patterns, can contribute to building resilience in the face of climate change and minimizing potential impacts on communities, ecosystems, and economies.

Bibliography

Abbaspour, K. and Ashraf Vaghefi, S. (2019). "Harmonized World Soil Database in SWAT Format". In: *PANGAEA*. DOI: 10.1594/PANGAEA.901309.

Abbaspour, K., Vaghefi, S., and Srinivasan, R. (2017). "A Guideline for Successful Calibration and Uncertainty Analysis for Soil and Water Assessment: A Review of Papers from the 2016 International SWAT Conference". In: *Water* 10.2, p. 6. DOI: 10.3390/w10010006.

Abbass, K., Qasim, M. Z., Song, H., Murshed, M., Mahmood, H., and Younis, I. (2022). "A review of the global climate change impacts, adaptation, and sustainable mitigation measures". In: *Environmental Science and Pollution Research* 29.28, pp. 42539–42559. DOI: 10.1007/S11356-022-19718-6.

Acero Triana, J. S., Chu, M. L., Guzman, J. A., Moriasi, D. N., and Steiner, J. L. (2019). "Beyond model metrics: The perils of calibrating hydrologic models". In: *Journal of Hydrology* 578, p. 124032. DOI: 10.1016/J.JHYDROL.2019.124032.

Aguilar-Lome, J., Espinoza-Villar, R., Espinoza, J. C., Rojas-Acuña, J., Willems, B. L., and Leyva-Molina, W. M. (2019). "Elevation-dependent warming of land surface temperatures in the Andes assessed using MODIS LST time series (2000–2017)". In: *International Journal of Applied Earth Observation and Geoinformation* 77, pp. 119–128. DOI: 10.1016/J.JAG.2018.12.013.

Alemayehu, T., van Griensven, A., Woldegiorgis, B. T., and Bauwens, W. (2017). "An improved SWAT vegetation growth module and its evaluation for four tropical ecosystems". In: *Hydrology and Earth System Sciences* 21.9, pp. 4449–4467. DOI: 10.5194/hess-21-4449-2017.

Alfieri, L., Lorini, V., Hirpa, F. A., Harrigan, S., Zsoter, E., Prudhomme, C., and Salamon, P. (2020). "A global streamflow reanalysis for 1980–2018". In: *Journal of Hydrology X* 6, p. 100049. DOI: 10.1016/j.hydroa.2019.100049.

Almazroui, M., Ashfaq, M., Islam, M. N., Rashid, I. U., Kamil, S., Abid, M. A., O'Brien, E., Ismail, M., Reboita, M. S., Sörensson, A. A., Arias, P. A., Alves, L. M., Tippett, M. K., Saeed, S., Haarsma, R., Doblas-Reyes, F. J., Saeed, F., Kucharski, F., Nadeem, I., Silva-Vidal, Y., Rivera, J. A., Ehsan, M. A., Martínez-Castro, D., Muñoz, Á. G., Ali, M. A., Coppola, E., and Sylla, M. B. (2021). "Assessment of CMIP6 Performance and Projected Temperature and Precipitation Changes Over South America". In: *Earth Systems and Environment* 5.2, pp. 155–183. DOI: 10.1007/S41748-021-00233-6.

ANA (2012). *Recursos hídricos en el Perú*. Tech. rep. Autoridad Nacional del Agua.

Andres, N., Vegas Galdos, F., Lavado Casimiro, W. S., and Zappa, M. (2014). "Water resources and climate change impact modelling on a daily time scale in the Peruvian Andes". In: *Hydrological Sciences Journal* 59.11, pp. 2043–2059. DOI: 10.1080/02626667.2013.862336.

Arias, P. A., Garreaud, R., Poveda, G., Espinoza, J. C., Molina-Carpio, J., Masiokas, M., Viale, M., Scaff, L., and van Oevelen, P. J. (2021a). "Hydroclimate of the Andes Part II: Hydroclimate Variability and Sub-Continental Patterns". In: *Frontiers in Earth Science* 8. DOI: 10.3389/feart.2020.505467.

Arias, P. A., Ortega, G., Villegas, L. D., Martínez, J. A., Arias, P. A., Ortega, G., Villegas, L. D., and Martínez, J. A. (2021b). "Colombian climatology in CMIP5/CMIP6 models: Persistent biases and improvements". In: *Revista Facultad de Ingeniería Universidad de Antioquia* 100, pp. 75–96. DOI: 10.17533/UDEA.REDIN.20210525.

Armijos, E., Crave, A., Vauchel, P., Fraizy, P., Santini, W., Moquet, J. S., Arevalo, N., Carranza, J., and Guyot, J. L. (2013). "Suspended sediment dynamics in the Amazon River of Peru". In: *Journal of South American Earth Sciences* 44, pp. 75–84. DOI: 10.1016/j.jsames.2012.09.002.

Arnold, J. G., Srinivasan, R., Muttiah, R. S., and Williams, J. R. (1998). "Large area hydrologic modeling and assessment part I: model development". In: *Journal of the American Water Resources Association* 34.1, pp. 73–89. DOI: 10.1111/j.1752-1688.1998.tb05961.x.

Arnold, J. G. and Allen, P. M. (1999). "Automated methods for estimating baseflow and ground water recharge from streamflow records". In: *Journal of the American Water Resources Association* 35.2, pp. 411–424. DOI: 10.1111/j.1752-1688.1999.tb03599.x.

Arnold, J. G., Allen, P. M., Muttiah, R., and Bernhardt, G. (1995). "Automated Base Flow Separation and Recession Analysis Techniques". In: *Ground Water* 33.6, pp. 1010–1018. DOI: 10.1111/j.1745-6584.1995.tb00046.x.

Arnold, J. G., Moriasi, D. N., Gassman, P. W., Abbaspour, K. C., White, M. J., Srinivasan, R., Santhi, C., Harmel, R. D., Griensven, a. V., VanLiew, M. W., Kannan, N., and Jha, M. K. (2012). "Swat: Model Use, Calibration, and Validation". In: *Asabe* 55.4, pp. 1491–1508.

Asurza-Véliz, F. A. and Lavado-Casimiro, W. S. (2020). "Regional Parameter Estimation of the SWAT Model: Methodology and Application to River Basins in the Peruvian Pacific Drainage". In: *Water* 12.11, p. 3198. DOI: 10.3390/W12113198.

Atieh, M., Taylor, G., M.A. Sattar, A., and Gharabaghi, B. (2017). "Prediction of flow duration curves for ungauged basins". In: *Journal of Hydrology* 545, pp. 383–394. DOI: 10.1016/j.jhydrol.2016.12.048.

Aybar, C., Fernández, C., Huerta, A., Lavado, W., Vega, F., and Felipe-Obando, O. (2020). "Construction of a high-resolution gridded rainfall dataset for Peru from 1981 to the present day". In: *Hydrological Sciences Journal* 65.5, pp. 770–785. DOI: 10.1080/02626667.2019.1649411.

Baez-Villanueva, O. M., Zambrano-Bigiarini, M., Beck, H. E., McNamara, I., Ribbe, L., Nauditt, A., Birkel, C., Verbist, K., Giraldo-Osorio, J. D., and Xuan Thinh, N. (2020). "RF-MEP: A novel Random Forest method for merging gridded precipitation products and ground-based measurements". In: *Remote Sensing of Environment* 239, p. 111606. DOI: 10.1016/j.rse.2019.111606.

Baez-Villanueva, O. M., Zambrano-Bigiarini, M., Ribbe, L., Nauditt, A., Giraldo-Osorio, J. D., and Thinh, N. X. (2018). "Temporal and spatial evaluation of satellite rainfall estimates over different regions in Latin-America". In: *Atmospheric Research* 213, pp. 34–50. DOI: 10.1016/j.atmosres.2018.05.011.

Bai, P. and Liu, X. (2018). "Evaluation of five satellite-based precipitation products in two gauge-scarce basins on the Tibetan Plateau". In: *Remote Sensing* 10.8, p. 1316. DOI: 10.3390/RS10081316.

Ballarin, A. S., Sone, J. S., Gesualdo, G. C., Schwamback, D., Reis, A., Almagro, A., and Wendland, E. C. (2023). "CLIMBra - Climate Change Dataset for Brazil". In: *Scientific Data* 10.1, pp. 1–16. DOI: 10.1038/s41597-023-01956-z.

Beck, H. E., van Dijk, A. I. J. M., Levizzani, V., Schellekens, J., Miralles, D. G., Martens, B., and de Roo, A. (2017). "MSWEP: 3-hourly 0.25° global gridded precipitation (1979–2015) by

merging gauge, satellite, and reanalysis data". In: *Hydrology and Earth System Sciences* 21.1, pp. 589–615. DOI: 10.5194/hess-21-589-2017.

Beck, H. E., van Dijk, A. I. J. M., Miralles, D. G., de Jeu, R. A. M., Sampurno Bruijnzeel, L. A., McVicar, T. R., and Schellekens, J. (2013). "Global patterns in base flow index and recession based on streamflow observations from 3394 catchments". In: *Water Resources Research* 49.12, pp. 7843–7863. DOI: 10.1002/2013WR013918.

Beck, H. E., Pan, M., Roy, T., Weedon, G. P., Pappenberger, F., van Dijk, A. I. J. M., Huffman, G. J., Adler, R. F., and Wood, E. F. (2019a). "Daily evaluation of 26 precipitation datasets using Stage-IV gauge-radar data for the CONUS". In: *Hydrology and Earth System Sciences* 23.1, pp. 207–224. DOI: 10.5194/hess-23-207-2019.

Beck, H. E., Vergopolan, N., Pan, M., Levizzani, V., van Dijk, A. I., Weedon, G. P., Brocca, L., Pappenberger, F., Huffman, G. J., and Wood, E. F. (2020a). "Global-scale evaluation of 22 precipitation datasets using gauge observations and hydrological modeling". In: *Advances in Global Change Research*. Ed. by Levizzani, V., Kidd, C., Kirschbaum, D., Kummerow, C., Nakamura, K., and Turk, F. Vol. 69. Cham: Springer International Publishing, pp. 625–653. DOI: 10.1007/978-3-030-35798-6_9.

Beck, H. E., Wood, E. F., McVicar, T. R., Zambrano-Bigiarini, M., Alvarez-Garreton, C., Baez-Villanueva, O. M., Sheffield, J., and Karger, D. N. (2020b). "Bias correction of global high-resolution precipitation climatologies using streamflow observations from 9372 catchments". In: *Journal of Climate* 33.4, pp. 1299–1315. DOI: 10.1175/JCLI-D-19-0332.1.

Beck, H. E., Wood, E. F., Pan, M., Fisher, C. K., Miralles, D. G., van Dijk, A. I. J. M., McVicar, T. R., and Adler, R. F. (2019b). "MSWEP V2 Global 3-Hourly 0.1° Precipitation: Methodology and Quantitative Assessment". In: *Bulletin of the American Meteorological Society* 100.3, pp. 473–500. DOI: 10.1175/BAMS-D-17-0138.1.

Benestad, R. E., Lussana Id, C., Lutz Id, J., Dobler, A., Landgrenid, O., Haugenid, J. E., Mezghaniid, A., Casatiid, B., and Pardingid, K. M. (2022). "Global hydro-climatological indicators and changes in the global hydrological cycle and rainfall patterns". In: *PLOS Climate* 1.5, e0000029. DOI: 10.1371/JOURNAL.PCLM.0000029.

Bergmann, J., Vinke, K., Fernandez Palomino, C., Gornott, C., Gleixner, S., Laudien, R., Lobanova, A., Ludescher, J., and Schellnhuber, H. J. (2021). *Assessing the Evidence: Climate Change and Migration in Peru*. Potsdam and Geneva: Potsdam Institute for Climate Impact Research (PIK) and International Organisation for Migration (IOM).

Beven, K. (2006). "A manifesto for the equifinality thesis". In: *Journal of Hydrology* 320.1, pp. 18–36. DOI: 10.1016/j.jhydrol.2005.07.007.

Bhuiyan, M. A. E., Nikolopoulos, E. I., and Anagnostou, E. N. (2019). "Machine learning–based blending of satellite and reanalysis precipitation datasets: A multiregional tropical complex terrain evaluation". In: *Journal of Hydrometeorology* 20.11, pp. 2147–2161. DOI: 10.1175/JHM-D-19-0073.1.

Boers, N., Marwan, N., Barbosa, H. M., and Kurths, J. (2017). "A deforestation-induced tipping point for the South American monsoon system". In: *Scientific Reports* 7.1, pp. 1–9. DOI: 10.1038/srep41489.

Boucher, O., Servonnat, J., Albright, A. L., Aumont, O., Balkanski, Y., Bastrikov, V., Bekki, S., Bonnet, R., Bony, S., Bopp, L., Braconnot, P., Brockmann, P., Cadule, P., Caubel, A., Cheruy, F., Codron, F., Cozic, A., Cugnet, D., D'Andrea, F., Davini, P., de Lavergne, C., Denvil, S., Deshayes, J., Devilliers, M., Ducharne, A., Dufresne, J. L., Dupont, E., Éthé, C., Fairhead, L., Falletti, L., Flavoni, S., Foujols, M. A., Gardoll, S., Gastineau, G., Ghattas, J., Grandpeix, J. Y., Guenet, B., Guez Lionel, E., Guilyardi, E., Guimberteau, M., Hauglustaine, D., Hourdin, F., Idelkadi, A., Joussaume, S., Kageyama, M., Khodri, M., Krinner, G., Lebas, N., Levavasseur, G., Lévy, C., Li, L., Lott, F., Lurton, T., Luyssaert, S., Madec, G., Madeleine, J. B., Maignan, F., Marchand, M., Marti, O., Mellul, L., Meurdesoif, Y., Mignot, J., Musat, I., Ottlé, C., Peylin, P., Planton, Y., Polcher, J., Rio, C., Rochetin, N., Rousset, C., Sepulchre, P., Sima, A., Swingedouw, D., Thiéblemont, R., Traore, A. K., Vancoppenolle, M., Vial, J., Vialard, J., Viovy, N., and Vuichard, N. (2020). "Presentation and Evaluation of the IPSL-CM6A-LR Climate Model". In: *Journal of Advances in Modeling Earth Systems* 12.7, e2019MS002010. DOI: 10.1029/2019MS002010.

Boulton, C. A., Lenton, T. M., and Boers, N. (2022). "Pronounced loss of Amazon rainforest resilience since the early 2000s". In: *Nature Climate Change* 12.3, pp. 271–278. DOI: 10.1038/s41558-022-01287-8.

Bradley, R. S., Vuille, M., Diaz, H. F., and Vergara, W. (2006). "Threats to water supplies in the tropical andes". In: *Science* 312.5781, pp. 1755–1756. DOI: 10.1126/science.1128087.

Brêda, J. P. L. F., de Paiva, R. C. D., Collischon, W., Bravo, J. M., Siqueira, V. A., and Steinke, E. B. (2020). "Climate change impacts on South American water balance from a continental-scale hydrological model driven by CMIP5 projections". In: *Climatic Change* 159.4, pp. 503–522. DOI: 10.1007/S10584-020-02667-9.

Breiman, L. (2001). "Random forests". In: *Machine Learning* 45.1, pp. 5–32. DOI: 10.1023/A:1010933404324.

Brocca, L., Moramarco, T., Melone, F., and Wagner, W. (2013). "A new method for rainfall estimation through soil moisture observations". In: *Geophysical Research Letters* 40.5, pp. 853–858. DOI: 10.1002/grl.50173.

Brocca, L., Filippucci, P., Hahn, S., Ciabatta, L., Massari, C., Camici, S., Schüller, L., Bojkov, B., and Wagner, W. (2019). "SM2RAIN–ASCAT (2007–2018): global daily satellite rainfall data from ASCAT soil moisture observations". In: *Earth System Science Data* 11.4, pp. 1583–1601. DOI: 10.5194/essd-11-1583-2019.

Brocca, L., Massari, C., Pellarin, T., Filippucci, P., Ciabatta, L., Camici, S., Kerr, Y. H., and Fernández-Prieto, D. (2020). "River flow prediction in data scarce regions: soil moisture integrated satellite rainfall products outperform rain gauge observations in West Africa". In: *Scientific Reports* 10.1, p. 12517. DOI: 10.1038/s41598-020-69343-x.

Bronstert, A., Kolokotronis, V., Schwandt, D., and Straub, H. (2007). "Comparison and evaluation of regional climate scenarios for hydrological impact analysis: General scheme and application example". In: *International Journal of Climatology* 27.12, pp. 1579–1594. DOI: 10.1002/JOC.1621.

Brouziyne, Y., Abouabdillah, A., Bouabid, R., Benaabidate, L., and Oueslati, O. (2017). "SWAT manual calibration and parameters sensitivity analysis in a semi-arid watershed in Northwestern Morocco". In: *Arabian Journal of Geosciences* 10.19, p. 427. DOI: 10.1007/s12517-017-3220-9.

Bruijnzeel, L. A., Mulligan, M., and Scatena, F. N. (2011). "Hydrometeorology of tropical montane cloud forests: Emerging patterns". In: *Hydrological Processes* 25.3, pp. 465–498. DOI: 10.1002/hyp.7974.

Buchhorn, M., Smets, B., Bertels, L., Lesiv, M., Tsendbazar, N.-E., Herold, M., and Fritz, S. (2019). "Copernicus Global Land Service: Land Cover 100m: epoch 2015: Globe. Dataset of the global component of the Copernicus Land Monitoring Service." In: *Zenodo*. DOI: 10.5281/zenodo.3243509.

Builes-Jaramillo, A. and Poveda, G. (2018). "Conjoint Analysis of Surface and Atmospheric Water Balances in the Andes-Amazon System". In: *Water Resources Research* 54.5, pp. 3472–3489. DOI: 10.1029/2017WR021338.

Buytaert, W., Iñiguez, V., and Bièvre, B. D. (2007). "The effects of afforestation and cultivation on water yield in the Andean páramo". In: *Forest Ecology and Management* 251.1-2, pp. 22–30. DOI: 10.1016/j.foreco.2007.06.035.

Buytaert, W., Moulds, S., Acosta, L., De Bièvre, B., Olmos, C., Villacis, M., Tovar, C., and Verbist, K. M. (2017). "Glacial melt content of water use in the tropical Andes". In: *Environmental Research Letters* 12.11, p. 114014. DOI: 10.1088/1748-9326/AA926C.

Cai, W., Ng, B., Geng, T., Jia, F., Wu, L., Wang, G., Liu, Y., Gan, B., Yang, K., Santoso, A., Lin, X., Li, Z., Liu, Y., Yang, Y., Jin, F. F., Collins, M., and McPhaden, M. J. (2023). "Anthropogenic impacts on twentieth-century ENSO variability changes". In: *Nature Reviews Earth & Environment* 4.6, pp. 407–418. DOI: 10.1038/s43017-023-00427-8.

Cárdenas, M. F., Tobón, C., and Buytaert, W. (2017). "Contribution of occult precipitation to the water balance of páramo ecosystems in the Colombian Andes". In: *Hydrological Processes* 31.24, pp. 4440–4449. DOI: 10.1002/hyp.11374.

Carrillo-Rojas, G., Silva, B., Rollenbeck, R., Célleri, R., and Bendix, J. (2019). "The breathing of the Andean highlands: Net ecosystem exchange and evapotranspiration over the páramo of

southern Ecuador". In: *Agricultural and Forest Meteorology* 265, pp. 30–47. DOI: `10.1016/j.agrformet.2018.11.006`.

Catacora-Acevedo, E. A. (2008). "Predicciones del comportamiento de caudales de la C.H. Machupicchu mediante análisis ARIMA de series temporales". PhD thesis. Universidad Nacional de Ingeniería - Perú.

Cayo, E. Y. T., Borja, M. O., Espinoza-Villar, R., Moreno, N., Camargo, R., Almeida, C., Hopfgartner, K., Yarleque, C., and Souza, C. M. (2022). "Mapping Three Decades of Changes in the Tropical Andean Glaciers Using Landsat Data Processed in the Earth Engine". In: *Remote Sensing* 14.9, p. 1974. DOI: `10.3390/RS14091974`.

Chavez, S. P. and Takahashi, K. (2017). "Orographic rainfall hot spots in the Andes-Amazon transition according to the TRMM precipitation radar and in situ data". In: *Journal of Geophysical Research: Atmospheres* 122.11, pp. 5870–5882. DOI: `10.1002/2016JD026282`.

Chen, Y., Chen, X., Xu, C.-Y., Zhang, M., Liu, M., and Gao, L. (2018). "Toward Improved Calibration of SWAT Using Season-Based Multi-Objective Optimization: a Case Study in the Jinjiang Basin in Southeastern China". In: *Water Resources Management* 32.4, pp. 1193–1207. DOI: `10.1007/s11269-017-1862-8`.

Chilkoti, V., Bolisetti, T., and Balachandar, R. (2018). "Multi-objective autocalibration of SWAT model for improved low flow performance for a small snowfed catchment". In: *Hydrological Sciences Journal* 63.10, pp. 1482–1501. DOI: `10.1080/02626667.2018.1505047`.

Chilkoti, V., Bolisetti, T., and Balachandar, R. (2019). "Diagnostic Evaluation of Hydrologic Models Employing Flow Duration Curve". In: *Journal of Hydrologic Engineering* 24.6. DOI: `10.1061/(ASCE)HE.1943-5584.0001778`.

Clark, K. E., Torres, M. A., West, A. J., Hilton, R. G., New, M., Horwath, A. B., Fisher, J. B., Rapp, J. M., Caceres, A. R., and Malhi, Y. (2014). "The hydrological regime of a forested tropical Andean catchment". In: *Hydrol. Earth Syst. Sci* 18, pp. 5377–5397. DOI: `10.5194/hess-18-5377-2014`.

Condom, T., Martínez, R., Pabón, J. D., Costa, F., Pineda, L., Nieto, J. J., López, F., and Villacis, M. (2020). "Climatological and Hydrological Observations for the South American Andes: In situ Stations, Satellite, and Reanalysis Data Sets". In: *Frontiers in Earth Science* 8. DOI: `10.3389/FEART.2020.00092`.

Conradt, T., Wechsung, F., and Bronstert, A. (2013). "Three perceptions of the evapotranspiration landscape: Comparing spatial patterns from a distributed hydrological model, remotely sensed surface temperatures, and sub-basin water balances". In: *Hydrology and Earth System Sciences* 17.7, pp. 2947–2966. DOI: `10.5194/HESS-17-2947-2013`.

Dalagnol, R., Borma, L. d. S., Mateus, P., and Rodriguez, D. A. (2017). "Assessment of climate change impacts on water resources of the Purus Basin in the southwestern Amazon". In: *Acta Amazonica* 47.3, pp. 213–226. DOI: `10.1590/1809-4392201601993`.

De Paiva, R. C. D., Buarque, D. C., Collischonn, W., Bonnet, M. P., Frappart, F., Calmant, S., and Bulhões Mendes, C. A. (2013). "Large-scale hydrologic and hydrodynamic modeling of the Amazon River basin". In: *Water Resources Research* 49.3, pp. 1226–1243. DOI: `10.1002/WRCR.20067`.

Dee, D. P., Uppala, S. M., Simmons, A. J., Berrisford, P., Poli, P., Kobayashi, S., Andrae, U., Balmaseda, M. A., Balsamo, G., Bauer, P., Bechtold, P., Beljaars, A. C., van de Berg, L., Bidlot, J., Bormann, N., Delsol, C., Dragani, R., Fuentes, M., Geer, A. J., Haimberger, L., Healy, S. B., Hersbach, H., Hólm, E. V., Isaksen, L., Kållberg, P., Köhler, M., Matricardi, M., Mcnally, A. P., Monge-Sanz, B. M., Morcrette, J. J., Park, B. K., Peubey, C., de Rosnay, P., Tavolato, C., Thépaut, J. N., and Vitart, F. (2011). "The ERA-Interim reanalysis: Configuration and performance of the data assimilation system". In: *Quarterly Journal of the Royal Meteorological Society* 137.656, pp. 553–597. DOI: `10.1002/qj.828`.

Delclaux, F., Coudrain, A., and Condom, T. (2007). "Evaporation estimation on Lake Titicaca: a synthesis review and modelling". In: *Hydrological Processes* 21.13, pp. 1664–1677. DOI: `10.1002/hyp.6360`.

Dereczynski, C., Chan Chou, S., Lyra, A., Sondermann, M., Regoto, P., Tavares, P., Chagas, D., Gomes, J. L., Rodrigues, D. C., and Skansi, M. d. l. M. (2020). "Downscaling of climate extremes over South America – Part I: Model evaluation in the reference climate". In: *Weather and Climate Extremes* 29, p. 100273. DOI: `10.1016/J.WACE.2020.100273`.

Derin, Y., Anagnostou, E., Berne, A., Borga, M., Boudevillain, B., Buytaert, W., Chang, C.-H., Chen, H., Delrieu, G., Hsu, Y., Lavado-Casimiro, W., Manz, B., Moges, S., Nikolopoulos, E., Sahlu, D., Salerno, F., Rodríguez-Sánchez, J.-P., Vergara, H., and Yilmaz, K. (2019). "Evaluation of GPM-era Global Satellite Precipitation Products over Multiple Complex Terrain Regions". In: *Remote Sensing* 11.24, p. 2936. DOI: 10.3390/rs11242936.

Devak, M. and Dhanya, C. T. (2017). "Sensitivity analysis of hydrological models: review and way forward". In: *Journal of Water and Climate Change* 8.4, pp. 557–575. DOI: 10.2166/wcc.2017.149.

Di Marco, N., Avesani, D., Righetti, M., Zaramella, M., Majone, B., and Borga, M. (2021). "Reducing hydrological modelling uncertainty by using MODIS snow cover data and a topography-based distribution function snowmelt model". In: *Journal of Hydrology* 599, p. 126020. DOI: 10.1016/J.JHYDROL.2021.126020.

Dile, Y. T., Ayana, E. K., Worqlul, A. W., Xie, H., Srinivasan, R., Lefore, N., You, L., and Clarke, N. (2020). "Evaluating satellite-based evapotranspiration estimates for hydrological applications in data-scarce regions: A case in Ethiopia". In: *Science of the Total Environment* 743, p. 140702. DOI: 10.1016/j.scitotenv.2020.140702.

Döscher, R., Acosta, M., Alessandri, A., Anthoni, P., Arsouze, T., Bergman, T., Bernardello, R., Boussetta, S., Caron, L. P., Carver, G., Castrillo, M., Catalano, F., Cvijanovic, I., Davini, P., Dekker, E., Doblas-Reyes, F. J., Docquier, D., Echevarria, P., Fladrich, U., Fuentes-Franco, R., Gröger, M., Hardenberg, J. V., Hieronymus, J., Karami, M. P., Keskinen, J. P., Koenigk, T., Makkonen, R., Massonnet, F., Ménégoz, M., Miller, P. A., Moreno-Chamarro, E., Nieradzik, L., Van Noije, T., Nolan, P., O'donnell, D., Ollinaho, P., Van Den Oord, G., Ortega, P., Prims, O. T., Ramos, A., Reerink, T., Rousset, C., Ruprich-Robert, Y., Le Sager, P., Schmith, T., Schrödner, R., Serva, F., Sicardi, V., Sloth Madsen, M., Smith, B., Tian, T., Tourigny, E., Uotila, P., Vancoppenolle, M., Wang, S., Wårlind, D., Willén, U., Wyser, K., Yang, S., Yepes-Arbós, X., and Zhang, Q. (2022). "The EC-Earth3 Earth system model for the Coupled Model Intercomparison Project 6". In: *Geoscientific Model Development* 15.7, pp. 2973–3020. DOI: 10.5194/GMD-15-2973-2022.

Dunne, J. P., Horowitz, L. W., Adcroft, A. J., Ginoux, P., Held, I. M., John, J. G., Krasting, J. P., Malyshev, S., Naik, V., Paulot, F., Shevliakova, E., Stock, C. A., Zadeh, N., Balaji, V., Blanton, C., Dunne, K. A., Dupuis, C., Durachta, J., Dussin, R., Gauthier, P. P., Griffies, S. M., Guo, H., Hallberg, R. W., Harrison, M., He, J., Hurlin, W., McHugh, C., Menzel, R., Milly, P. C., Nikonov, S., Paynter, D. J., Ploshay, J., Radhakrishnan, A., Rand, K., Reichl, B. G., Robinson, T., Schwarzkopf, D. M., Sentman, L. T., Underwood, S., Vahlenkamp, H., Winton, M., Wittenberg, A. T., Wyman, B., Zeng, Y., and Zhao, M. (2020). "The GFDL Earth System Model Version 4.1 (GFDL-ESM 4.1): Overall Coupled Model Description and Simulation Characteristics". In: *Journal of Advances in Modeling Earth Systems* 12.11, e2019MS002015. DOI: 10.1029/2019MS002015.

Eini, M. R., Massari, C., and Piniewski, M. (2023). "Satellite-based soil moisture enhances the reliability of agro-hydrological modeling in large transboundary river basins". In: *Science of The Total Environment* 873, p. 162396. DOI: 10.1016/J.SCITOTENV.2023.162396.

Erazo, B., Bourrel, L., Frappart, F., Chimborazo, O., Labat, D., Dominguez-Granda, L., Matamoros, D., and Mejia, R. (2018). "Validation of Satellite Estimates (Tropical Rainfall Measuring Mission, TRMM) for Rainfall Variability over the Pacific Slope and Coast of Ecuador". In: *Water* 10.2, p. 213. DOI: 10.3390/w10020213.

Espinoza, J. C., Chavez, S., Ronchail, J., Junquas, C., Takahashi, K., and Lavado, W. (2015). "Rainfall hotspots over the southern tropical Andes: Spatial distribution, rainfall intensity, and relations with large-scale atmospheric circulation". In: *Water Resources Research* 51.5, pp. 3459–3475. DOI: 10.1002/2014WR016273.

Espinoza, J. C., Garreaud, R., Poveda, G., Arias, P. A., Molina-Carpio, J., Masiokas, M., Viale, M., and Scaff, L. (2020). "Hydroclimate of the Andes Part I: Main Climatic Features". In: *Frontiers in Earth Science* 8. DOI: 10.3389/FEART.2020.00064.

Espinoza, J. C., Ronchail, J., Marengo, J. A., and Segura, H. (2019). "Contrasting North–South changes in Amazon wet-day and dry-day frequency and related atmospheric features (1981–2017)". In: *Climate Dynamics* 52.9-10, pp. 5413–5430. DOI: 10.1007/S00382-018-4462-2.

Espinoza, J. C., Segura, H., Ronchail, J., Drapeau, G., and Gutierrez-Cori, O. (2016). "Evolution of wet-day and dry-day frequency in the western Amazon basin: Relationship with atmospheric circulation and impacts on vegetation". In: *Water Resources Research* 52.11, pp. 8546–8560. DOI: 10.1002/2016WR019305.

Espinoza Villar, J. C., Guyot, J. L., Ronchail, J., Cochonneau, G., Filizola, N., Fraizy, P., Labat, D., de Oliveira, E., Ordoñez, J. J., and Vauchel, P. (2009a). "Contrasting regional discharge evolutions in the Amazon basin (1974–2004)". In: *Journal of Hydrology* 375.3-4, pp. 297–311. DOI: 10.1016/J.JHYDROL.2009.03.004.

Espinoza Villar, J. C., Ronchail, J., Guyot, J. L., Cochonneau, G., Naziano, F., Lavado, W., De Oliveira, E., Pombosa, R., and Vauchel, P. (2009b). "Spatio-temporal rainfall variability in the Amazon basin countries (Brazil, Peru, Bolivia, Colombia, and Ecuador)". In: *International Journal of Climatology* 29.11, pp. 1574–1594. DOI: 10.1002/joc.1791.

Eyring, V., Bony, S., Meehl, G. A., Senior, C. A., Stevens, B., Stouffer, R. J., and Taylor, K. E. (2016). "Overview of the Coupled Model Intercomparison Project Phase 6 (CMIP6) experimental design and organization". In: *Geoscientific Model Development* 9.5, pp. 1937–1958. DOI: 10.5194/GMD-9-1937-2016.

Eyring, V., Mishra, V., Griffith, G. P., Chen, L., Keenan, T., Turetsky, M. R., Brown, S., Jotzo, F., Moore, F. C., and van der Linden, S. (2021). "Reflections and projections on a decade of climate science". In: *Nature Climate Change* 11.4, pp. 279–285. DOI: 10.1038/s41558-021-01020-x.

Fallah, A., Rakhshandehroo, G. R., Berg, P., O, S., and Orth, R. (2020). "Evaluation of precipitation datasets against local observations in southwestern Iran". In: *International Journal of Climatology*, joc.6445. DOI: 10.1002/joc.6445.

Fan, Y., Li, H., and Miguez-Macho, G. (2013). "Global patterns of groundwater table depth". In: *Science* 339.6122, pp. 940–943. DOI: 10.1126/science.1229881.

FAO-UNESCO (1988). "Soil Map of the World, Revised Legend, with corrections and updates". In: *World Soil Resources Report* 60, p. 140.

Fernandez-Palomino, C. A., Hattermann, F. F., Krysanova, V., Lobanova, A., Vega-Jácome, F., Lavado, W., Santini, W., Aybar, C., and Bronstert, A. (2021). "Rain for Peru and Ecuador (RAIN4PE). V. 1.0". In: *GFZ Data Services*. DOI: 10.5880/pik.2020.010.

Fernandez-Palomino, C. A., Hattermann, F. F., Krysanova, V., Lobanova, A., Vega-Jácome, F., Lavado, W., Santini, W., Aybar, C., and Bronstert, A. (2022). "A Novel High-Resolution Gridded Precipitation Dataset for Peruvian and Ecuadorian Watersheds: Development and Hydrological Evaluation". In: *Journal of Hydrometeorology* 23.3, pp. 309–336. DOI: 10.1175/JHM-D-20-0285.1.

Fernandez-Palomino, C. A., Hattermann, F. F., Krysanova, V., Vega-Jácome, F., and Bronstert, A. (2020). "Towards a more consistent eco-hydrological modelling through multi-objective calibration: a case study in the Andean Vilcanota River basin, Peru". In: *Hydrological Sciences Journal* 66.1, pp. 59–74. DOI: 10.1080/02626667.2020.1846740.

Fernandez-Palomino, C. A., Hattermann, F. F., Krysanova, V., Vega-Jácome, F., Lavado, W., Santini, W., Gutiérrez, R. R., and Bronstert, A. (2023a). "Pan-Peruvian Simulation of Present and Projected Future Hydrological Conditions Using Novel Data Products and CMIP6 Climate Projections". In: *SSRN*. DOI: 10.2139/SSRN.4602668.

Fernandez-Palomino, C. A., Hattermann, F. F., Krysanova, V., Vega-Jácome, F., Menz, C., Gleixner, S., and Bronstert, A. (2023b). "BASD-CMIP6-PE: bias-adjusted and statistically downscaled CMIP6 projections over Peru and Ecuador." In: *GFZ Data Services*. DOI: 10.5880/pik.2023.001.

Fernandez-Palomino, C. A., Hattermann, F. F., Krysanova, V., Vega-Jácome, F., Menz, C., Gleixner, S., and Bronstert, A. (2024). "High-resolution climate projection dataset based on CMIP6 for Peru and Ecuador: BASD-CMIP6-PE". In: *Scientific Data* 11.1, pp. 1–14. DOI: 10.1038/s41597-023-02863-z.

Fernández-Palomino, C. A. and Lavado-Casimiro, W. S. (2017). "Regional maximum rainfall analysis using L-moments at the Titicaca Lake drainage, Peru". In: *Theoretical and Applied Climatology* 129.3-4, pp. 1295–1307. DOI: 10.1007/S00704-016-1845-3.

Ficklin, D. L. and Barnhart, B. L. (2014). "SWAT hydrologic model parameter uncertainty and its implications for hydroclimatic projections in snowmelt-dependent watersheds". In: *Journal of Hydrology* 519, pp. 2081–2090. DOI: 10.1016/j.jhydrol.2014.09.082.

Fiedler, S., Crueger, T., D'Agostino, R., Peters, K., Becker, T., Leutwyler, D., Paccini, L., Burdanowitz, J., Buehler, S. A., Cortes, A. U., Dauhut, T., Dommenget, D., Fraedrich, K., Jungandreas, L., Maher, N., Naumann, A. K., Rugenstein, M., Sakradzija, M., Schmidt, H., Sielmann, F., Stephan, C., Timmreck, C., Zhu, X., and Stevens, B. (2020). "Simulated Tropical Precipitation Assessed across Three Major Phases of the Coupled Model Intercomparison Project (CMIP)". In: *Monthly Weather Review* 148.9, pp. 3653–3680. DOI: 10.1175/MWR-D-19-0404.1.

Firpo, M. Â. F., Guimarães, B. d. S., Dantas, L. G., Silva, M. G. B. d., Alves, L. M., Chadwick, R., Llopart, M. P., and Oliveira, G. S. d. (2022). "Assessment of CMIP6 models' performance in simulating present-day climate in Brazil". In: *Frontiers in Climate* 0, p. 170. DOI: 10.3389/FCLIM.2022.948499.

Fox, E. W., Ver Hoef, J. M., and Olsen, A. R. (2020). "Comparing spatial regression to random forests for large environmental data sets". In: *PLoS ONE* 15.3, e0229509. DOI: 10.1371/journal.pone.0229509.

Francesconi, W., Srinivasan, R., Pérez-Miñana, E., Willcock, S. P., and Quintero, M. (2016). "Using the Soil and Water Assessment Tool (SWAT) to model ecosystem services: A systematic review". In: *Journal of Hydrology* 535, pp. 625–636. DOI: 10.1016/j.jhydrol.2016.01.034.

Funk, C., Peterson, P., Landsfeld, M., Pedreros, D., Verdin, J., Shukla, S., Husak, G., Rowland, J., Harrison, L., Hoell, A., and Michaelsen, J. (2015a). "The climate hazards infrared precipitation with stations - A new environmental record for monitoring extremes". In: *Scientific Data* 2.1, pp. 1–21. DOI: 10.1038/sdata.2015.66.

Funk, C., Verdin, A., Michaelsen, J., Peterson, P., Pedreros, D., and Husak, G. (2015b). "A global satellite-assisted precipitation climatology". In: *Earth System Science Data* 7.2, pp. 275–287. DOI: 10.5194/essd-7-275-2015.

Gassman, P. W., Reyes, M. R., Green, C. H., and Arnold, J. G. (2007). "The Soil and Water Assessment Tool : historical development, applications, and future research directions". In: *Transactions of the ASAE* 50.4, pp. 1211–1250. DOI: 10.1.1.88.6554.

Gassman, P. W., Sadeghi, A. M., and Srinivasan, R. (2014). "Applications of the SWAT Model Special Section: Overview and Insights". In: *Journal of Environmental Quality* 43.1, pp. 1–8. DOI: 10.2134/jeq2013.11.0466.

Gennaretti, F., Sangelantoni, L., and Grenier, P. (2015). "Toward daily climate scenarios for Canadian Arctic coastal zones with more realistic temperature-precipitation interdependence". In: *Journal of Geophysical Research: Atmospheres* 120.23, pp. 11862–11877. DOI: 10.1002/2015JD023890.

Gleixner, S., Demissie, T., and Diro, G. T. (2020). "Did ERA5 Improve Temperature and Precipitation Reanalysis over East Africa?" In: *Atmosphere* 11.9, p. 996. DOI: 10.3390/atmos11090996.

Gloor, M., Barichivich, J., Ziv, G., Brienen, R., Schöngart, J., Peylin, P., Ladvocat Cintra, B. B., Feldpausch, T., Phillips, O., and Baker, J. (2015). "Recent Amazon climate as background for possible ongoing and future changes of Amazon humid forests". In: *Global Biogeochemical Cycles* 29.9, pp. 1384–1399. DOI: 10.1002/2014GB005080.

Gloor, M., Brienen, R. J., Galbraith, D., Feldpausch, T. R., Schöngart, J., Guyot, J. L., Espinoza, J. C., Lloyd, J., and Phillips, O. L. (2013). "Intensification of the Amazon hydrological cycle over the last two decades". In: *Geophysical Research Letters* 40.9, pp. 1729–1733. DOI: 10.1002/GRL.50377.

Gomez-Peralta, D., Oberbauer, S. F., McClain, M. E., and Philippi, T. E. (2008). "Rainfall and cloud-water interception in tropical montane forests in the eastern Andes of Central Peru". In: *Forest Ecology and Management* 255.3-4, pp. 1315–1325. DOI: 10.1016/j.foreco.2007.10.058.

Goyburo, A., Rau, P., Lavado-Casimiro, W., Buytaert, W., Cuadros-Adriazola, J., and Horna, D. (2023). "Assessment of Present and Future Water Security under Anthropogenic and Climate Changes Using WEAP Model in the Vilcanota-Urubamba Catchment, Cusco, Perú". In: *Water* 15.7, p. 1439. DOI: 10.3390/W15071439.

Grenier, P. (2018). "Two Types of Physical Inconsistency to Avoid with Univariate Quantile Mapping: A Case Study over North America Concerning Relative Humidity and Its Parent Variables". In: *Journal of Applied Meteorology and Climatology* 57.2, pp. 347–364. DOI: 10.1175/JAMC-D-17-0177.1.

Gudmundsson, L., Leonard, M., Do, H. X., Westra, S., and Seneviratne, S. I. (2019). "Observed Trends in Global Indicators of Mean and Extreme Streamflow". In: *Geophysical Research Letters* 46.2, pp. 756–766. DOI: 10.1029/2018GL079725.

Guimberteau, M., Drapeau, G., Ronchail, J., Sultan, B., Polcher, J., Martinez, J.-M., Prigent, C., Guyot, J.-L., Cochonneau, G., Espinoza, J. C., Filizola, N., Fraizy, P., Lavado, W., De Oliveira, E., Pombosa, R., Noriega, L., and Vauchel, P. (2012). "Discharge simulation in the sub-basins of the Amazon using ORCHIDEE forced by new datasets". In: *Hydrology and Earth System Sciences* 16.3, pp. 911–935. DOI: 10.5194/hess-16-911-2012.

Guo, Y., Zhang, Y., Zhang, L., and Wang, Z. (2021). "Regionalization of hydrological modeling for predicting streamflow in ungauged catchments: A comprehensive review". In: *Wiley Interdisciplinary Reviews: Water* 8.1. DOI: 10.1002/WAT2.1487.

Gupta, H. V., Kling, H., Yilmaz, K. K., and Martinez, G. F. (2009). "Decomposition of the mean squared error and NSE performance criteria: Implications for improving hydrological modelling". In: *Journal of Hydrology* 377.1-2, pp. 80–91. DOI: 10.1016/j.jhydrol.2009.08.003.

Gupta, H. V., Sorooshian, S., and Yapo, P. O. (1998). "Toward improved calibration of hydrologic models: Multiple and noncommensurable measures of information". In: *Water Resources Research* 34.4, pp. 751–763. DOI: 10.1029/97WR03495.

Gupta, H. V., Sorooshian, S., and Yapo, P. O. (1999). "Status of Automatic Calibration for Hydrologic Models: Comparison with Multilevel Expert Calibration". In: *Journal of Hydrologic Engineering* 4.2, pp. 135–143. DOI: 10.1061/(ASCE)1084-0699(1999)4:2(135).

Guse, B., Pfannerstill, M., Gafurov, A., Fohrer, N., and Gupta, H. (2016). "Demasking the integrated information of discharge: Advancing sensitivity analysis to consider different hydrological components and their rates of change". In: *Water Resources Research* 52.11, pp. 8724–8743. DOI: 10.1002/2016WR018894.

Gutierrez, R. A., Junquas, C., Armijos, E., Sörensson, A. A., and Espinoza, J. C. (2024). "Performance of Regional Climate Model Precipitation Simulations Over the Terrain-Complex Andes-Amazon Transition Region". In: *Journal of Geophysical Research: Atmospheres* 129.1, e2023JD038618. DOI: 10.1029/2023JD038618.

Guzmán, P., Batelaan, O., Huysmans, M., and Wyseure, G. (2015). "Comparative analysis of baseflow characteristics of two Andean catchments, Ecuador". In: *Hydrological Processes* 29.14, pp. 3051–3064. DOI: 10.1002/hyp.10422.

Ha, L., Bastiaanssen, W., Van Griensven, A., Van Dijk, A., and Senay, G. (2018). "Calibration of Spatially Distributed Hydrological Processes and Model Parameters in SWAT Using Remote Sensing Data and an Auto-Calibration Procedure: A Case Study in a Vietnamese River Basin". In: *Water* 10.2, p. 212. DOI: 10.3390/w10020212.

Hadka, D. and Reed, P. (2012). "Diagnostic assessment of search controls and failure modes in many-objective evolutionary optimization". In: *Evolutionary Computation* 20.3, pp. 423–452. DOI: 10.1162/EVCO_a_00053.

Hadka, D. and Reed, P. (2013). "Borg: An Auto-Adaptive Many-Objective Evolutionary Computing Framework". In: *Evolutionary Computation* 21.2, pp. 231–259. DOI: 10.1162/EVCO_a_00075.

Hakala, K., Addor, N., and Seibert, J. (2018). "Hydrological Modeling to Evaluate Climate Model Simulations and Their Bias Correction". In: *Journal of Hydrometeorology* 19.8, pp. 1321–1337. DOI: 10.1175/JHM-D-17-0189.1.

Hansen, J., Sato, M., Kharecha, P., and Von Schuckmann, K. (2011). "Earth's energy imbalance and implications". In: *Atmospheric Chemistry and Physics* 11.24, pp. 13421–13449. DOI: 10.5194/acp-11-13421-2011.

Hansen, J., Nazarenko, L., Ruedy, R., Sato, M., Willis, J., Del Genio, A., Koch, D., Lacis, A., Lo, K., Menon, S., Novakov, T., Perlwitz, J., Russell, G., Schmidt, G. A., and Tausnev, N. (2005). "Climate Change: Earth's energy imbalance: Confirmation and implications". In: *Science* 308.5727, pp. 1431–1435. DOI: 10.1126/science.1110252.

Harifidy, R. Z., Hiroshi, I., Kazuyoshi, S., Jun, M., Zy, R., Harivelo, M., and Fernández-Palomino, C. A. (2024). "Multi-gauge calibration comparison for simulating streamflow across the Major River Basins in Madagascar: SWAT + Toolbox, R-SWAT, and SWAT + Editor Hard calibration". In: *Hydrology Research*. DOI: 10.2166/NH.2024.188.

Harris, I., Osborn, T. J., Jones, P., and Lister, D. (2020). "Version 4 of the CRU TS monthly high-resolution gridded multivariate climate dataset". In: *Scientific Data* 7.1, pp. 1–18. DOI: 10.1038/s41597-020-0453-3.

Hattermann, F. F., Krysanova, V., Gosling, S. N., Dankers, R., Daggupati, P., Donnelly, C., Flörke, M., Huang, S., Motovilov, Y., Buda, S., Yang, T., Müller, C., Leng, G., Tang, Q., Portmann, F. T., Hagemann, S., Gerten, D., Wada, Y., Masaki, Y., Alemayehu, T., Satoh, Y., and Samaniego, L. (2017). "Cross-scale intercomparison of climate change impacts simulated by regional and global hydrological models in eleven large river basins". In: *Climatic Change* 141.3, pp. 561–576. DOI: 10.1007/S10584-016-1829-4.

Hattermann, F. F., Vetter, T., Breuer, L., Su, B., Daggupati, P., Donnelly, C., Fekete, B., Florke, F., Gosling, S. N., Hoffmann, P., Liersch, S., Masaki, Y., Motovilov, Y., Muller, C., Samaniego, L., Stacke, T., Wada, Y., Yang, T., and Krysnaova, V. (2018). "Sources of uncertainty in hydrological climate impact assessment: a cross-scale study". In: *Environmental Research Letters* 13.1, p. 015006. DOI: 10.1088/1748-9326/AA9938.

Hattermann, F. F., Wattenbach, M., Krysanova, V., and Wechsung, F. (2005). "Runoff simulations on the macroscale with the ecohydrological model SWIM in the Elbe catchment - Validation and uncertainty analysis". In: *Hydrological Processes* 19.3, pp. 693–714. DOI: 10.1002/hyp.5625.

He, J., Yang, K., Tang, W., Lu, H., Qin, J., Chen, Y., and Li, X. (2020). "The first high-resolution meteorological forcing dataset for land process studies over China". In: *Scientific Data* 7.1, pp. 1–11. DOI: 10.1038/s41597-020-0369-y.

Helmer, E. H., Gerson, E. A., Baggett, L. S., Bird, B. J., Ruzycki, T. S., and Voggesser, S. M. (2019). "Neotropical cloud forests and páramo to contract and dry from declines in cloud immersion and frost". In: *PLOS ONE* 14.4. Ed. by Lötters, S., e0213155. DOI: 10.1371/journal.pone.0213155.

Hengl, T., Nussbaum, M., Wright, M. N., Heuvelink, G. B., and Gräler, B. (2018). "Random forest as a generic framework for predictive modeling of spatial and spatio-temporal variables". In: *PeerJ* 2018.8. DOI: 10.7717/peerj.5518.

Henn, B., Clark, M. P., Kavetski, D., and Lundquist, J. D. (2015). "Estimating mountain basin-mean precipitation from streamflow using Bayesian inference". In: *Water Resources Research* 51.10, pp. 8012–8033. DOI: 10.1002/2014WR016736.

Henn, B., Clark, M. P., Kavetski, D., Newman, A. J., Hughes, M., McGurk, B., and Lundquist, J. D. (2018). "Spatiotemporal patterns of precipitation inferred from streamflow observations across the Sierra Nevada mountain range". In: *Journal of Hydrology* 556, pp. 993–1012. DOI: 10.1016/j.jhydrol.2016.08.009.

Her, Y. and Chaubey, I. (2015). "Impact of the numbers of observations and calibration parameters on equifinality, model performance, and output and parameter uncertainty". In: *Hydrological Processes* 29.19, pp. 4220–4237. DOI: 10.1002/hyp.10487.

Herrnegger, M., Nachtnebel, H. P., and Schulz, K. (2015). "From runoff to rainfall: inverse rainfall–runoff modelling in a high temporal resolution". In: *Hydrology and Earth System Sciences* 19.11, pp. 4619–4639. DOI: 10.5194/hess-19-4619-2015.

Hersbach, H., Bell, B., Berrisford, P., Hirahara, S., Horányi, A., Muñoz-Sabater, J., Nicolas, J., Peubey, C., Radu, R., Schepers, D., Simmons, A., Soci, C., Abdalla, S., Abellan, X., Balsamo, G., Bechtold, P., Biavati, G., Bidlot, J., Bonavita, M., Chiara, G., Dahlgren, P., Dee, D., Diamantakis, M., Dragani, R., Flemming, J., Forbes, R., Fuentes, M., Geer, A., Haimberger, L., Healy, S., Hogan, R. J., Hólm, E., Janisková, M., Keeley, S., Laloyaux, P., Lopez, P., Lupu, C., Radnoti, G., Rosnay, P., Rozum, I., Vamborg, F., Villaume, S., and Thépaut, J.-N. (2020). "The ERA5 Global Reanalysis". In: *Quarterly Journal of the Royal Meteorological Society* 146.730, pp. 1999–2049. DOI: 10.1002/qj.3803.

Hill, A. F., Stallard, R. F., and Rittger, K. (2018). "Clarifying regional hydrologic controls of the Marañón River, Peru through rapid assessment to inform system-wide basin planning

approaches". In: *Elementa: Science of the Anthropocene* 6.1, p. 37. DOI: `10.1525/element a.290`.

Hock, R., Rasul, G., Adler, C., Cáceres, B., Gruber, S., Hirabayashi, Y., Jackson, M., Kääb, A., Kang, S., Kutuzov, S., Milner, A., Molau, U., Morin, S., Orlove, B., and Steltzer, H. (2019). "High Mountain Areas". In: *IPCC Special Report on the Ocean and Cryosphere in a Changing Climate*. Ed. by Pörtner, H.-O., Roberts, D., Masson-Delmotte, V., Zhai, P., Tignor, M., Poloczanska, E., Mintenbeck, K., Alegría, A., Nicolai, M., Okem, A., Petzold, J., Rama, B., and Weyer, N. Cambridge, UK and New York, NY, USA: Cambridge University Press. Chap. Chapter 2, pp. 131–202. DOI: `10.1017/9781009157964.004`.

Hong, Z., Han, Z., Li, X., Long, D., Tang, G., and Wang, J. (2021). "Generation of an improved precipitation data set from multisource information over the Tibetan Plateau". In: *Journal of Hydrometeorology* -1.aop. DOI: `10.1175/JHM-D-20-0252.1`.

Hrachowitz, M., Fovet, O., Ruiz, L., Euser, T., Gharari, S., Nijzink, R., Freer, J., Savenije, H. H. G., and Gascuel-Odoux, C. (2014). "Process consistency in models: The importance of system signatures, expert knowledge, and process complexity". In: *Water Resources Research* 50.9, pp. 7445–7469. DOI: `10.1002/2014WR015484`.

Hsu, K.-l., Gao, X., Sorooshian, S., Gupta, H. V., Hsu, K.-l., Gao, X., Sorooshian, S., and Gupta, H. V. (1997). "Precipitation Estimation from Remotely Sensed Information Using Artificial Neural Networks". In: *Journal of Applied Meteorology* 36.9, pp. 1176–1190. DOI: `10.1175/1520-0450(1997)036<1176:PEFRSI>2.0.CO;2`.

Huerta, A., Aybar, C., and Lavado-Casimiro, W. (2018). *PISCO temperatura v.1.1. SENAMHI - DHI-2018, Lima-Perú*. Tech. rep.

Huerta, A., Bonnesoeur, V., Cuadros-Adriazola, J., Gutierrez, L., Ochoa-Tocachi, B. F., Román-Dañobeytia, F., and Lavado-Casimiro, W. (2022). "PISCOeo_pm, a reference evapotranspiration gridded database based on FAO Penman-Monteith in Peru". In: *Scientific Data* 9.1, pp. 1–18. DOI: `10.1038/s41597-022-01373-8`.

Huffman, G. J., Bolvin, D. T., Braithwaite, D., Hsu, K., Joyce, R., Kidd, C., Nelkin, E. J., Sorooshian, S., Tan, J., and Xie, P. (2019). *NASA Global Precipitation Measurement (GPM) Integrated Multi-satellitE Retrievals for GPM (IMERG)*. Tech. rep.

Huffman, G. J., Bolvin, D. T., Nelkin, E. J., Wolff, D. B., Adler, R. F., Gu, G., Hong, Y., Bowman, K. P., and Stocker, E. F. (2007). "The TRMM Multisatellite Precipitation Analysis (TMPA): Quasi-Global, Multiyear, Combined-Sensor Precipitation Estimates at Fine Scales". In: *Journal of Hydrometeorology* 8.1, pp. 38–55. DOI: `10.1175/JHM560.1`.

Hunziker, S., Gubler, S., Calle, J., Moreno, I., Andrade, M., Velarde, F., Ticona, L., Carrasco, G., Castellón, Y., Oria, C., Croci-Maspoli, M., Konzelmann, T., Rohrer, M., and Brönnimann, S. (2017). "Identifying, attributing, and overcoming common data quality issues of manned station observations". In: *International Journal of Climatology* 37.11, pp. 4131–4145. DOI: `10.1002/joc.5037`.

Huss, M. and Hock, R. (2018). "Global-scale hydrological response to future glacier mass loss". In: *Nature Climate Change* 8.2, pp. 135–140. DOI: `10.1038/s41558-017-0049-x`.

Imfeld, N., Sedlmeier, K., Gubler, S., Correa Marrou, K., Davila, C. P., Huerta, A., Lavado-Casimiro, W., Rohrer, M., Scherrer, S. C., and Schwierz, C. (2021). "A combined view on precipitation and temperature climatology and trends in the southern Andes of Peru". In: *International Journal of Climatology* 41.1, pp. 679–698. DOI: `10.1002/JOC.6645`.

INAIGEM (2018). *Inventario Nacional de Glaciares*. Huaraz: INAIGEM.

IPCC (2007). *Climate Change 2007 - The Physical Science Basis: Working Group I Contribution to the Fourth Assessment Report of the Intergovernmental Panel on Climate Change*. Cambridge: Cambridge University Press.

IPCC (2014). *Climate Change 2013 – The Physical Science Basis: Working Group I Contribution to the Fifth Assessment Report of the Intergovernmental Panel on Climate Change*. Cambridge: Cambridge University Press. DOI: `10.1017/CB09781107415324`.

IPCC (2023a). "Annex I: Glossary". In: *Climate Change 2022 - Mitigation of Climate Change: Working Group III Contribution to the Sixth Assessment Report of the Intergovernmental Panel on Climate Change*. Ed. by (IPCC), I. P. o. C. C. Cambridge: Cambridge University Press, pp. 1793–1820. DOI: `10.1017/9781009157926.020`.

IPCC (2023b). "Changing State of the Climate System". In: *Climate Change 2021 – The Physical Science Basis: Working Group I Contribution to the Sixth Assessment Report of the Intergovernmental Panel on Climate Change*. Cambridge: Cambridge University Press, pp. 287–422. DOI: 10.1017/9781009157896.004.

IPCC (2023c). *Climate Change 2021 – The Physical Science Basis: Working Group I Contribution to the Sixth Assessment Report of the Intergovernmental Panel on Climate Change*. Cambridge: Cambridge University Press. DOI: 10.1017/9781009157896.

IPCC (2023d). "Water". In: *Climate Change 2022 – Impacts, Adaptation and Vulnerability: Working Group II Contribution to the Sixth Assessment Report of the Intergovernmental Panel on Climate Change*. Cambridge: Cambridge University Press, pp. 551–712. DOI: 10.1017/9781009325844.006.

IPCC (2023e). "Water Cycle Changes". In: *Climate Change 2021 – The Physical Science Basis: Working Group I Contribution to the Sixth Assessment Report of the Intergovernmental Panel on Climate Change*. Cambridge: Cambridge University Press, pp. 1055–1210. DOI: 10.1017/9781009157896.010.

IPCC (2023f). "Weather and Climate Extreme Events in a Changing Climate". In: *Climate Change 2021 – The Physical Science Basis: Working Group I Contribution to the Sixth Assessment Report of the Intergovernmental Panel on Climate Change*. Cambridge: Cambridge University Press, pp. 1513–1766. DOI: 10.1017/9781009157896.013.

Jajarmizadeh, M., Sidek, L. M., Harun, S., and Salarpour, M. (2017). "Optimal Calibration and Uncertainty Analysis of SWAT for an Arid Climate". In: *Air, Soil and Water Research* 10, p. 117862211773179. DOI: 10.1177/1178622117731792.

Jang, W. S., Engel, B., and Ryu, J. (2018). "Efficient flow calibration method for accurate estimation of baseflow using a watershed scale hydrological model (SWAT)". In: *Ecological Engineering* 125, pp. 50–67. DOI: 10.1016/j.ecoleng.2018.10.007.

Jarvis A, H., Reuter, A., Nelson, A., and Guevara, E. (2008). "Hole-filled SRTM for the globe Version 4, available from the CGIAR-CSI SRTM 90m Database". In: *CGIAR Consortium for Spatial Information (CGIAR-CSI)*.

Jones, P. W. (1999). "First- and Second-Order Conservative Remapping Schemes for Grids in Spherical Coordinates". In: *Monthly Weather Review* 127.9, pp. 2204–2210. DOI: 10.1175/1520-0493(1999)127<2204:FASOCR>2.0.CO;2.

Joyce, R. J., Janowiak, J. E., Arkin, P. A., Xie, P., Joyce, R. J., Janowiak, J. E., Arkin, P. A., and Xie, P. (2004). "CMORPH: A Method that Produces Global Precipitation Estimates from Passive Microwave and Infrared Data at High Spatial and Temporal Resolution". In: *Journal of Hydrometeorology* 5.3, pp. 487–503. DOI: 10.1175/1525-7541(2004)005<0487:CAMTPG>2.0.CO;2.

Juen, I., Kaser, G., and Georges, C. (2007). "Modelling observed and future runoff from a glacierized tropical catchment (Cordillera Blanca, Perú)". In: *Global and Planetary Change* 59.1-4, pp. 37–48. DOI: 10.1016/J.GLOPLACHA.2006.11.038.

Juřicová, A. and Fratianni, S. (2018). "Climate change and its relation to the fluctuation in glacier mass balance in the Cordillera Blanca, Peru: A review". In: *Acta Universitatis Carolinae, Geographica* 53.1, pp. 106–118. DOI: 10.14712/23361980.2018.10.

Kirchner, J. W. (2009). "Catchments as simple dynamical systems: Catchment characterization, rainfall-runoff modeling, and doing hydrology backward". In: *Water Resources Research* 45.2. DOI: 10.1029/2008WR006912.

Kling, H., Fuchs, M., and Paulin, M. (2012). "Runoff conditions in the upper Danube basin under an ensemble of climate change scenarios". In: *Journal of Hydrology* 424-425, pp. 264–277. DOI: 10.1016/j.jhydrol.2012.01.011.

Kneis, D., Chatterjee, C., and Singh, R. (2014). "Evaluation of TRMM rainfall estimates over a large Indian river basin (Mahanadi)". In: *Hydrology and Earth System Sciences* 18.7, pp. 2493–2502. DOI: 10.5194/hess-18-2493-2014.

Kobayashi, S., Ota, Y., Harada, Y., Ebita, A., Moriya, M., Onoda, H., Onogi, K., Kamahori, H., Kobayashi, C., Endo, H., Miyaoka, K., and Takahashi, K. (2015). "The JRA-55 Reanalysis: General Specifications and Basic Characteristics". In: *Journal of the Meteorological Society of Japan. Ser. II* 93.1, pp. 5–48. DOI: 10.2151/jmsj.2015-001.

Krause, P., Boyle, D. P., and Bäse, F. (2005). "Comparison of different efficiency criteria for hydrological model assessment". In: *Advances in Geosciences* 5, pp. 89–97. DOI: 10.5194/adgeo-5-89-2005.

Krier, R., Matgen, P., Goergen, K., Pfister, L., Hoffmann, L., Kirchner, J. W., Uhlenbrook, S., and Savenije, H. H. G. (2012). "Inferring catchment precipitation by doing hydrology backward: A test in 24 small and mesoscale catchments in Luxembourg". In: *Water Resources Research* 48.10. DOI: 10.1029/2011WR010657.

Krysanova, V. and Arnold, J. G. (2008). "Advances in ecohydrological modelling with SWAT-a review". In: *Hydrological Sciences Journal* 53.5, pp. 939–947. DOI: 10.1623/hysj.53.5.939.

Krysanova, V., Donnelly, C., Gelfan, A., Gerten, D., Arheimer, B., Hattermann, F., and Kundzewicz, Z. W. (2018). "How the performance of hydrological models relates to credibility of projections under climate change". In: *Hydrological Sciences Journal* 63.5, pp. 696–720. DOI: 10.1080/02626667.2018.1446214.

Krysanova, V., Kundzewicz, Z. W., Piniewski, M., and Singh, V. P. (2016). "Assessment of climate change impacts on water resources". In: *Handbook of applied hydrology*. McGraw-Hill Education, pp. 141–148.

Krysanova, V., Müller-Wohlfeil, D. I., and Becker, A. (1998). "Development and test of a spatially distributed hydrological/water quality model for mesoscale watersheds". In: *Ecological Modelling* 106.2-3, pp. 261–289. DOI: 10.1016/S0304-3800(97)00204-4.

Lange, S. (2019). "Trend-preserving bias adjustment and statistical downscaling with ISIMIP3BASD (v1.0)". In: *Geoscientific Model Development* 12.7, pp. 3055–3070. DOI: 10.5194/GMD-12-3055-2019.

Lange, S. (2021a). *ISIMIP3b bias adjustment fact sheet*. Tech. rep.

Lange, S. (2021b). "ISIMIP3BASD (2.5.0)". In: *Zenodo*. DOI: 10.5281/ZENODO.4686991.

Lange, S. and Büchner, M. (2021). "ISIMIP3b bias-adjusted atmospheric climate input data". In: *ISIMIP Repository*. DOI: 10.48364/ISIMIP.842396.1.

Lange, S. and Büchner, M. (2022). "Secondary ISIMIP3b bias-adjusted atmospheric climate input data". In: *ISIMIP Repository*. DOI: 10.48364/ISIMIP.581124.

Lange, S., Menz, C., Gleixner, S., Cucchi, M., Weedon, G. P., Amici, A., Bellouin, N., Schmied, H. M., Hersbach, H., Buontempo, C., and Cagnazzo, C. (2021). "WFDE5 over land merged with ERA5 over the ocean (W5E5 v2.0)". In: *ISIMIP Repository*. DOI: 10.48364/ISIMIP.342217.

Larabi, S., St-Hilaire, A., Chebana, F., and Latraverse, M. (2018). "Multi-Criteria Process-Based Calibration Using Functional Data Analysis to Improve Hydrological Model Realism". In: *Water Resources Management* 32.1, pp. 195–211. DOI: 10.1007/s11269-017-1803-6.

Laraque, A., Ronchail, J., Cochonneau, G., Pombosa, R., and Guyot, J. L. (2007). "Heterogeneous distribution of rainfall and discharge regimes in the Ecuadorian Amazon basin". In: *Journal of Hydrometeorology* 8.6, pp. 1364–1381. DOI: 10.1175/2007JHM784.1.

Lavado Casimiro, W. S., Labat, D., Guyot, J. L., and Ardoin-Bardin, S. (2011). "Assessment of climate change impacts on the hydrology of the Peruvian Amazon–Andes basin". In: *Hydrological Processes* 25.24, pp. 3721–3734. DOI: 10.1002/HYP.8097.

Lavado Casimiro, W. S., Labat, D., Ronchail, J., Espinoza, J. C., and Guyot, J. L. (2013). "Trends in rainfall and temperature in the Peruvian Amazon–Andes basin over the last 40 years (1965–2007)". In: *Hydrological Processes* 27.20, pp. 2944–2957. DOI: 10.1002/HYP.9418.

Lavado Casimiro, W. S., Ronchail, J., Labat, D., Espinoza, J. C., and Guyot, J. L. (2012). "Basin-scale analysis of rainfall and runoff in Peru (1969–2004): Pacific, Titicaca and Amazonas drainages". In: *Hydrological Sciences Journal* 57.4, pp. 625–642. DOI: 10.1080/02626667.2012.672985.

Lavado-Casimiro, W., Traverso-Yucra, K., and Gutierrez, L. (2021). *Atlas de hidrología superficial del Perú: una evaluación presente y futura*. Servicio Nacional de Meteorología e Hidrología del Perú.

Le Moine, N., Hendrickx, F., Gailhard, J., Garçon, R., and Gottardi, F. (2015). "Hydrologically Aided Interpolation of Daily Precipitation and Temperature Fields in a Mesoscale Alpine Catchment". In: *Journal of Hydrometeorology* 16.6, pp. 2595–2618. DOI: 10.1175/JHM-D-14-0162.1.

Lenton, T. M. (2011). "Early warning of climate tipping points". In: *Nature Climate Change* 1.4, pp. 201–209. DOI: 10.1038/nclimate1143.

Li, G. and Xie, S. P. (2014). "Tropical Biases in CMIP5 Multimodel Ensemble: The Excessive Equatorial Pacific Cold Tongue and Double ITCZ Problems". In: *Journal of Climate* 27.4, pp. 1765–1780. DOI: 10.1175/JCLI-D-13-00337.1.

Liang, X., Lettenmaier, D. P., Wood, E. F., and Burges, S. J. (1994). "A simple hydrologically based model of land surface water and energy fluxes for general circulation models". In: *Journal of Geophysical Research* 99.D7, pp. 14415–14428. DOI: 10.1029/94jd00483.

Liaw, A. and Wiener, M. (2002). "Classification and Regression by randomForest". In: *R news* 2.3, pp. 18–22.

Lim, K. J., Engel, B. A., Tang, Z., Choi, J., Kim, K.-S., Muthukrishnan, S., and Tripathy, D. (2005). "AUTOMATED WEB GIS BASED HYDROGRAPH ANALYSIS TOOL, WHAT". In: *Journal of the American Water Resources Association* 41.6, pp. 1407–1416. DOI: 10.1111/j.1752-1688.2005.tb03808.x.

Lindström, G., Pers, C., Rosberg, J., Strömqvist, J., and Arheimer, B. (2010). "Development and testing of the HYPE (Hydrological Predictions for the Environment) water quality model for different spatial scales". In: *Hydrology Research* 41.3-4, pp. 295–319. DOI: 10.2166/nh.2010.007.

Llauca, H., Lavado-Casimiro, W., Montesinos, C., Santini, W., and Rau, P. (2021). "PISCO_HyM_GR2M: A Model of Monthly Water Balance in Peru (1981–2020)". In: *Water* 13.8, p. 1048. DOI: 10.3390/W13081048.

Llauca, H., Leon, K., and Lavado-Casimiro, W. (2023). "Construction of a daily streamflow dataset for Peru using a similarity-based regionalization approach and a hybrid hydrological modeling framework". In: *Journal of Hydrology: Regional Studies* 47, p. 101381. DOI: 10.1016/J.EJRH.2023.101381.

Lloyd, E. A., Bukovsky, M., and Mearns, L. O. (2021). "An analysis of the disagreement about added value by regional climate models". In: *Synthese* 198.12, pp. 11645–11672. DOI: 10.1007/S11229-020-02821-X.

Luo, Y., Arnold, J., Allen, P., and Chen, X. (2012). "Baseflow simulation using SWAT model in an inland river basin in Tianshan Mountains, Northwest China". In: *Hydrology and Earth System Sciences* 16.4, pp. 1259–1267. DOI: 10.5194/hess-16-1259-2012.

Ma, T., Duan, Z., Li, R., and Song, X. (2019). "Enhancing SWAT with remotely sensed LAI for improved modelling of ecohydrological process in subtropics". In: *Journal of Hydrology* 570, pp. 802–815. DOI: 10.1016/J.JHYDROL.2019.01.024.

Mantas, V. M., Liu, Z., Caro, C., and Pereira, A. J. S. C. (2014). "Validation of TRMM multi-satellite precipitation analysis (TMPA) products in the Peruvian Andes". In: *Atmospheric Research* 163, pp. 132–145. DOI: 10.1016/j.atmosres.2014.11.012.

Manz, B., Buytaert, W., Zulkafli, Z., Lavado, W., Willems, B., Robles, L. A., and Rodríguez-Sánchez, J.-P. (2016). "High-resolution satellite-gauge merged precipitation climatologies of the Tropical Andes". In: *Journal of Geophysical Research: Atmospheres* 121.3, pp. 1190–1207. DOI: 10.1002/2015JD023788.

Manz, B., Páez-Bimos, S., Horna, N., Buytaert, W., Ochoa-Tocachi, B., Lavado-Casimiro, W., Willems, B., Manz, B., Páez-Bimos, S., Horna, N., Buytaert, W., Ochoa-Tocachi, B., Lavado-Casimiro, W., and Willems, B. (2017). "Comparative Ground Validation of IMERG and TMPA at Variable Spatiotemporal Scales in the Tropical Andes". In: *Journal of Hydrometeorology* 18.9, pp. 2469–2489. DOI: 10.1175/JHM-D-16-0277.1.

Marengo, J. A. and Espinoza, J. C. (2016). "Extreme seasonal droughts and floods in Amazonia: causes, trends and impacts". In: *International Journal of Climatology* 36.3, pp. 1033–1050. DOI: 10.1002/JOC.4420.

Marengo, J. A., Souza, C. M., Thonicke, K., Burton, C., Halladay, K., Betts, R. A., Alves, L. M., and Soares, W. R. (2018). "Changes in Climate and Land Use Over the Amazon Region: Current and Future Variability and Trends". In: *Frontiers in Earth Science* 6, p. 228. DOI: 10.3389/FEART.2018.00228.

Martens, B., Miralles, D. G., Lievens, H., Van Der Schalie, R., De Jeu, R. A., Fernández-Prieto, D., Beck, H. E., Dorigo, W. A., and Verhoest, N. E. (2017). "GLEAM v3: Satellite-based

land evaporation and root-zone soil moisture". In: *Geoscientific Model Development* 10.5, pp. 1903–1925. DOI: 10.5194/GMD-10-1903-2017.

Masiokas, M. H., Rabatel, A., Rivera, A., Ruiz, L., Pitte, P., Ceballos, J. L., Barcaza, G., Soruco, A., Bown, F., Berthier, E., Dussaillant, I., and MacDonell, S. (2020). "A Review of the Current State and Recent Changes of the Andean Cryosphere". In: *Frontiers in Earth Science* 8, p. 99. DOI: 10.3389/FEART.2020.00099.

McMillan, H., Westerberg, I., and Branger, F. (2017). "Five guidelines for selecting hydrological signatures". In: *Hydrological Processes* 31.26, pp. 4757–4761. DOI: 10.1002/hyp.11300.

Meaurio, M., Zabaleta, A., Uriarte, J. A., Srinivasan, R., and Antigüedad, I. (2015). "Evaluation of SWAT models performance to simulate streamflow spatial origin. The case of a small forested watershed". In: *Journal of Hydrology* 525, pp. 326–334. DOI: 10.1016/J.JHYDROL.2015.03.050.

Miralles, D. G., Holmes, T. R., De Jeu, R. A., Gash, J. H., Meesters, A. G., and Dolman, A. J. (2011). "Global land-surface evaporation estimated from satellite-based observations". In: *Hydrology and Earth System Sciences* 15.2, pp. 453–469. DOI: 10.5194/HESS-15-453-2011.

Mishra, V., Bhatia, U., and Tiwari, A. D. (2020). "Bias-corrected climate projections for South Asia from Coupled Model Intercomparison Project-6". In: *Scientific Data* 7.1, pp. 1–13. DOI: 10.1038/s41597-020-00681-1.

Mohammed, R. and Scholz, M. (2018). "Flow–duration curve integration into digital filtering algorithms for simulating climate variability based on river baseflow". In: *Hydrological Sciences Journal* 63.10, pp. 1558–1573. DOI: 10.1080/02626667.2018.1519318.

Monteverde, C., De Sales, F., and Jones, C. (2022). "Evaluation of the CMIP6 Performance in Simulating Precipitation in the Amazon River Basin". In: *Climate* 10.8, p. 122. DOI: 10.3390/CLI10080122.

Morán-Tejeda, E., Bazo, J., López-Moreno, J. I., Aguilar, E., Azorín-Molina, C., Sanchez-Lorenzo, A., Martínez, R., Nieto, J. J., Mejía, R., Martín-Hernández, N., and Vicente-Serrano, S. M. (2016). "Climate trends and variability in Ecuador (1966-2011)". In: *International Journal of Climatology* 36.11, pp. 3839–3855. DOI: 10.1002/joc.4597.

Moriasi, D., Arnold, J., Van Liew, M., Binger, R., Harmel, R., and Veith, T. (2007). "Model evaluation guidelines for systematic quantification of accuracy in watershed simulations". In: *Transactions of the ASABE* 50.3, pp. 885–900. DOI: 10.13031/2013.23153.

Mosquera, G. M., Lazo, P. X., Célleri, R., Wilcox, B. P., and Crespo, P. (2015). "Runoff from tropical alpine grasslands increases with areal extent of wetlands". In: *CATENA* 125, pp. 120–128. DOI: 10.1016/J.CATENA.2014.10.010.

Motschmann, A., Teutsch, C., Huggel, C., Seidel, J., León, C. D., Muñoz, R., Sienel, J., Drenkhan, F., and Weimer-Jehle, W. (2022). "Current and future water balance for coupled human-natural systems – Insights from a glacierized catchment in Peru". In: *Journal of Hydrology: Regional Studies* 41, p. 101063. DOI: 10.1016/J.EJRH.2022.101063.

da Motta Paca, V. H., Espinoza-Dávalos, G. E., Moreira, D. M., and Comair, G. (2020). "Variability of Trends in Precipitation across the Amazon River Basin Determined from the CHIRPS Precipitation Product and from Station Records". In: *Water* 12.5, p. 1244. DOI: 10.3390/W12051244.

Mu, Q., Zhao, M., and Running, S. W. (2011). "Improvements to a MODIS global terrestrial evapotranspiration algorithm". In: *Remote Sensing of Environment* 115.8, pp. 1781–1800. DOI: 10.1016/J.RSE.2011.02.019.

Müller, W. A., Jungclaus, J. H., Mauritsen, T., Baehr, J., Bittner, M., Budich, R., Bunzel, F., Esch, M., Ghosh, R., Haak, H., Ilyina, T., Kleine, T., Kornblueh, L., Li, H., Modali, K., Notz, D., Pohlmann, H., Roeckner, E., Stemmler, I., Tian, F., and Marotzke, J. (2018). "A Higher-resolution Version of the Max Planck Institute Earth System Model (MPI-ESM1.2-HR)". In: *Journal of Advances in Modeling Earth Systems* 10.7, pp. 1383–1413. DOI: 10.1029/2017MS001217.

Nash, J. and Sutcliffe, J. (1970). "River flow forecasting through conceptual models part I — A discussion of principles". In: *Journal of Hydrology* 10.3, pp. 282–290. DOI: 10.1016/0022-1694(70)90255-6.

Neitsch, S., Arnold, J., Kiniry, J., and Williams, J. (2011). *Soil & Water Assessment Tool Theoretical Documentation Version 2009.* Tech. rep. Texas Water Resources Institute, pp. 1–647.

Nobre, C. A., Sampaio, G., Borma, L. S., Castilla-Rubio, J. C., Silva, J. S., and Cardoso, M. (2016). "Land-use and climate change risks in the amazon and the need of a novel sustainable development paradigm". In: *Proceedings of the National Academy of Sciences of the United States of America* 113.39, pp. 10759–10768. DOI: 10.1073/PNAS.1605516113.

Noël, T., Loukos, H., Defrance, D., Vrac, M., and Levavasseur, G. (2022). "Extending the global high-resolution downscaled projections dataset to include CMIP6 projections at increased resolution coherent with the ERA5-Land reanalysis". In: *Data in Brief* 45, p. 108669. DOI: 10.1016/J.DIB.2022.108669.

Núñez Mejía, S. X., Mendoza Paz, S., Tabari, H., and Willems, P. (2023). "Climate change impacts on hydrometeorological and river hydrological extremes in Quito, Ecuador". In: *Journal of Hydrology: Regional Studies* 49, p. 101522. DOI: 10.1016/J.EJRH.2023.101522.

Ochoa, A., Pineda, L., Crespo, P., and Willems, P. (2014). "Evaluation of TRMM 3B42 precipitation estimates and WRF retrospective precipitation simulation over the Pacific–Andean region of Ecuador and Peru". English. In: *Hydrology and Earth System Sciences* 18.8, pp. 3179–3193. DOI: 10.5194/hess-18-3179-2014.

Ochoa-Tocachi, B. F., Buytaert, W., De Bièvre, B., Célleri, R., Crespo, P., Villacís, M., Llerena, C. A., Acosta, L., Villazón, M., Guallpa, M., Gil-Ríos, J., Fuentes, P., Olaya, D., Viñas, P., Rojas, G., and Arias, S. (2016). "Impacts of land use on the hydrological response of tropical Andean catchments". In: *Hydrological Processes* 30.22, pp. 4074–4089. DOI: 10.1002/hyp.10980.

Olsson, T., Kämäräinen, M., Santos, D., Seitola, T., Tuomenvirta, H., Haavisto, R., and Lavado-Casimiro, W. (2017). "Downscaling climate projections for the Peruvian coastal Chancay-Huaral Basin to support river discharge modeling with WEAP". In: *Journal of Hydrology: Regional Studies* 13, pp. 26–42. DOI: 10.1016/J.EJRH.2017.05.011.

Opperman, J. J., Luster, R., McKenney, B. A., Roberts, M., and Meadows, A. W. (2010). "Ecologically Functional Floodplains: Connectivity, Flow Regime, and Scale1". In: *JAWRA Journal of the American Water Resources Association* 46.2, pp. 211–226. DOI: 10.1111/J.1752-1688.2010.00426.X.

Ortega, G., Arias, P. A., Villegas, J. C., Marquet, P. A., and Nobre, P. (2021). "Present-day and future climate over central and South America according to CMIP5/CMIP6 models". In: *International Journal of Climatology* 41.15, pp. 6713–6735. DOI: 10.1002/JOC.7221.

Pabón-Caicedo, J. D., Arias, P. A., Carril, A. F., Espinoza, J. C., Borrel, L. F., Goubanova, K., Lavado-Casimiro, W., Masiokas, M., Solman, S., and Villalba, R. (2020). "Observed and Projected Hydroclimate Changes in the Andes". In: *Frontiers in Earth Science* 8. DOI: 10.3389/FEART.2020.00061.

Paccini, L., Espinoza, J. C., Ronchail, J., and Segura, H. (2018). "Intra-seasonal rainfall variability in the Amazon basin related to large-scale circulation patterns: a focus on western Amazon-Andes transition region". In: *International Journal of Climatology* 38.5, pp. 2386–2399. DOI: 10.1002/joc.5341.

Paiva, R. C., Collischonn, W., and Tucci, C. E. (2011). "Large scale hydrologic and hydrodynamic modeling using limited data and a GIS based approach". In: *Journal of Hydrology* 406.3-4, pp. 170–181. DOI: 10.1016/j.jhydrol.2011.06.007.

Parra, B. G., Rojas, L. E. P., Barrios, M., and Estrada, J. C. M. (2016). "Uncertainty of discharge estimation in high-grade Andean streams". In: *Flow Measurement and Instrumentation* 48, pp. 42–50. DOI: 10.1016/j.flowmeasinst.2016.02.005.

Pelletier, J. D., Broxton, P. D., Hazenberg, P., Zeng, X., Troch, P. A., Niu, G.-Y., Williams, Z., Brunke, M. A., and Gochis, D. (2016). "A gridded global data set of soil, intact regolith, and sedimentary deposit thicknesses for regional and global land surface modeling". In: *Journal of Advances in Modeling Earth Systems* 8.1, pp. 41–65. DOI: 10.1002/2015MS000526.

Pfannerstill, M., Bieger, K., Guse, B., Bosch, D. D., Fohrer, N., and Arnold, J. G. (2017). "How to Constrain Multi-Objective Calibrations of the SWAT Model Using Water Balance Components". In: *JAWRA Journal of the American Water Resources Association* 53.3, pp. 532–546. DOI: 10.1111/1752-1688.12524.

Pfannerstill, M., Guse, B., and Fohrer, N. (2014). "Smart low flow signature metrics for an improved overall performance evaluation of hydrological models". In: *Journal of Hydrology* 510, pp. 447–458. DOI: 10.1016/J.JHYDROL.2013.12.044.

Pokhrel, P. and Yilmaz, K. K. (2012). "Multiple-criteria calibration of a distributed watershed model using spatial regularization and response signatures". In: *Journal of Hydrology* 418-419, pp. 49–60. DOI: 10.1016/J.JHYDROL.2008.12.004.

Pollock, M. D., O'Donnell, G., Quinn, P., Dutton, M., Black, A., Wilkinson, M. E., Colli, M., Stagnaro, M., Lanza, L. G., Lewis, E., Kilsby, C. G., and O'Connell, P. E. (2018). "Quantifying and Mitigating Wind-Induced Undercatch in Rainfall Measurements". In: *Water Resources Research* 54.6, pp. 3863–3875. DOI: 10.1029/2017WR022421.

Potter, E. R., Fyffe, C. L., Orr, A., Quincey, D. J., Ross, A. N., Rangecroft, S., Medina, K., Burns, H., Llacza, A., Jacome, G., Hellström, R., Castro, J., Cochachin, A., Montoya, N., Loarte, E., and Pellicciotti, F. (2023). "A future of extreme precipitation and droughts in the Peruvian Andes". In: *npj Climate and Atmospheric Science* 6.1, pp. 1–9. DOI: 10.1038/s41612-023-00409-z.

Poveda, G., Espinoza, J. C., Zuluaga, M. D., Solman, S. A., Garreaud, R., and van Oevelen, P. J. (2020). "High Impact Weather Events in the Andes". In: *Frontiers in Earth Science* 8. DOI: 10.3389/FEART.2020.00162.

Qi, J., Lee, S., Zhang, X., Yang, Q., McCarty, G. W., and Moglen, G. E. (2020). "Effects of surface runoff and infiltration partition methods on hydrological modeling: A comparison of four schemes in two watersheds in the Northeastern US". In: *Journal of Hydrology* 581, p. 124415. DOI: 10.1016/J.JHYDROL.2019.124415.

Rabatel, A., Francou, B., Soruco, A., Gomez, J., Cáceres, B., Ceballos, J. L., Basantes, R., Vuille, M., Sicart, J. E., Huggel, C., Scheel, M., Lejeune, Y., Arnaud, Y., Collet, M., Condom, T., Consoli, G., Favier, V., Jomelli, V., Galarraga, R., Ginot, P., Maisincho, L., Mendoza, J., Ménégoz, M., Ramirez, E., Ribstein, P., Suarez, W., Villacis, M., and Wagnon, P. (2013). "Current state of glaciers in the tropical Andes: A multi-century perspective on glacier evolution and climate change". In: *Cryosphere* 7.1, pp. 81–102. DOI: 10.5194/TC-7-81-2013.

Rajib, A., Evenson, G. R., Golden, H. E., and Lane, C. R. (2018). "Hydrologic model predictability improves with spatially explicit calibration using remotely sensed evapotranspiration and biophysical parameters". In: *Journal of Hydrology* 567, pp. 668–683. DOI: 10.1016/J.JHYDROL.2018.10.024.

Rane, N. L. and Jayaraj, G. K. (2023). "Enhancing SWAT model predictivity using multi-objective calibration: effects of integrating remotely sensed evapotranspiration and leaf area index". In: *International Journal of Environmental Science and Technology* 20.6, pp. 6449–6468. DOI: 10.1007/S13762-022-04293-7.

Rau, P., Bourrel, L., Labat, D., Ruelland, D., Frappart, F., Lavado, W., Dewitte, B., and Felipe, O. (2019). "Assessing multidecadal runoff (1970–2010) using regional hydrological modelling under data and water scarcity conditions in Peruvian Pacific catchments". In: *Hydrological Processes* 33.1, pp. 20–35. DOI: 10.1002/HYP.13318.

Razmkhah, H., AkhoundAli, A.-M., and Radmanesh, F. (2017). "Correlated Parameters Uncertainty Propagation in a Rainfall-Runoff Model, Considering 2-Copula; Case Study: Karoon III River Basin". In: *Environmental Modeling & Assessment* 22.5, pp. 503–521. DOI: 10.1007/s10666-017-9569-z.

Reichle, R. H., Liu, Q., Koster, R. D., Draper, C. S., Mahanama, S. P. P., and Partyka, G. S. (2017). "Land Surface Precipitation in MERRA-2". In: *Journal of Climate* 30.5, pp. 1643–1664. DOI: 10.1175/JCLI-D-16-0570.1.

Riahi, K., van Vuuren, D. P., Kriegler, E., Edmonds, J., O'Neill, B. C., Fujimori, S., Bauer, N., Calvin, K., Dellink, R., Fricko, O., Lutz, W., Popp, A., Cuaresma, J. C., KC, S., Leimbach, M., Jiang, L., Kram, T., Rao, S., Emmerling, J., Ebi, K., Hasegawa, T., Havlik, P., Humpenöder, F., Da Silva, L. A., Smith, S., Stehfest, E., Bosetti, V., Eom, J., Gernaat, D., Masui, T., Rogelj, J., Strefler, J., Drouet, L., Krey, V., Luderer, G., Harmsen, M., Takahashi, K., Baumstark, L., Doelman, J. C., Kainuma, M., Klimont, Z., Marangoni, G., Lotze-Campen, H., Obersteiner, M., Tabeau, A., and Tavoni, M. (2017). "The Shared Socioeconomic Pathways and their

energy, land use, and greenhouse gas emissions implications: An overview". In: *Global Environmental Change* 42, pp. 153–168. DOI: 10.1016/j.gloenvcha.2016.05.009.

Román-Cascón, C., Pellarin, T., Gibon, F., Brocca, L., Cosme, E., Crow, W., Fernández-Prieto, D., Kerr, Y. H., and Massari, C. (2017). "Correcting satellite-based precipitation products through SMOS soil moisture data assimilation in two land-surface models of different complexity: API and SURFEX". In: *Remote Sensing of Environment* 200, pp. 295–310. DOI: 10.1016/j.rse.2017.08.022.

Rosas, M. A., Vanacker, V., Viveen, W., Gutierrez, R. R., and Huggel, C. (2020). "The potential impact of climate variability on siltation of Andean reservoirs". In: *Journal of Hydrology* 581, p. 124396. DOI: 10.1016/J.JHYDROL.2019.124396.

Ross, C. W., Prihodko, L., Anchang, J., Kumar, S., Ji, W., and Hanan, N. P. (2018). "HYSOGs250m, global gridded hydrologic soil groups for curve-number-based runoff modeling". In: *Scientific Data* 5.1, p. 180091. DOI: 10.1038/sdata.2018.91.

Russell, A. M., Gnanadesikan, A., and Zaitchik, B. (2017). "Are the Central Andes Mountains a Warming Hot Spot?" In: *Journal of Climate* 30.10, pp. 3589–3608. DOI: 10.1175/JCLI-D-16-0268.1.

Saha, S., Moorthi, S., Pan, H. L., Wu, X., Wang, J., Nadiga, S., Tripp, P., Kistler, R., Woollen, J., Behringer, D., Liu, H., Stokes, D., Grumbine, R., Gayno, G., Wang, J., Hou, Y. T., Chuang, H. Y., Juang, H. M. H., Sela, J., Iredell, M., Treadon, R., Kleist, D., Van Delst, P., Keyser, D., Derber, J., Ek, M., Meng, J., Wei, H., Yang, R., Lord, S., Van Den Dool, H., Kumar, A., Wang, W., Long, C., Chelliah, M., Xue, Y., Huang, B., Schemm, J. K., Ebisuzaki, W., Lin, R., Xie, P., Chen, M., Zhou, S., Higgins, W., Zou, C. Z., Liu, Q., Chen, Y., Han, Y., Cucurull, L., Reynolds, R. W., Rutledge, G., and Goldberg, M. (2010). "The NCEP climate forecast system reanalysis". In: *Bulletin of the American Meteorological Society* 91.8, pp. 1015–1057. DOI: 10.1175/2010BAMS3001.1.

Sahraei, S., Asadzadeh, M., and Unduche, F. (2020). "Signature-based multi-modelling and multi-objective calibration of hydrologic models: Application in flood forecasting for Canadian Prairies". In: *Journal of Hydrology* 588, p. 125095. DOI: 10.1016/j.jhydrol.2020.125095.

Salazar, L. F. and Nobre, C. A. (2010). "Climate change and thresholds of biome shifts in Amazonia". In: *Geophysical Research Letters* 37.17, p. 17706. DOI: 10.1029/2010GL043538.

Santini, W., Martinez, J.-M., Espinoza-Villar, R., Cochonneau, G., Vauchel, P., Moquet, J.-S., Baby, P., Espinoza, J.-C., Lavado, W., Carranza, J., and Guyot, J.-L. (2015). "Sediment budget in the Ucayali River basin, an Andean tributary of the Amazon River". In: *Proceedings of the International Association of Hydrological Sciences* 367, pp. 320–325. DOI: 10.5194/piahs-367-320-2015.

Santini, W. (2020). "Caractérisation de la dynamique hydro-sédimentaire du bassin de l'Ucayali (Pérou), par une approche intégrant réseau de mesures, télédétection et modélisation hydrologique". PhD thesis. Toulouse: Université Toulouse III - Paul Sabatier, pp. 1–479.

Santini, W., Camenen, B., Le Coz, J., Vauchel, P., Guyot, J.-L., Lavado, W., Carranza, J., Paredes, M. A., Pérez Arévalo, J. J., Arévalo, N., Espinoza Villar, R., Julien, F., and Martinez, J.-M. (2019). "An index concentration method for suspended load monitoring in large rivers of the Amazonian foreland". In: *Earth Surface Dynamics* 7.2, pp. 515–536. DOI: 10.5194/esurf-7-515-2019.

Satgé, F., Bonnet, M.-P., Gosset, M., Molina, J., Hernan Yuque Lima, W., Pillco Zolá, R., Timouk, F., and Garnier, J. (2016). "Assessment of satellite rainfall products over the Andean plateau". In: *Atmospheric Research* 167, pp. 1–14. DOI: 10.1016/j.atmosres.2015.07.012.

Satgé, F., Hussain, Y., Molina-Carpio, J., Pillco, R., Laugner, C., Akhter, G., and Bonnet, M.-P. (2020). "Reliability of SM2RAIN precipitation datasets in comparison to gauge observations and hydrological modelling over arid regions". In: *International Journal of Climatology* 41.S1, E517–E536. DOI: 10.1002/joc.6704.

Satgé, F., Ruelland, D., Bonnet, M.-P., Molina, J., and Pillco, R. (2019). "Consistency of satellite-based precipitation products in space and over time compared with gauge observations and snow- hydrological modelling in the Lake Titicaca region". In: *Hydrology and Earth System Sciences* 23.1, pp. 595–619. DOI: 10.5194/hess-23-595-2019.

Scheel, M. L. M., Rohrer, M., Huggel, C., Santos Villar, D., Silvestre, E., and Huffman, G. J. (2011). "Evaluation of TRMM Multi-satellite Precipitation Analysis (TMPA) performance in the Central Andes region and its dependency on spatial and temporal resolution". English. In: *Hydrology and Earth System Sciences* 15.8, pp. 2649–2663. DOI: 10.5194/hess-15-2649-2011.

Séférian, R., Nabat, P., Michou, M., Saint-Martin, D., Voldoire, A., Colin, J., Decharme, B., Delire, C., Berthet, S., Chevallier, M., Sénési, S., Franchisteguy, L., Vial, J., Mallet, M., Joetzjer, E., Geoffroy, O., Guérémy, J. F., Moine, M. P., Msadek, R., Ribes, A., Rocher, M., Roehrig, R., Salas-y-Mélia, D., Sanchez, E., Terray, L., Valcke, S., Waldman, R., Aumont, O., Bopp, L., Deshayes, J., Éthé, C., and Madec, G. (2019). "Evaluation of CNRM Earth System Model, CNRM-ESM2-1: Role of Earth System Processes in Present-Day and Future Climate". In: *Journal of Advances in Modeling Earth Systems* 11.12, pp. 4182–4227. DOI: 10.1029/2019MS001791.

Segura, H., Espinoza, J. C., Junquas, C., Lebel, T., Vuille, M., and Garreaud, R. (2020). "Recent changes in the precipitation-driving processes over the southern tropical Andes/western Amazon". In: *Climate Dynamics* 54.5-6, pp. 2613–2631. DOI: 10.1007/S00382-020-05132-6.

Segura, H., Junquas, C., Espinoza, J. C., Vuille, M., Jauregui, Y. R., Rabatel, A., Condom, T., and Lebel, T. (2019). "New insights into the rainfall variability in the tropical Andes on seasonal and interannual time scales". In: *Climate Dynamics* 53.1-2, pp. 405–426. DOI: 10.1007/s00382-018-4590-8.

Seiler, C., Hutjes, R. W., and Kabat, P. (2013). "Likely Ranges of Climate Change in Bolivia". In: *Journal of Applied Meteorology and Climatology* 52.6, pp. 1303–1317. DOI: 10.1175/JAMC-D-12-0224.1.

Sekulić, A., Kilibarda, M., Heuvelink, G. B., Nikolić, M., and Bajat, B. (2020). "Random Forest Spatial Interpolation". In: *Remote Sensing* 12.10, p. 1687. DOI: 10.3390/rs12101687.

Sellar, A. A., Jones, C. G., Mulcahy, J. P., Tang, Y., Yool, A., Wiltshire, A., O'Connor, F. M., Stringer, M., Hill, R., Palmieri, J., Woodward, S., de Mora, L., Kuhlbrodt, T., Rumbold, S. T., Kelley, D. I., Ellis, R., Johnson, C. E., Walton, J., Abraham, N. L., Andrews, M. B., Andrews, T., Archibald, A. T., Berthou, S., Burke, E., Blockley, E., Carslaw, K., Dalvi, M., Edwards, J., Folberth, G. A., Gedney, N., Griffiths, P. T., Harper, A. B., Hendry, M. A., Hewitt, A. J., Johnson, B., Jones, A., Jones, C. D., Keeble, J., Liddicoat, S., Morgenstern, O., Parker, R. J., Predoi, V., Robertson, E., Siahaan, A., Smith, R. S., Swaminathan, R., Woodhouse, M. T., Zeng, G., and Zerroukat, M. (2019). "UKESM1: Description and Evaluation of the U.K. Earth System Model". In: *Journal of Advances in Modeling Earth Systems* 11.12, pp. 4513–4558. DOI: 10.1029/2019MS001739.

Shafii, M. and De Smedt, F. (2009). "Multi-objective calibration of a distributed hydrological model (WetSpa) using a genetic algorithm". In: *Hydrology and Earth System Sciences* 13.11, pp. 2137–2149. DOI: 10.5194/hess-13-2137-2009.

Shafii, M., Basu, N., Craig, J. R., Schiff, S. L., and Van Cappellen, P. (2017). "A diagnostic approach to constraining flow partitioning in hydrologic models using a multiobjective optimization framework". In: *Water Resources Research* 53.4, pp. 3279–3301. DOI: 10.1002/2016WR019736.

Shafii, M. and Tolson, B. A. (2015). "Optimizing hydrological consistency by incorporating hydrological signatures into model calibration objectives". In: *Water Resources Research* 51.5, pp. 3796–3814. DOI: 10.1002/2014WR016520.

Shen, Z. Y., Chen, L., and Chen, T. (2012). "Analysis of parameter uncertainty in hydrological and sediment modeling using GLUE method: a case study of SWAT model applied to Three Gorges Reservoir Region, China". English. In: *Hydrology and Earth System Sciences* 16.1, pp. 121–132. DOI: 10.5194/hess-16-121-2012.

Shepard, D. (1968). "A two-dimensional interpolation function for irregularly-spaced data". In: *ACM 68: Proceedings of the 1968 23rd ACM National Conference*. Association for Computing Machinery, pp. 517–524. DOI: 10.1145/800186.810616.

da Silva Júnior, J. C., Medeiros, V., Garrozi, C., Montenegro, A., and Gonçalves, G. E. (2019). "Random forest techniques for spatial interpolation of evapotranspiration data from Brazilian's

Northeast". In: *Computers and Electronics in Agriculture* 166, p. 105017. DOI: 10.1016/j.compag.2019.105017.

Singh, S. K., Pahlow, M., Booker, D. J., Shankar, U., and Chamorro, A. (2019). "Towards baseflow index characterisation at national scale in New Zealand". In: *Journal of Hydrology* 568, pp. 646–657. DOI: 10.1016/j.jhydrol.2018.11.025.

Somers, L. D., McKenzie, J. M., Mark, B. G., Lagos, P., Ng, G.-H. C., Wickert, A. D., Yarleque, C., Baraër, M., and Silva, Y. (2019). "Groundwater Buffers Decreasing Glacier Melt in an Andean Watershed—But Not Forever". In: *Geophysical Research Letters* 46.22, pp. 13016–13026. DOI: 10.1029/2019GL084730.

Song, X., Zhang, J., Zhan, C., Xuan, Y., Ye, M., and Xu, C. (2015). *Global sensitivity analysis in hydrological modeling: Review of concepts, methods, theoretical framework, and applications*. DOI: 10.1016/j.jhydrol.2015.02.013.

Staal, A., Tuinenburg, O. A., Bosmans, J. H., Holmgren, M., Van Nes, E. H., Scheffer, M., Zemp, D. C., and Dekker, S. C. (2018). "Forest-rainfall cascades buffer against drought across the Amazon". In: *Nature Climate Change* 8.6, pp. 539–543. DOI: 10.1038/s41558-018-0177-y.

Strauch, M., Kumar, R., Eisner, S., Mulligan, M., Reinhardt, J., Santini, W., Vetter, T., and Friesen, J. (2017). "Adjustment of global precipitation data for enhanced hydrologic modeling of tropical Andean watersheds". In: *Climatic Change* 141.3, pp. 547–560. DOI: 10.1007/s10584-016-1706-1.

Strauch, M. and Volk, M. (2013). "SWAT plant growth modification for improved modeling of perennial vegetation in the tropics". In: *Ecological Modelling* 269, pp. 98–112. DOI: 10.1016/J.ECOLMODEL.2013.08.013.

Sun, Q., Miao, C., Duan, Q., Ashouri, H., Sorooshian, S., and Hsu, K.-L. (2018). "A Review of Global Precipitation Data Sets: Data Sources, Estimation, and Intercomparisons". In: *Reviews of Geophysics* 56.1, pp. 79–107. DOI: 10.1002/2017RG000574.

Swart, N. C., Cole, J. N., Kharin, V. V., Lazare, M., Scinocca, J. F., Gillett, N. P., Anstey, J., Arora, V., Christian, J. R., Hanna, S., Jiao, Y., Lee, W. G., Majaess, F., Saenko, O. A., Seiler, C., Seinen, C., Shao, A., Sigmond, M., Solheim, L., Von Salzen, K., Yang, D., and Winter, B. (2019). "The Canadian Earth System Model version 5 (CanESM5.0.3)". In: *Geoscientific Model Development* 12.11, pp. 4823–4873. DOI: 10.5194/GMD-12-4823-2019.

Tall, M., Albergel, C., Bonan, B., Zheng, Y., Guichard, F., Dramé, M. S., Gaye, A. T., Sintondji, L. O., Hountondji, F. C., Nikiema, P. M., and Calvet, J. C. (2019). "Towards a long-term reanalysis of land surface variables over western Africa: LDAS-Monde applied over Burkina Faso from 2001 to 2018". In: *Remote Sensing* 11.6, p. 735. DOI: 10.3390/RS11060735.

Tamayo, G. G. (2017). "Evaluación de los caudales líquidos y de producción de sedimentos estimados con el modelo Soil Water Assessment Tool (SWAT) y su relación con los caudales líquidos y sólidos observados". PhD thesis. Quito: Escuela Politécnica Nacional.

Tan, M. L., Gassman, P. W., Yang, X., and Haywood, J. (2020). "A review of SWAT applications, performance and future needs for simulation of hydro-climatic extremes". In: *Advances in Water Resources* 143, p. 103662. DOI: 10.1016/j.advwatres.2020.103662.

Tang, W. (2019). "Dataset of high-resolution (3 hour, 10 km) global surface solar radiation (1983-2018)". In: *National Tibetan Plateau Data Center*. DOI: 10.11888/Meteoro.tpdc.270112.

Tang, W., Yang, K., Qin, J., Li, X., and Niu, X. (2019). "A 16-year dataset (2000–2015) of high-resolution (3 h, 10 km) global surface solar radiation". In: *Earth System Science Data* 11.4, pp. 1905–1915. DOI: 10.5194/essd-11-1905-2019.

Tarek, M., Brissette, F. P., and Arsenault, R. (2020). "Evaluation of the ERA5 reanalysis as a potential reference dataset for hydrological modelling over North America". In: *Hydrology and Earth System Sciences* 24.5, pp. 2527–2544. DOI: 10.5194/hess-24-2527-2020.

Tatebe, H., Ogura, T., Nitta, T., Komuro, Y., Ogochi, K., Takemura, T., Sudo, K., Sekiguchi, M., Abe, M., Saito, F., Chikira, M., Watanabe, S., Mori, M., Hirota, N., Kawatani, Y., Mochizuki, T., Yoshimura, K., Takata, K., O'Ishi, R., Yamazaki, D., Suzuki, T., Kurogi, M., Kataoka, T., Watanabe, M., and Kimoto, M. (2019). "Description and basic evaluation of simulated mean state, internal variability, and climate sensitivity in MIROC6". In: *Geoscientific Model Development* 12.7, pp. 2727–2765. DOI: 10.5194/GMD-12-2727-2019.

Taylor, K. E. (2001). "Summarizing multiple aspects of model performance in a single diagram". In: *Journal of Geophysical Research* 106.D7, p. 7183. DOI: 10.1029/2000JD900719.

Teuling, A. J., Lehner, I., Kirchner, J. W., and Seneviratne, S. I. (2010). "Catchments as simple dynamical systems: Experience from a Swiss prealpine catchment". In: *Water Resources Research* 46.10. DOI: 10.1029/2009WR008777.

Themeßl, M. J., Gobiet, A., and Heinrich, G. (2012). "Empirical-statistical downscaling and error correction of regional climate models and its impact on the climate change signal". In: *Climatic Change* 112.2, pp. 449–468. DOI: 10.1007/S10584-011-0224-4.

Thrasher, B., Maurer, E. P., McKellar, C., and Duffy, P. B. (2012). "Technical Note: Bias correcting climate model simulated daily temperature extremes with quantile mapping". In: *Hydrology and Earth System Sciences* 16.9, pp. 3309–3314. DOI: 10.5194/HESS-16-3309-2012.

Thrasher, B., Wang, W., Michaelis, A., Melton, F., Lee, T., and Nemani, R. (2022). "NASA Global Daily Downscaled Projections, CMIP6". In: *Scientific Data* 9.1, pp. 1–6. DOI: 10.1038/s41597-022-01393-4.

Tobar, V. and Wyseure, G. (2018). "Seasonal rainfall patterns classification, relationship to ENSO and rainfall trends in Ecuador". In: *International Journal of Climatology* 38.4, pp. 1808–1819. DOI: 10.1002/joc.5297.

Tomkins, K. M. (2014). "Uncertainty in streamflow rating curves: Methods, controls and consequences". In: *Hydrological Processes* 28.3, pp. 464–481. DOI: 10.1002/hyp.9567.

Torres-Batlló, J. and Martí-Cardona, B. (2020). "Precipitation trends over the southern Andean Altiplano from 1981 to 2018". In: *Journal of Hydrology* 590, p. 125485. DOI: 10.1016/J.JHYDROL.2020.125485.

Towner, J., Cloke, H. L., Zsoter, E., Flamig, Z., Hoch, J. M., Bazo, J., De Perez, E. C., and Stephens, E. M. (2019). "Assessing the performance of global hydrological models for capturing peak river flows in the Amazon basin". In: *Hydrology and Earth System Sciences* 23.7, pp. 3057–3080. DOI: 10.5194/HESS-23-3057-2019.

Trenberth, K. E. and Cheng, L. (2022). "A perspective on climate change from Earth's energy imbalance". In: *Environmental Research: Climate* 1.1, p. 013001. DOI: 10.1088/2752-5295/AC6F74.

Veettil, B. K. and Kamp, U. (2019). "Global Disappearance of Tropical Mountain Glaciers: Observations, Causes, and Challenges". In: *Geosciences* 9.5, p. 196. DOI: 10.3390/GEOSCIENCES9050196.

Vega-Jácome, F., Lavado-Casimiro, W. S., and Felipe-Obando, O. G. (2018). "Assessing hydrological changes in a regulated river system over the last 90 years in Rimac Basin (Peru)". In: *Theoretical and Applied Climatology* 132.1-2, pp. 347–362. DOI: 10.1007/S00704-017-2084-Y.

Vicente-Serrano, S. M., López-Moreno, J. I., Correa, K., Avalos, G., Bazo, J., Azorin-Molina, C., Domínguez-Castro, F., Kenawy, A. E., Gimeno, L., and Nieto, R. (2018). "Recent changes in monthly surface air temperature over Peru, 1964–2014". In: *International Journal of Climatology* 38.1, pp. 283–306. DOI: 10.1002/JOC.5176.

Vicente-Serrano, S. M., Peña-Angulo, D., Beguería, S., Domínguez-Castro, F., Tomás-Burguera, M., Noguera, I., Gimeno-Sotelo, L., and El Kenawy, A. (2022). "Global drought trends and future projections". In: *Philosophical Transactions of the Royal Society A* 380.2238. DOI: 10.1098/RSTA.2021.0285.

Voldoire, A., Saint-Martin, D., Sénési, S., Decharme, B., Alias, A., Chevallier, M., Colin, J., Guérémy, J. F., Michou, M., Moine, M. P., Nabat, P., Roehrig, R., Salas y Mélia, D., Séférian, R., Valcke, S., Beau, I., Belamari, S., Berthet, S., Cassou, C., Cattiaux, J., Deshayes, J., Douville, H., Ethé, C., Franchistéguy, L., Geoffroy, O., Lévy, C., Madec, G., Meurdesoif, Y., Msadek, R., Ribes, A., Sanchez-Gomez, E., Terray, L., and Waldman, R. (2019). "Evaluation of CMIP6 DECK Experiments With CNRM-CM6-1". In: *Journal of Advances in Modeling Earth Systems* 11.7, pp. 2177–2213. DOI: 10.1029/2019MS001683.

Vormoor, K., Lawrence, D., Heistermann, M., and Bronstert, A. (2015). "Climate change impacts on the seasonality and generation processes of floods – projections and uncertainties for catchments with mixed snowmelt/rainfall regimes". In: *Hydrology and Earth System Sciences* 19.2, pp. 913–931. DOI: 10.5194/HESS-19-913-2015.

Vuille, M., Carey, M., Huggel, C., Buytaert, W., Rabatel, A., Jacobsen, D., Soruco, A., Villacis, M., Yarleque, C., Elison Timm, O., Condom, T., Salzmann, N., and Sicart, J. E. (2018). "Rapid

decline of snow and ice in the tropical Andes – Impacts, uncertainties and challenges ahead". In: *Earth-Science Reviews* 176, pp. 195–213. DOI: 10.1016/J.EARSCIREV.2017.09.019.

Vuille, M., Franquist, E., Garreaud, R., Lavado Casimiro, W. S., and Cáceres, B. (2015). "Impact of the global warming hiatus on Andean temperature". In: *Journal of Geophysical Research: Atmospheres* 120.9, pp. 3745–3757. DOI: 10.1002/2015JD023126.

Wagener, T., Boyle, D. P., Lees, M. J., Wheater, H. S., Gupta, H. V., and Sorooshian, S. (2001). "A framework for development and application of hydrological models". In: *Hydrology and Earth System Sciences* 5.1, pp. 13–26. DOI: 10.5194/hess-5-13-2001.

Wang, H., Gong, W., Duan, Q., and Di, Z. (2020). "Evaluation of parameter interaction effect of hydrological models using the sparse polynomial chaos (SPC) method". In: *Environmental Modelling & Software* 125, p. 104612. DOI: 10.1016/J.ENVSOFT.2019.104612.

Wang, J., Zhuo, L., Han, D., Liu, Y., and Rico-Ramirez, M. A. (2023). "Hydrological Model Adaptability to Rainfall Inputs of Varied Quality". In: *Water Resources Research* 59.2, e2022WR032484. DOI: 10.1029/2022WR032484.

Weedon, G. P., Balsamo, G., Bellouin, N., Gomes, S., Best, M. J., and Viterbo, P. (2014). "The WFDEI meteorological forcing data set: WATCH Forcing data methodology applied to ERA-Interim reanalysis data". In: *Water Resources Research* 50.9, pp. 7505–7514. DOI: 10.1002/2014WR015638.

Wei, Z., Zhang, B., Liu, Y., and Xu, D. (2018). "The Application of a Modified Version of the SWAT Model at the Daily Temporal Scale and the Hydrological Response unit Spatial Scale: A Case Study Covering an Irrigation District in the Hei River Basin". In: *Water* 10.8, p. 1064. DOI: 10.3390/w10081064.

van Werkhoven, K., Wagener, T., Reed, P., and Tang, Y. (2009). "Sensitivity-guided reduction of parametric dimensionality for multi-objective calibration of watershed models". In: *Advances in Water Resources* 32.8, pp. 1154–1169. DOI: 10.1016/J.ADVWATRES.2009.03.002.

Wongchuig Correa, S., Paiva, R. C. D. d., Espinoza, J. C., and Collischonn, W. (2017). "Multi-decadal Hydrological Retrospective: Case study of Amazon floods and droughts". In: *Journal of Hydrology* 549, pp. 667–684. DOI: 10.1016/j.jhydrol.2017.04.019.

Wu, W., Li, Y., Luo, X., Zhang, Y., Ji, X., and Li, X. (2019). "Performance evaluation of the CHIRPS precipitation dataset and its utility in drought monitoring over Yunnan Province, China". In: *Geomatics, Natural Hazards and Risk* 10.1, pp. 2145–2162. DOI: 10.1080/19475705.2019.1683082.

Wunderlich, W., Lang, M., Keating, K., Perez, W. B., and Oshun, J. (2023). "The role of peat-forming bofedales in sustaining baseflow in the humid puna". In: *Journal of Hydrology: Regional Studies* 47, p. 101394. DOI: 10.1016/J.EJRH.2023.101394.

Xavier, A. C., King, C. W., and Scanlon, B. R. (2016). "Daily gridded meteorological variables in Brazil (1980–2013)". In: *International Journal of Climatology* 36.6, pp. 2644–2659. DOI: 10.1002/joc.4518.

Xavier, A. C., King, C. W., and Scanlon, B. R. (2017). "An update of Xavier, King and Scanlon (2016) daily precipitation gridded data set for the Brazil". In: *XVIII Simpósio Brasileiro de Sensoriamento Remoto*. São Paulo, Brazil, INPE, pp. 28–31.

Xu, X., Frey, S. K., Boluwade, A., Erler, A. R., Khader, O., Lapen, D. R., and Sudicky, E. (2019a). "Evaluation of variability among different precipitation products in the Northern Great Plains". In: *Journal of Hydrology: Regional Studies* 24, p. 100608. DOI: 10.1016/j.ejrh.2019.100608.

Xu, Z., Wu, Z., He, H., Wu, X., Zhou, J., Zhang, Y., and Guo, X. (2019b). "Evaluating the accuracy of MSWEP V2.1 and its performance for drought monitoring over mainland China". In: *Atmospheric Research* 226, pp. 17–31. DOI: 10.1016/j.atmosres.2019.04.008.

Xu, Z., Han, Y., Tam, C. Y., Yang, Z. L., and Fu, C. (2021). "Bias-corrected CMIP6 global dataset for dynamical downscaling of the historical and future climate (1979–2100)". In: *Scientific Data* 8.1, pp. 1–11. DOI: 10.1038/s41597-021-01079-3.

Xue, X., Zhang, K., Hong, Y., Gourley, J. J., Kellogg, W., McPherson, R. A., Wan, Z., and Austin, B. N. (2016). "New Multisite Cascading Calibration Approach for Hydrological Models: Case Study in the Red River Basin Using the VIC Model". In: *Journal of Hydrologic Engineering* 21.2, p. 05015019. DOI: 10.1061/(ASCE)HE.1943-5584.0001282.

Yamazaki, D., Ikeshima, D., Tawatari, R., Yamaguchi, T., O'Loughlin, F., Neal, J. C., Sampson, C. C., Kanae, S., and Bates, P. D. (2017). "A high-accuracy map of global terrain elevations". In: *Geophysical Research Letters* 44.11, pp. 5844–5853. DOI: 10.1002/2017GL072874.

Yamazaki, D., Kanae, S., Kim, H., and Oki, T. (2011). "A physically based description of floodplain inundation dynamics in a global river routing model". In: *Water Resources Research* 47.4, p. 4501. DOI: 10.1029/2010WR009726.

Ye, B., Yang, D., and Ma, L. (2012). "Effect of precipitation bias correction on water budget calculation in Upper Yellow River, China". In: *Environmental Research Letters* 7.2, p. 025201. DOI: 10.1088/1748-9326/7/2/025201.

Yesuf, H. M., Melesse, A. M., Zeleke, G., and Alamirew, T. (2016). "Streamflow prediction uncertainty analysis and verification of SWAT model in a tropical watershed". In: *Environmental Earth Sciences* 75.9, p. 806. DOI: 10.1007/s12665-016-5636-z.

Yilmaz, K. K., Gupta, H. V., and Wagener, T. (2008). "A process-based diagnostic approach to model evaluation: Application to the NWS distributed hydrologic model". In: *Water Resources Research* 44.9. DOI: 10.1029/2007WR006716.

Yuan, H., Dai, Y., Xiao, Z., Ji, D., and Shangguan, W. (2011). "Reprocessing the MODIS Leaf Area Index products for land surface and climate modelling". In: *Remote Sensing of Environment* 115.5, pp. 1171–1187. DOI: 10.1016/J.RSE.2011.01.001.

Yukimoto, S., Kawai, H., Koshiro, T., Oshima, N., Yoshida, K., Urakawa, S., Tsujino, H., Deushi, M., Tanaka, T., Hosaka, M., Yabu, S., Yoshimura, H., Shindo, E., Mizuta, R., Obata, A., Adachi, Y., and Ishii, M. (2019). "The Meteorological Research Institute Earth System Model Version 2.0, MRI-ESM2.0: Description and Basic Evaluation of the Physical Component". In: *Journal of the Meteorological Society of Japan. Ser. II* 97.5, pp. 931–965. DOI: 10.2151/JMSJ.2019-051.

Zambrano-Bigiarini, M., Nauditt, A., Birkel, C., Verbist, K., and Ribbe, L. (2017). "Temporal and spatial evaluation of satellite-based rainfall estimates across the complex topographical and climatic gradients of Chile". In: *Hydrology and Earth System Sciences* 21.2, pp. 1295–1320. DOI: 10.5194/hess-21-1295-2017.

Zhang, J., Lei, X., and Li, Q. (2018a). "Two Model Performance Comparisons with Multisite Observations Based on Uncertainty Methods for Modeling Hydrologic Dynamics". In: *Journal of Irrigation and Drainage Engineering* 144.1, p. 04017060. DOI: 10.1061/(ASCE)IR.1943-4774.0001284.

Zhang, R., Liu, J., Gao, H., and Mao, G. (2018b). "Can multi-objective calibration of streamflow guarantee better hydrological model accuracy?" In: *Journal of Hydroinformatics* 20.3, pp. 687–698. DOI: 10.2166/hydro.2018.131.

Zhang, S., Zhou, L., Zhang, L., Yang, Y., Wei, Z., Zhou, S., Yang, D., Yang, X., Wu, X., Zhang, Y., Li, X., and Dai, Y. (2022). "Reconciling disagreement on global river flood changes in a warming climate". In: *Nature Climate Change* 12.12, pp. 1160–1167. DOI: 10.1038/s41558-022-01539-7.

Zubieta, R., Getirana, A., Espinoza, J. C., and Lavado, W. (2015). "Impacts of satellite-based precipitation datasets on rainfall–runoff modeling of the Western Amazon basin of Peru and Ecuador". In: *Journal of Hydrology* 528, pp. 599–612. DOI: 10.1016/j.jhydrol.2015.06.064.

Zubieta, R., Getirana, A., Espinoza, J. C., Lavado-Casimiro, W., and Aragon, L. (2017). "Hydrological modeling of the Peruvian–Ecuadorian Amazon Basin using GPM-IMERG satellite-based precipitation dataset". In: *Hydrology and Earth System Sciences* 21.7, pp. 3543–3555. DOI: 10.5194/hess-21-3543-2017.

Zubieta, R., Molina-Carpio, J., Laqui, W., Sulca, J., and Ilbay, M. (2021). "Comparative Analysis of Climate Change Impacts on Meteorological, Hydrological, and Agricultural Droughts in the Lake Titicaca Basin". In: *Water* 13.2, p. 175. DOI: 10.3390/W13020175.

Zulkafli, Z., Buytaert, W., Manz, B., Rosas, C. V., Willems, P., Lavado-Casimiro, W., Guyot, J. L., and Santini, W. (2016). "Projected increases in the annual flood pulse of the Western Amazon". In: *Environmental Research Letters* 11.1, p. 014013. DOI: 10.1088/1748-9326/11/1/014013.

Zulkafli, Z., Buytaert, W., Onof, C., Manz, B., Tarnavsky, E., Lavado, W., and Guyot, J. L. (2014). "A Comparative Performance Analysis of TRMM 3B42 (TMPA) Versions 6 and 7 for Hydro-

logical Applications over Andean–Amazon River Basins". In: *Journal of Hydrometeorology* 15.2, pp. 581–592. DOI: 10.1175/JHM-D-13-094.1.